

MAY 1984

EXPERIMENTAL INVESTIGATION OF SHOCK-CELL NOISE REDUCTION FOR SINGLE-STREAM NOZZLES IN SIMULATED FLIGHT

Contract NAS3-22514

(NASA-CR-168234-Vol-3) EXPERIMENTAL
INVESTIGATION OF SHOCK-CELL NOISE REDUCTION
FOR SINGLE-STREAM NOZZLES IN SIMULATED
FLIGHT, COMPREHENSIVE DATA REPORT. VOLUME
3: SHADOWGRAPH PHOTOS AND FACILITY (General G3/71)

N84-33150

Unclassified
20344

Comprehensive Data Report

VOLUME III

Shadowgraph Photos and Facility Description

by

K. Yamamoto

J.F. Brausch

B.A. Janardan

D.J. Hoerst

A.O. Price

P.R. Knott

GENERAL  ELECTRIC

For



National Aeronautics and Space Administration
Lewis Research Center
21000 Brookpark Road
Cleveland, Ohio 44134

REPRODUCED BY
U.S. DEPARTMENT OF COMMERCE
NATIONAL TECHNICAL
INFORMATION SERVICE
SPRINGFIELD, VA 22161

MAY 1984

EXPERIMENTAL INVESTIGATION OF SHOCK-CELL NOISE REDUCTION FOR SINGLE-STREAM NOZZLES IN SIMULATED FLIGHT

Contract NAS3-22514

Comprehensive Data Report VOLUME III

Shadowgraph Photos and Facility Description

by

K. Yamamoto

J.F. Brausch

B.A. Janardan

D.J. Hoerst

A.O. Price

P.R. Knott

GENERAL  ELECTRIC

For

**National Aeronautics and Space Administration
Lewis Research Center
21000 Brookpark Road
Cleveland, Ohio 44135**

**ORIGINAL PAGE IS
OF POOR QUALITY**

1. Report No. NASA CR-168234	2. Government Accession No.	3. Recipient's Catalog No.	
4. Title and Subtitle Experimental Investigation of Shock-Cell Noise Reduction for Single-Stream Nozzles in Simulated Flight - Comprehensive Data Report Volume I.		5. Report Date May 1984	
7. Author(s) K.J.Yamamoto, J.F.Brausch, B.A.Janardan, D.J.Hoerst, A.O.Price, P.R.Knott		6. Performing Organization Code	
9. Performing Organization Name and Address General Electric Company Aircraft Engine Group Cincinnati, Ohio 45215		8. Performing Organization Report No. R82AEB491	
12. Sponsoring Agency Name and Address National Aeronautics and Space Administration Washington, D.C. 20546		10. Work Unit No.	
15. Supplementary Notes Project Manager, James R. Stone NASA-Lewis Research Center Cleveland, Ohio 44135		11. Contract or Grant No. NAS3-22514	
18. Abstract This Comprehensive Data Report, composing three volumes, includes the basic test description and test results which are analyzed and documented in the companion Final Report. Volume I contains a description of the model nozzle configurations, acoustic test conditions, and detailed test results from the hot static and simulated flight acoustic tests at the General Electric Anechoic Chamber. Volume II presents the diagnostic laser velocimeter test results. Volume III contains the diagnostic flow visualization test results obtained by shadowgraph along with a description of test facilities and data acquisition and reduction techniques. Design drawings of scale model nozzles are also included in Volume III.		13. Type of Report and Period Covered Comprehensive Data Report	
17. Key Words (Suggested by Author(s)) Shock-Cell Noise Convergent-Divergent Diagnostic Laser Velocimeter Tests Shadowgraph		18. Distribution Statement Unclassified - Unlimited	
19. Security Classif. (of this report) Unclassified	20. Security Classif. (of this page) Unclassified	21. No. of Pages	22. Price*

* For sale by the National Technical Information Service, Springfield, Virginia 22161

VOLUME III
SHADOWGRAPH PHOTOS AND FACILITY DESCRIPTION

TABLE OF CONTENTS

VOLUME I -- TEST NOZZLES AND ACOUSTIC DATA

<u>Section</u>		<u>Page</u>
1.0	INTRODUCTION	1
2.0	SCALE MODEL NOZZLE CONFIGURATIONS	2
	2.1 Model 1: Baseline Conical-Convergent Nozzle	3
	2.2 Model 2: Circular Convergent-Divergent Nozzle	3
	2.3 Model 3: Baseline Contoured Convergent Annular Plug Nozzle	4
	2.4 Model 3 with Tabs: Baseline Contoured Convergent Annular Plug Nozzle with Shock Screech Tabs	4
	2.5 Model 4: Convergent-Divergent Annular Plug Nozzle	5
	2.6 Model 5: 20 Chute Annular Plug Suppressor, Convergent Flow Element Terminations	6
	2.7 Model 6: 20 Chute Annular Plug Suppressor, Convergent-Divergent Flow Element Terminations	7
3.0	TEST POINT DEFINITION	33
	3.1 Definition of Variables	33
	3.2 Test Matrix of Model 1	38
	3.3 Test Matrix of Model 2	41
	3.4 Test Matrix of Model 3	46
	3.5 Test Matrix of Model 4	51
	3.6 Test Matrix of Model 5	58
	3.7 Test Matrix of Model 6	61
4.0	ACOUSTIC TEST RESULTS	67
	4.1 Description of Acoustic Data Tables	67
	4.2 Acoustic Data of Model 1	72
	4.3 Acoustic Data of Model 2	114
	4.4 Acoustic Data of Model 3	221
	4.5 Acoustic Data of Model 4	297
	4.6 Acoustic Data of Model 5	451
	4.7 Acoustic Data of Model 6	509

PRECEDING PAGE BLANK NOT FILMED

TABLE OF CONTENTS

VOLUME II -- LASER VELOCIMETER DATA

<u>Section</u>		<u>Page</u>
5.0	LASER VELOCIMETER TESTS	591
5.1	Test Matrix and Aerodynamic Conditions of Test Points	591
5.2	Laser Velocimeter Test Data	592
5.2.1	Tabulations of Laser Velocimeter Data	592
5.2.2	General Remarks on LV Mean Velocity Traces	593
5.2.3	Laser Velocimeter Data of Model 1	771
5.2.4	Laser Velocimeter Data of Model 2	832
5.2.5	Laser Velocimeter Data of Model 3	899
5.2.6	Laser Velocimeter Data of Model 4	991
5.2.7	Laser Velocimeter Data of Model 5	1075
5.2.8	Laser Velocimeter Data of Model 6	1221

VOLUME III -- SHADOWGRAPH PHOTOS AND FACILITY DESCRIPTION

6.0	SHADOWGRAPH PHOTO TESTS	1365
6.1	Scope and Details of Tests	1365
6.2	Shadowgraph Photo Test Results	1380
6.2.1	Shadowgraph Photos of Model 1	1380
6.2.2	Shadowgraph Photos of Model 2	1396
6.2.3	Shadowgraph Photos of Model 3	1413
6.2.4	Shadowgraph Photos of Model 4	1427
6.2.5	Shadowgraph Photos of Model 5	1438
6.2.6	Shadowgraph Photos of Model 6	1451
7.0	STATIC PRESSURE DATA	1471
7.1	Diagnostic Static Pressure Data	1471
7.2	Suppressor Base Pressure Data	1483
8.0	NOMENCLATURE	1489
9.0	REFERENCES	1491

APPENDICES

Appendix I	Acoustic Test Facility	1494
Appendix II	Acoustic Data Acquisition and Reduction Procedures	1503
Appendix III	Aerodynamic Data Acquisition and Reduction Procedures	1517
Appendix IV	Laser Velocimeter System	1521
Appendix V	Shadowgraph System	1529
Appendix VI	Design Drawings of Scale Model Nozzles	1531

LIST OF TABLES
IN VOLUME III

	<u>Page</u>
6.1 Summary of Shadowgraph Tests.	1366
6.2 Test Details of Shadowgraph Photographs. thru 6.7	1367
7.1 Diagnostic Static Pressure Data of Circular Convergent-Divergent Nozzle (Model 2).	1475
7.2 Diagnostic Static Pressure Data of Annular Convergent-Divergent Nozzle (Model 4).	1477
7.3 Diagnostic Static Pressure Data of Convergent-Divergent 20-Shallow-Chute Suppressor Nozzle (Model 6).	1481
7.4 Summary of Aerodynamic Flow Conditions of Base Pressure Tests with Model 6.	1485
7.5 Summary of Measured Base Pressure Data for Model 6.	1486
IV-1 Estimated Percent Error in the LV Measurement of Mean Velocity with 95% Confidence.	1527
IV-2 Estimated Percent Error for LV Turbulent Velocity Measurements with 95% Confidence.	1527
VI-1 Summarization Scale Model Nozzles with Applicable Text and Appendix Figures.	1532

LIST OF ILLUSTRATIONS

IN VOLUME III

	<u>Page</u>
7.1 Application of P _s Instrumentation to Circular Convergent-Divergent Nozzle (Model 2).	1472
7.2 Application of P _s Instrumentation to Annular Convergent-Divergent Nozzle (Model 4).	1473
7.3 Application of P _s Instrumentation to C-D Flow Passage of 20-Shallow-Chute Suppressor Nozzle (Model 6).	1474
7.4 Application of Base Pressure Instrumentation to 20-Shallow-Chute Suppressor Nozzle (Model 6)	1484
I-1 Schematic of the General Electric Anechoic Free-Jet Acoustic Facility.	1495
I-2 Operating Domain of General Electric's Anechoic Chamber.	1496
I-3 Free-Jet Arrangement in Anechoic Facility (Cell 41).	1497
I-4 Overhead View of the Tertiary Exhaust Surrounding a Conical Test Nozzle.	1498
I-5 Comparison of Coannular Jet Noise Spectra with Tertiary (Background) Noise Spectra at θ _i = 50°.	1499
I-6 Comparison of Coannular Jet Noise Spectra with Tertiary (Background) Noise Spectra at θ _i = 90°.	1500
I-7 Comparison of Coannular Jet Noise Spectra with Tertiary (Background) Noise Spectra at θ _i = 150°.	1501
II-1 Acoustic Data Acquisition and Reduction System.	1510
II-2 Acoustic Data Processing Flow Chart.	1511
II-3 Algorithm Description.	1512
III-1 General Electric Anechoic Chamber Aerodynamic Data Processing System.	1518
IV-1 Laser System in the GE Anechoic Jet Noise Test Facility.	1525
IV-2 Laser Velocimeter Optics Package.	1525
IV-3 Schematic of Laser Velocity Measurements.	1526
V-1 Schematic Arrangement of the Shadowgraph Setup in the Anechoic Jet Facility.	1530
VI-1 Drawing of Model 1, Baseline Conical-Convergent Nozzle, 4013096-981, Item 8, P07.	1533
VI-2 Drawing of Model 2's Transition Shroud, JNT040181P01.	1534
VI-3 Drawing of Model 2's C-D Nozzle, JNT040181P02.	1535
VI-4 Photo of Model 2's Transition Shroud, JNT040181P01.	1536
VI-5 Photo of Model 2's C-D Nozzle, JNT040181P02.	1537
VI-6 Drawing of Model 3's & 4's Plug Forebody, 4013266-525, Item 3, P02.	153

LIST OF ILLUSTRATIONS

IN VOLUME III

CONT'D

Page

VI-7.	Photo of Model 3's & 4's Plug Forebody, 4013266-525, Item 3, P02.	1539
VI-8.	Drawing of Model 3's & 4's Plug Crown, 4013266-525, Item 4, P03.	1540
VI-9.	Photo of Model 3's & 4's Plug Crown, 4013266-525, Item 4, P03.	1541
VI-10.	Drawing of Model 3's & 4's Plug Closure, 4013266-525, Item 7, P06.	1542
VI-11.	Photo of Model 3's & 4's Plug Closure, 4013266-525, Item 7, P06.	1543
VI-12.	Drawing of Model 3's & 4's Transition & Centering Sleeve, 4013266-525, Item 11, P10.	1544
VI-13.	Photo of Model 3's & 4's Transition & Centering Sleeve, 4013266-525, Item 11, P10.	1545
VI-14.	Drawing of Model 3's & 4's Core Nozzle Support Structure, 4013266-525, Item 12, P11.	1546
VI-15.	Photo of Model 3's & 4's Core Nozzle Support Structure, 4013266-525, Item 12, P11, Side View.	1547
VI-16.	Photo of Model 3's & 4's Core Nozzle Support Structure, 4013266-525, Item 12, P11, End View.	1548
VI-17.	Drawing of Model 3's & 4's Aft Free Stream Closure, 4013266-525, Item 14, P13.	1549
VI-18.	Photo of Model 3's & 4's Aft Free Stream Closure, 4013266-525, Item 14, P13.	1550
VI-19.	Drawing of Model 3's & 4's Centering Strut/Pad Assembly, 4013266-525, Item 19, P17.	1551
VI-20.	Photo of Model 3's & 4's Centering Strut/Pad Assembly, 4013266-525, Item 19, P17.	1552
VI-21.	Drawing of Model 3's Convergent Annular Sleeve, JNT030981-1, P01.	1553
VI-22.	Drawing of Model 4's Convergent-Divergent Annular Sleeve, 4013266-525, Item 8, P07.	1554
VI-23.	Photo of Model 4's Convergent-Divergent Annular Sleeve, 4013266-525, Item 8, P07.	1555
VI-24.	Drawing of Static Pressure Instrumentation Application to Model 4's Plug Crown, 4013266-525, Item 4, P03.	1556

LIST OF ILLUSTRATIONS

IN VOLUME III

CONCLUDED

	<u>Page</u>
VI-25. Drawing of Static Pressure Instrumentation Application to Model 4's Plug Closure, 4013266-525, Item 7, P06.	1557
VI-26. Drawing of Static Pressure Instrumentation Application to Model 4's C-D Annular Sleeve, 4013266-525, Item 8, P07.	1558
VI-27. Assembly Drawing, Model 6.	1559
VI-28. Assembly Drawing, Model 5.	1560
VI-29. Detailed Drawing, Model 6.	1561
VI-30. Detailed Drawing, Models 5 & 6.	1562
VI-31. Detailed Drawing, Models 5 & 6,	1563
VI-32. Photo of Model 5 Components.	1564
VI-33. Photo of Model 6 Components.	1565
VI-34. Application of P_s Instrumentation to C-D Flow Passage of Model 6's C-D Chute Suppressor.	1566
VI-35. Application of P_s Instrumentation to Base Area of Model 6's C-D Chute Suppressor.	1567

6.0 SHADOWGRAPH PHOTO TESTS

A total of 142 shadowgraph photographs were taken on 43 different plumes that were distributed over the six nozzle configurations of this program using the 9.5 inch diameter collimated light beam of the shadowgraph setup described in Appendix V. Aerodynamic flow conditions of the shadowgraph test points, the location and identification of each of the photographs, and copies of the pictures taken are presented in this section.

6.1 SCOPE AND DETAILS OF TESTS

The total scope of the shadowgraph test efforts are summarized in Table 6.1. The individual test details associated with each of the test models are provided in Tables 6.2 through 6.7. For easy cross-reference, the following information is provided on each of these tables:

- o Shadowgraph test plume designation
- o Test plume aerodynamic flow conditions --
Pictures taken with a flow condition for a given nozzle constitute a set of shadowgraphs.
- o Identification of each of the pictures in a given set with a shadowgraph number
- o Actual center location of each of the pictures relative to a referenced origin
- o Pictorial description of a shadowgraph set for each of the test plumes with the individual pictures identified by their shadowgraph numbers
- o Identification, if any, of the available and matching acoustic and laser velocimeter test plume numbers

The copies of individual shadowgraph photographs for each of the six test models are presented in Section 6.2 (Subsections 6.2.1 - 6.2.6).

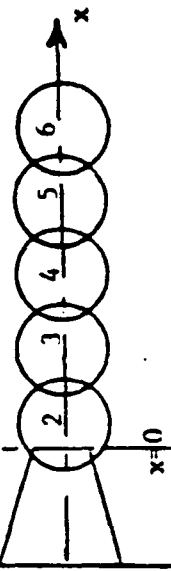
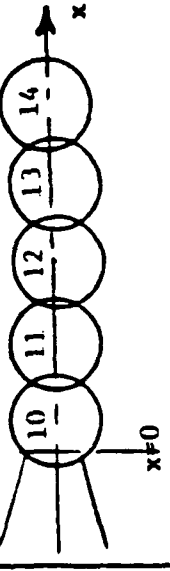
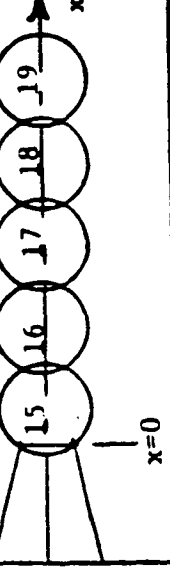
Table 6.1 Summary of Shadowgraph Tests

Model No.	Nozzle Description	Shadowgraph Details		
		No. of Test Plumes	No. of Pictures Taken	Test Details
1	Conical Convergent	5	25	Table 6.2
2	Conical C-D	8	27	Subsection 6.2.1
3	Annular Convergent	7	23	Table 6.3
4	Annular C-D	5	17	Subsection 6.2.2
5	Suppressor Convergent	8	24	Table 6.4
6	Suppressor C-D	10	26	Subsection 6.2.3
				Table 6.5
				Table 6.6
				Table 6.7
				Subsection 6.2.4
				Subsection 6.2.5
				Subsection 6.2.6

- 1

Table 6.2 Test Details of Shadowgraph Photographs with Circular Convergent Nozzle (Model 1).

ORIGINAL PAGE IS
OF POOR QUALITY

Test Point	Shadowgraph Test Flow Conditions				Photograph Details			Matching Acoustic Test Point	Matching LV Test Point
	$V_{a/c.}$ fps	P_r	T_r °R	V_j fps	No.	Shadowgraph Center Location X (in.) Along Centerline	Pictorial Representation		
113	0	3.12	1718	2411	2	3.33		113	113
					3	10.50			
					4	17.67			
					5	24.42			
					6	31.45			
114	400	3.13	1721	2414	10	3.19		114	114
					11	10.50			
					12	17.67			
					13	24.42			
					14	31.45			
5114	400	3.23	834	1689	15	3.38		-	-
					16	10.20			
					17	18.08			
					18	24.96			
					19	31.85			

ORIGINAL PAGE IS
OF POOR QUALITY

Table 6.2 (Concluded)

1368

Test Point	Shadowgraph Test Flow Conditions				Photograph Details			Matching Acoustic Test Point	Matching LV Test Point
	$V_{a/c}$, fps	P_r	T_r , °R	V_j , fps	No.	Shadowgraph Center Location X (In.) Along Centerline	Pictorial Representation		
5113	0	3.22	839	1693	20	3.00		-	-
					21	10.74			
					22	17.77			
					23	24.66			
					24	31.19			
7113	0	3.24	537	1358	30	3.51		-	-
					31	10.26			
					32	16.50			
					33	23.39			
					34	30.92			

Table 6.3 Test Details of Shadowgraph Photographs with Circular Convergent-Divergent Nozzle (Model 2).

ORIGINAL PAGE IS
OF POOR QUALITY

Test Point	Shadowgraph Test Flow Conditions				Photograph Details		Matching Acoustic Test Point	Matching LV Test Point
	$V_{a/c}$, fps	P_r	T_r , °R	V_j , fps	No.	Shadowgraph Center Location X (In.) Along Centerline	Pictorial Representation	
213	0	3.12	1716	2408	1	3.16		213
					2	9.91		
					3	16.65		
221	0	3.31	1710	2458	4	3.20		221
					5	9.95		
					6	16.69		
222	400	3.31	1706	2454	7	3.18		222
					8	9.93		
					9	16.67		
214	400	3.11	1707	2400	10	3.18		214
					11	10.14		
					12	16.67		

Table 6.3 (Concluded).

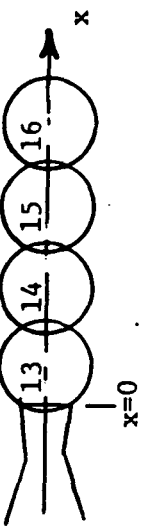
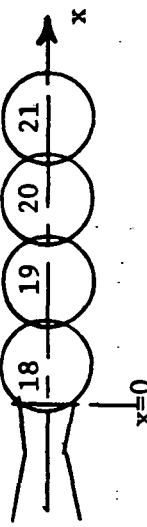
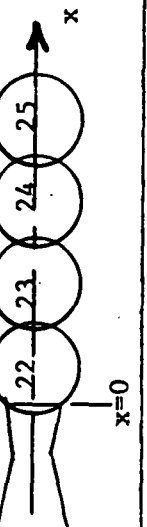
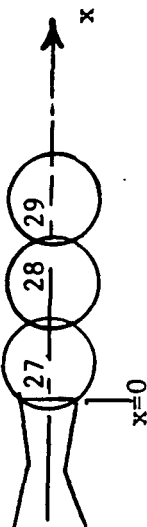
Test Point	Shadowgraph Test Flow Conditions				No.	Shadowgraph Center Location X (In.) Along Centerline	Photograph Details		Matching Acoustic Test Point	Matching LV Test Point
	$V_{a/c}$, fps	P_r	T_T , °R	V_j , fps			Pictorial Representation			
7214	400	3.24	559	1384	13	3.32		-	-	-
					14	10.07				
					15	16.81				
					16	23.56				
7213	0	3.24	517	1332	18	3.16		-	-	-
					19	10.62				
					20	17.36				
					21	24.11				
7211	0	3.21	514	1323	22	3.20		-	-	-
					23	9.95				
					24	16.69				
					25	23.44				
1211	0	3.16	866	1708	27	3.16		1211	-	-
					28	9.91				
					29	16.65				

Table 6.4 Test Details of Shadowgraph Photographs with Annular Convergent Nozzle (Model 3).

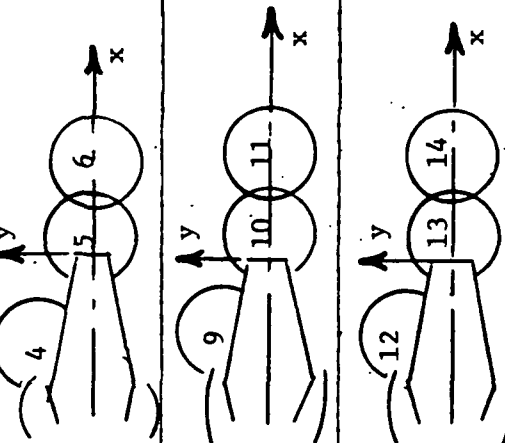
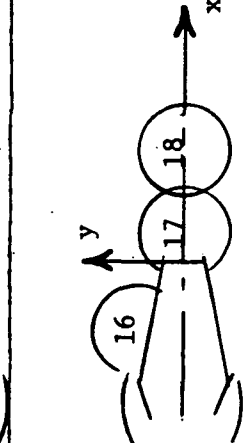
Test Point	Shadowgraph Test Flow Conditions				Photograph Details		Matching Acoustic Test Point	Matching LV Test Point
	$V_{a/c}$, fps	P_r	T_r , °R	V_j , fps	No.	Shadowgraph Center Location X (In) Y (In)	Pictorial Representation	
4313 (With Tabs)	0	3.11	1726	2413	4	-9.9 4.02		4313
4321 (With Tabs)	0	3.33	1688	2444	9	-9.68 4.02		4321
5323 (With Tabs)	0	3.39	856	1740	12	-9.39 4.02		5323
1313	0	3.22	866	1720	16	-9.31 3.69		1313

Table 6.4 (Concluded).

Test Point	Shadowgraph Test Flow Conditions				Photograph Details		Matching Acoustic Test Point	Matching LV Test Point
	$V_{a/c}$, $f_{p,j}$	P_r	T_T , σ_R	V_j , f_{ps}	No.			
					Shadowgraph Center Location	X (In)	Y (In)	
313	0	3.14	1731	2424	20	-9.35	4.03	
					21	-2.40	4.03	
					22	2.43	0.0	
					23	9.53	0.0	
314	400	3.14	1709	2410	25	-9.73	4.05	
					26	-2.63	4.05	
					27	2.20	0.0	
					28	9.30	0.0	
322	400	3.31	1715	2460	30	-9.42	4.03	
					31	2.51	0.0	

Table 6.5 Test Details of Shadowgraph Photographs With Annular Convergent-Divergent Nozzle (Model 4).

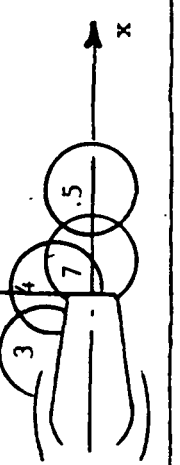
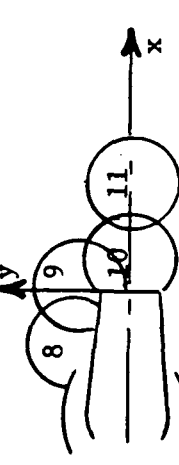
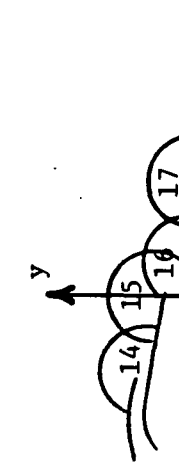
Test Point	Shadowgraph Test Flow Conditions				No.	Shadowgraph Center Location X (In)	Y (In)	Photograph Details		Matching Acoustic Test Point	Matching LV Test Point
	$V_{a/c}$, f/s	P_r	T_r , °R	V_j , f/s				Pictorial Representation			
413	0	3.10	1687	2382	3	-6.94	3.1			413	413
					4	0.23	3.1				
					7	2.08	0.0				
					5	9.18	0.0				
411	0	3.07	1704	2387	8	-6.85	3.1			411	411
					9	0.32	3.1				
					10	2.17	0.0				
					11	9.27	0.0				
421	0	3.32	1687	2442	14	-6.85	3.1			421	421
					15	0.32	3.1				
					16	2.17	0.0				
					17	9.27	0.0				

Table 6.5 (Concluded).

Test Point	Shadowgraph Test Flow Conditions					Photograph Details		Matching Acoustic Test Point	Matching LV Test Point
	$V_{a/c}$, fps	P_r	T_r , °R	V_j , fps	No. Center	Shadowgraph X (In) Y (In)	Pictorial Representation		
422	400	3.34	1693	2451	18	-7.09	3.1	422	422
					19	0.08	3.1		
					20	1.93	0.0		
414	400	3.09	1700	2389	21	-7.09	3.1	414	414
					22	0.08	3.1		
					23	1.93	0.0		
					24	9.03	0.0		

ORIGINAL PAGE IS
OF POOR QUALITY

Table 6-6. Test Details of Shadowgraph Photographs with Convergent Suppressor Nozzle (Model 5).

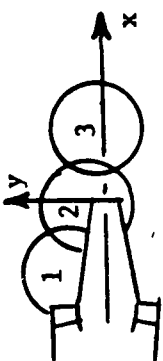
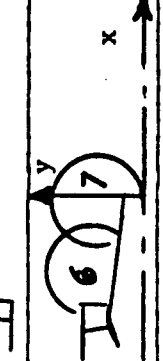
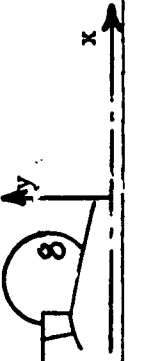
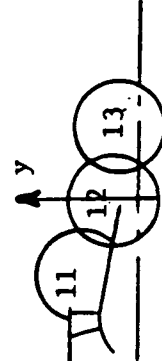
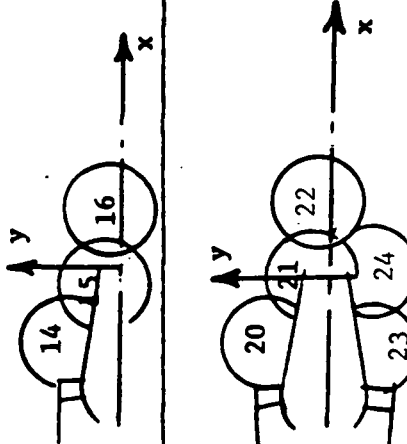
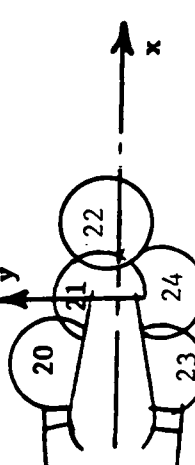
Test Point	Shadowgraph Test Flow Conditions				Photograph Details			Matching Acoustic Test Point	Matching LV Test Point
	$V_{a/c}$, f_{ps}	P_r	T_r^* σ_r	V_j^* fps	No.	Shadowgraph Center Location X (In) Y (In)	Pictorial Representation		
1513	0	3.21	849	1701	1			1513	1513
1521	0	3.37	852	1733	4			1521	-
513	0	3.12	1717	2411	6			513	513
514	400	3.13	1725	2420	8			514	514
1514	400	3.22	849	1702	11			-	1514

Table 6-6. (Concluded).

Test Point	Shadowgraph Test Flow Conditions				Photograph Details		Matching Acoustic Test Point	Matching LV Test Point
	$V_{a/c}$, fps	P_r	T_r' or R	V_j' fps	No.	Shadowgraph Center Location	Pictorial Representation	
					X (In)	Y (In)		
1522	400	3.37	859	1740	14			-
7513	0	3.27	542	1368	20			-

ORIGINAL PAGE IS
OF POOR QUALITY

Table 6.7. Test Details of Shadowgraph Photographs with Convergent-Divergent Suppressor Nozzle (Model 6)

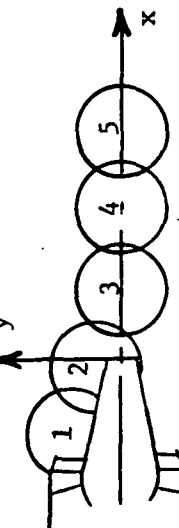
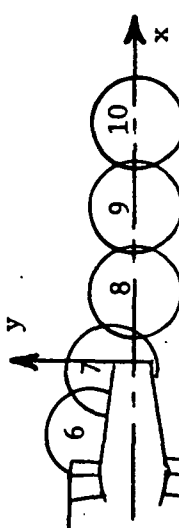
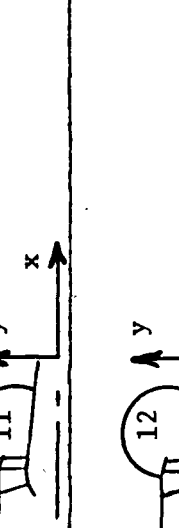
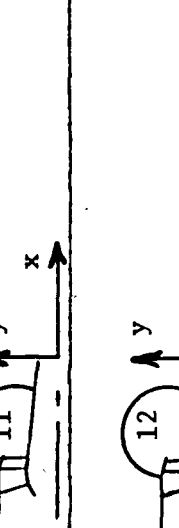
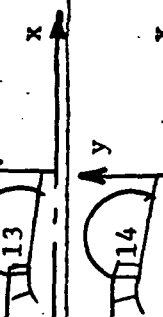
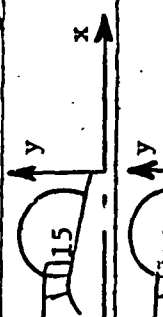
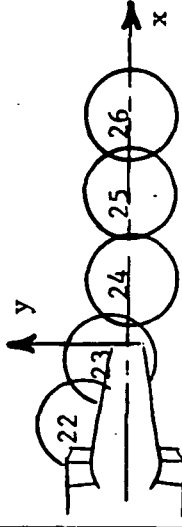
Test Point	Shadowgraph Test Flow Conditions				Photograph Details				Matching Acoustic Test Point	Matching LV Test Point
	$V_{a/c}$, f/s	P_r	T_r , °R	V_j , f/s	No.	Shadowgraph Center Location X (In)	Y (In)	Pictorial Representation		
613	0	3.13	1715	2412	1	-6.57	4.28		613	613
614	400	3.13	1712	2410	6	-6.57	4.28		614	614
4614	400	3.72	1726	2566	11	-6.57	4.28		-	-
4612	400	3.42	1730	2499	12	-6.57	4.28		-	-

Table 6.7 (Continued).

Test Point	Shadowgraph Test Flow Conditions				Photograph Details			Matching Acoustic Test Point	Matching LV Test Point
	V _{a/c} , fps	P _r	T _r , °R	V _j , fps	No.	Shadowgraph Center Location X (In)	Y (In)		
4610	400	3.21	1740	2451	13	-6.57	4.28		-
4606	400	3.02	1733	2390	14	-6.57	4.28		-
4604	400	2.72	1732	2290	15	-6.57	4.28		-
4602	400	2.37	1591	2055	16	-6.57	4.28		-
7614	400	3.26	609	1448	17	-5.52	3.52		-
					18	1.58	0.99		
					19	8.68	0.0		
					20	15.78	0.0		
					21	22.88	0.0		

ORIGINAL PAGE IS
OF POOR QUALITY

Table 6.7 (Concluded).

Test Point	Shadowgraph Test Flow Conditions				Photograph Details				Matching Acoustic Test Point	Matching LV Test Point
	V_a/γ_s , fps	P_r	T_T^* , °R	V_j^* , fps	No.	Shadowgraph Center Location X (In)	Y (In)	Pictorial Representation		
7613	0	3.26	560	1389	22	-6.3	3.52		-	-

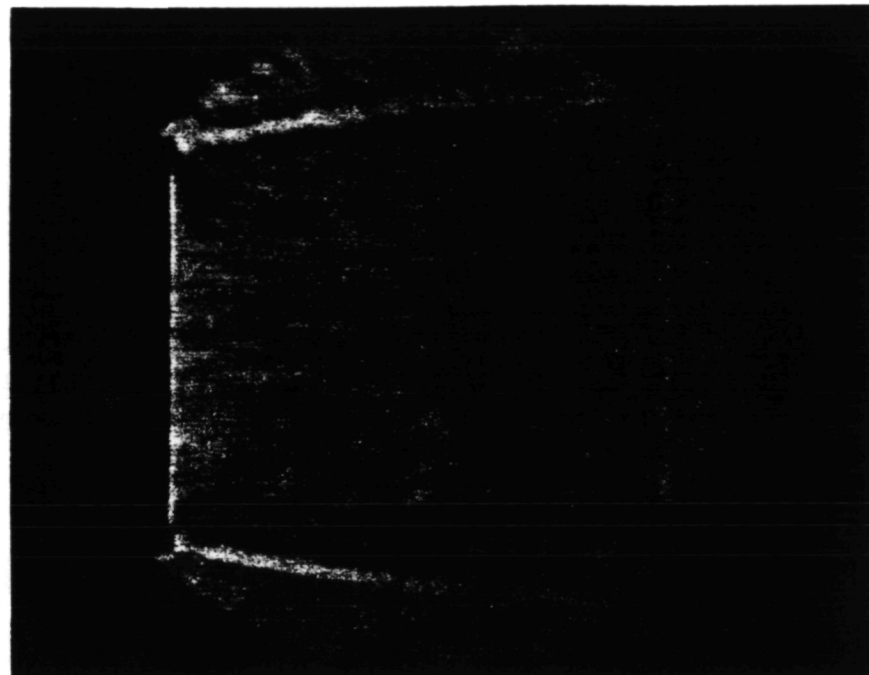
6.2 SHADOWGRAPH PHOTO TEST RESULTS

6.2.1 Shadowgraph Photos of Model 1

The shadowgraph test details associated with this model are provided in Table 6.2. The copies of the individual shadowgraph photographs taken with this model are presented next in this section.

ORIGINAL PAGE IS
OF POOR QUALITY

Configuration	/
Test Point	/13
Shadowgraph No.	2

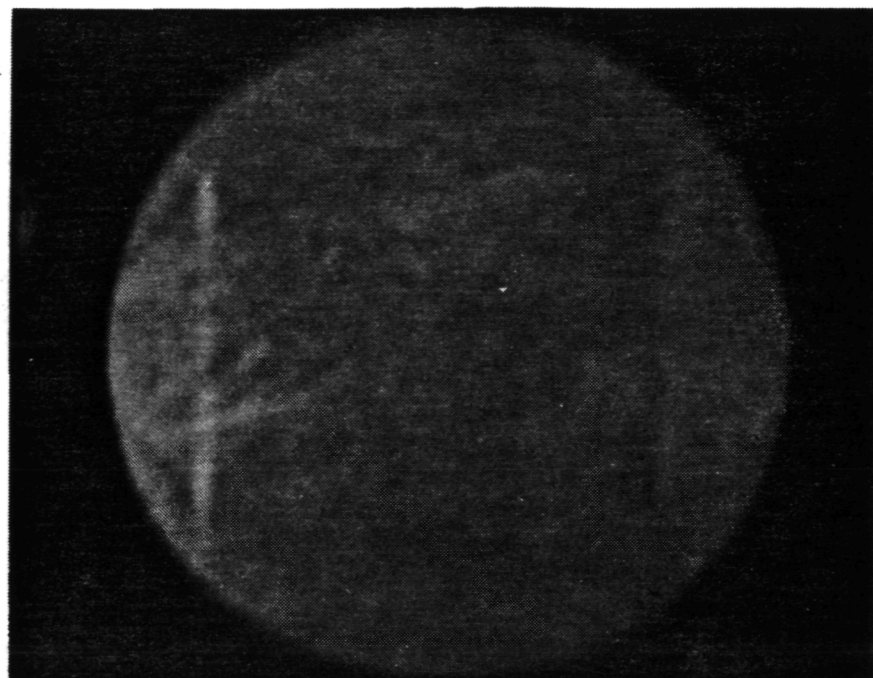


Configuration	/
Test Point	/13
Shadowgraph No.	3

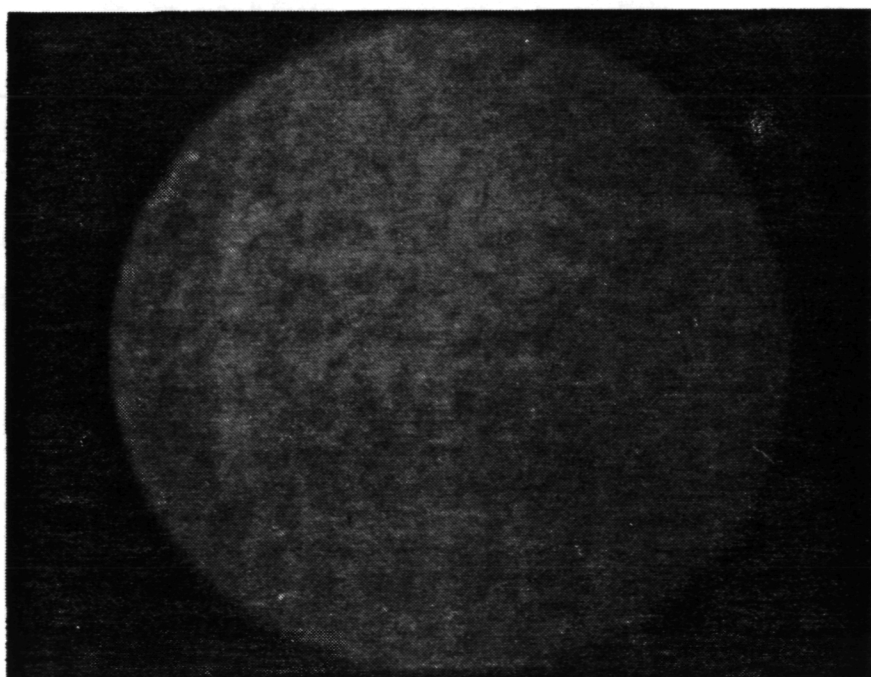


ORIGINAL PAGE IS
OF POOR QUALITY

Configuration	/
Test Point	113
Shadowgraph No.	4

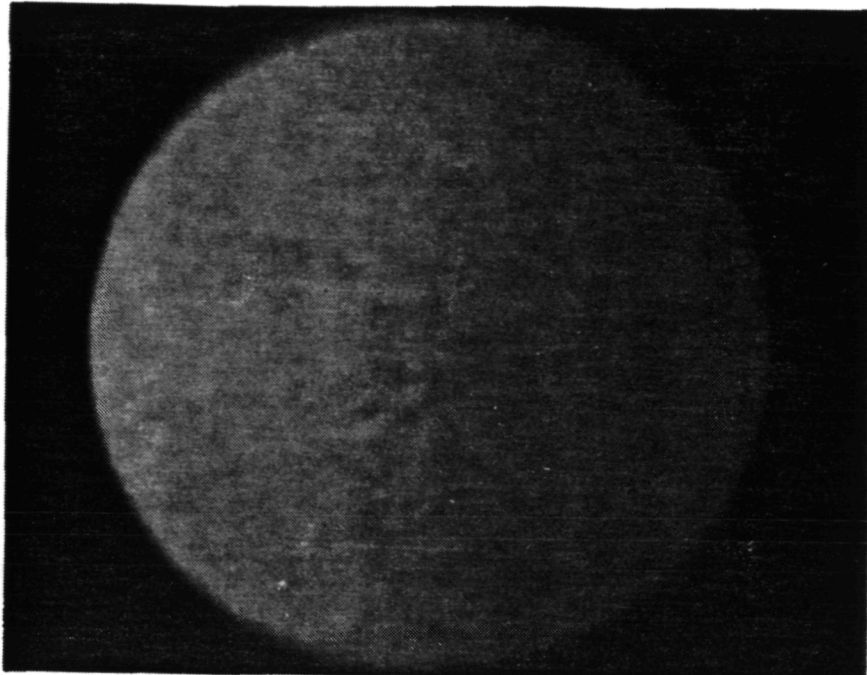


Configuration	/
Test Point	113
Shadowgraph No.	5



ORIGINAL PAGE IS
OF POOR QUALITY

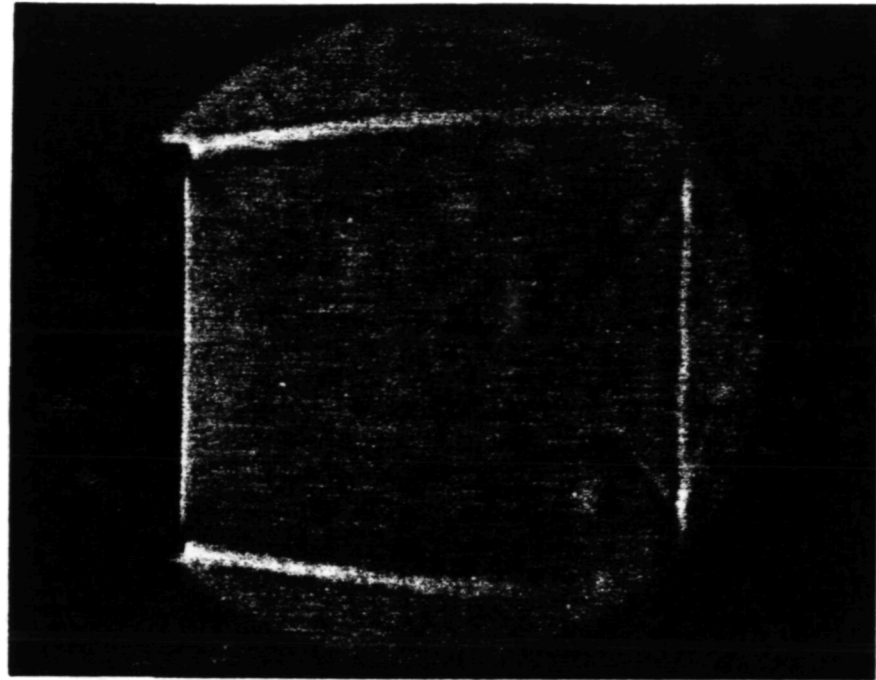
Configuration	/
Test Point	113
Shadowgraph No.	6



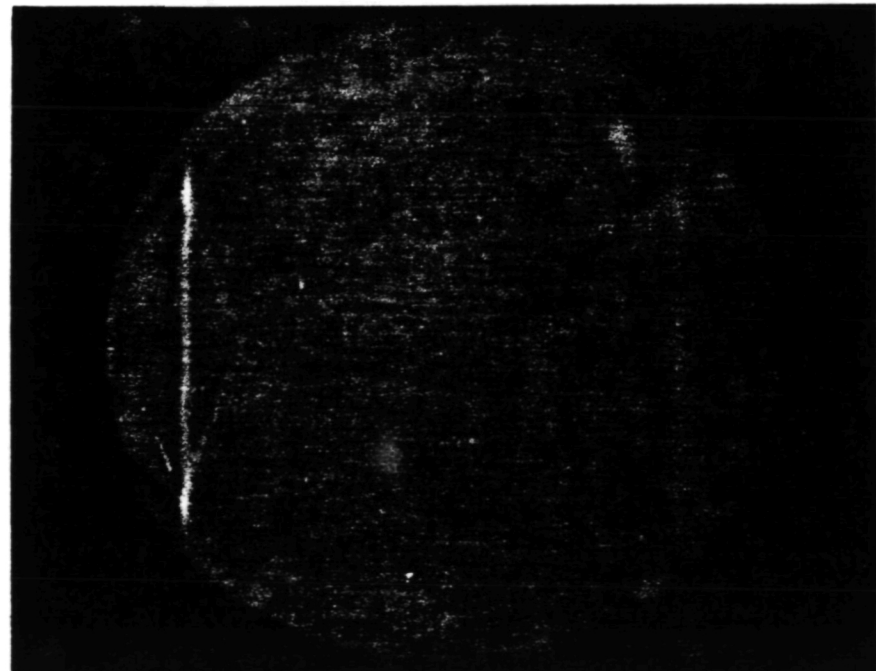
1383

ORIGINAL PAGE IS
OF POOR QUALITY

Configuration	/
Test Point	//4
Shadowgraph No.	/0

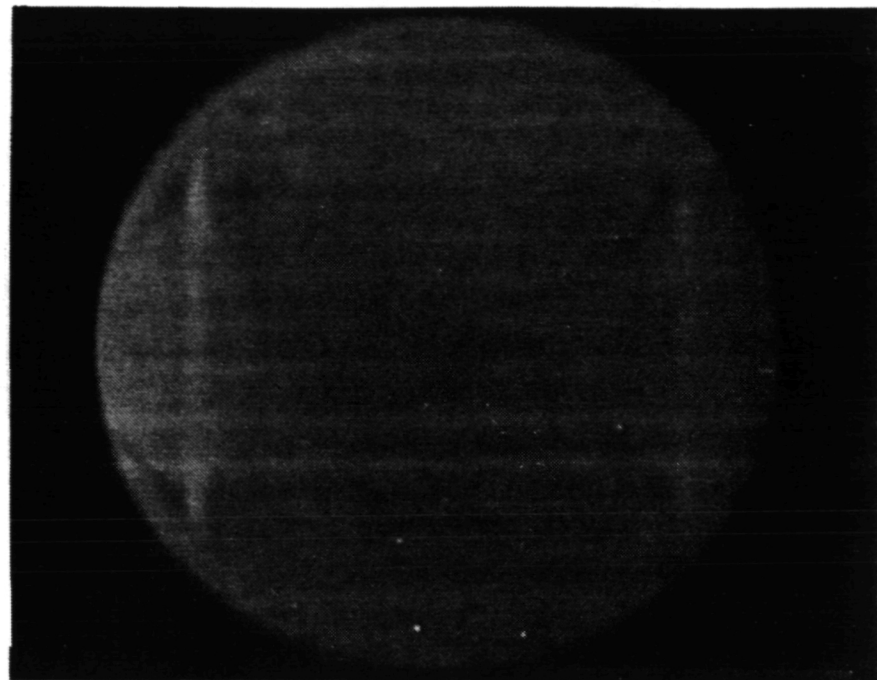


Configuration	/
Test Point	//4
Shadowgraph No.	//

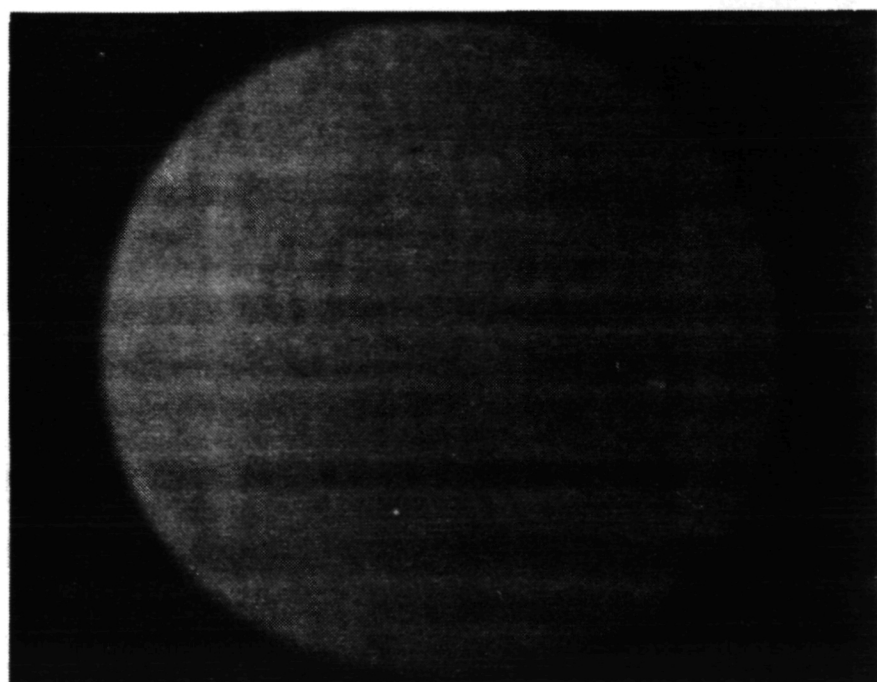


ORIGINAL PAGE IS
OF POOR QUALITY

Configuration	/4
Test Point	/4
Shadowgraph No.	/2

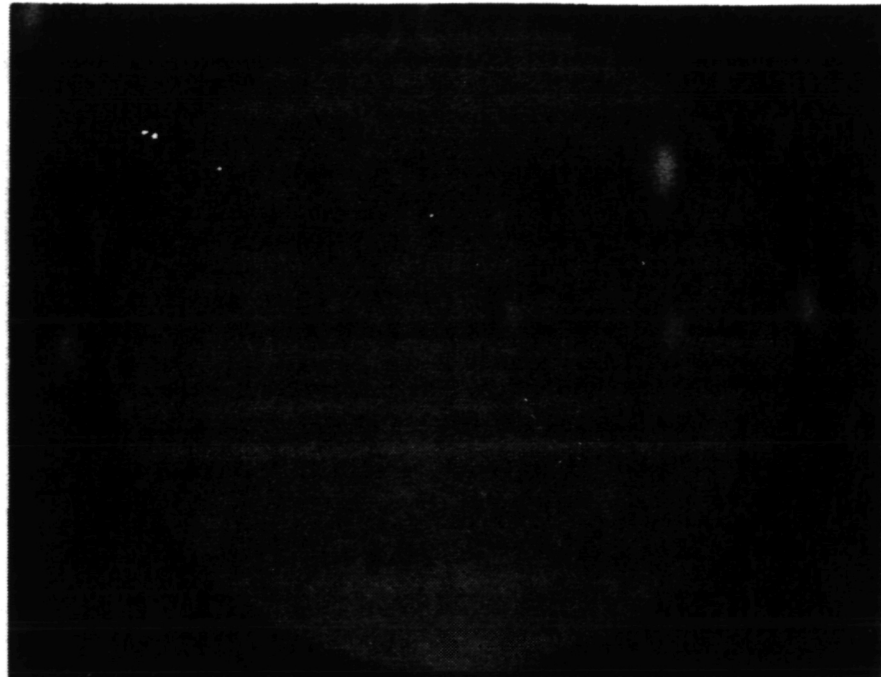


Configuration	/
Test Point	/4
Shadowgraph No.	/3



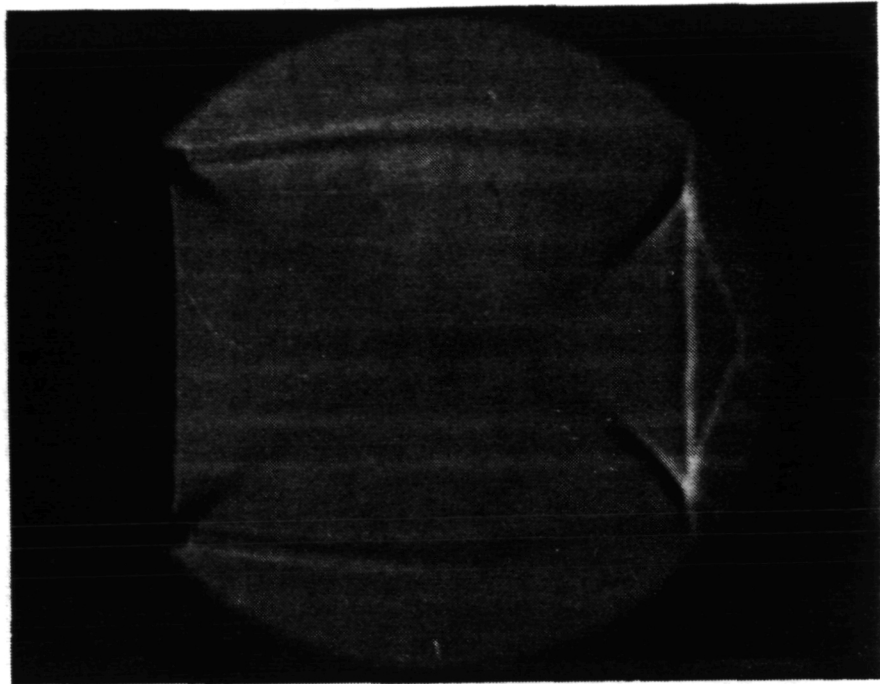
ORIGINAL PAGE IS
OF POOR QUALITY

Configuration 1
Test Point 114
Shadowgraph No. 14

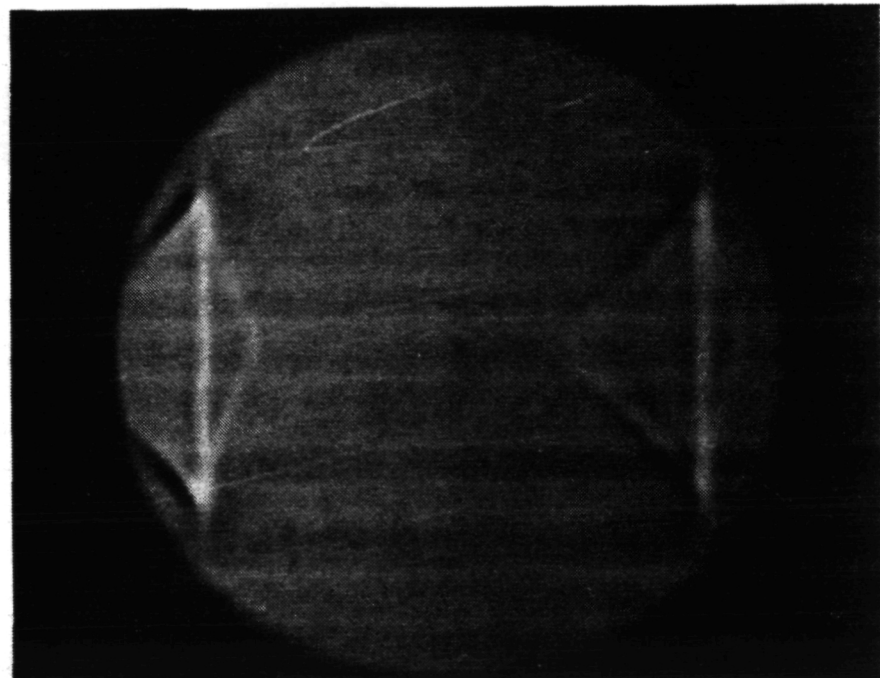


ORIGINAL PAGE IS
OF POOR QUALITY

Configuration	/	5114
Test Point	/	5114
Shadowgraph No.	/	15

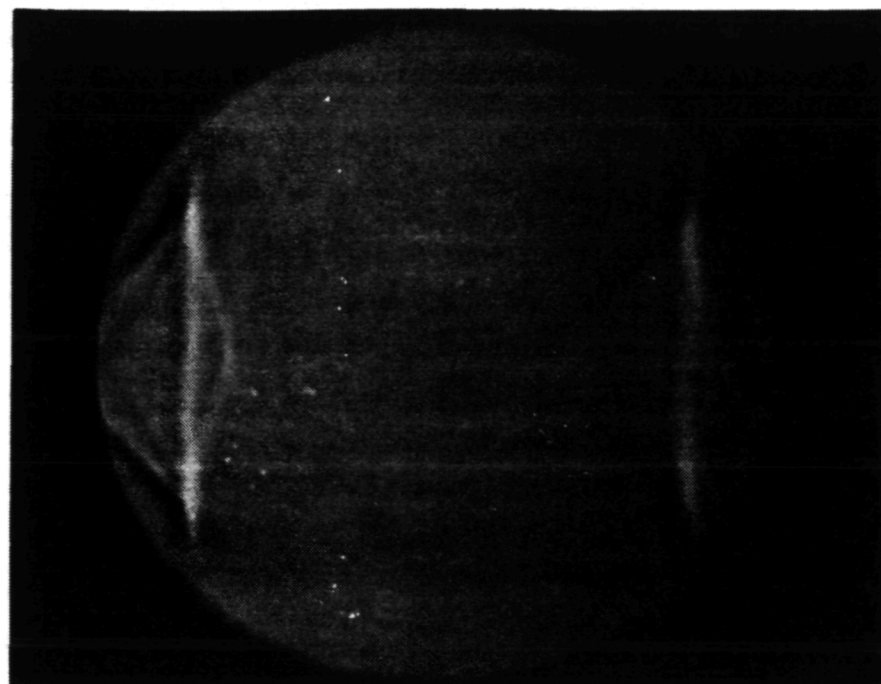


Configuration	/	5114
Test Point	/	5114
Shadowgraph No.	/	16

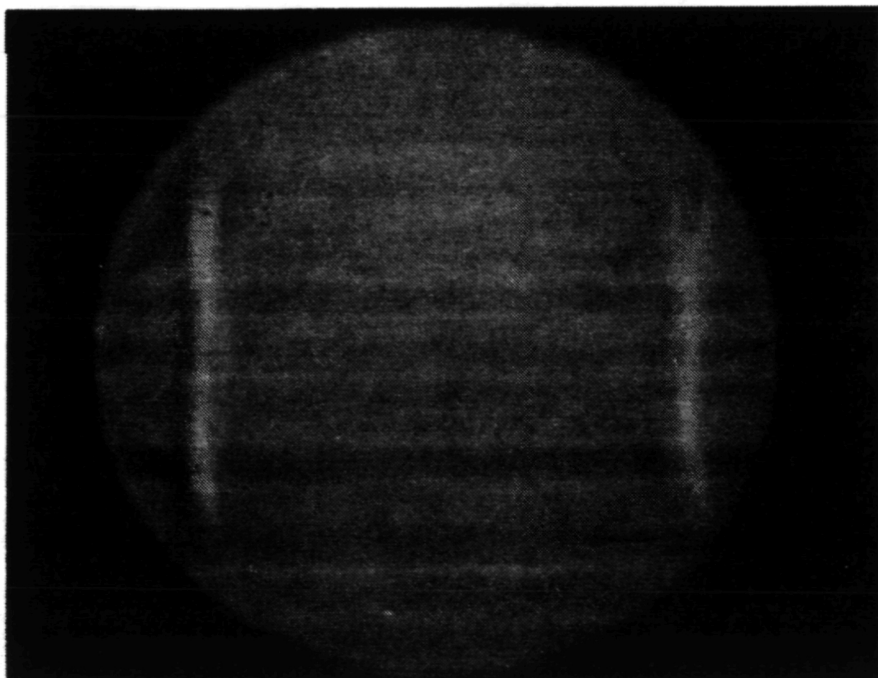


ORIGINAL PAGE IS
OF POOR QUALITY

Configuration	<u>1</u>
Test Point	<u>5114</u>
Shadowgraph No.	<u>17</u>

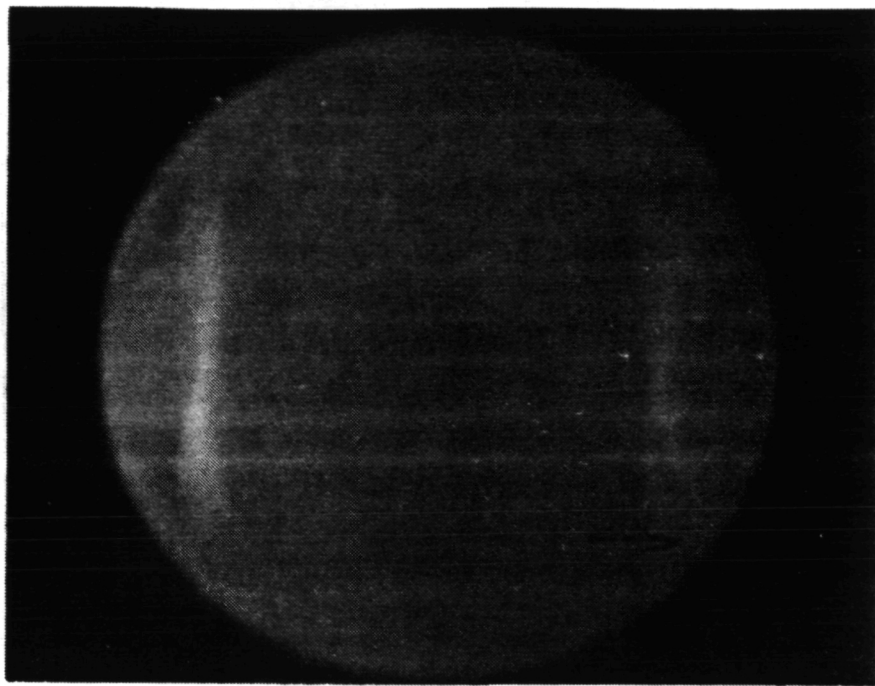


Configuration	<u>1</u>
Test Point	<u>5114</u>
Shadowgraph No.	<u>18</u>



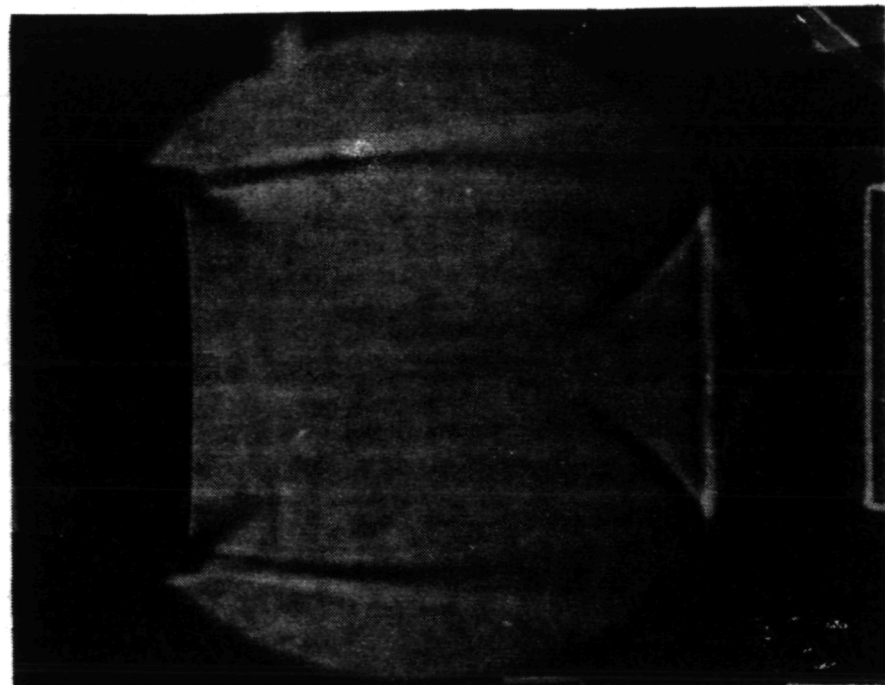
ORIGINAL PAGE IS
OF POOR QUALITY

Configuration	/
Test Point	<u>5112</u>
Shadowgraph No.	<u>19</u>

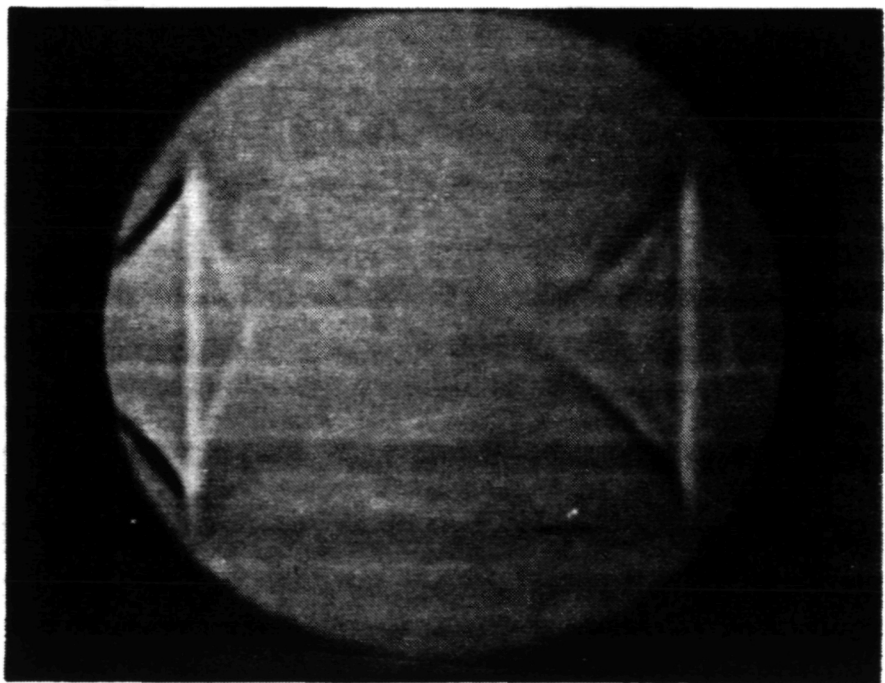


ORIGINAL PAGE IS
OF POOR QUALITY

Configuration 1
Test Point 5113
Shadowgraph No. 20

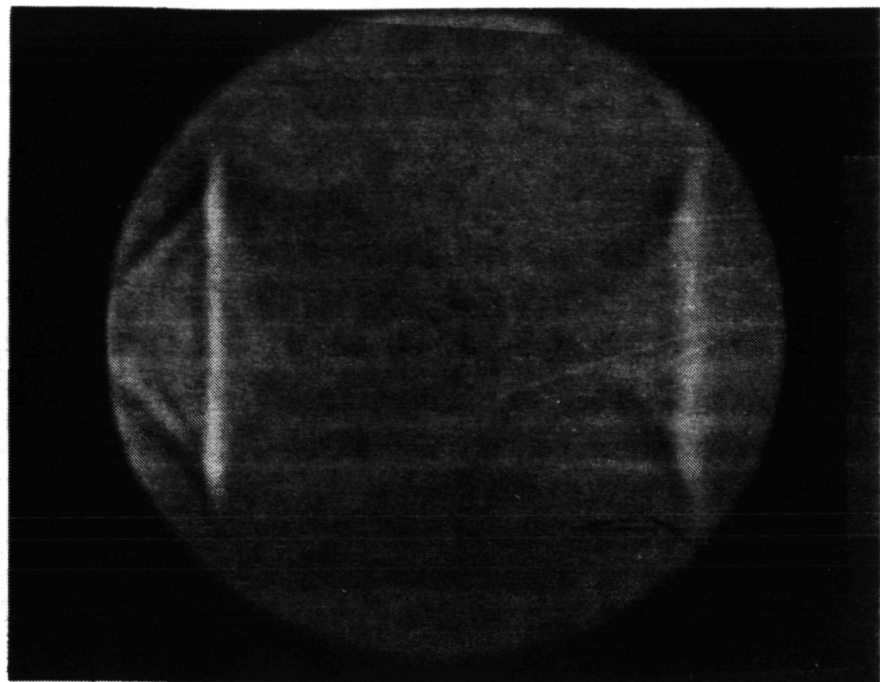


Configuration 1
Test Point 5113
Shadowgraph No. 21

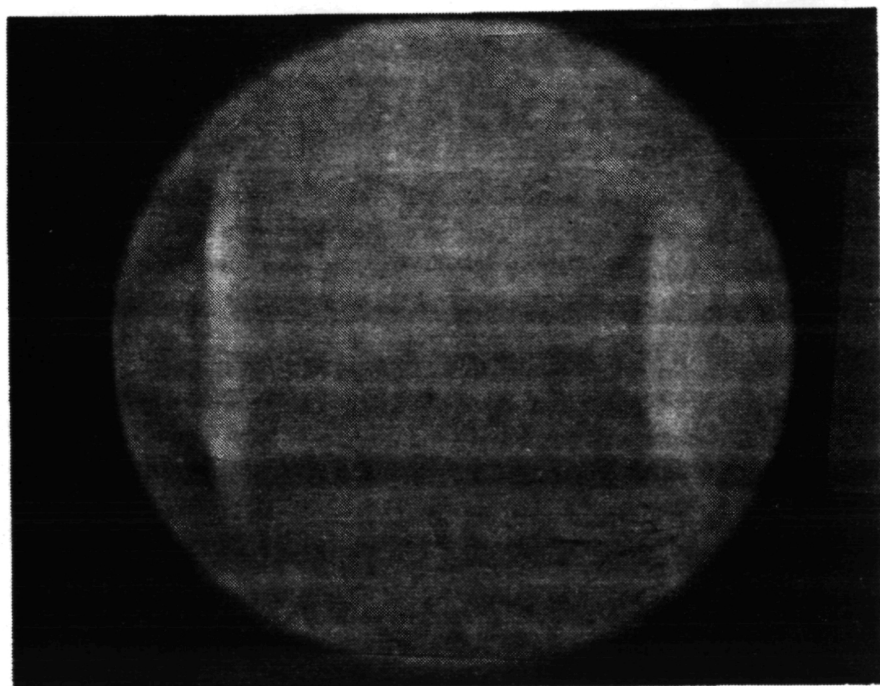


ORIGINAL PAGE IS
OF POOR QUALITY

Configuration	<u>1</u>
Test Point	<u>5113</u>
Shadowgraph No.	<u>22</u>

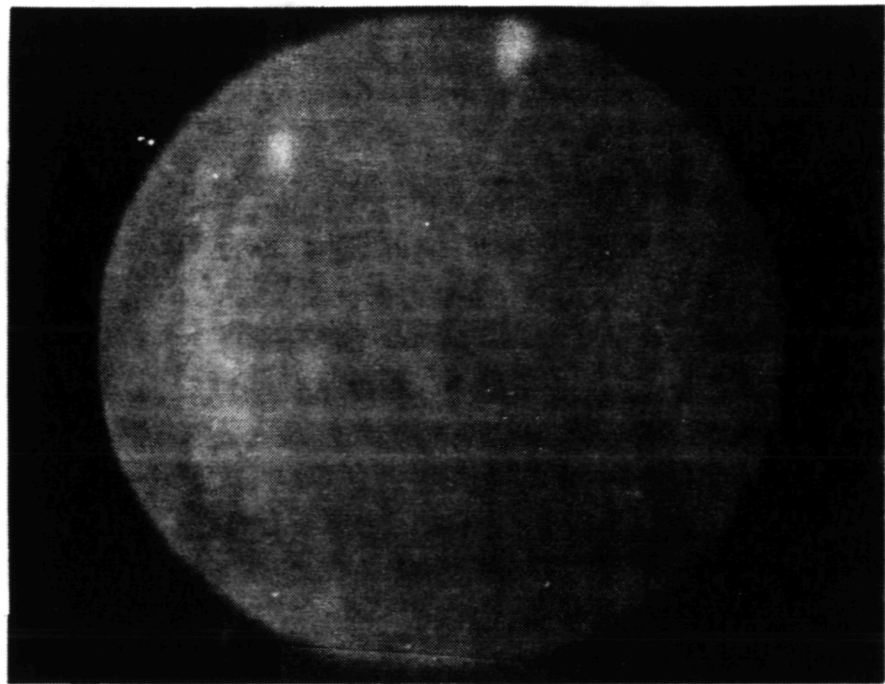


Configuration	<u>1</u>
Test Point	<u>5113</u>
Shadowgraph No.	<u>23</u>



ORIGINAL PAGE IS
OF POOR QUALITY

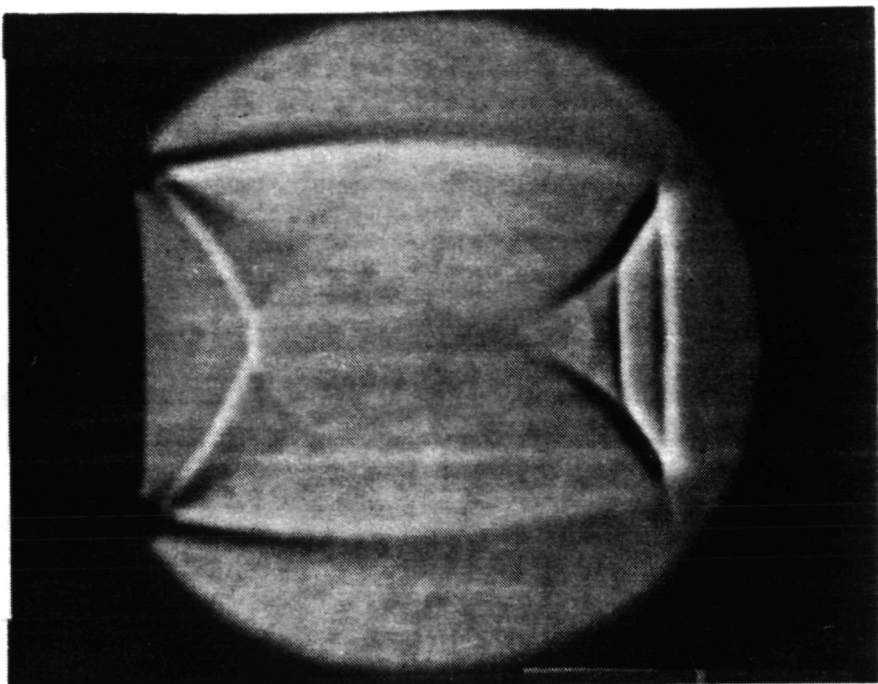
Configuration	<u>1</u>
Test Point	<u>5113</u>
Shadowgraph No.	<u>24</u>



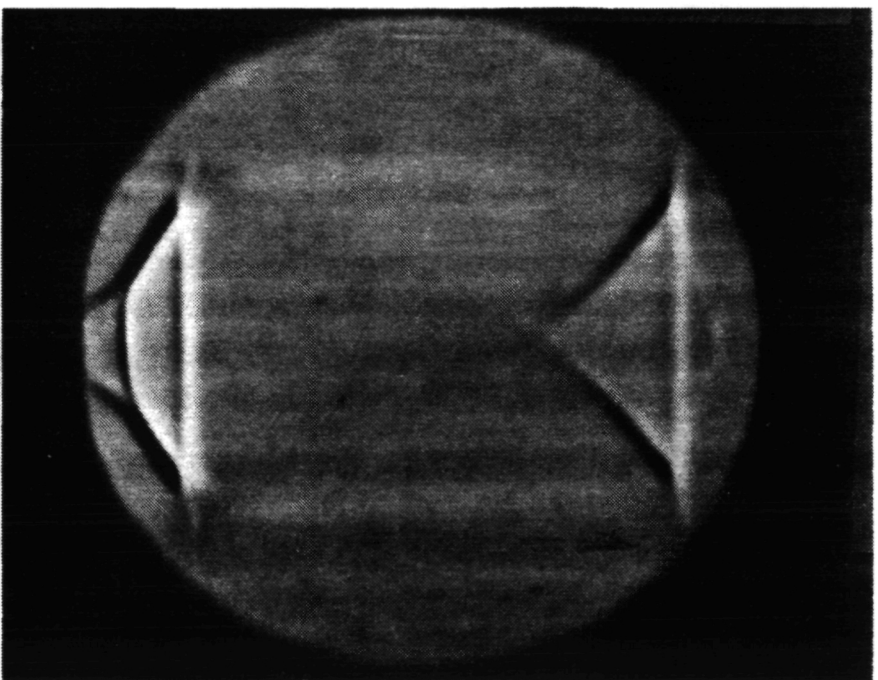
1392

ORIGINAL PAGE IS
OF POOR QUALITY.

Configuration	/
Test Point	7113
Shadowgraph No.	30

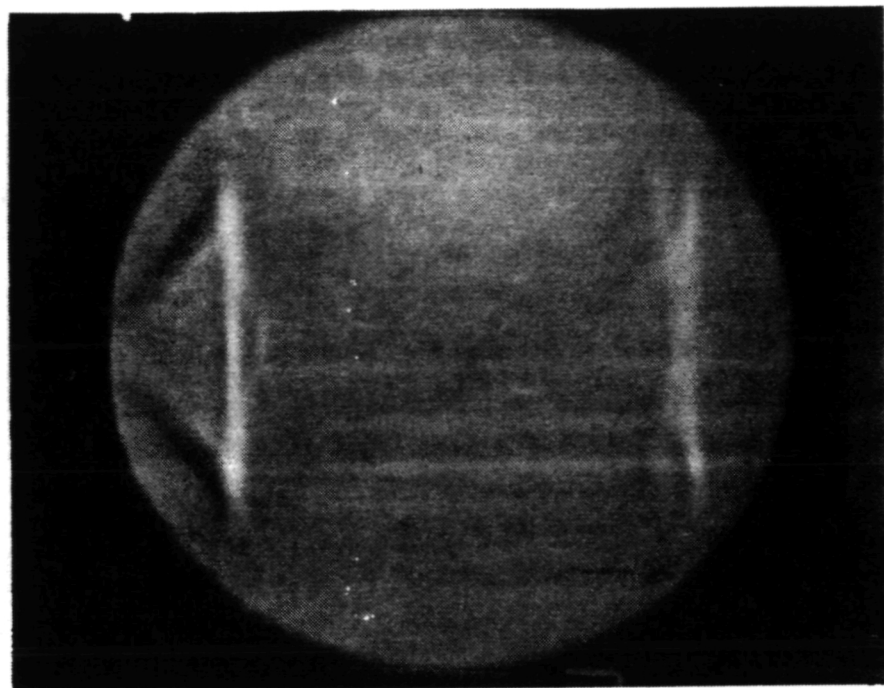


Configuration	/
Test Point	7113
Shadowgraph No.	31

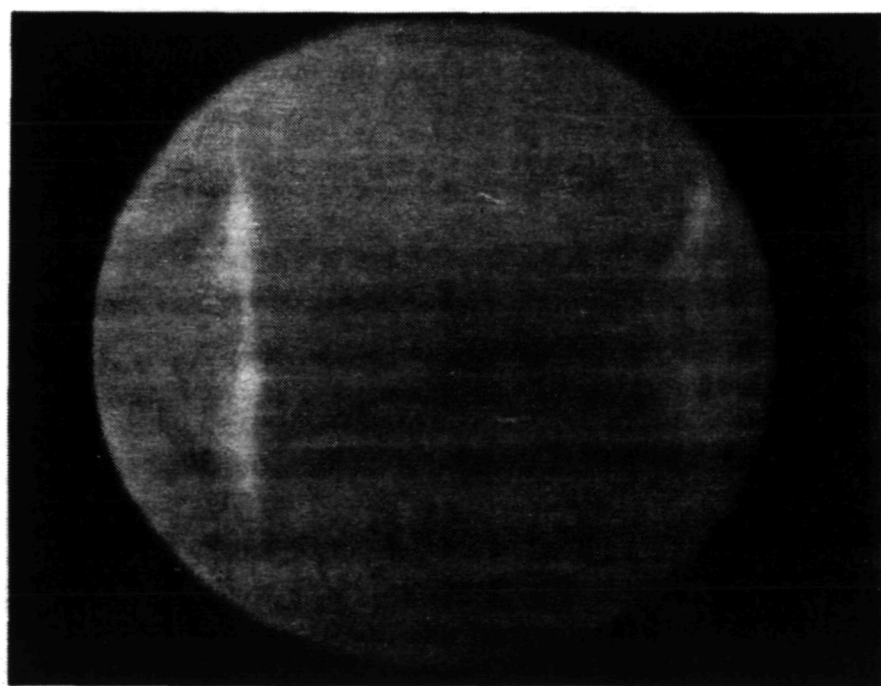


ORIGINAL PAGE IS
OF POOR QUALITY

Configuration	/
Test Point	<u>7113</u>
Shadowgraph No.	<u>32</u>

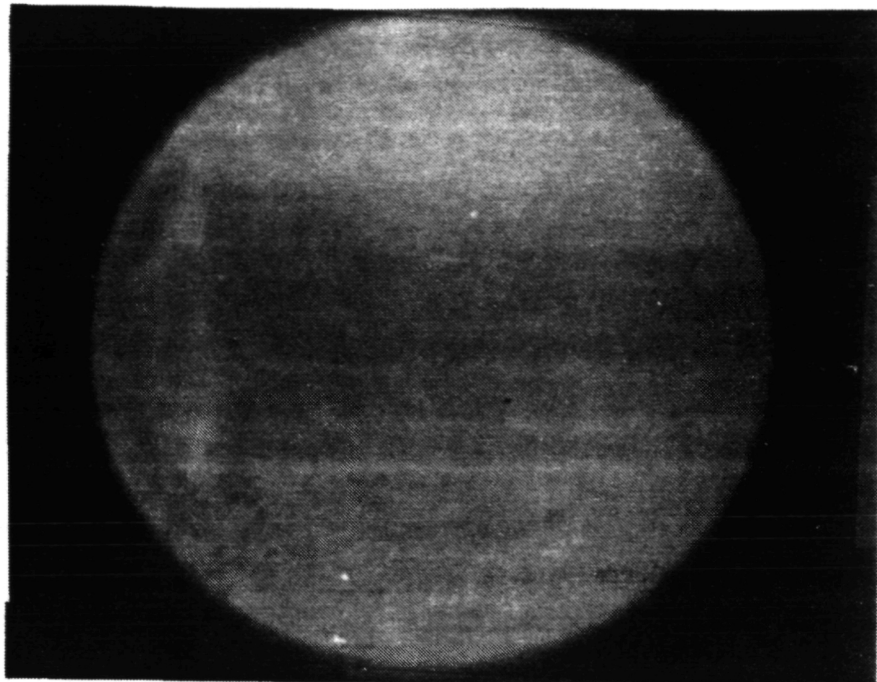


Configuration	/
Test Point	<u>7113</u>
Shadowgraph No.	<u>33</u>



ORIGINAL PAGE IS
OF POOR QUALITY

Configuration	<u>1</u>
Test Point	<u>7113</u>
Shadowgraph No.	<u>34</u>

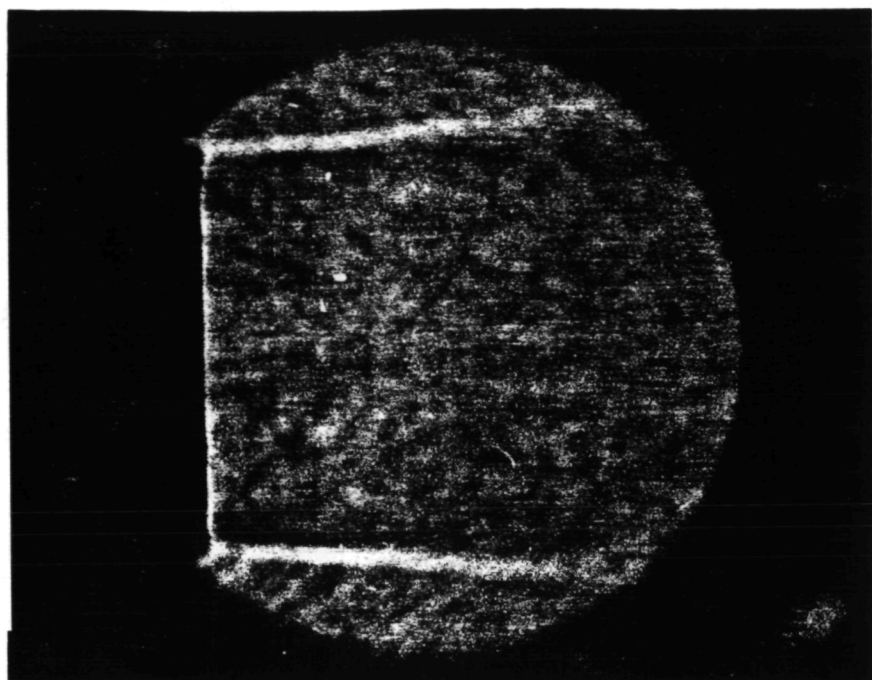


6.2.2 Shadowgraph Photos of Model 2

The shadowgraph test details associated with this model are provided in Table 6.3. The copies of the individual shadowgraph photographs taken with this model are presented next in this section.

ORIGINAL PAGE IS
OF POOR QUALITY

Configuration	2
Test Point	21.3
Shadowgraph No.	/

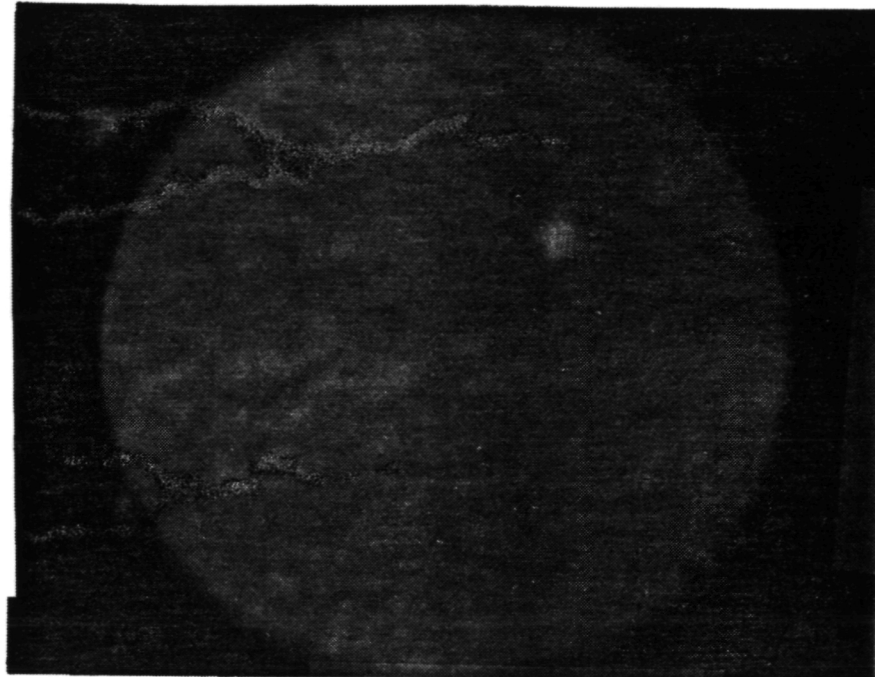


Configuration	2
Test Point	21.3
Shadowgraph No.	2



ORIGINAL PAGE IS
OF POOR QUALITY

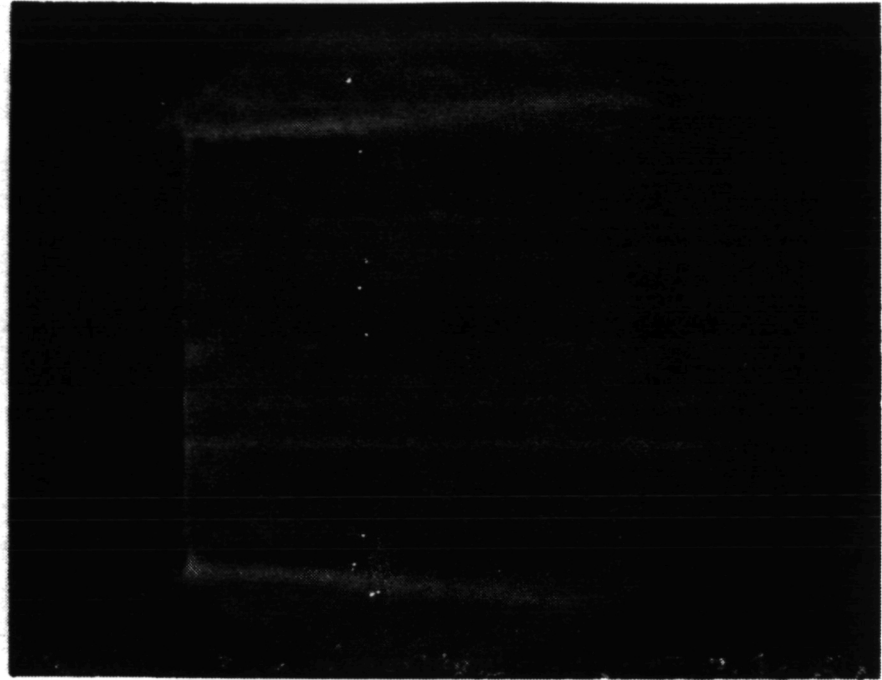
Configuration	<u>2</u>
Test Point	<u>2 / 3</u>
Shadowgraph No.	<u>3</u>



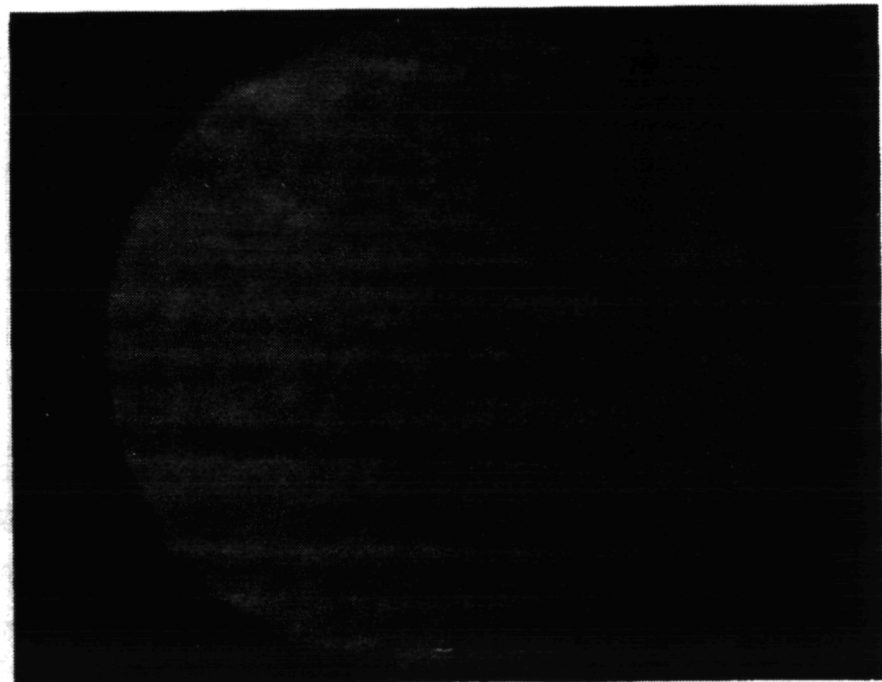
1398

ORIGINAL PAGE IS
OF POOR QUALITY

Configuration	<u>2</u>
Test Point	<u>221</u>
Shadowgraph No.	<u>4</u>



Configuration	<u>2</u>
Test Point	<u>221</u>
Shadowgraph No.	<u>5</u>



1399

1399

ORIGINAL PAGE IS
OF POOR QUALITY

Configuration	<u>2</u>
Test Point	<u>221</u>
Shadowgraph No.	<u>6</u>

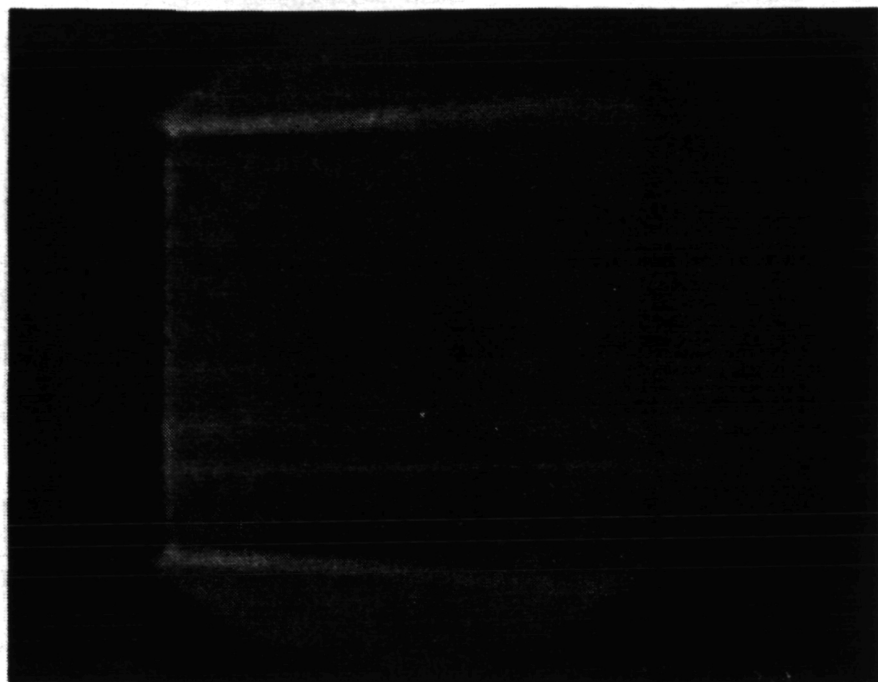


1400

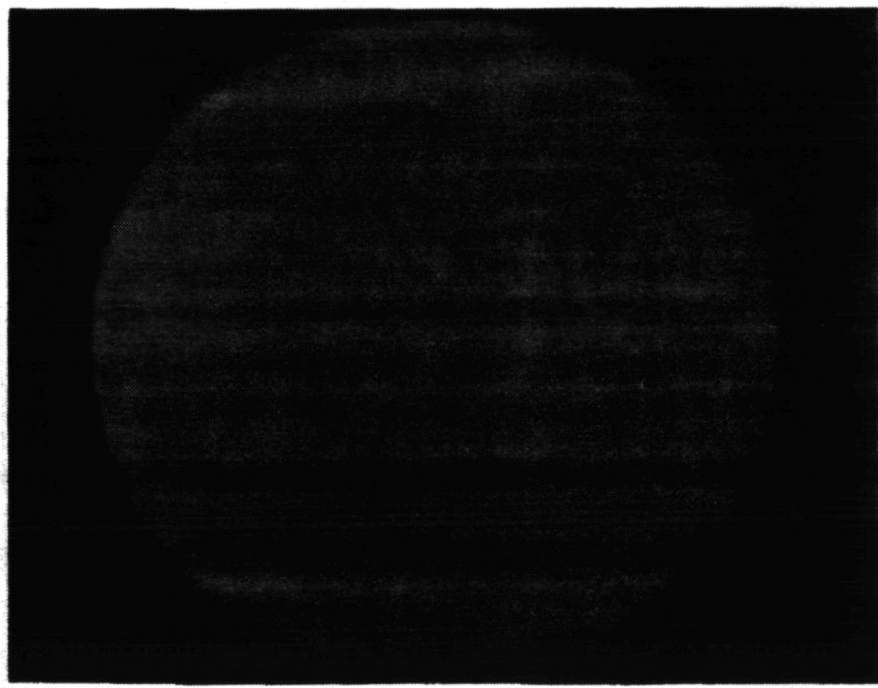
1400

ORIGINAL PAGE IS
OF POOR QUALITY

Configuration	<u>2</u>
Test Point	<u>222</u>
Shadowgraph No.	<u>7</u>

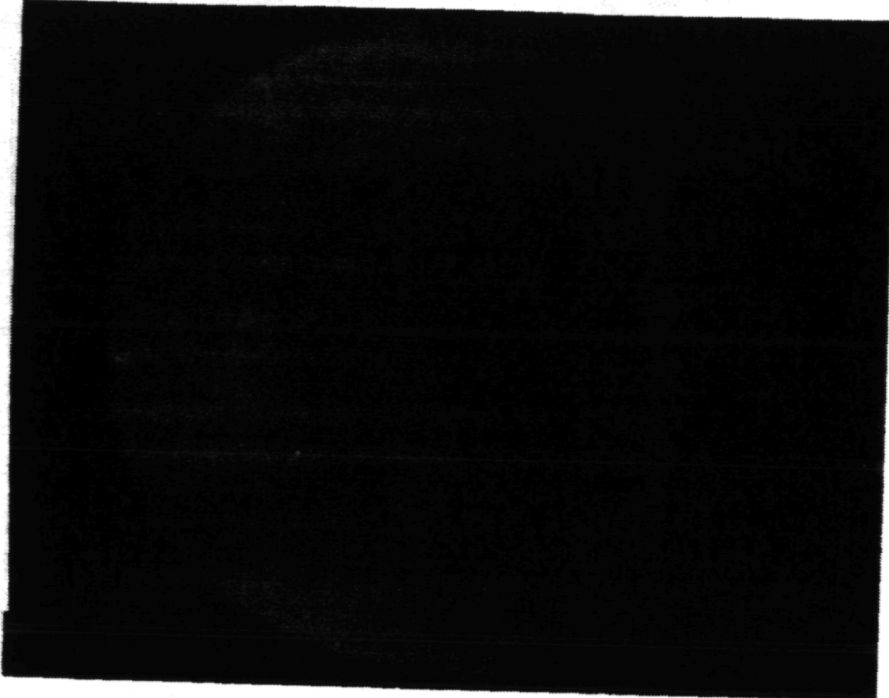


Configuration	<u>2</u>
Test Point	<u>222</u>
Shadowgraph No.	<u>8</u>



ORIGINAL PAGE IS
OF POOR QUALITY

Configuration 2
Test Point 222
Shadowgraph No. 9

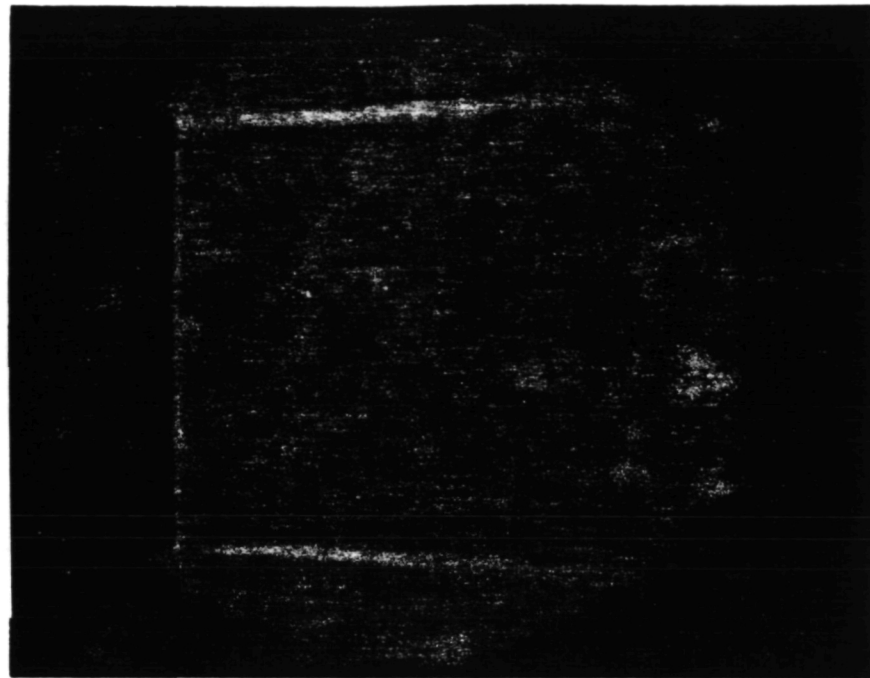


1402

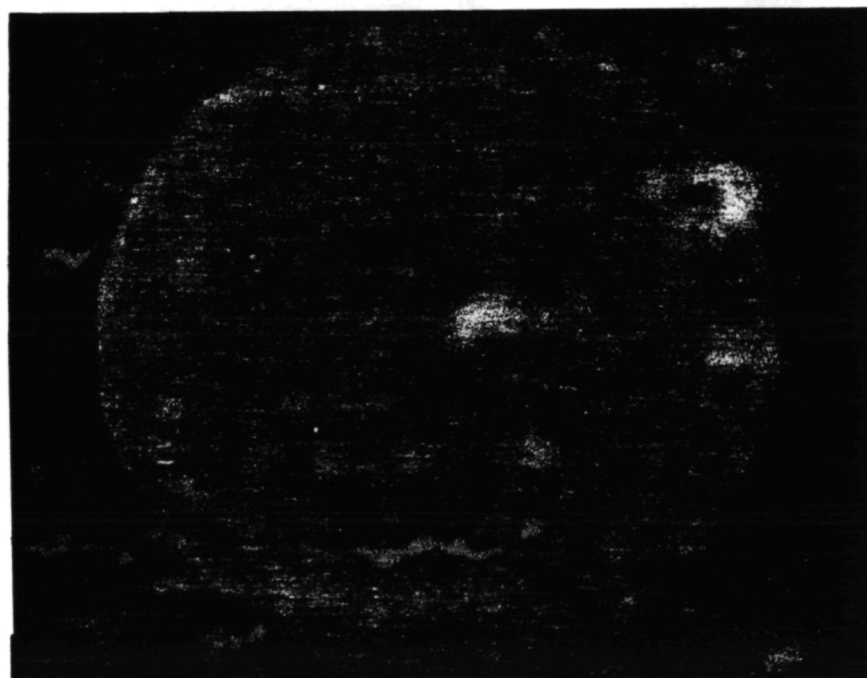
1402

ORIGINAL PAGE IS
OF POOR QUALITY

Configuration 2
Test Point 214
Shadowgraph No. 10



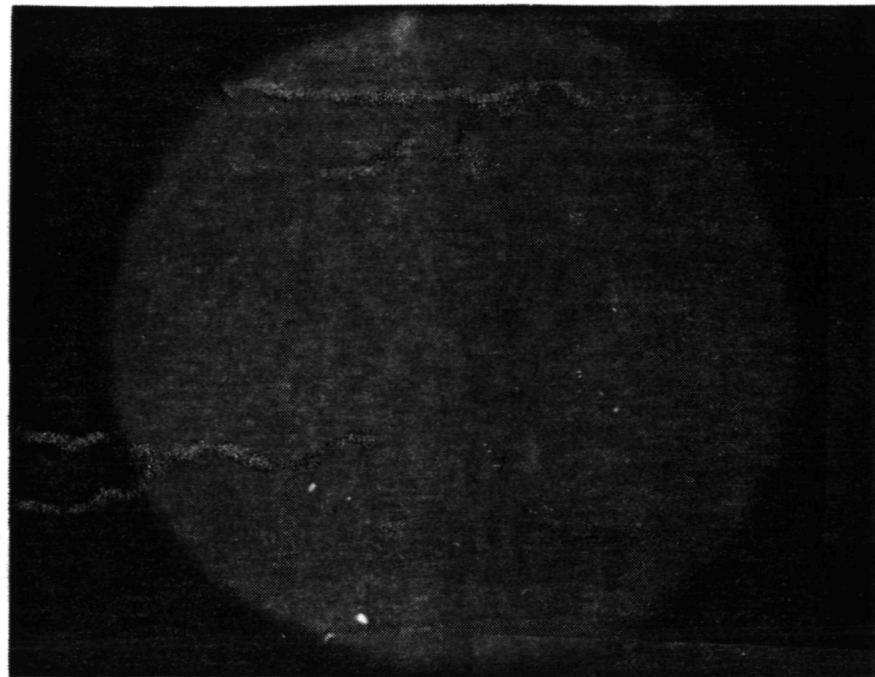
Configuration 2
Test Point 214
Shadowgraph No. 11



1403

ORIGINAL PAGE IS
OF POOR QUALITY

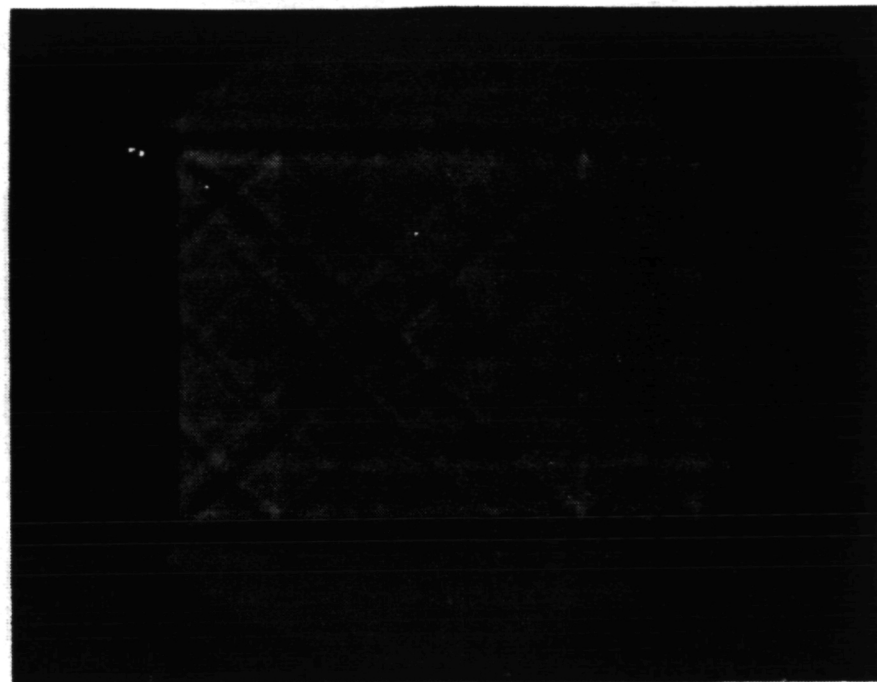
Configuration	<u>2</u>
Test Point	<u>214</u>
Shadowgraph No.	<u>12</u>



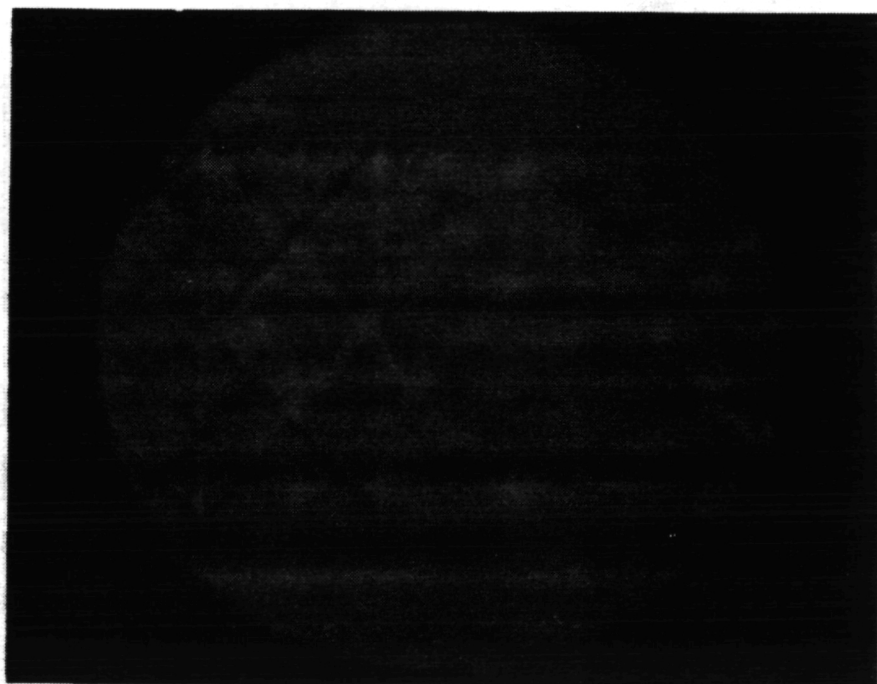
1404

**ORIGINAL PAGE IS
OF POOR QUALITY**

Configuration	<u>2</u>
Test Point	<u>72/4</u>
Shadowgraph No.	<u>13</u>



Configuration	<u>2</u>
Test Point	<u>72/4</u>
Shadowgraph No.	<u>14</u>



ORIGINAL PAGE IS
OF POOR QUALITY

Configuration 2
Test Point 7214
Shadowgraph No. 15



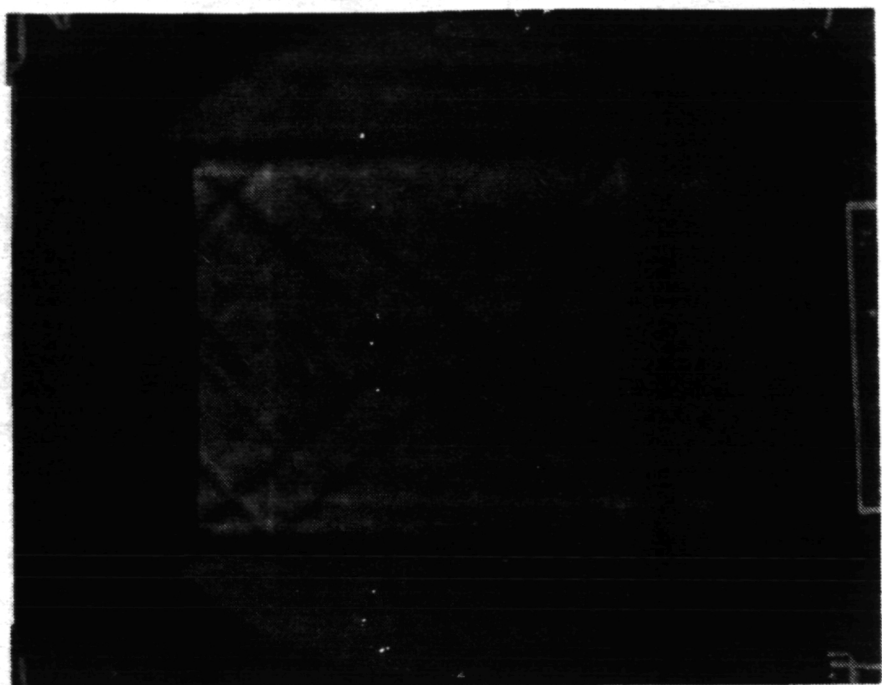
Configuration 2
Test Point 7214
Shadowgraph No. 16



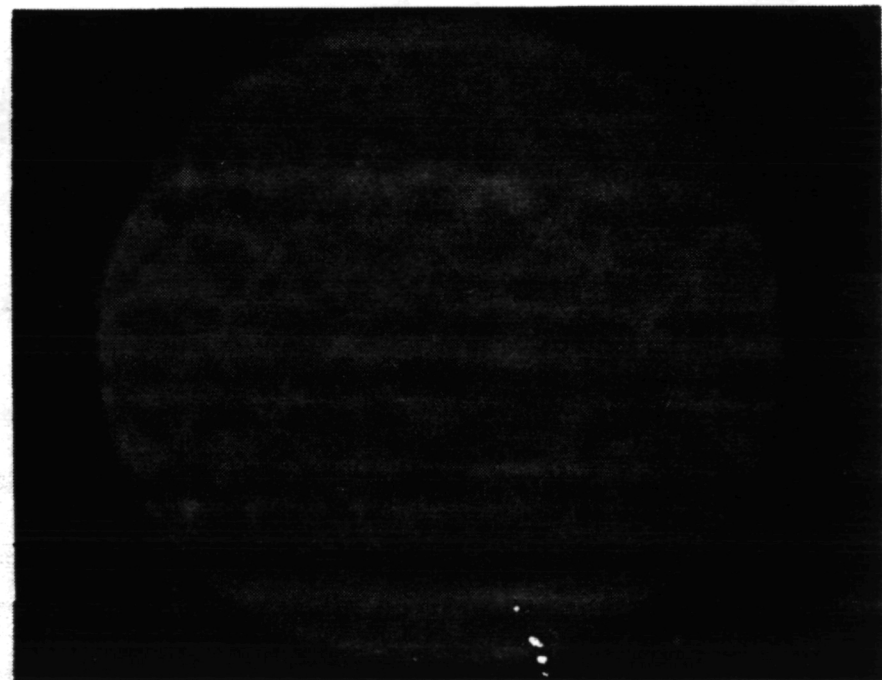
Fig 10 Light

ORIGINAL PAGE IS
OF POOR QUALITY

Configuration 2
Test Point 7213
Shadowgraph No. 18



Configuration 2
Test Point 7213
Shadowgraph No. 19

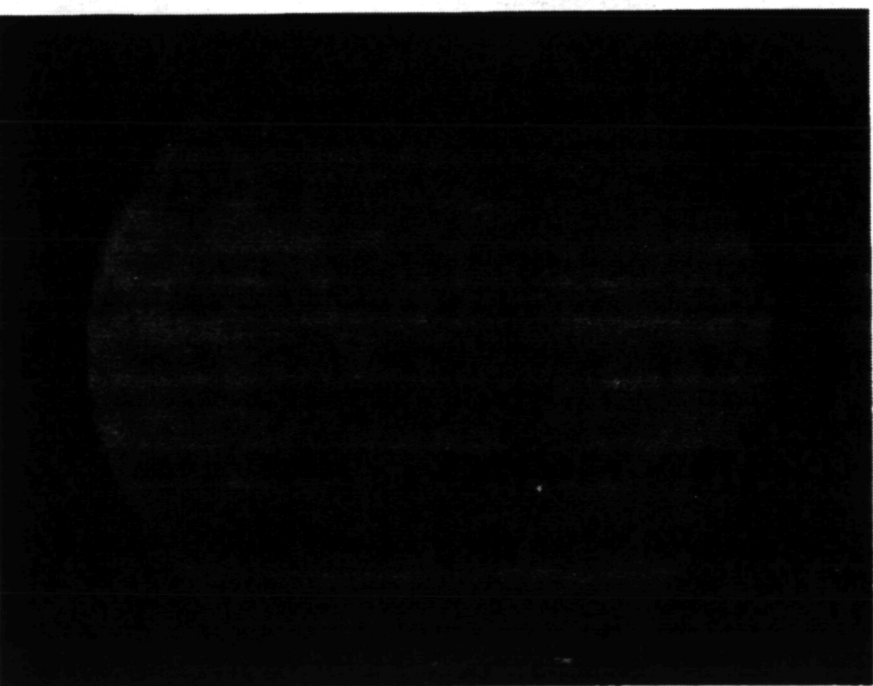


ORIGINAL PAGE IS
OF POOR QUALITY.

Configuration	<u>2</u>
Test Point	<u>7213</u>
Shadowgraph No.	<u>20</u>

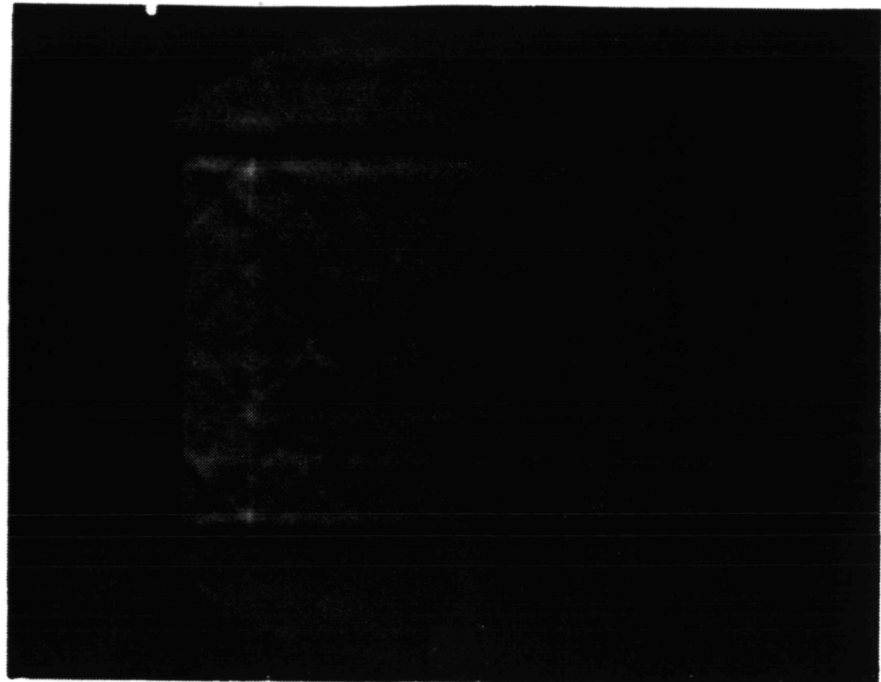


Configuration	<u>2</u>
Test Point	<u>7213</u>
Shadowgraph No.	<u>21</u>



ORIGINAL PAGE IS
OF POOR QUALITY

Configuration	<u>2</u>
Test Point	<u>7211</u>
Shadowgraph No.	<u>22</u>

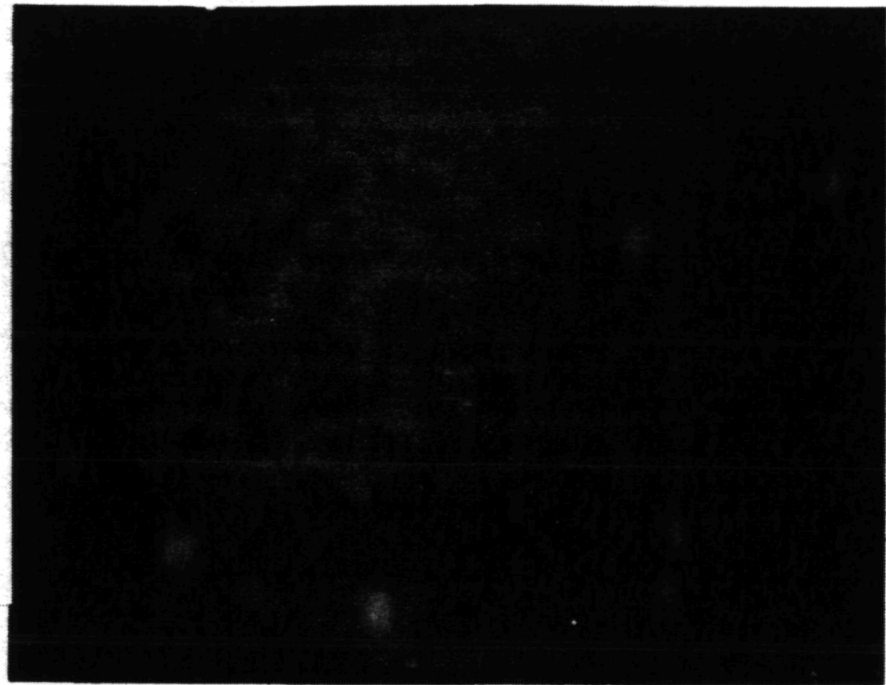


Configuration	<u>2</u>
Test Point	<u>7211</u>
Shadowgraph No.	<u>23</u>

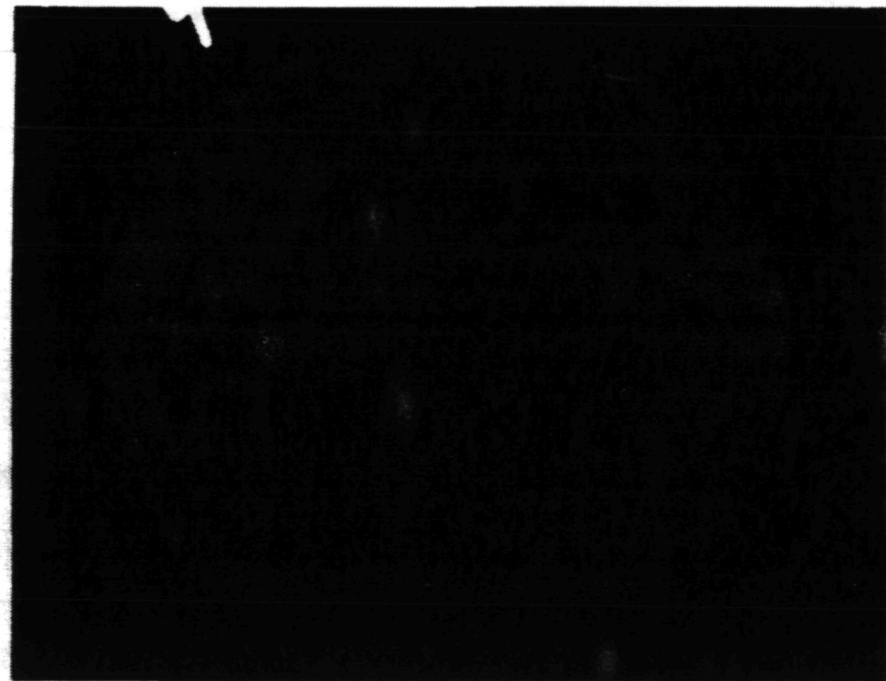


**ORIGINAL PAGE IS
OF POOR QUALITY**

Configuration	<u>2</u>
Test Point	<u>7211</u>
Shadowgraph No.	<u>24</u>



Configuration	<u>2</u>
Test Point	<u>7211</u>
Shadowgraph No.	<u>25</u>

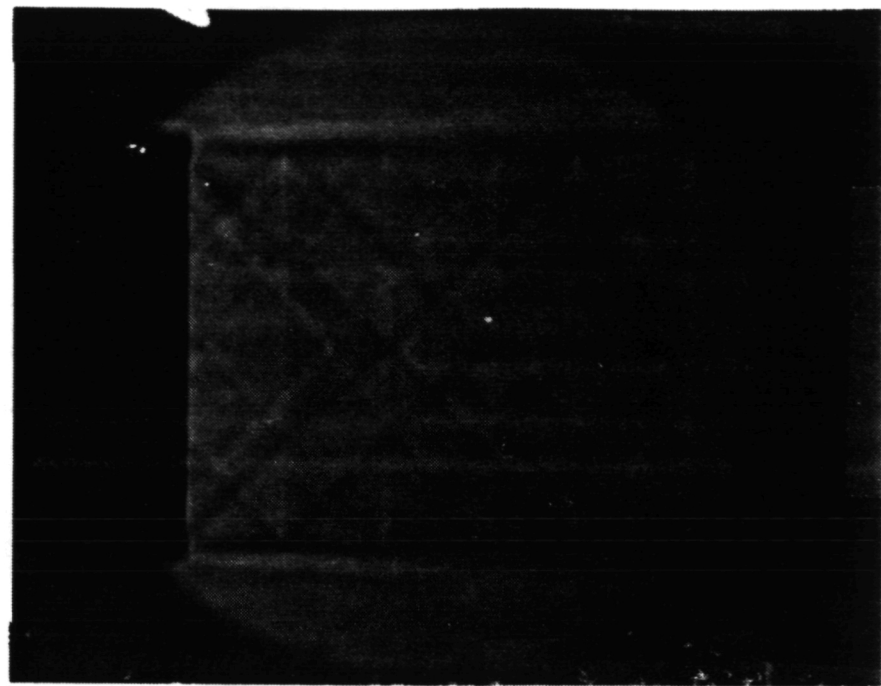


1416

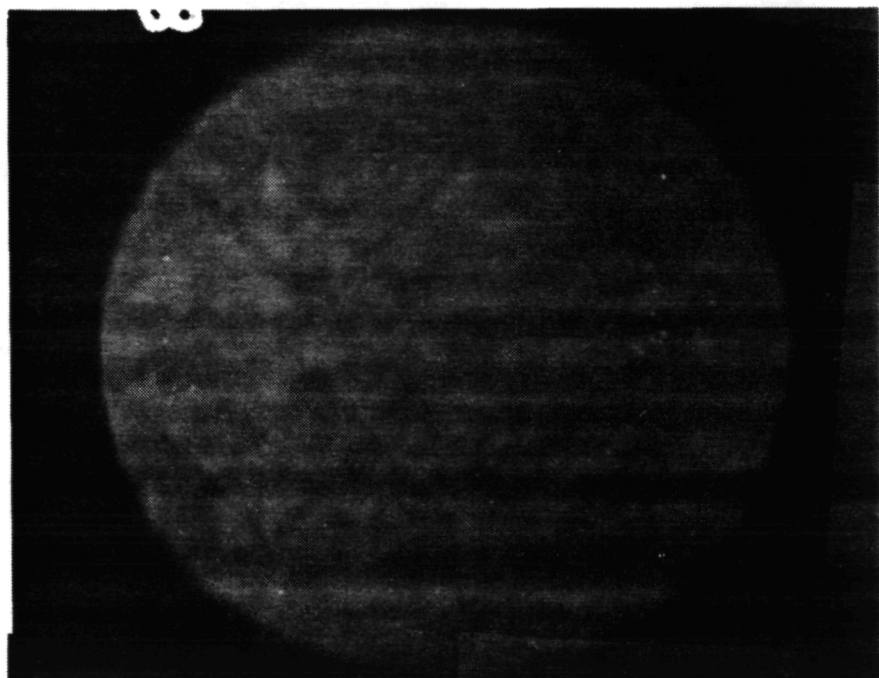
1410

ORIGINAL PAGE IS
OF POOR QUALITY

Configuration 2
Test Point 12//
Shadowgraph No. 27

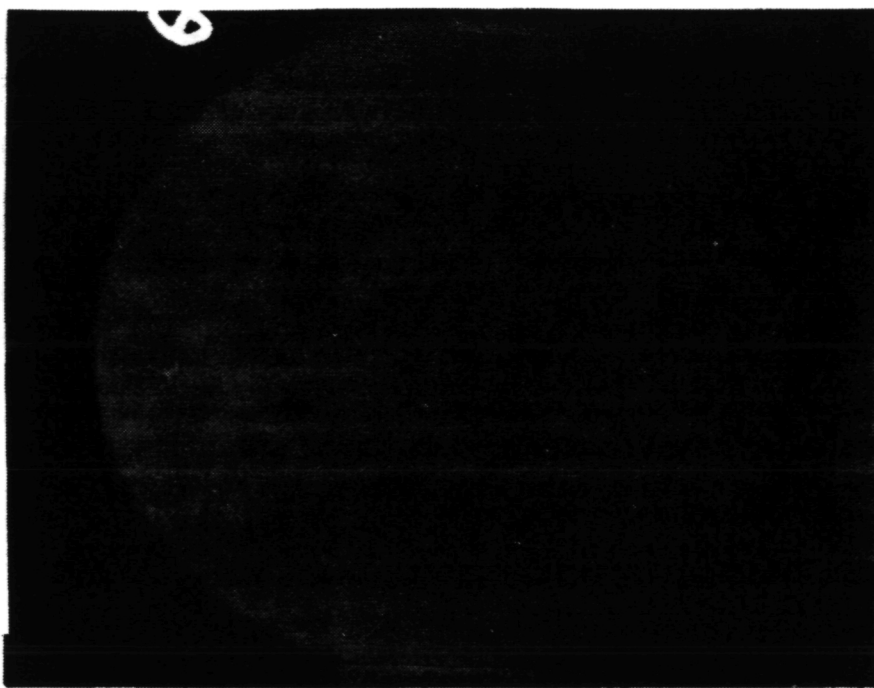


Configuration 2
Test Point 12//
Shadowgraph No. 28



ORIGINAL PAGE IS
OF POOR QUALITY

Configuration	<u>2</u>
Test Point	<u>1211</u>
Shadowgraph No.	<u>29</u>

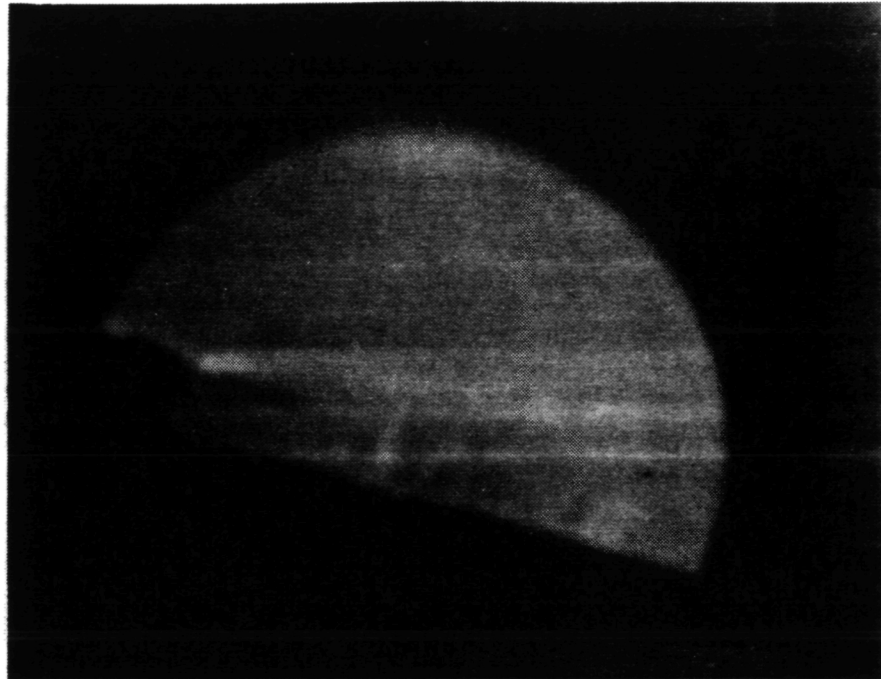


6.2.3 Shadowgraph Photos of Model 3

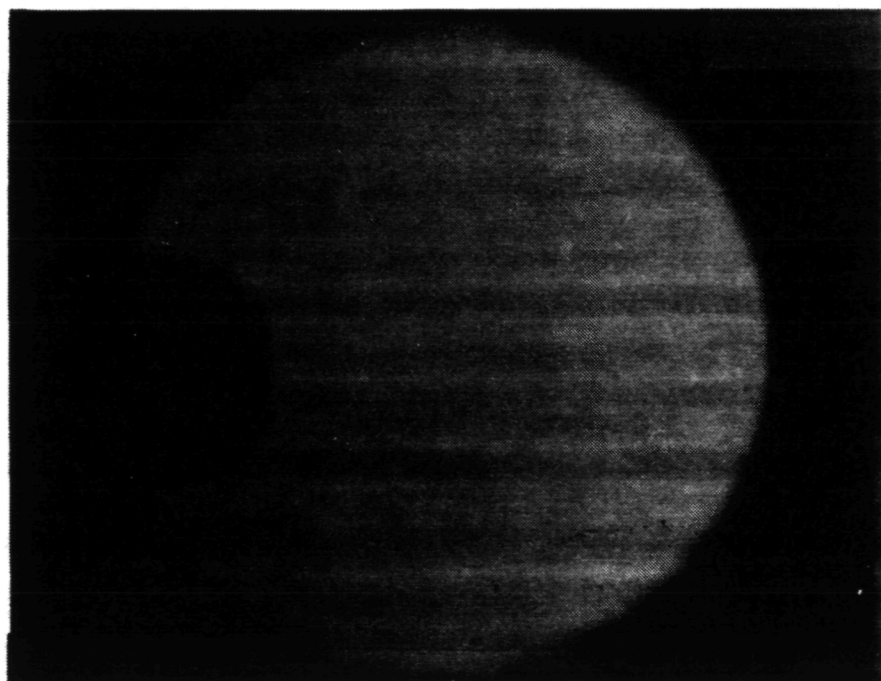
The shadowgraph test details associated with this model are provided in Table 6.4. The copies of the individual shadowgraph photographs taken with this model are presented next in this section.

ORIGINAL PAGE IS
OF POOR QUALITY.

Configuration 3
Test Point 4.313
Shadowgraph No. 4

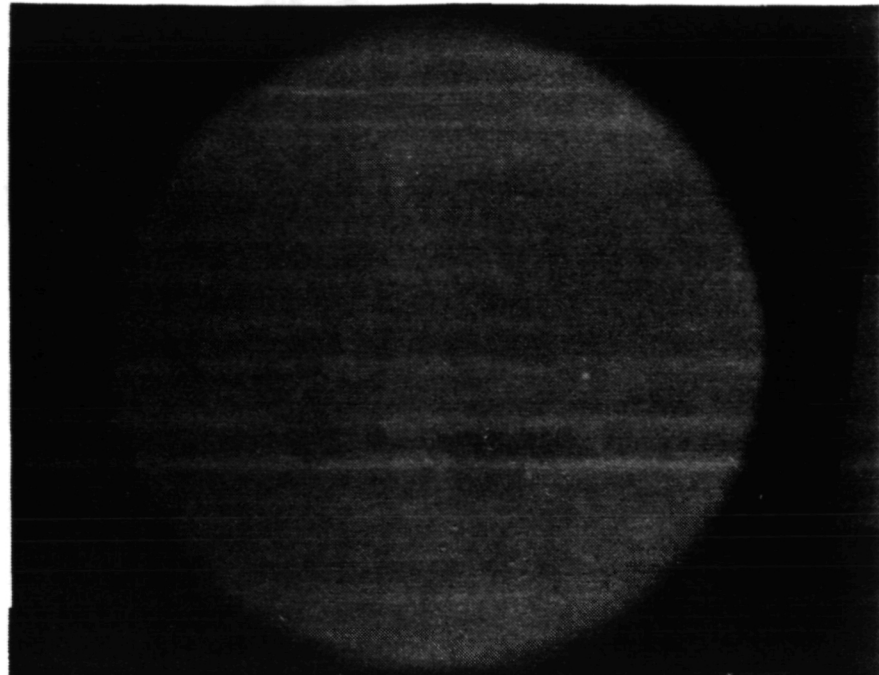


Configuration 3
Test Point 4.313
Shadowgraph No. 5



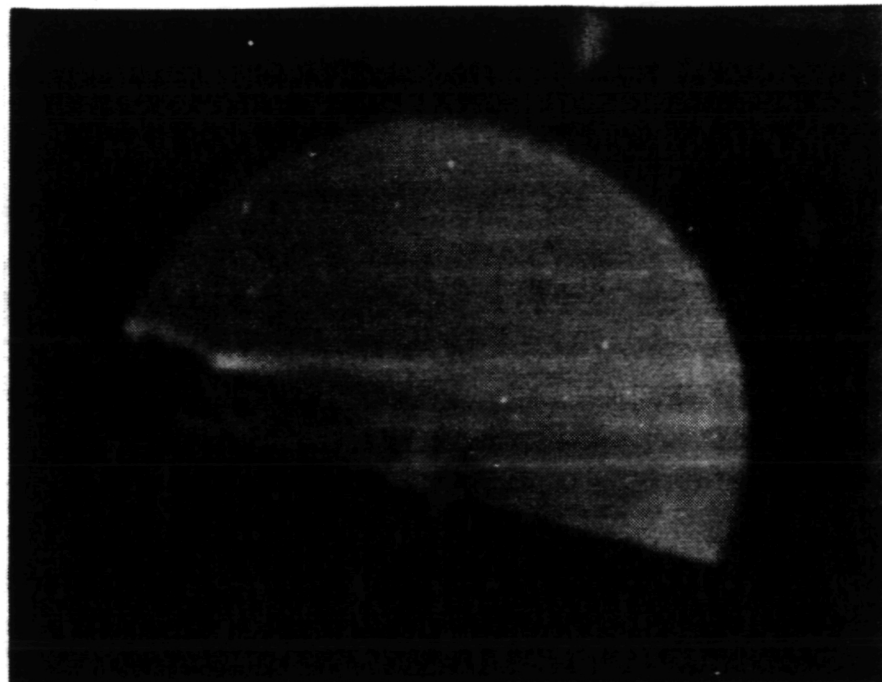
ORIGINAL PAGE IS
OF POOR QUALITY

Configuration	<u>3</u>
Test Point	<u>4.3/3</u>
Shadowgraph No.	<u>6</u>

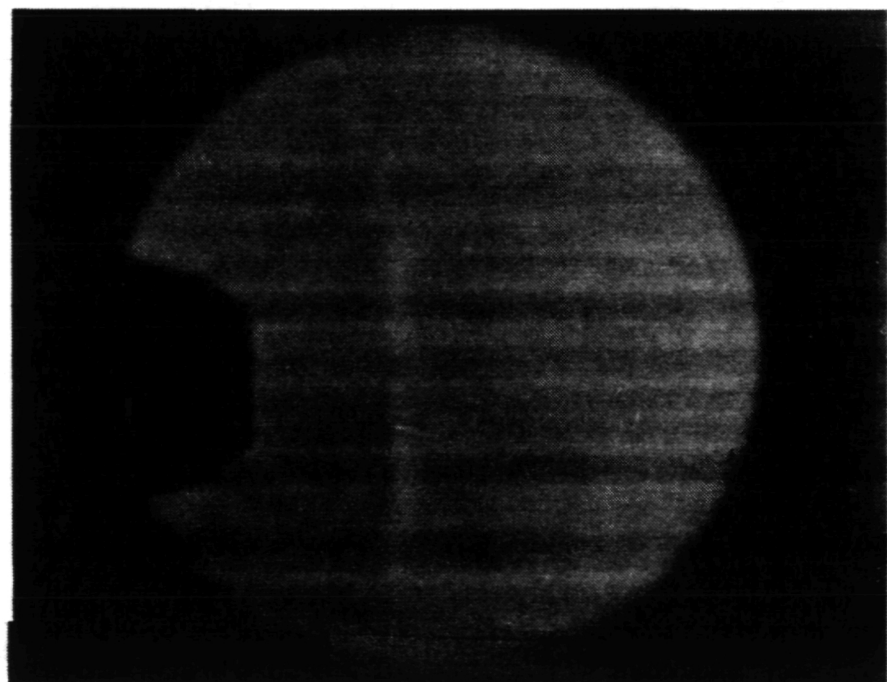


ORIGINAL PAGE IS
OF POOR QUALITY

Configuration	3
Test Point	4321
Shadowgraph No.	9

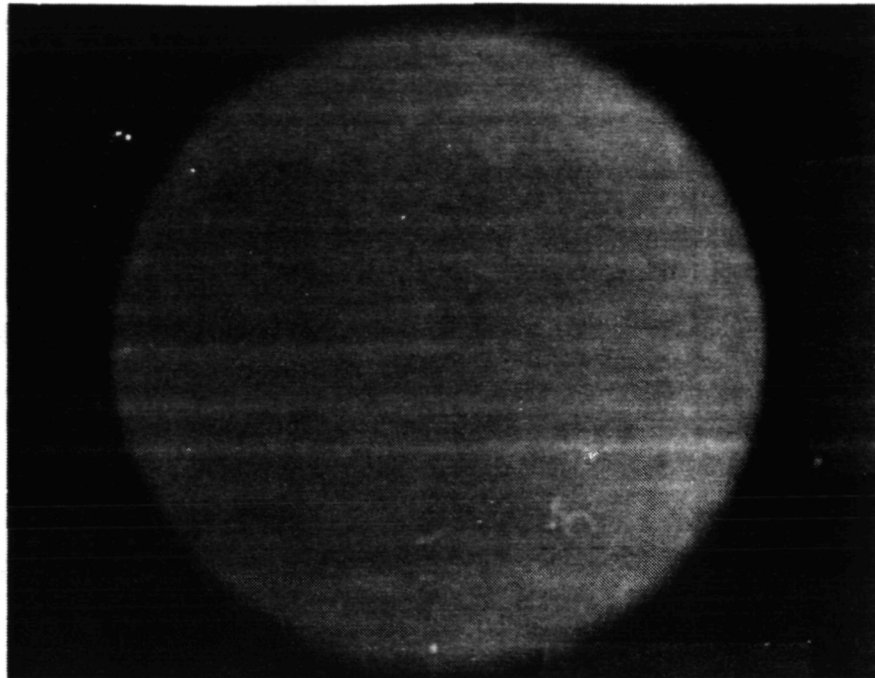


Configuration	3
Test Point	4321
Shadowgraph No.	10



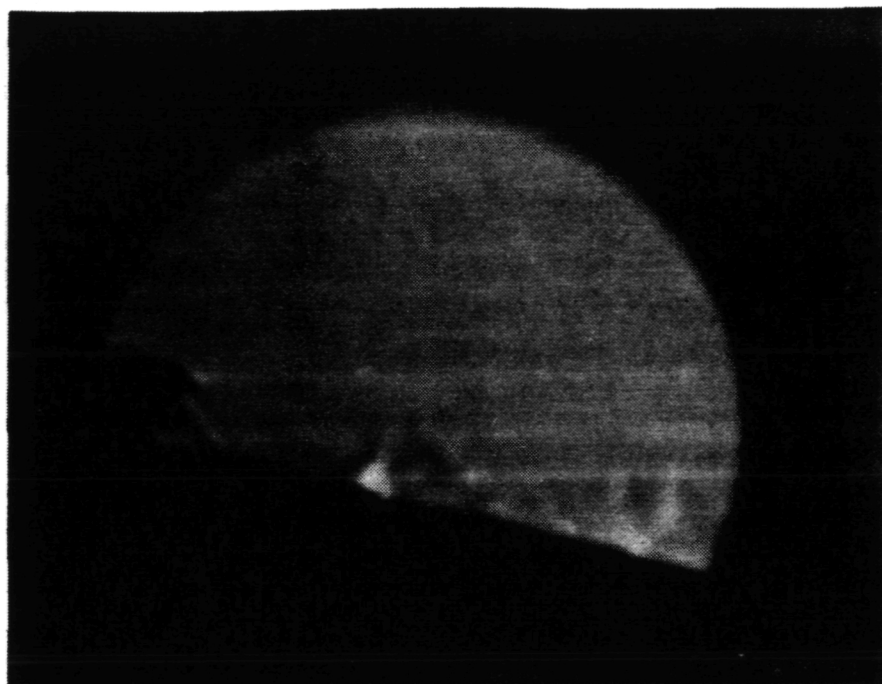
ORIGINAL FACE IS
OF POOR QUALITY

Configuration	<u>3</u>
Test Point	<u>4321</u>
Shadowgraph No.	<u>11</u>

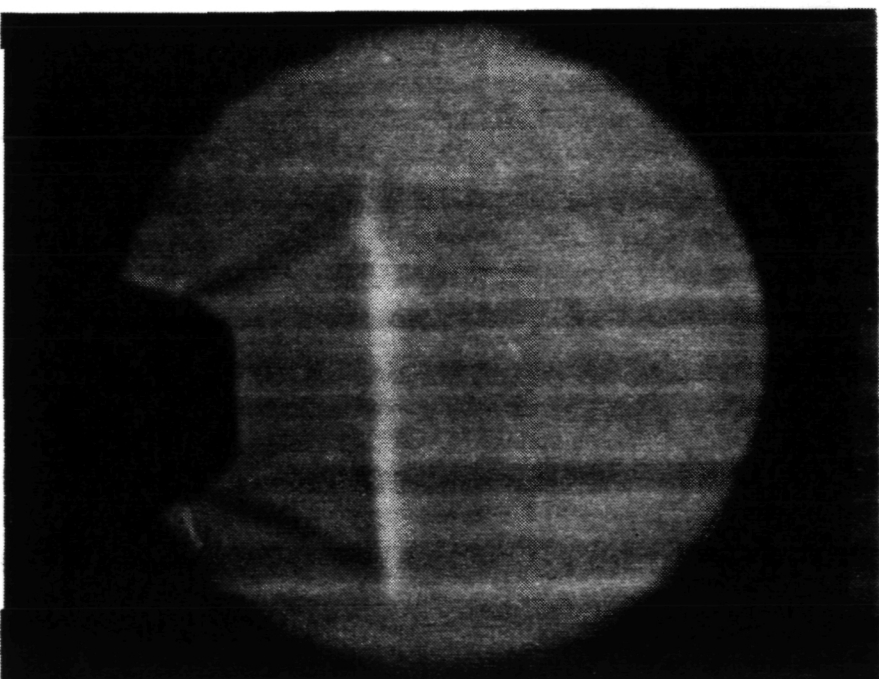


ORIGINAL PAGE IS
OF POOR QUALITY

Configuration	<u>3</u>
Test Point	<u>5323</u>
Shadowgraph No.	<u>12</u>

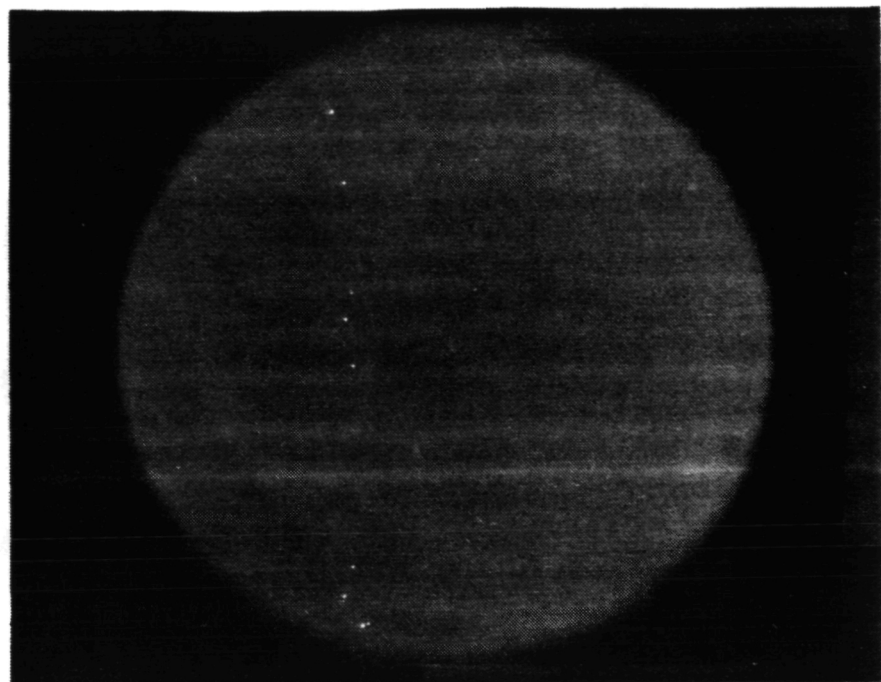


Configuration	<u>3</u>
Test Point	<u>5323</u>
Shadowgraph No.	<u>13</u>



ORIGINAL PAGE IS
OF POOR QUALITY.

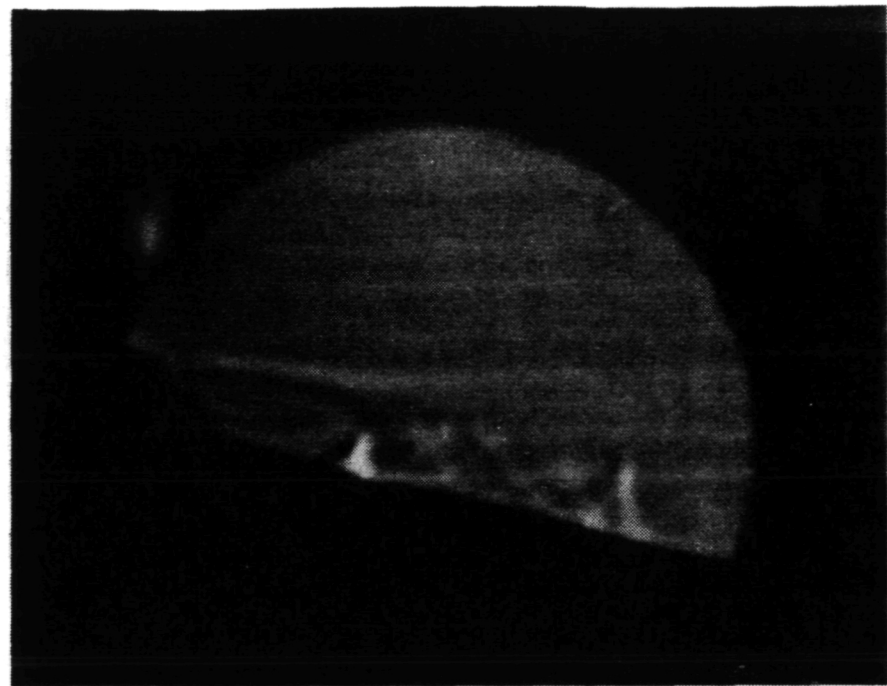
Configuration	<u>3</u>
Test Point	<u>5323</u>
Shadowgraph No.	<u>14</u>



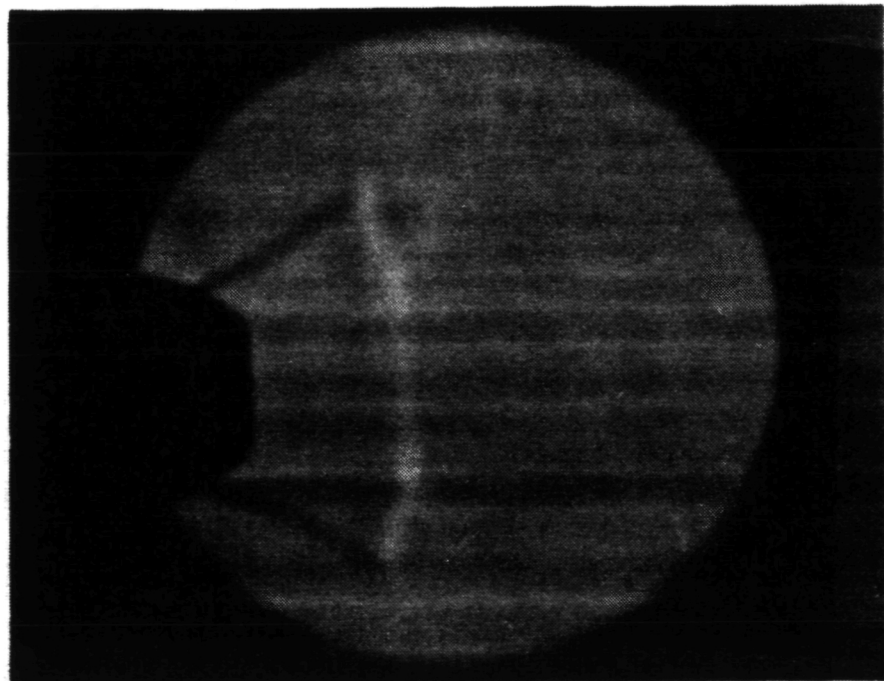
1419

ORIGINAL PAGE IS
OF POOR QUALITY

Configuration	3
Test Point	1313
Shadowgraph No.	16

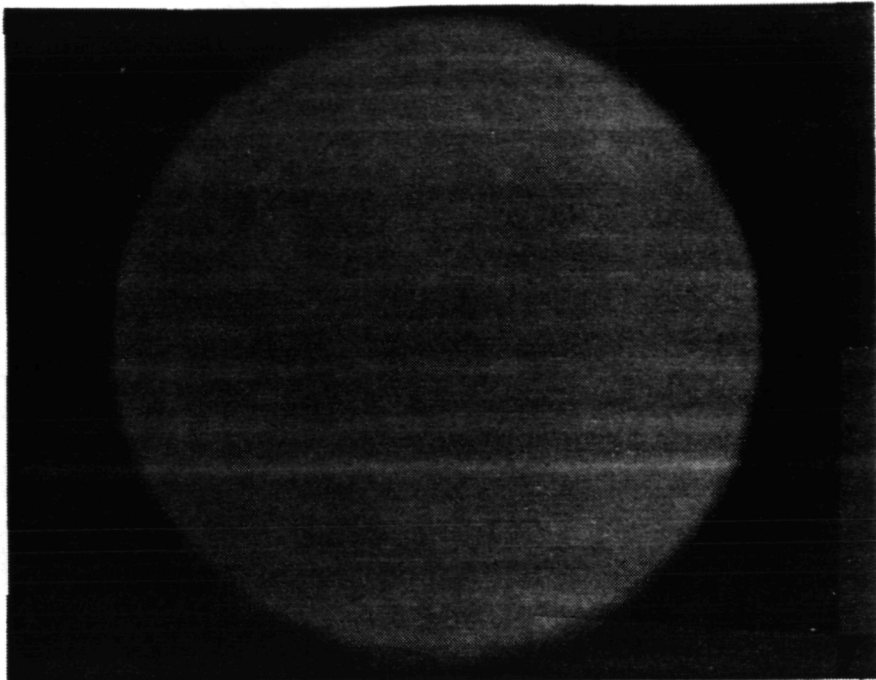


Configuration	3
Test Point	1313
Shadowgraph No.	17



ORIGINAL PAGE IS
OF POOR QUALITY

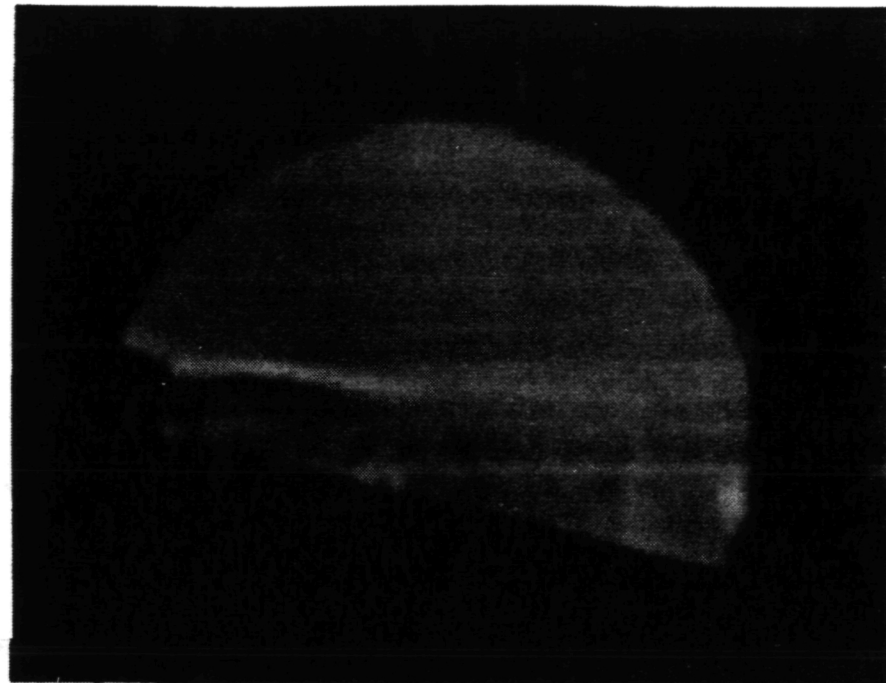
Configuration	<u>3</u>
Test Point	<u>1313</u>
Shadowgraph No.	<u>18</u>



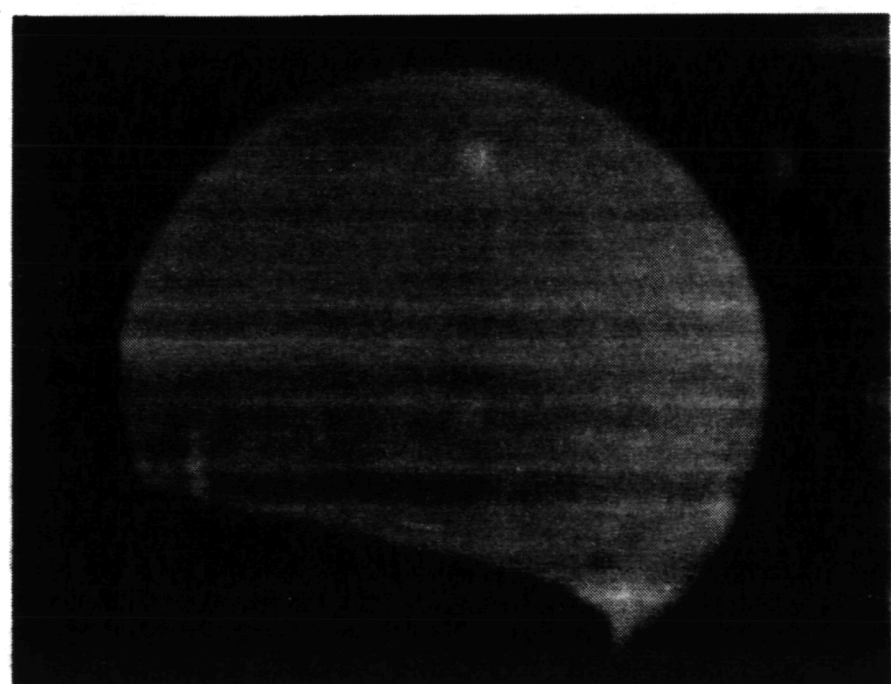
1421

ORIGINAL PAGE IS
OF POOR QUALITY

Configuration	3
Test Point	3/3
Shadowgraph No.	20



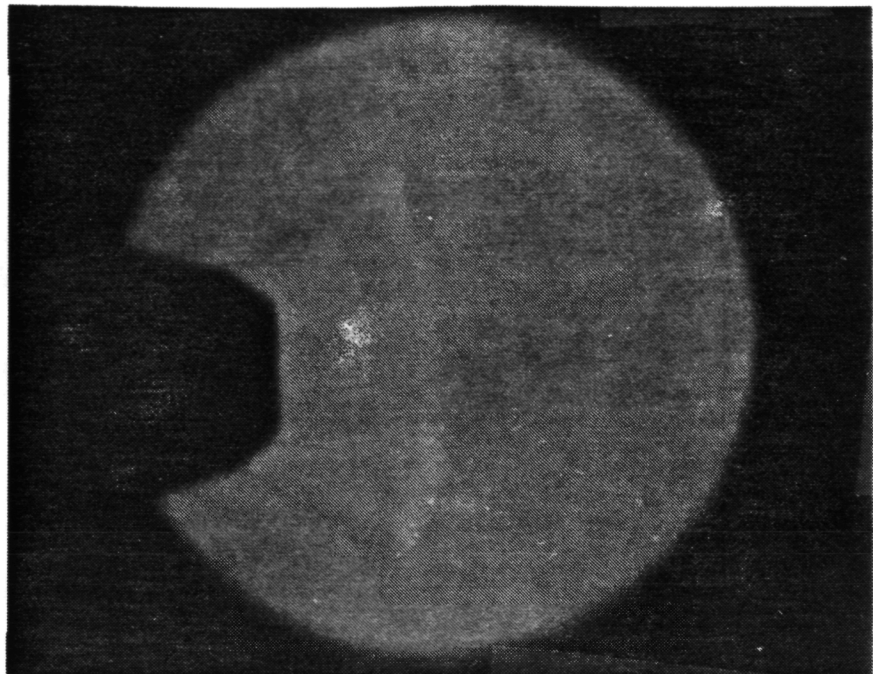
Configuration	3
Test Point	3/3
Shadowgraph No.	21



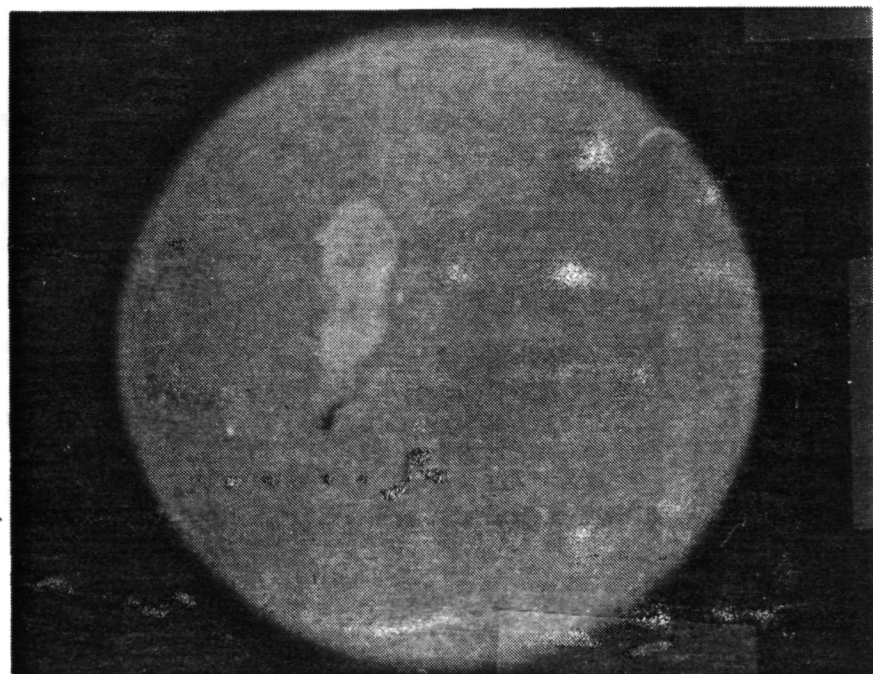
1422

ORIGINAL PAGE IS
OF POOR QUALITY.

Configuration 3
Test Point 3/3
Shadowgraph No. 22

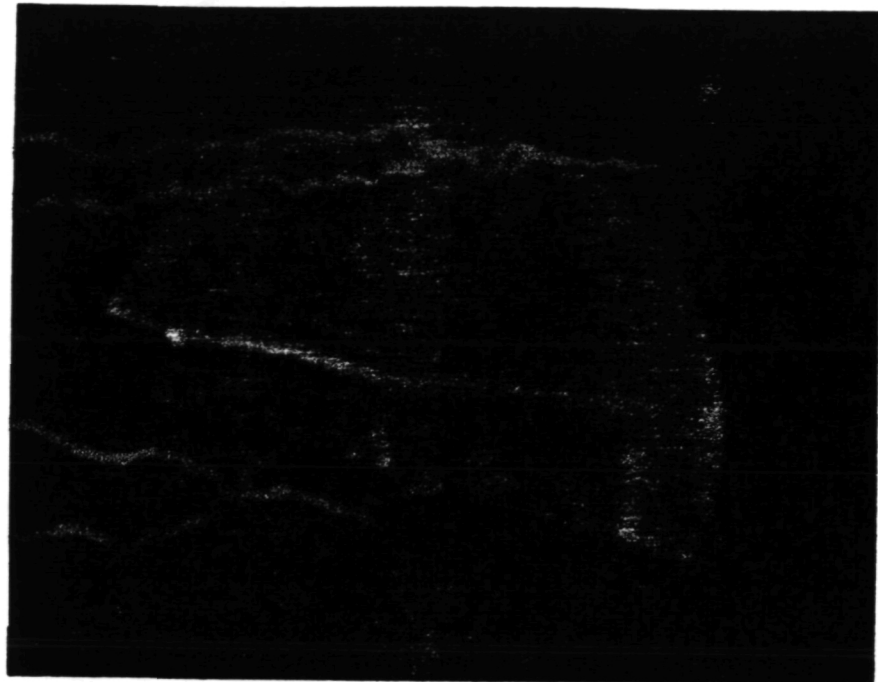


Configuration 3
Test Point 3/3
Shadowgraph No. 23

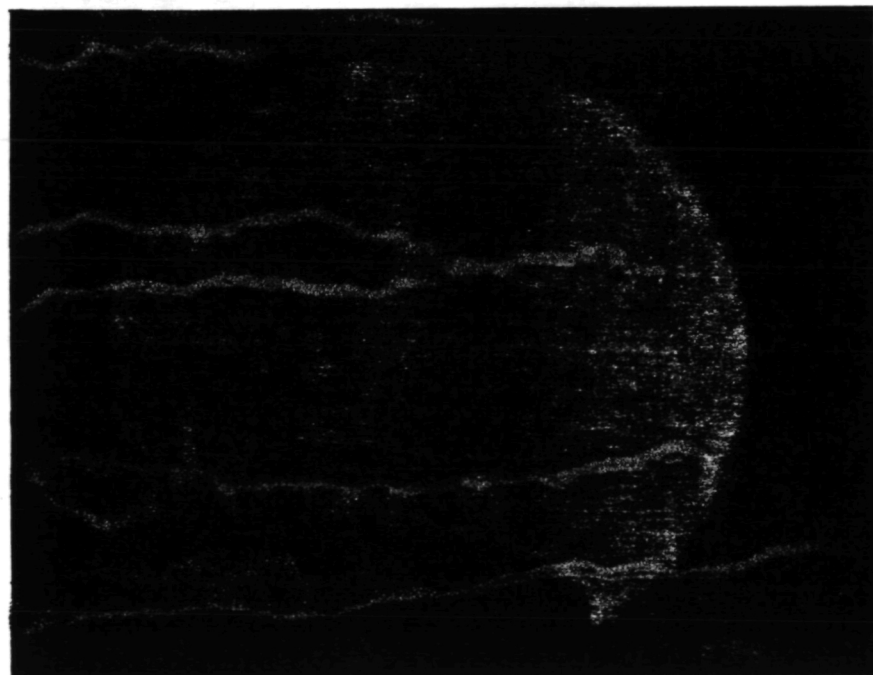


ORIGINAL PAGE IS
OF POOR QUALITY

Configuration	<u>3</u>
Test Point	<u>314</u>
Shadowgraph No.	<u>25</u>



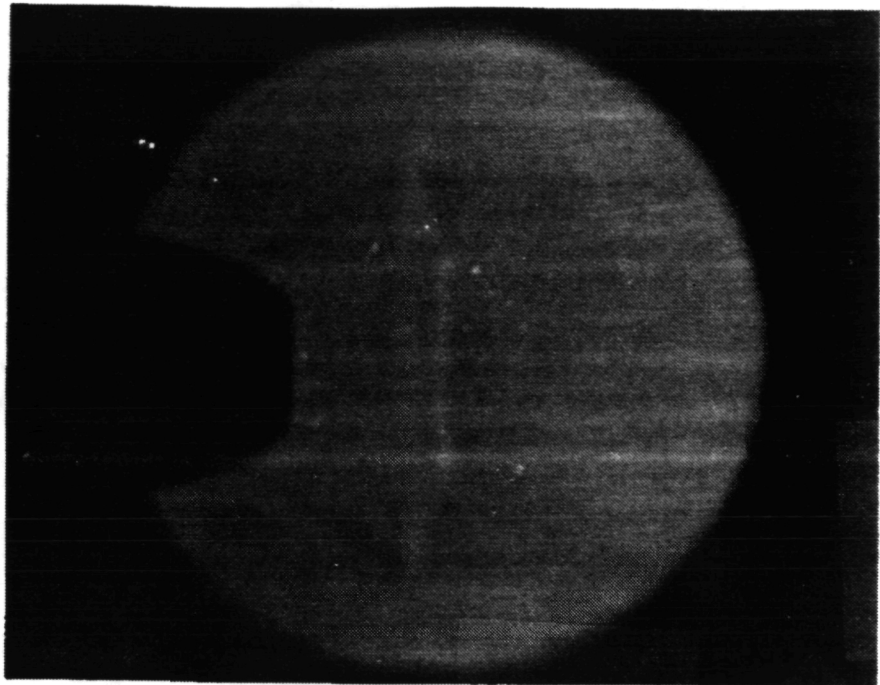
Configuration	<u>3</u>
Test Point	<u>314</u>
Shadowgraph No.	<u>26</u>



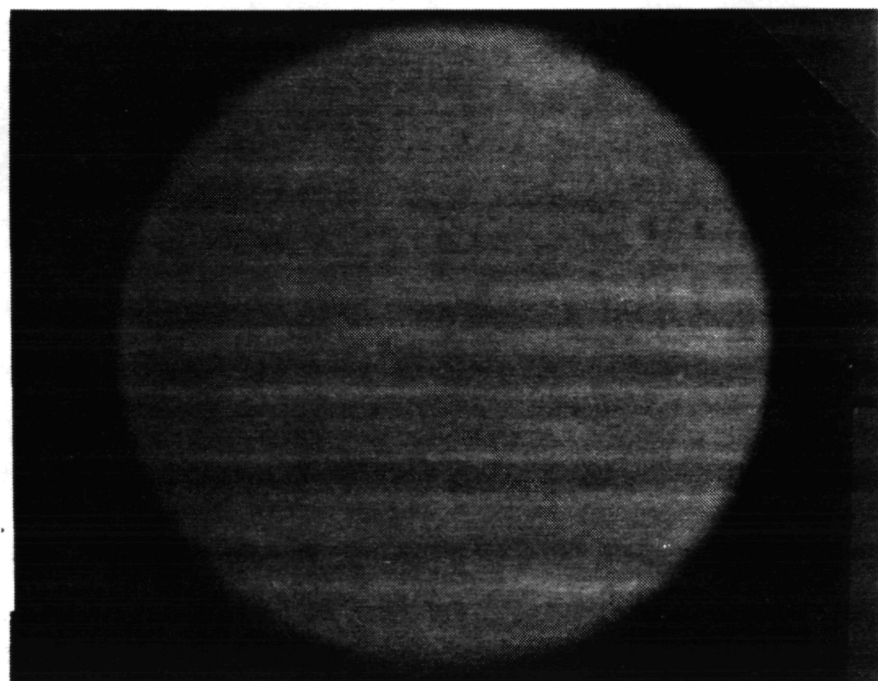
1424

ORIGINAL PAGE IS
OF POOR QUALITY

Configuration	<u>3</u>
Test Point	<u>314</u>
Shadowgraph No.	<u>27</u>

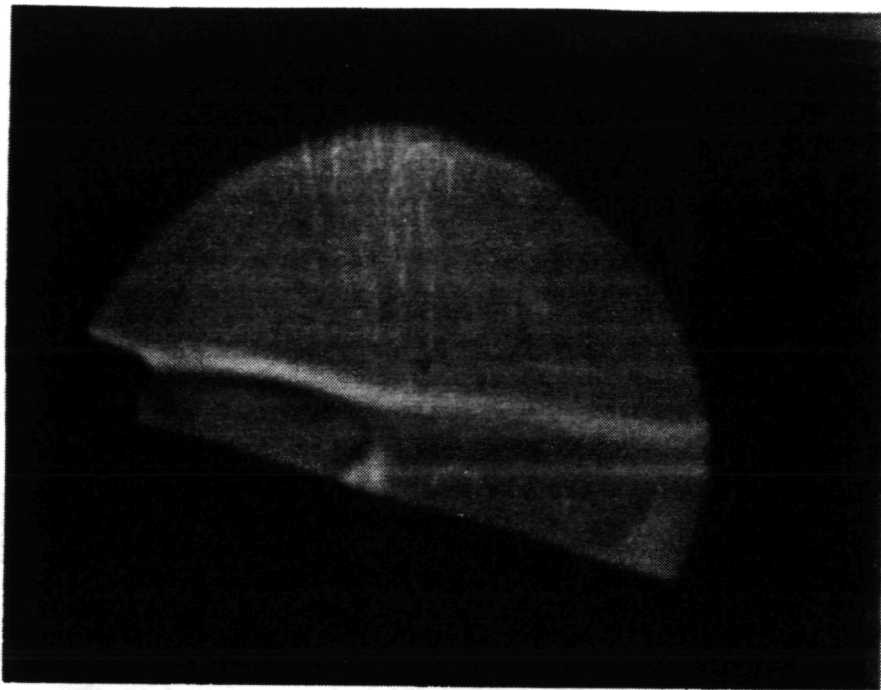


Configuration	<u>3</u>
Test Point	<u>314</u>
Shadowgraph No.	<u>28</u>

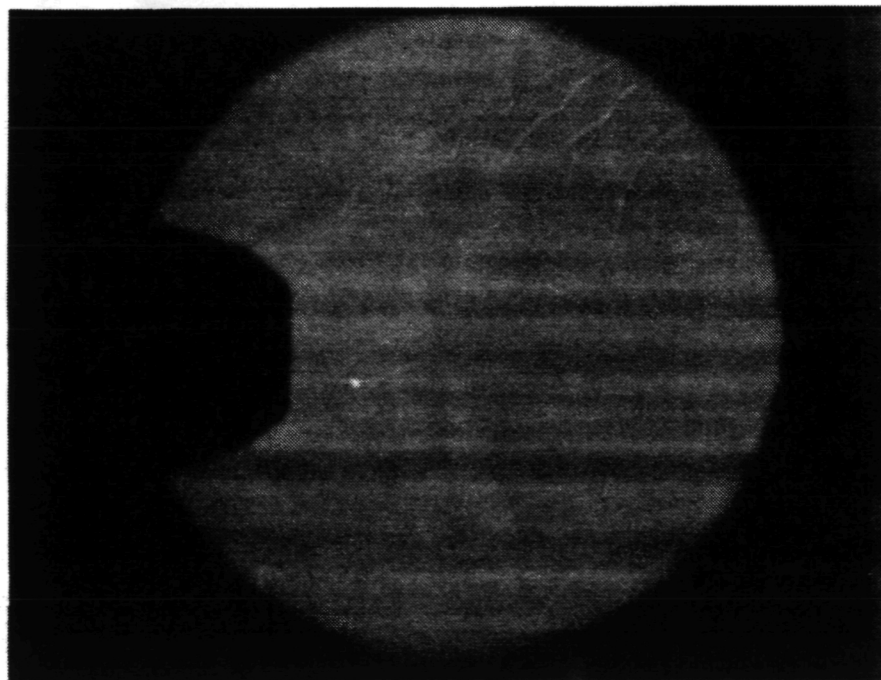


ORIGINAL PAGE IS
OF POOR QUALITY

Configuration	<u>3</u>
Test Point	<u>322</u>
Shadowgraph No.	<u>30</u>



Configuration	<u>3</u>
Test Point	<u>322</u>
Shadowgraph No.	<u>31</u>

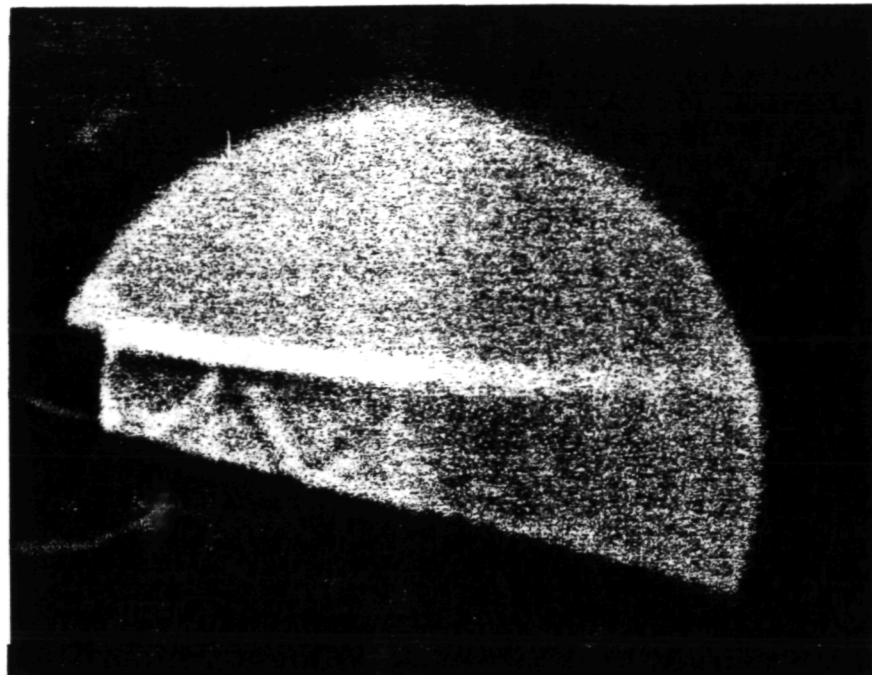


6.2.4 Shadowgraph Photos of Model 4

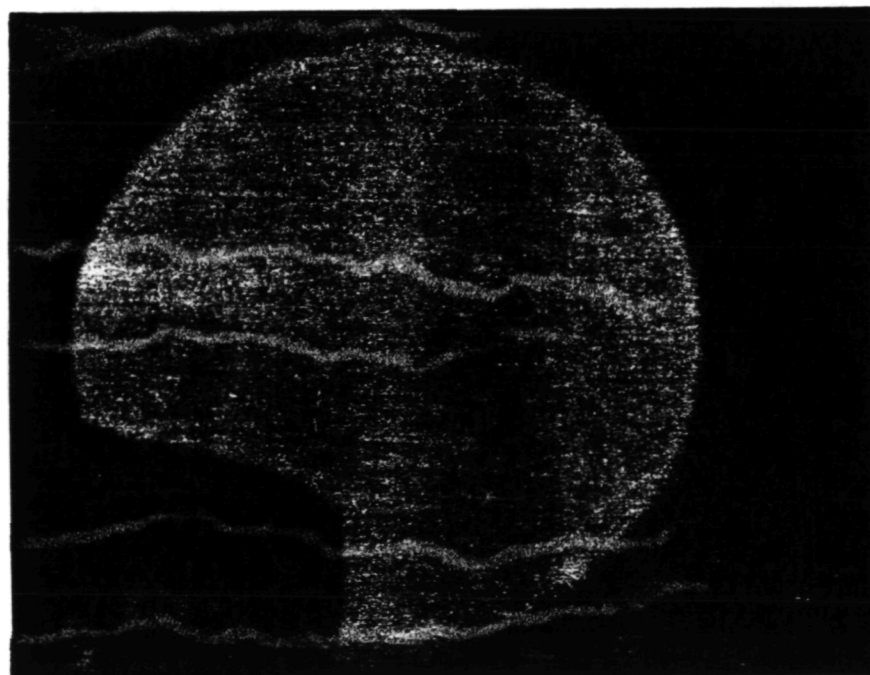
The shadowgraph test details associated with this model are provided in Table 6.5. The copies of the individual shadowgraph photographs taken with this model are presented next in this section.

ORIGINAL PAGE IS
OF POOR QUALITY

Configuration	4
Test Point	413
Shadowgraph No.	3



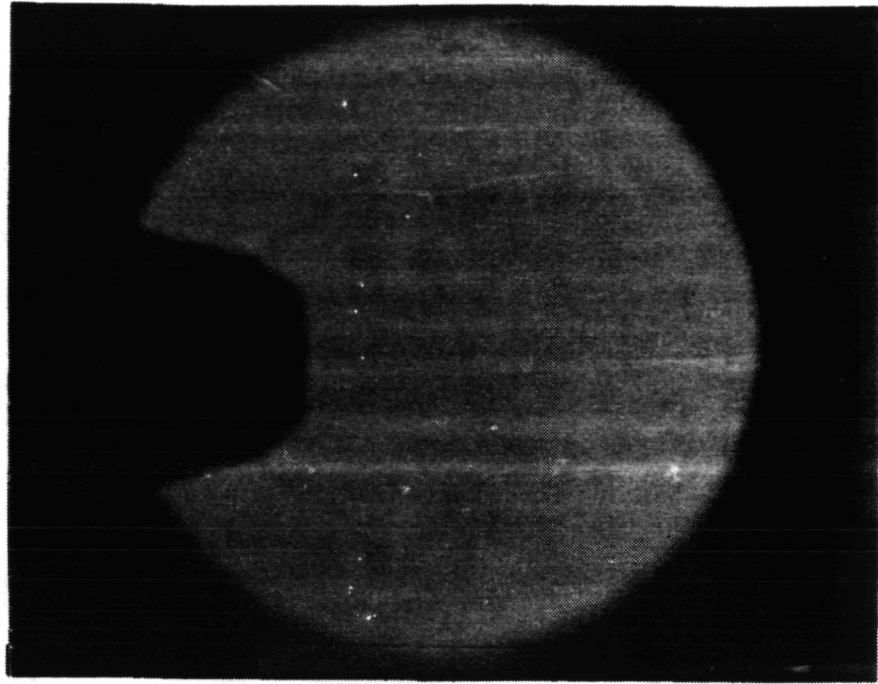
Configuration	4
Test Point	413
Shadowgraph No.	4



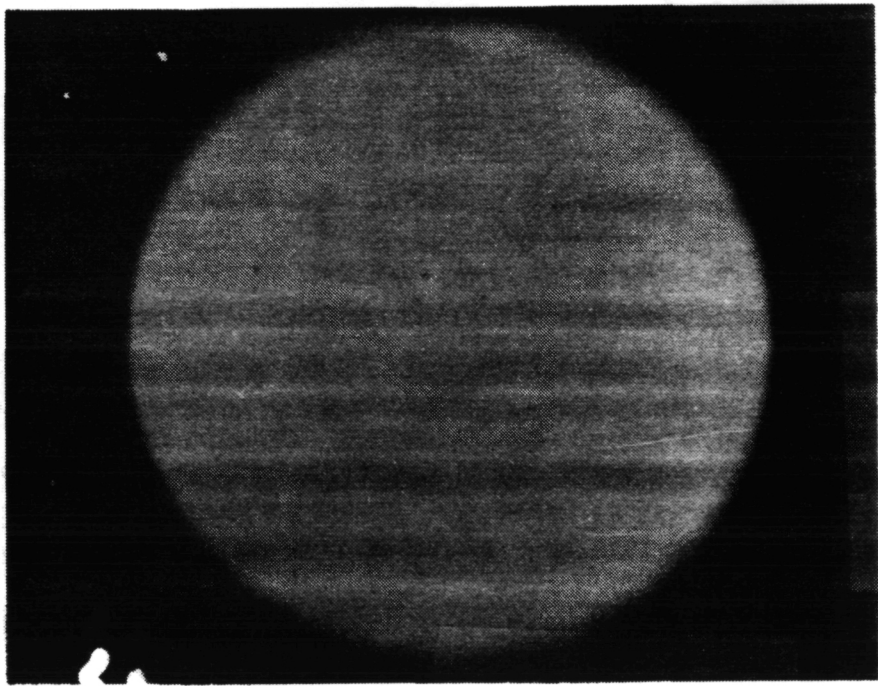
1428

ORIGINAL PAGE IS
OF POOR QUALITY

Configuration	4
Test Point	413
Shadowgraph No.	7



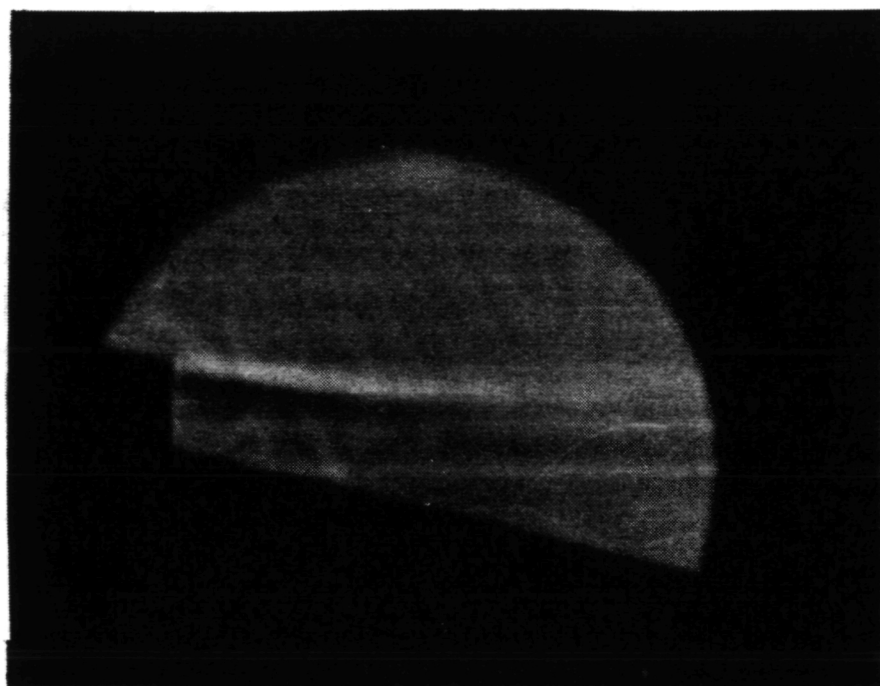
Configuration	4
Test Point	413
Shadowgraph No.	5



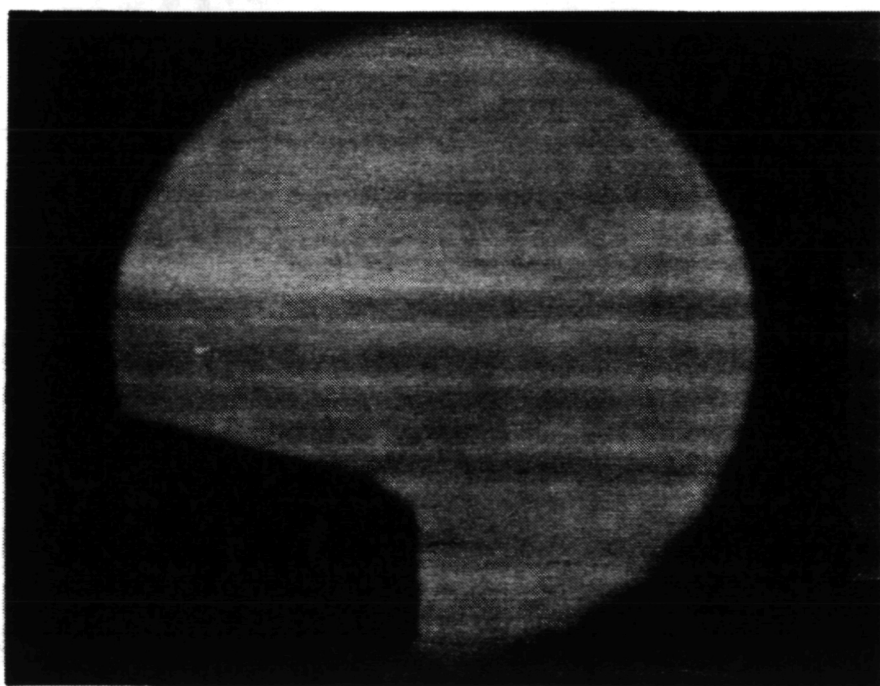
1438

ORIGINAL PAGE IS
OF POOR QUALITY.

Configuration	4
Test Point	411
Shadowgraph No.	8

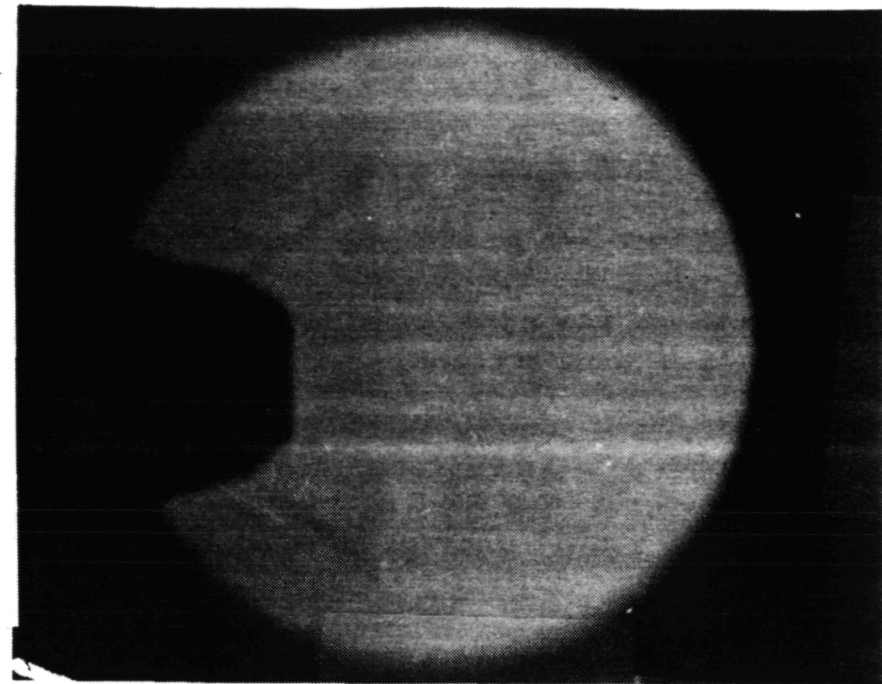


Configuration	4
Test Point	411
Shadowgraph No.	9

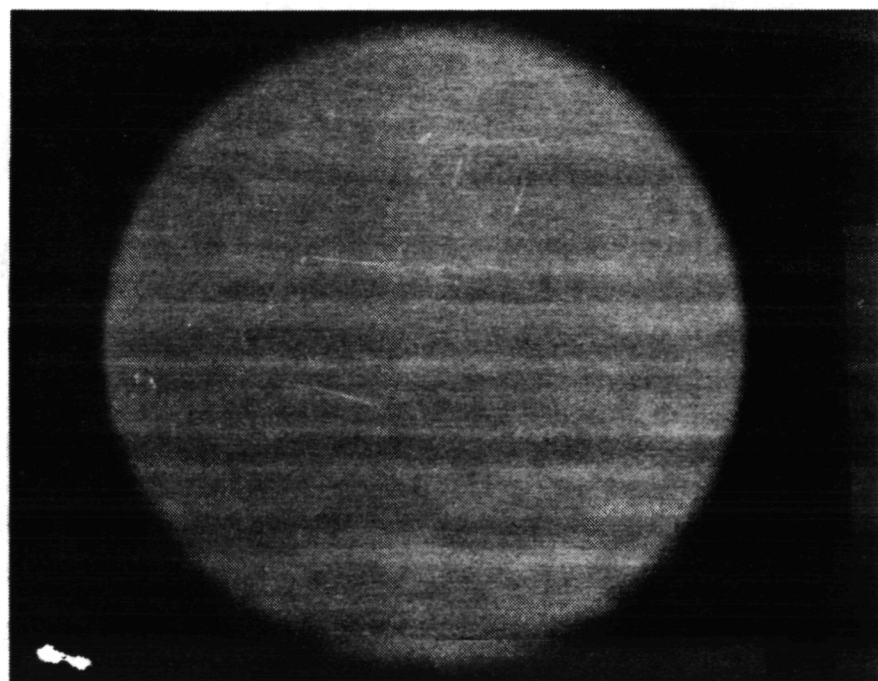


ORIGINAL PAGE IS
OF POOR QUALITY

Configuration	4
Test Point	411
Shadowgraph No.	10

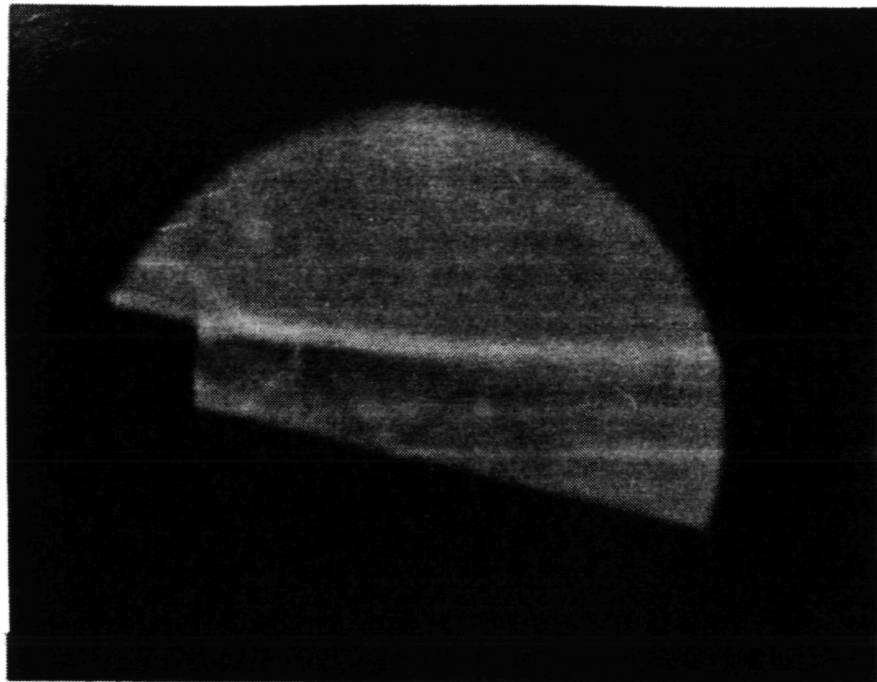


Configuration	4
Test Point	411
Shadowgraph No.	11

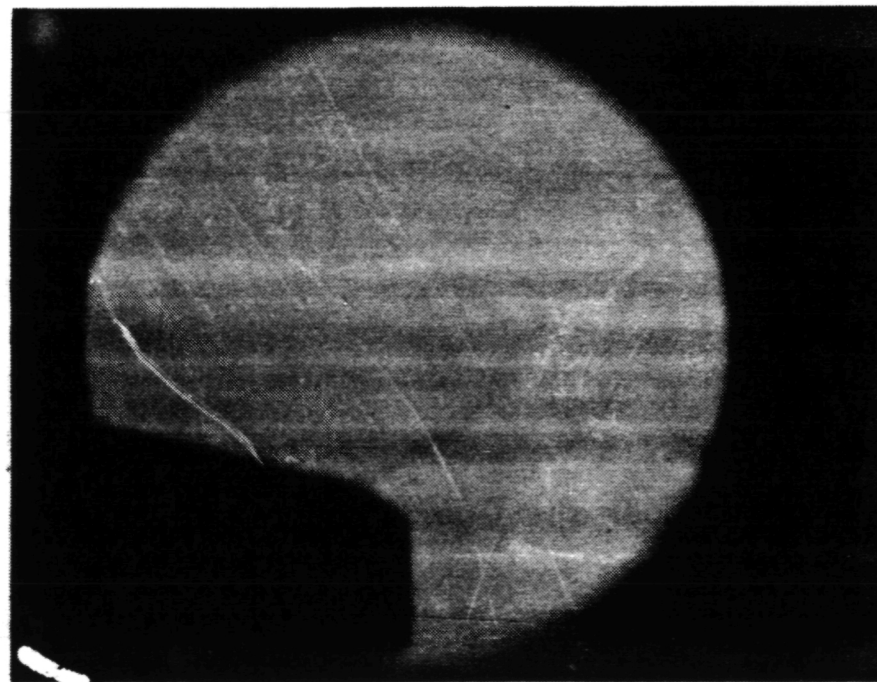


ORIGINAL PAGE IS
OF POOR QUALITY

Configuration	<u>4</u>
Test Point	<u>421</u>
Shadowgraph No.	<u>14</u>



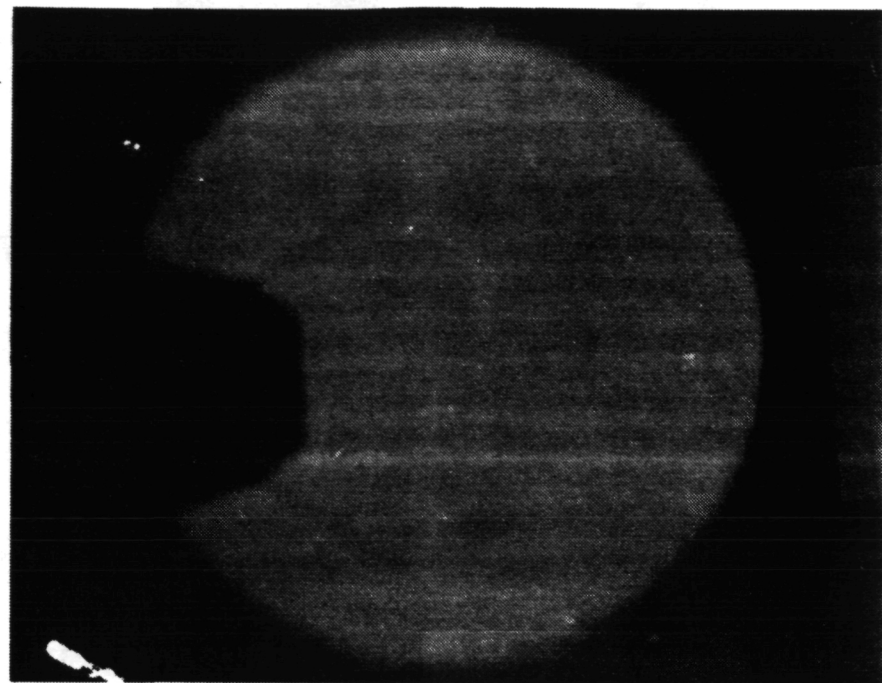
Configuration	<u>4</u>
Test Point	<u>421</u>
Shadowgraph No.	<u>15</u>



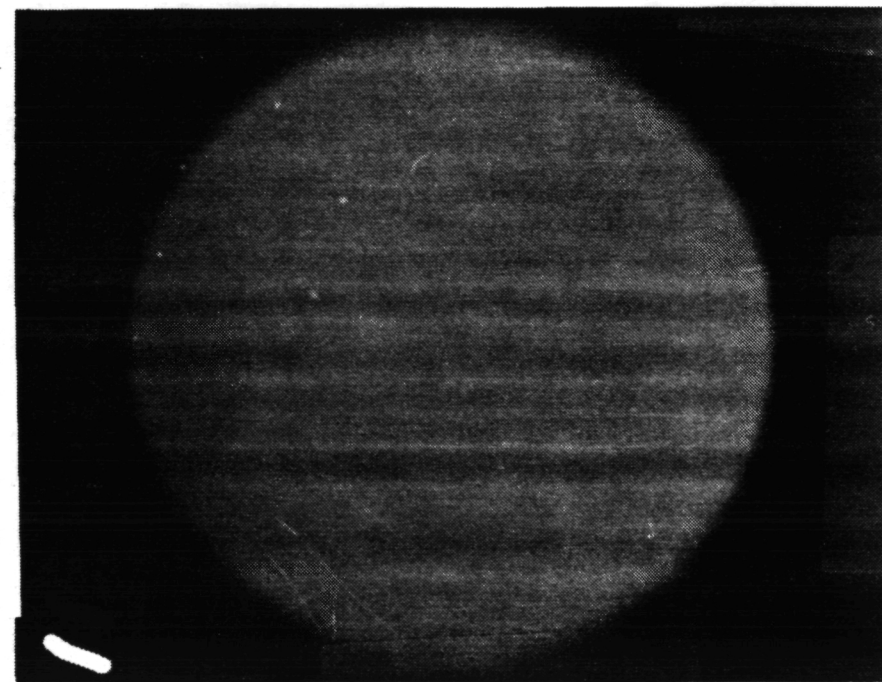
1432

ORIGINAL PAGE IS
OF POOR QUALITY

Configuration 4
Test Point 421
Shadowgraph No. 16

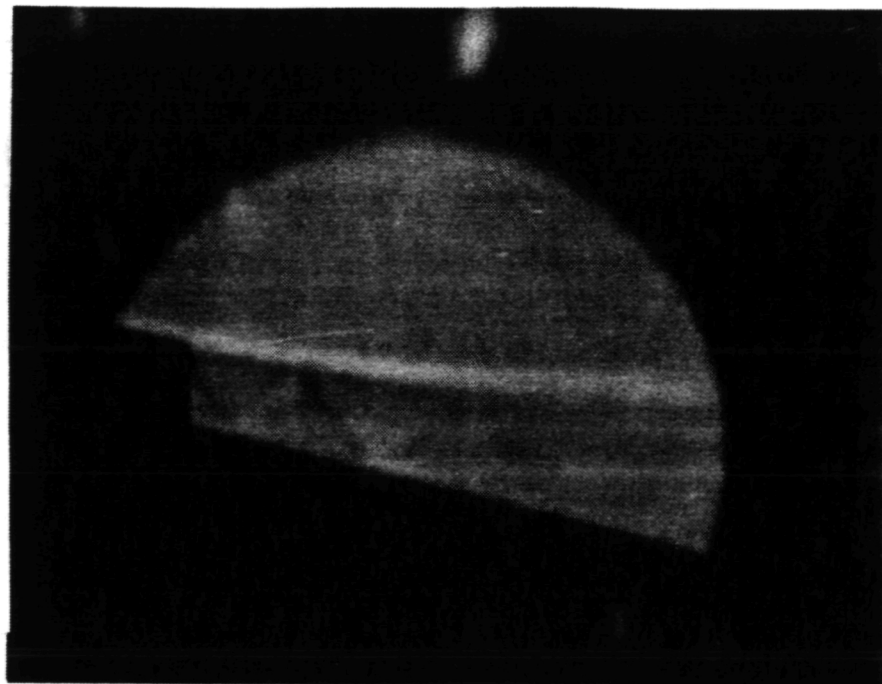


Configuration 4
Test Point 421
Shadowgraph No. 17

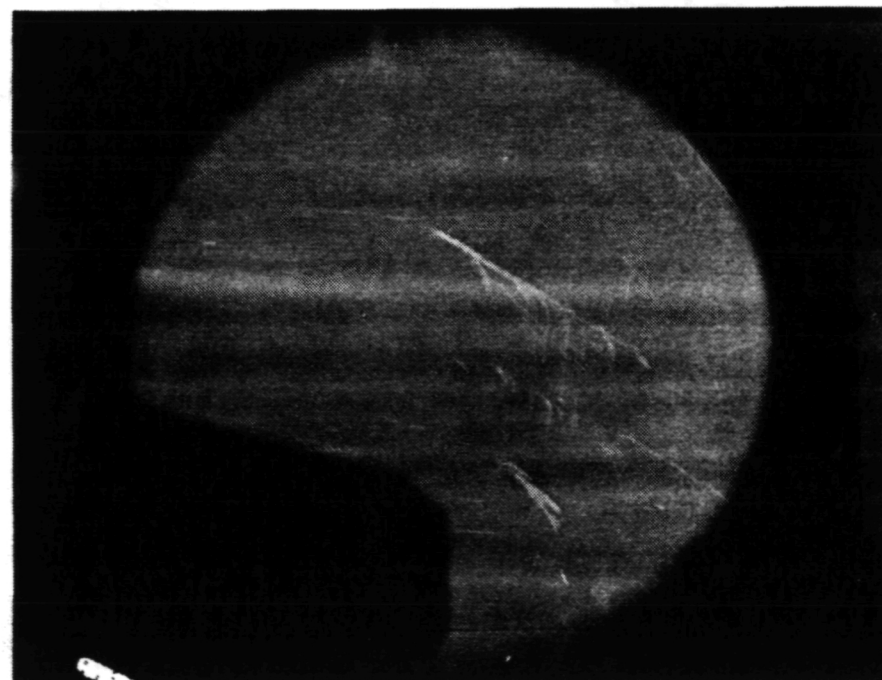


ORIGINAL PAGE IS
OF POOR QUALITY

Configuration	<u>4</u>
Test Point	<u>422</u>
Shadowgraph No.	<u>18</u>

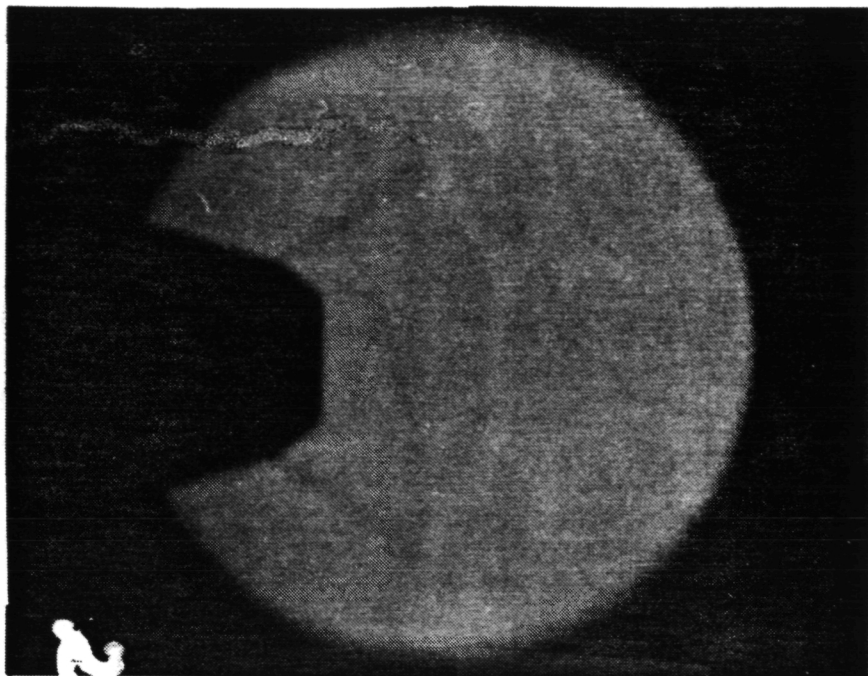


Configuration	<u>4</u>
Test Point	<u>422</u>
Shadowgraph No.	<u>19</u>



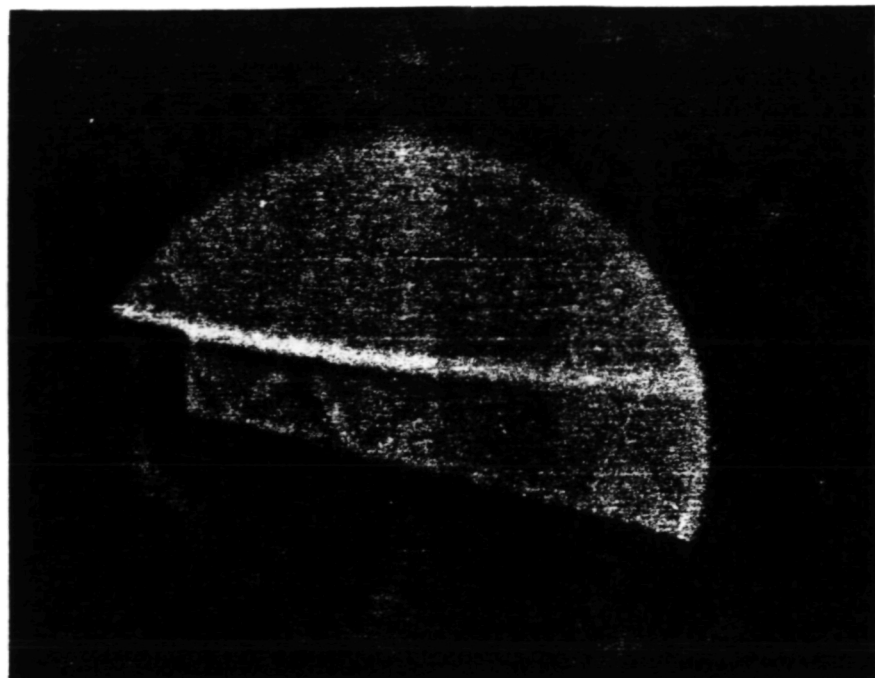
ORIGINAL PAGE IS
OF POOR QUALITY

Configuration	<u>4</u>
Test Point	<u>422</u>
Shadowgraph No.	<u>20</u>

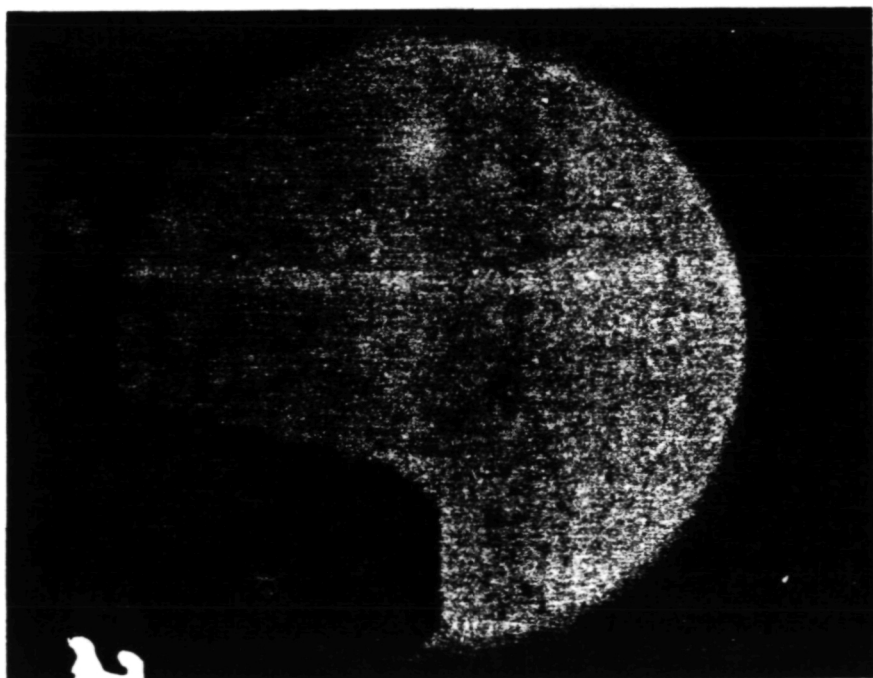


ORIGINAL PAGE 19
OF POOR QUALITY

Configuration	4
Test Point	414
Shadowgraph No.	21

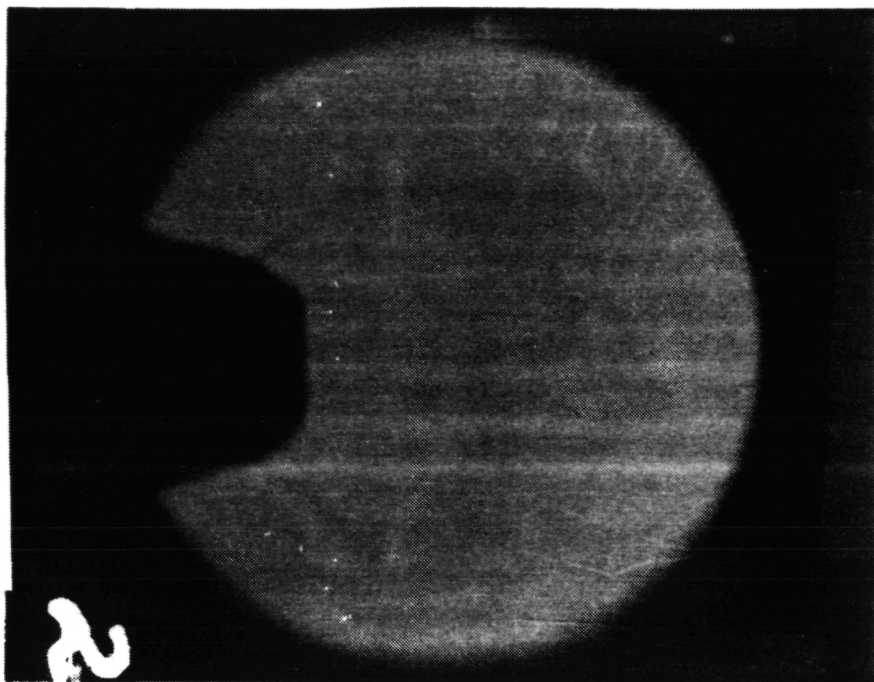


Configuration	4
Test Point	414
Shadowgraph No.	22



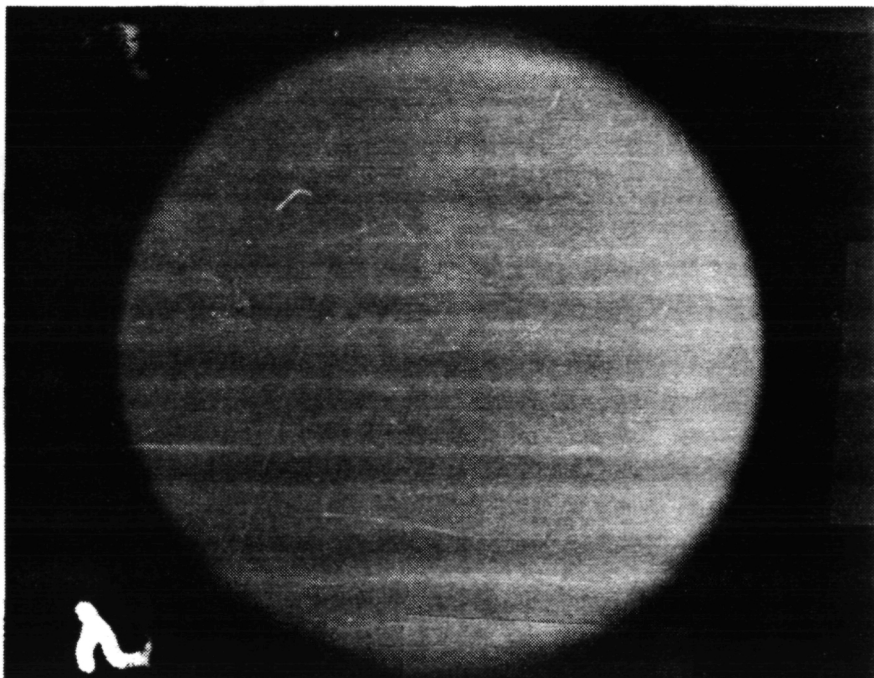
ORIGINAL PAGE IS
OF POOR QUALITY

Configuration 4
Test Point 4/4
Shadowgraph No. 23



2

Configuration 4
Test Point 4/4
Shadowgraph No. 24



2

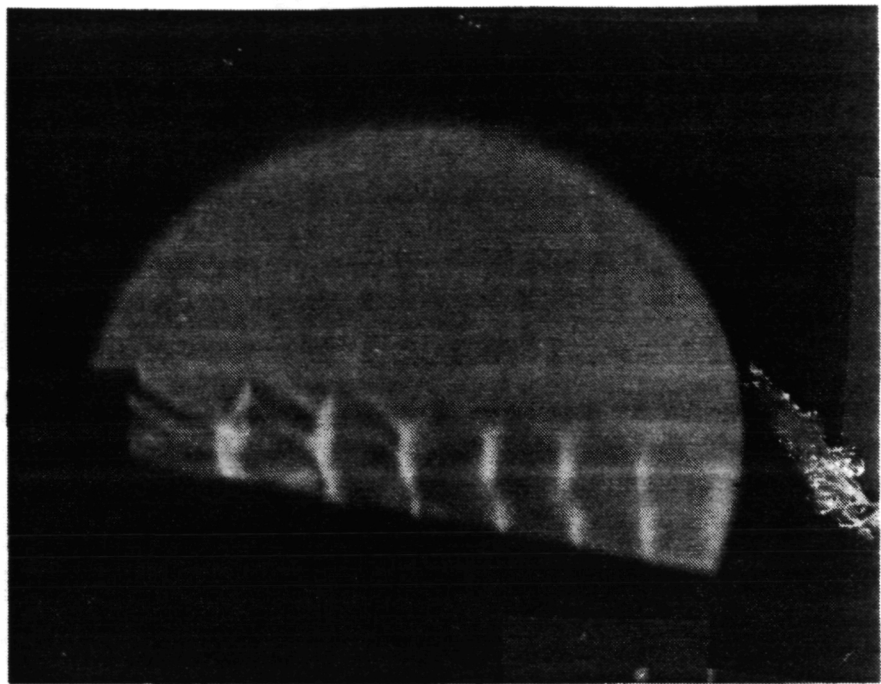
1437

6.2.5 Shadowgraph Photos of Model 5

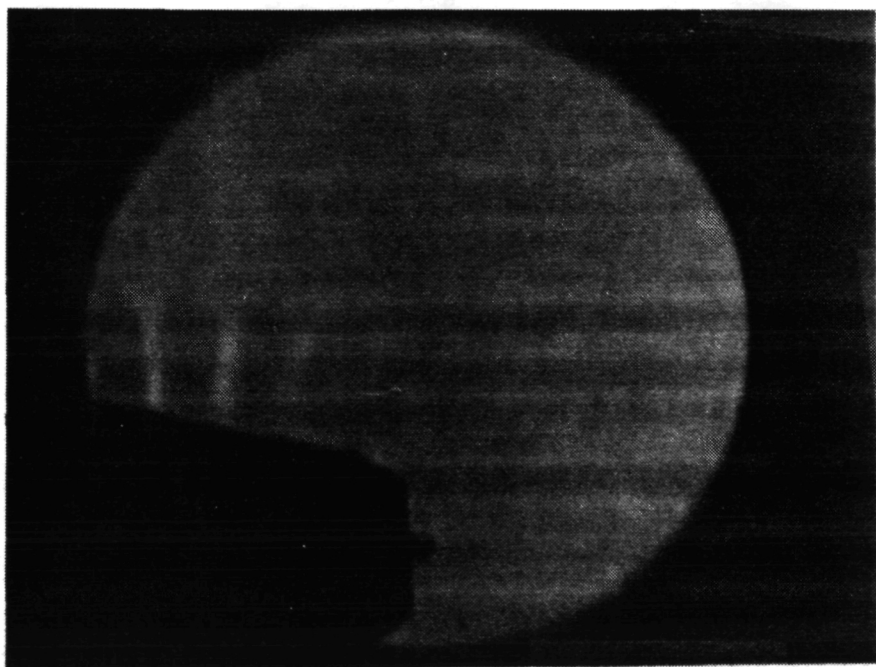
The shadowgraph test details associated with this model are provided in Table 6.6. The copies of the individual shadowgraph photographs taken with this model are presented next in this section.

ORIGINAL PAGE IS
OF POOR QUALITY.

Configuration 5
Test Point 1513
Shadowgraph No. 1



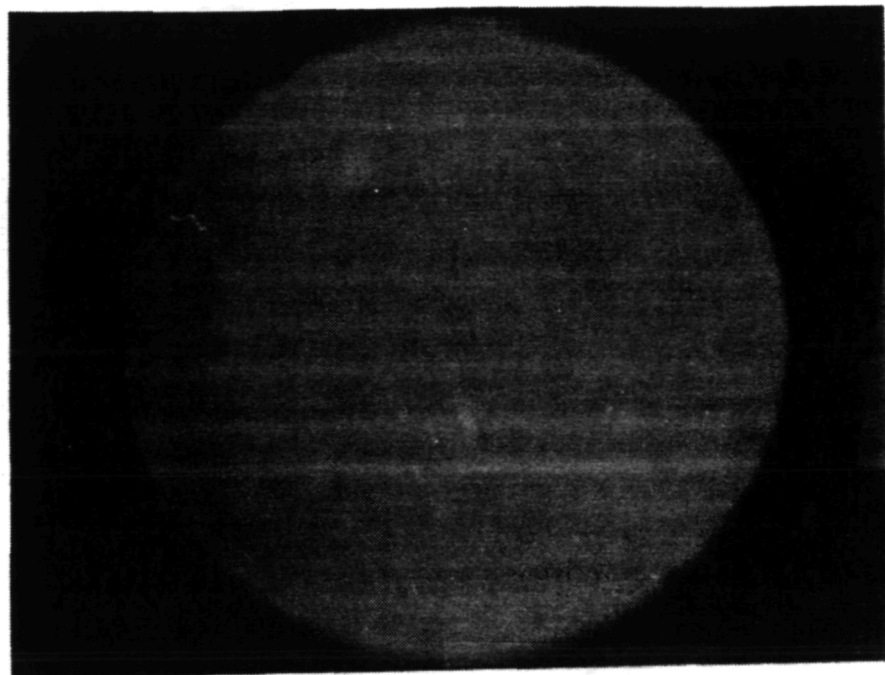
Configuration 5
Test Point 1513
Shadowgraph No. 2



1439

ORIGINAL PAGE IS
OF POOR QUALITY

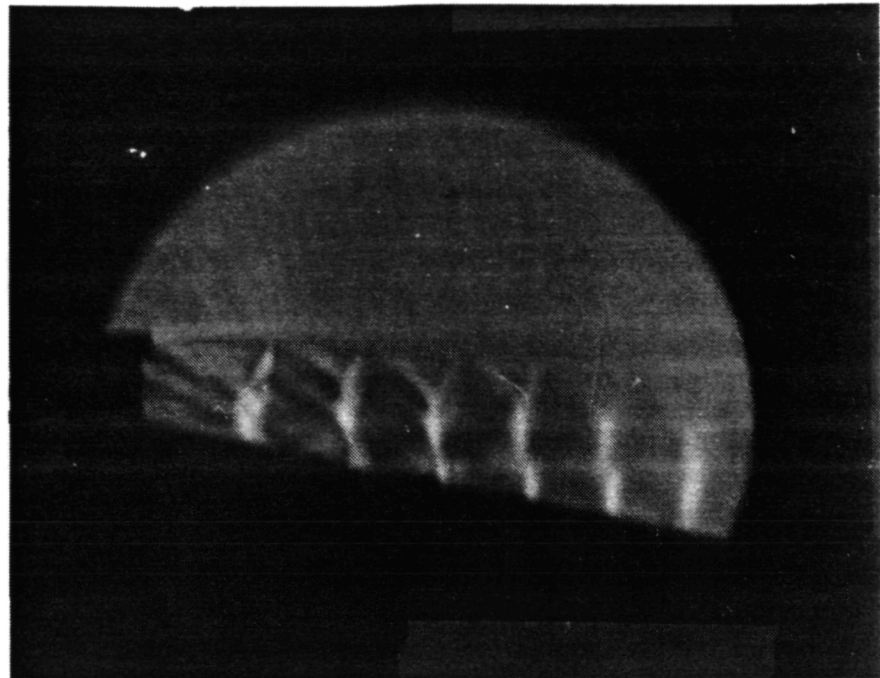
Configuration	<u>5</u>
Test Point	<u>1513</u>
Shadowgraph No.	<u>3</u>



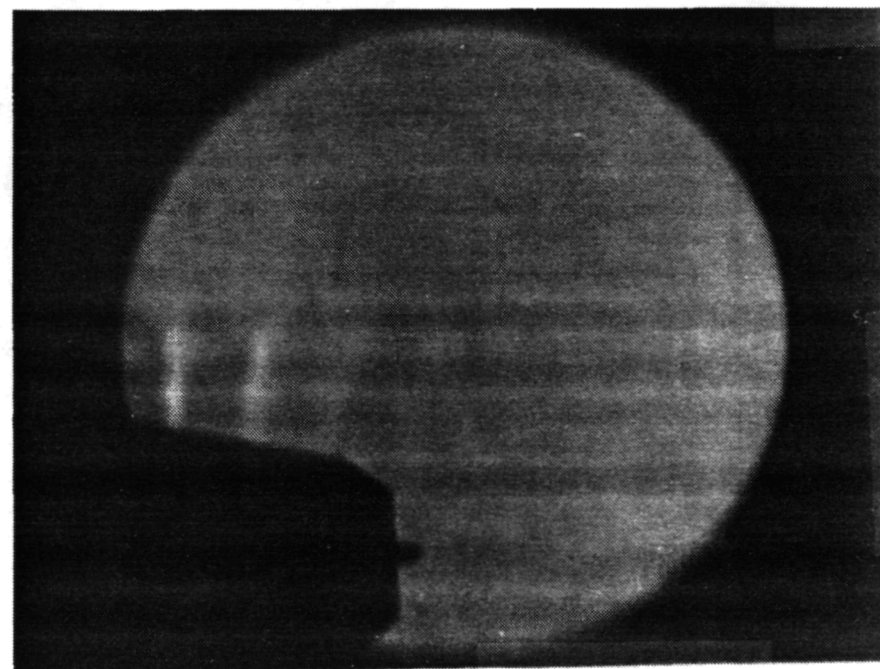
1440

ORIGINAL PAGE IS
OF POOR QUALITY

Configuration 5
Test Point 1521
Shadowgraph No. 4



Configuration 5
Test Point 1521
Shadowgraph No. 5

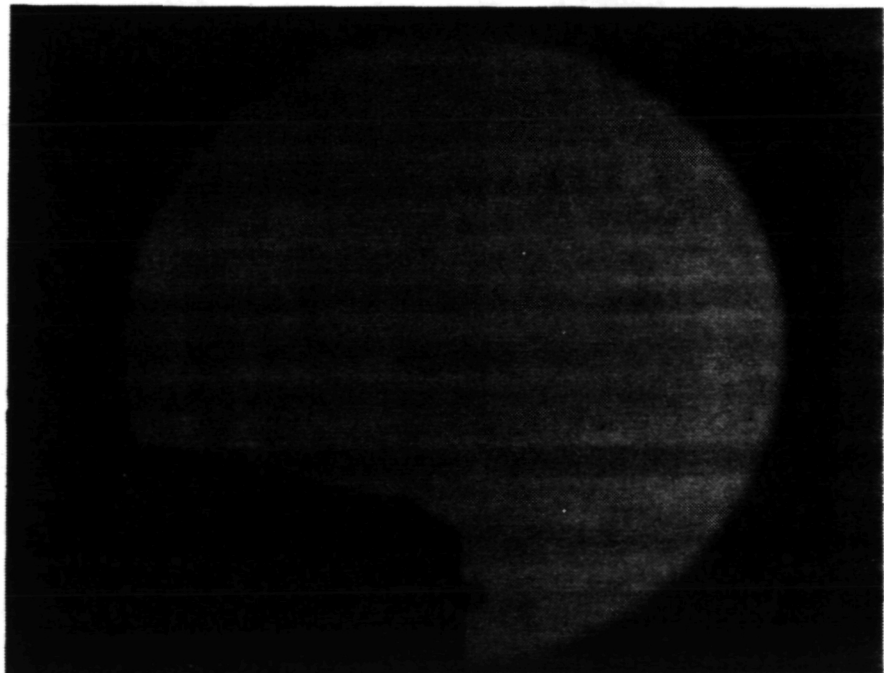
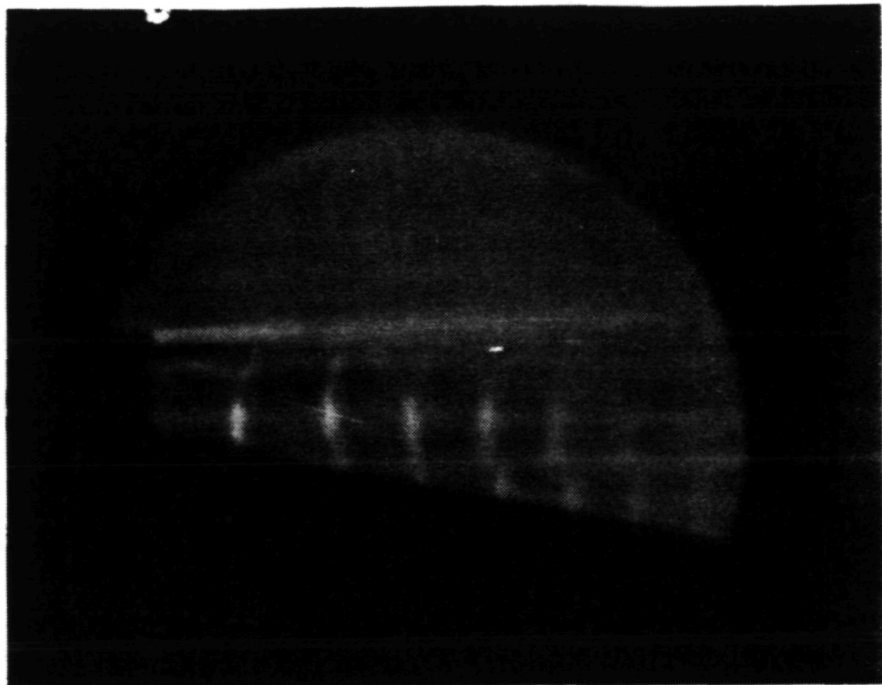


ORIGINAL PAGE IS
OF POOR QUALITY

Model	Test Point	P _r	T _T , (°R)	V _j (F/s)	V _{a/c} (F/s)
5	513	3.12	1717	2405	0

Configuration	5
Test Point	513
Shadowgraph No.	7

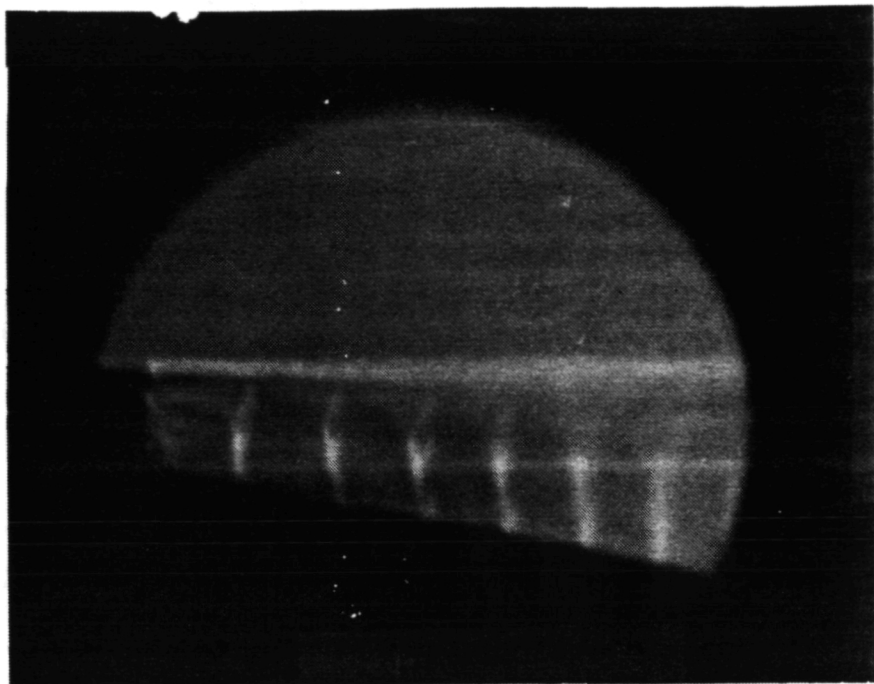
Configuration	5
Test Point	513
Shadowgraph No.	6



ORIGINAL PAGE IS
OF POOR QUALITY

Model	Test Point	P_r	T_r , (°R)	V_j (ft/s)	$V_{a/c}$ (ft/s)
5	514	3.13	1725	2414	400

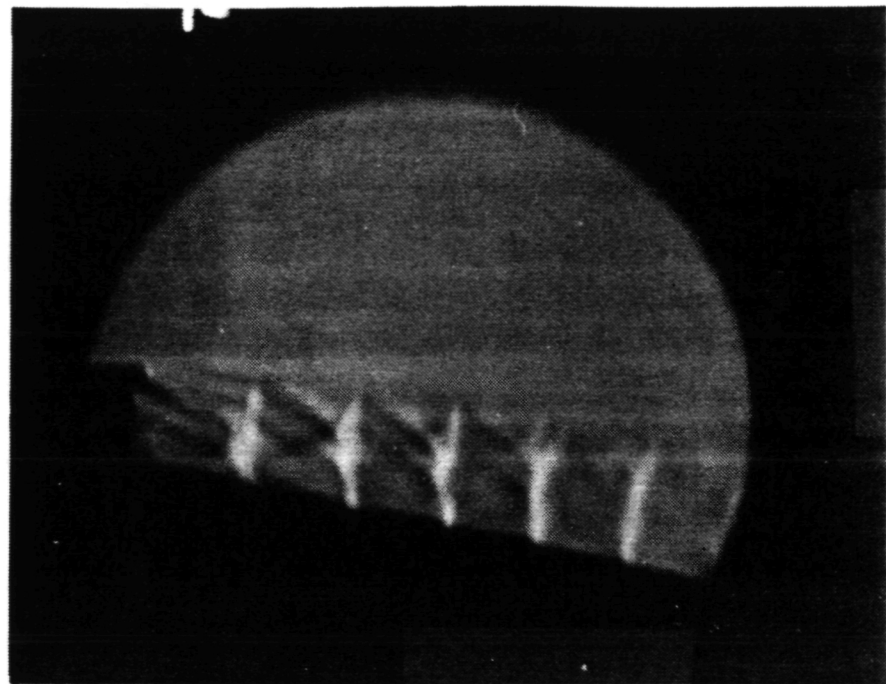
Configuration	<u>5</u>
Test Point	<u>514</u>
Shadowgraph No.	<u>8</u>



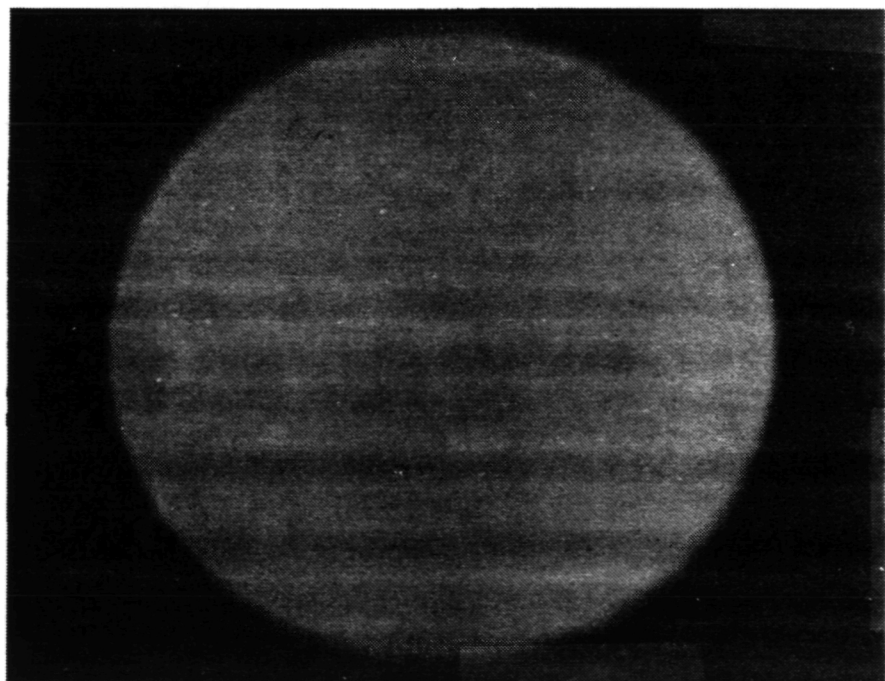
1443

ORIGINAL PAGE IS
OF POOR QUALITY

Configuration	5
Test Point	1514
Shadowgraph No.	11



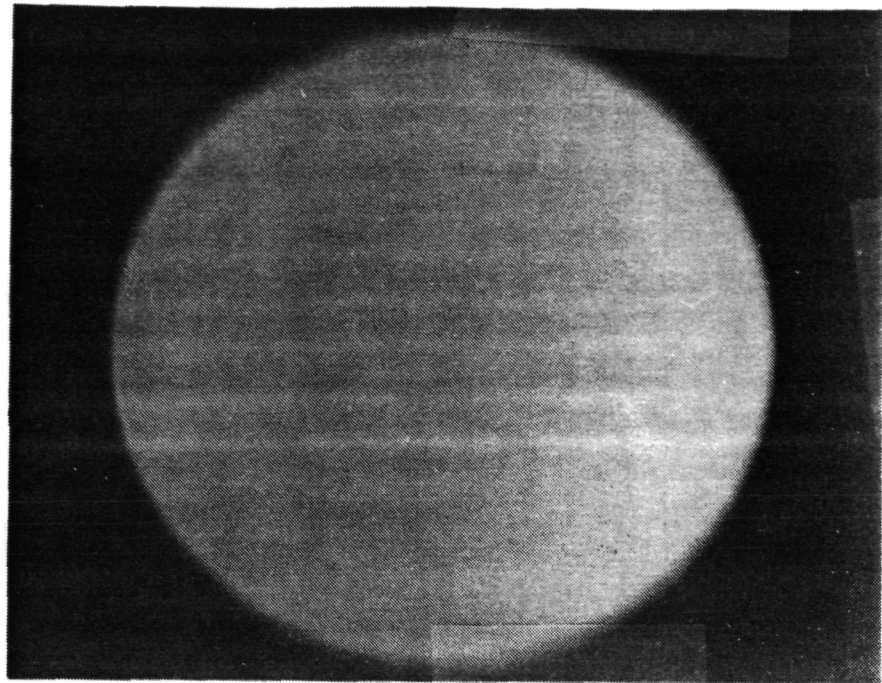
Configuration	5
Test Point	1514
Shadowgraph No.	12



1444

ORIGINAL PAGE IS
OF POOR QUALITY

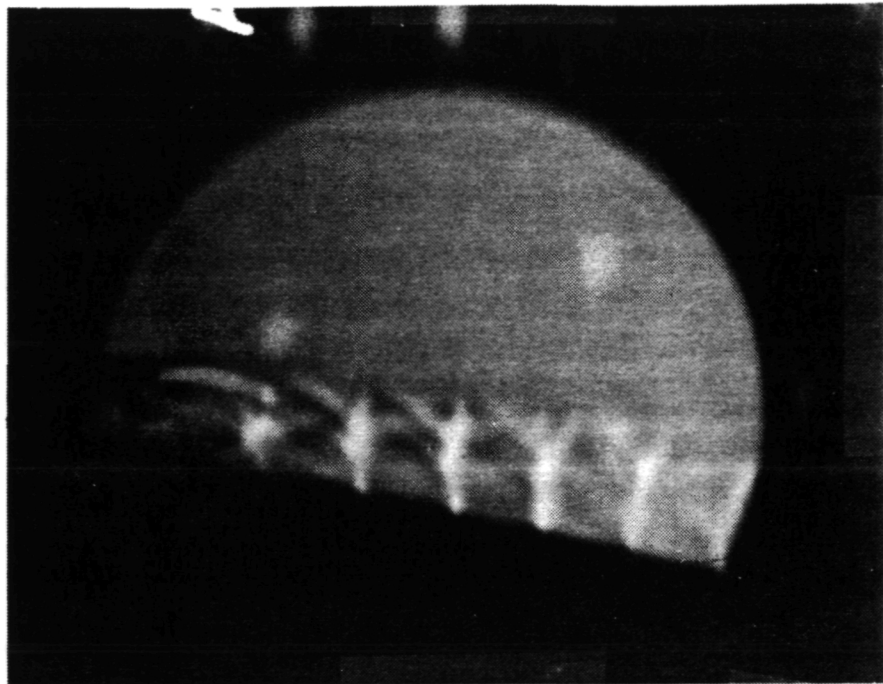
Configuration	<u>5</u>
Test Point	<u>1514</u>
Shadowgraph No.	<u>13</u>



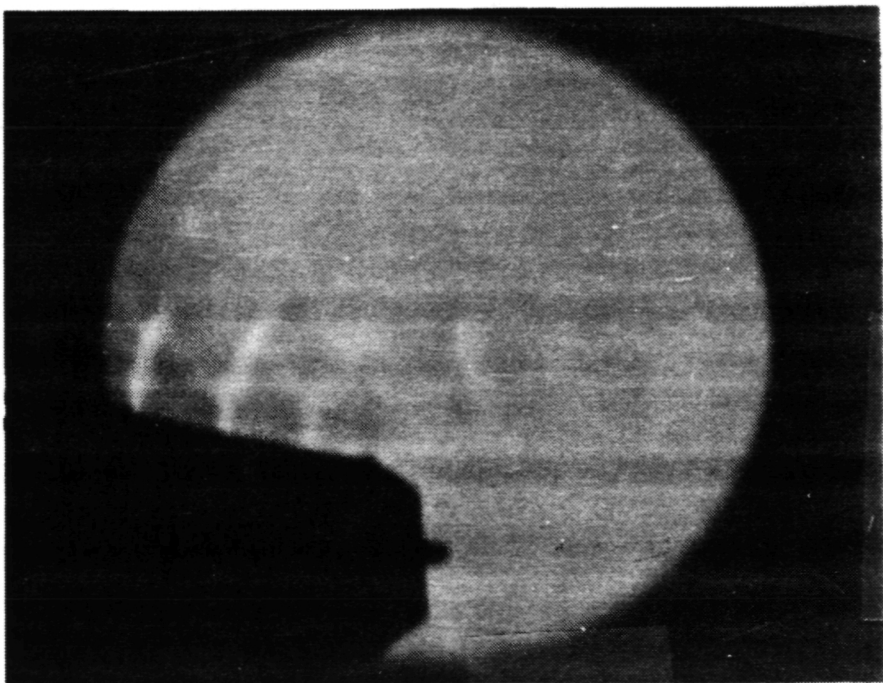
1445

ORIGINAL PAGE IS
OF POOR QUALITY

Configuration 5
Test Point 1522
Shadowgraph No. 14

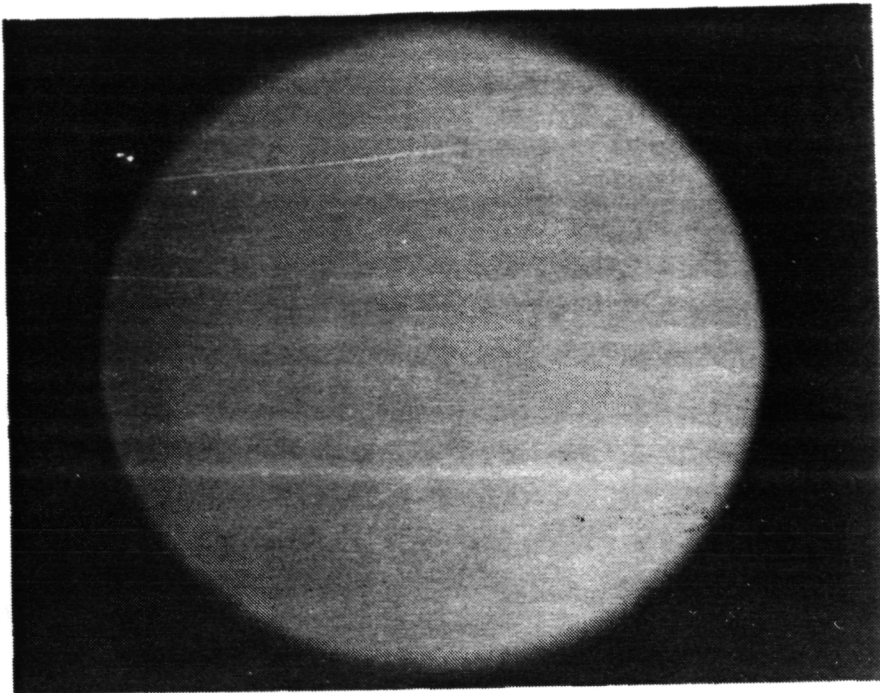


Configuration 5
Test Point 1522
Shadowgraph No. 15



ORIGINAL PAGE IS
OF POOR QUALITY

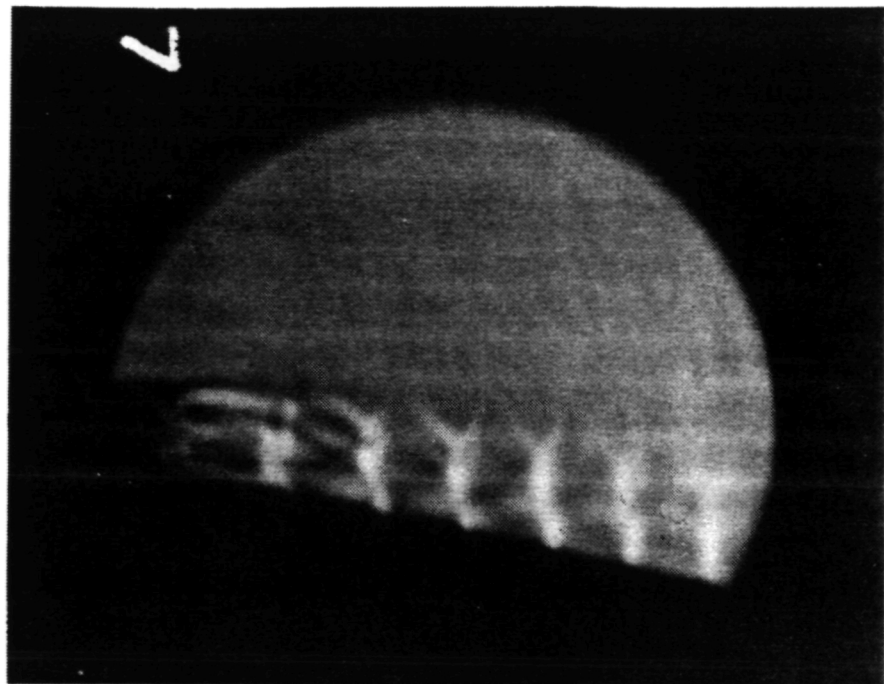
Configuration 5
Test Point 1522
Shadowgraph No. 16



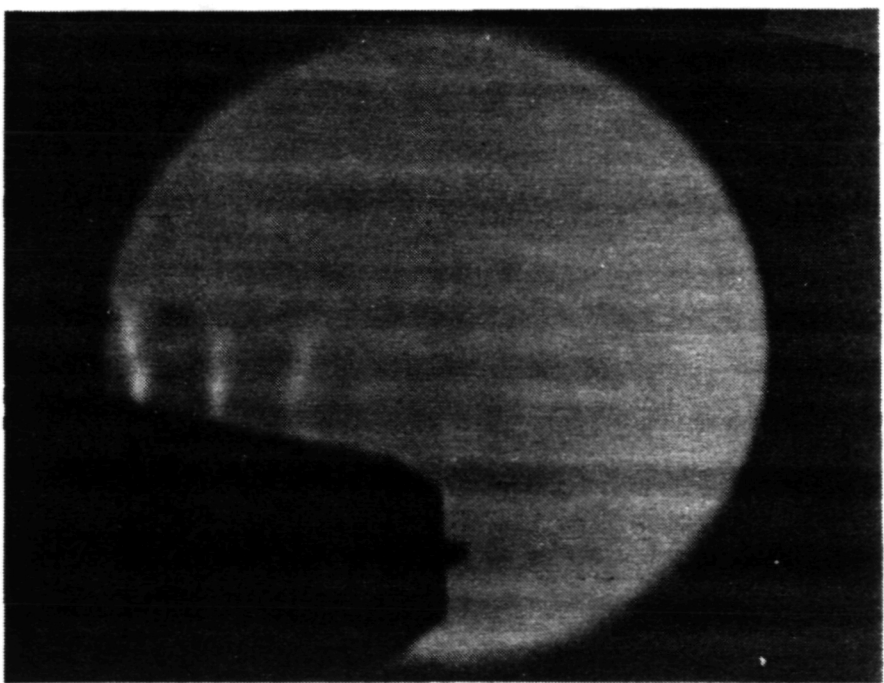
1547

ORIGINAL PAGE IS
OF POOR QUALITY

Configuration	5
Test Point	2513
Shadowgraph No.	20



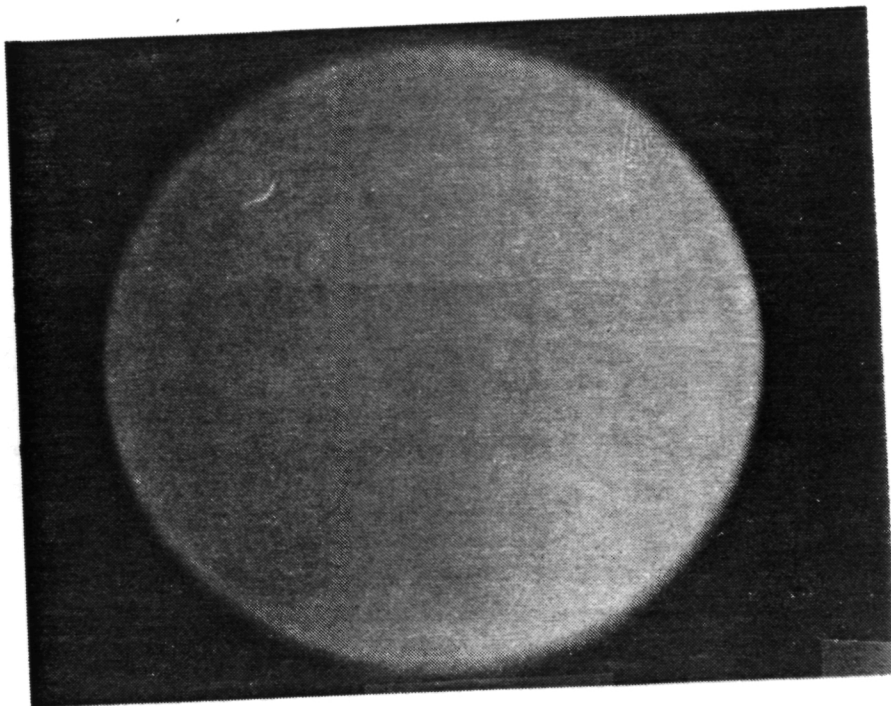
Configuration	5
Test Point	2513
Shadowgraph No.	21



1448

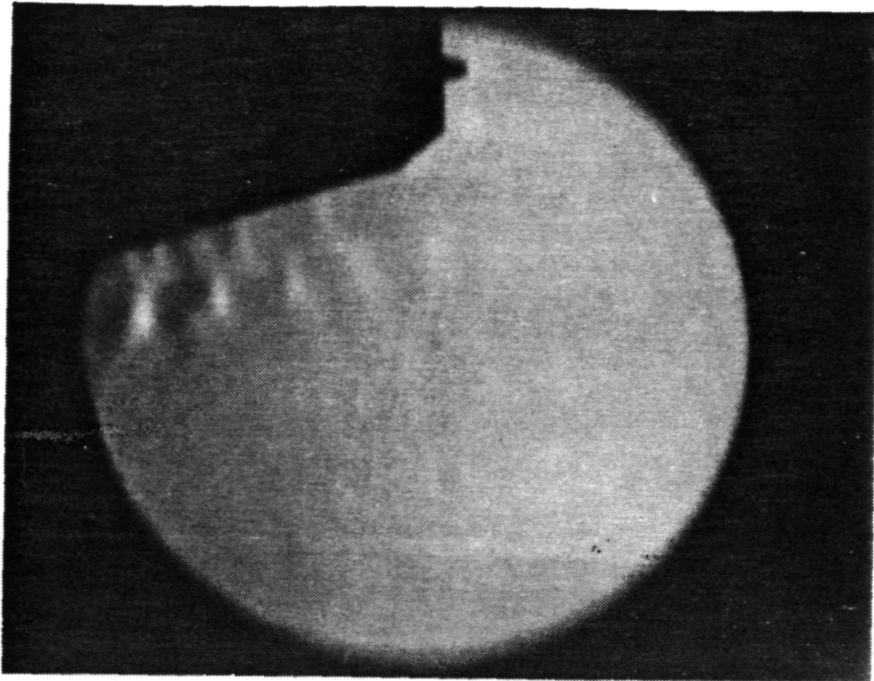
ORIGINAL PAGE IS
OF POOR QUALITY

Configuration 5
Test Point 7513
Shadowgraph No. 22

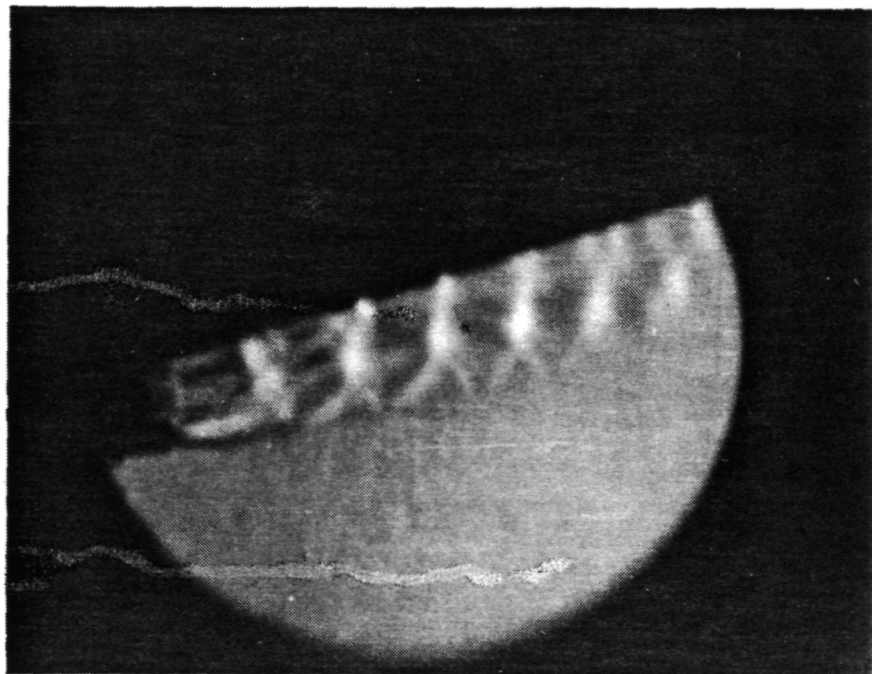


1414

ORIGINAL PAGE IS
OF POOR QUALITY



Configuration	5
Test Point	7513
Shadowgraph No.	24



Configuration	5
Test Point	7513
Shadowgraph No.	23

6.2.6 Shadowgraph Photos of Model 6

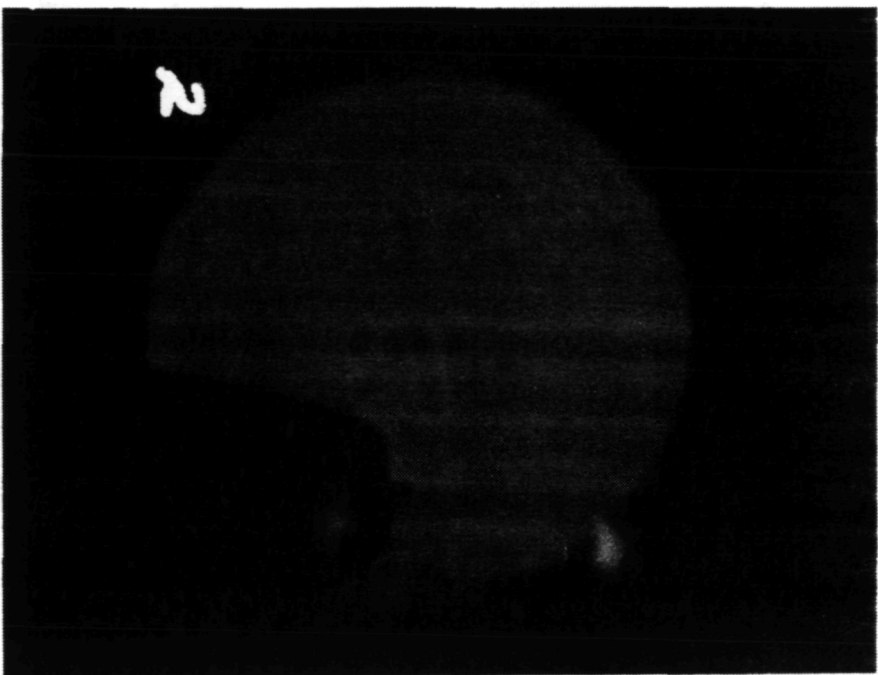
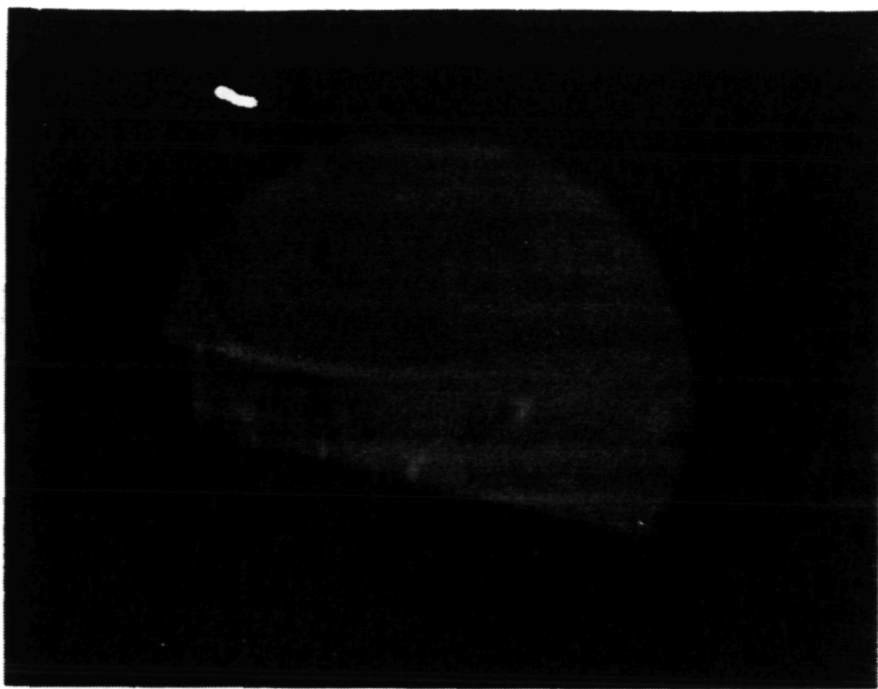
The shadowgraph test details associated with this model are provided in Table 6.7. The copies of the individual shadowgraph photographs taken with this model are presented next in this section.

ORIGINAL PAGE IS
OF POOR QUALITY

Model	Test Point	P_r	$T_T, ({}^{\circ}R)$	$V_j (f/s)$	$V_{a/c} (f/s)$
6	613	3.12	1735	2418	0

Configuration	6
Test Point	613
Shadowgraph No.	2

Configuration	6
Test Point	613
Shadowgraph No.	1

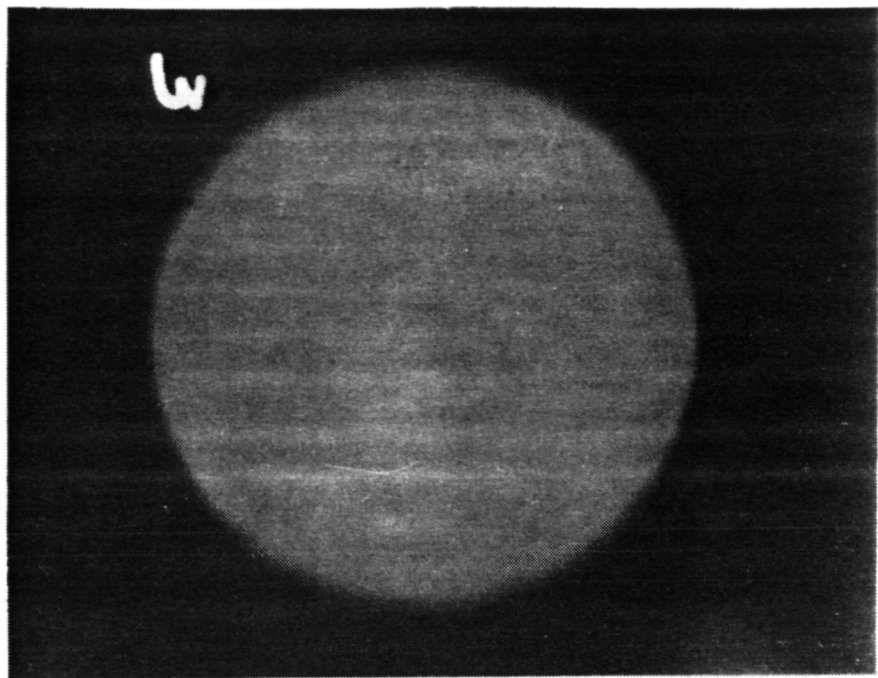


1452

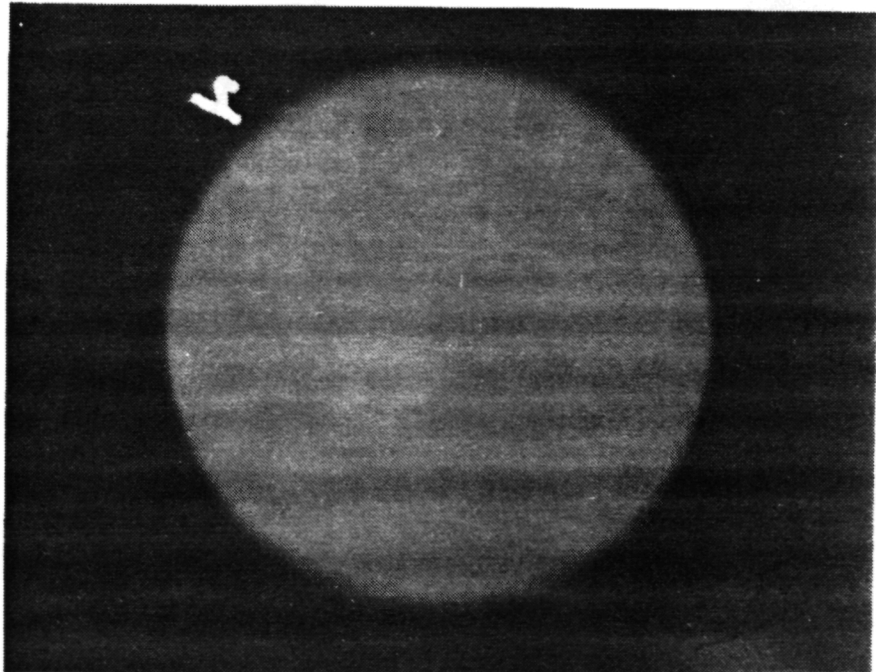
C - 2

ORIGINAL PAGE IS
OF POOR QUALITY

Configuration 6
Test Point 613
Shadowgraph No. 3

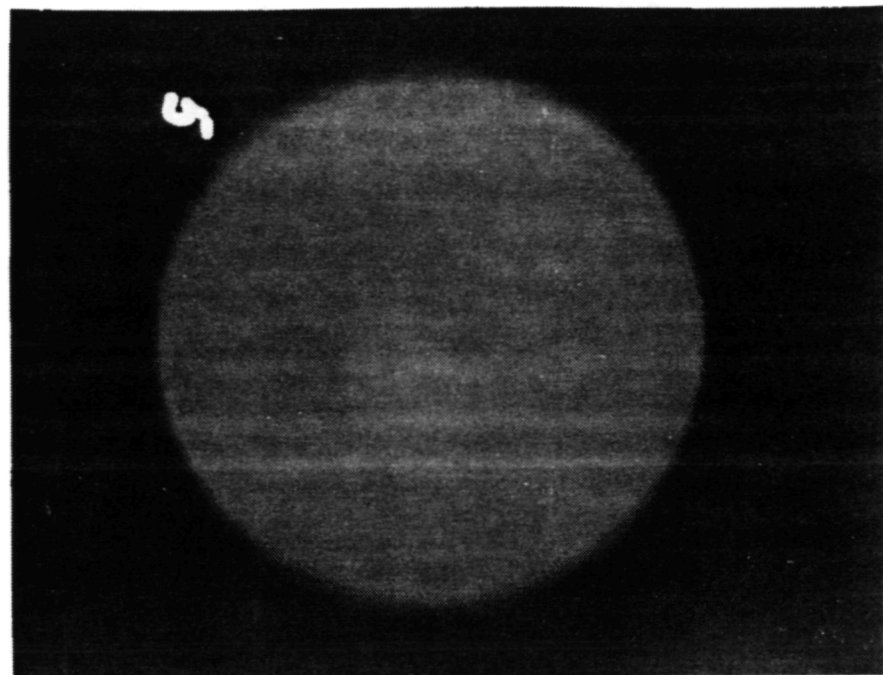


Configuration 6
Test Point 613
Shadowgraph No. 4



ORIGINAL PAGE IS
OF POOR QUALITY

Configuration	<u>6</u>
Test Point	<u>613</u>
Shadowgraph No.	<u>5</u>



ORIGINAL PAGE IS
OF POOR QUALITY.

Model	Test Point	P_r	T_r^* (°R)	V_j (ft/s)	$V_{a/c}$ (ft/s)
6	614	3.13	1711	2404	400

Configuration	6
Test Point	614
Shadowgraph No.	7

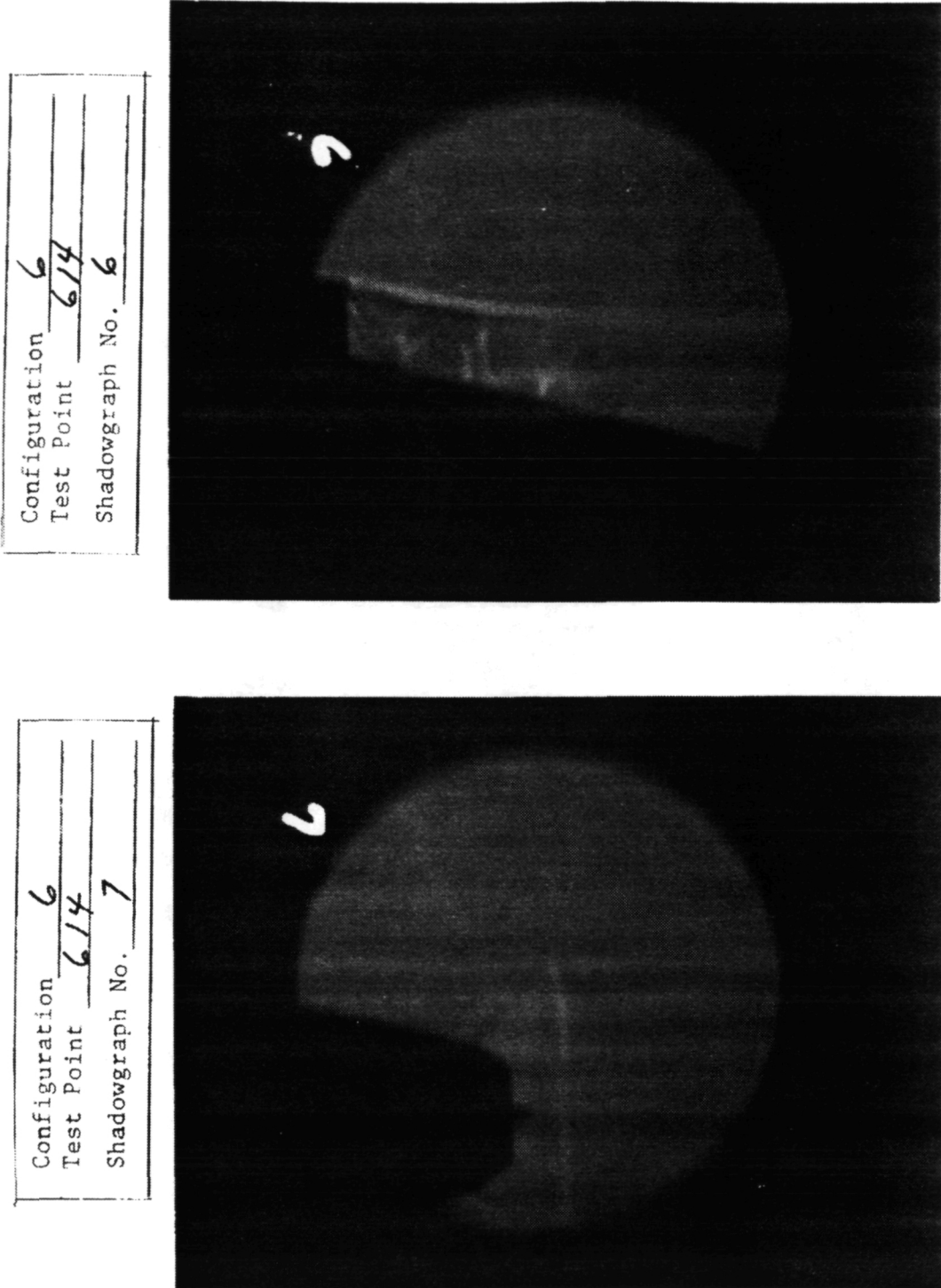
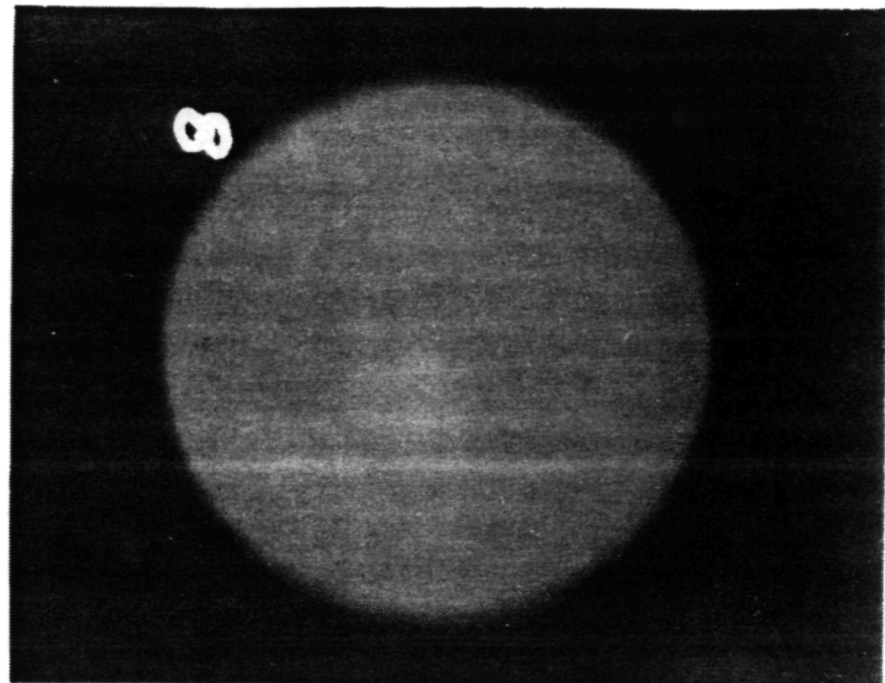


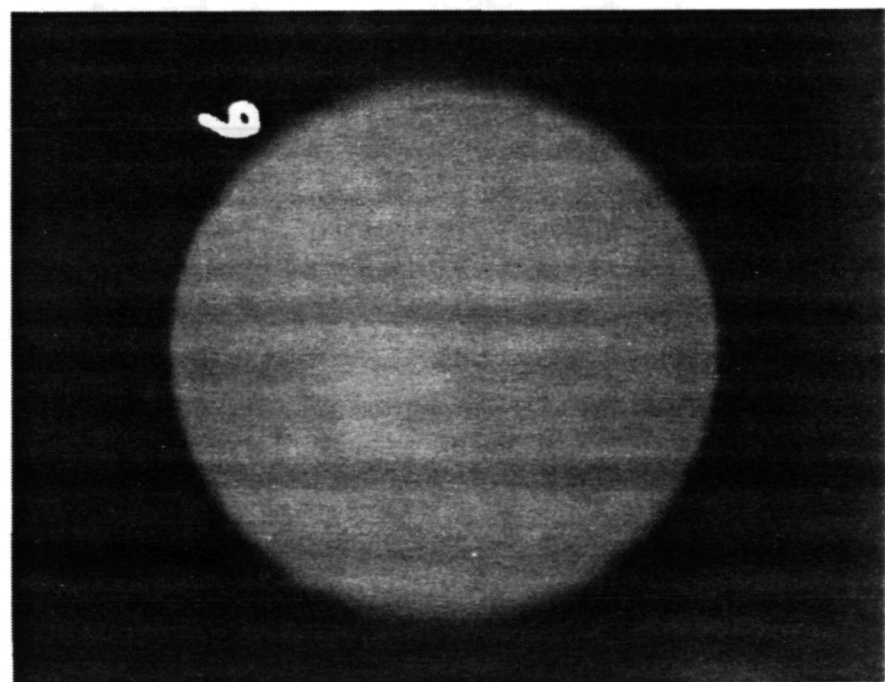
Figure 6-50 Shadowgraph Photos: Multi-Element C-D Suppressor Plug Nozzle (Model 6): With Free-Jet.

ORIGINAL PAGE IS
OF POOR QUALITY

Configuration 6
Test Point 614
Shadowgraph No. 8

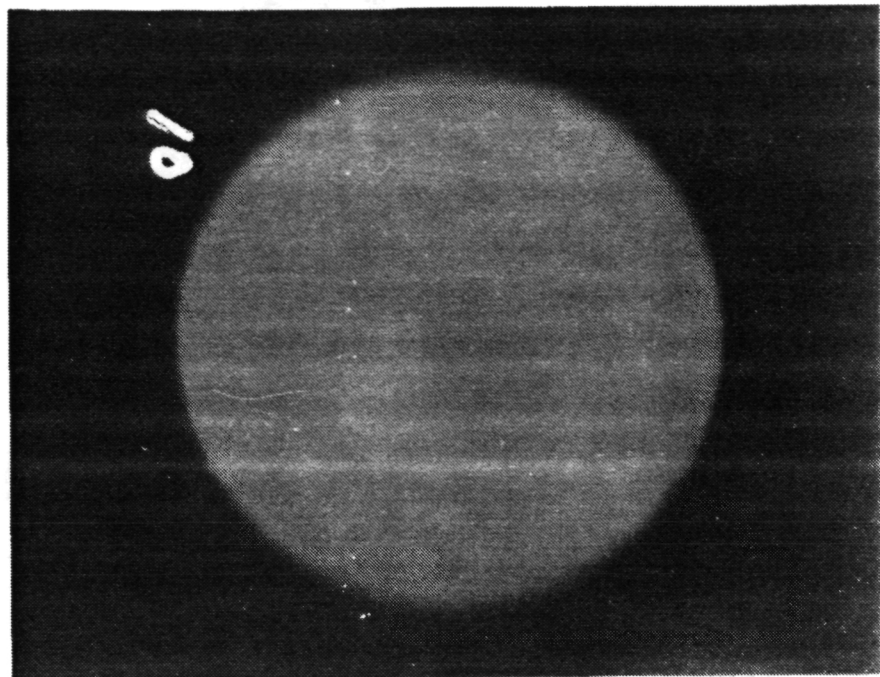


Configuration 6
Test Point 614
Shadowgraph No. 9



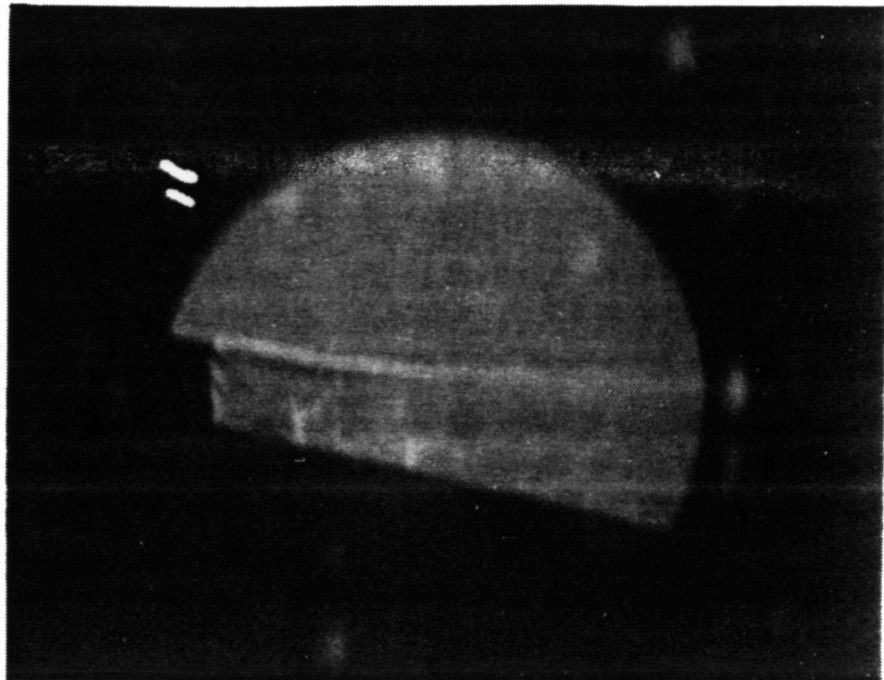
ORIGINAL PAGE IS
OF POOR QUALITY.

Configuration	6
Test Point	614
Shadowgraph No.	10



ORIGINAL PAGE IS
OF POOR QUALITY

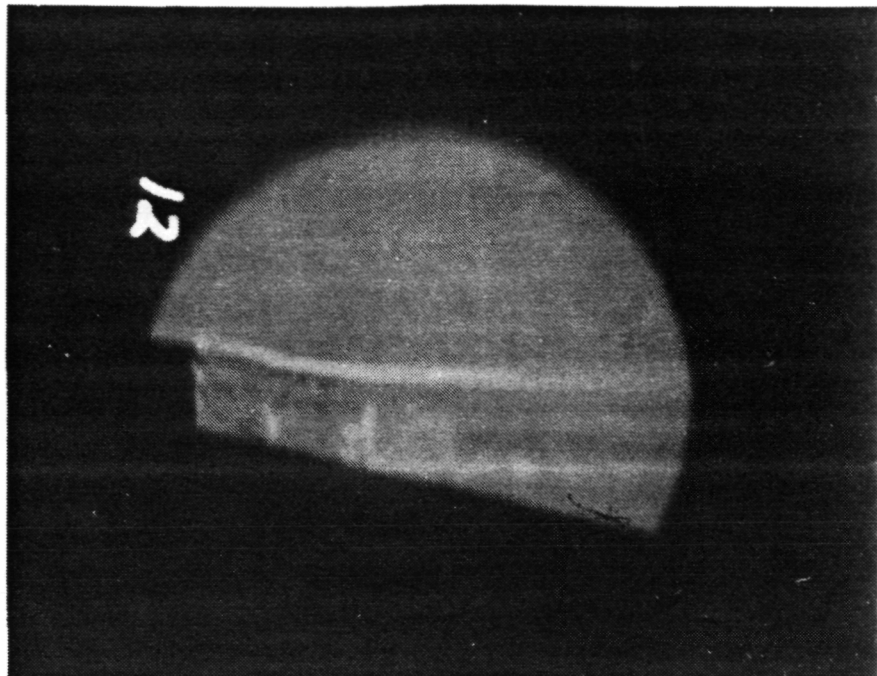
Configuration	6
Test Point	4614
Shadowgraph No.	//



1455

ORIGINAL PAGE IS
OF POOR QUALITY

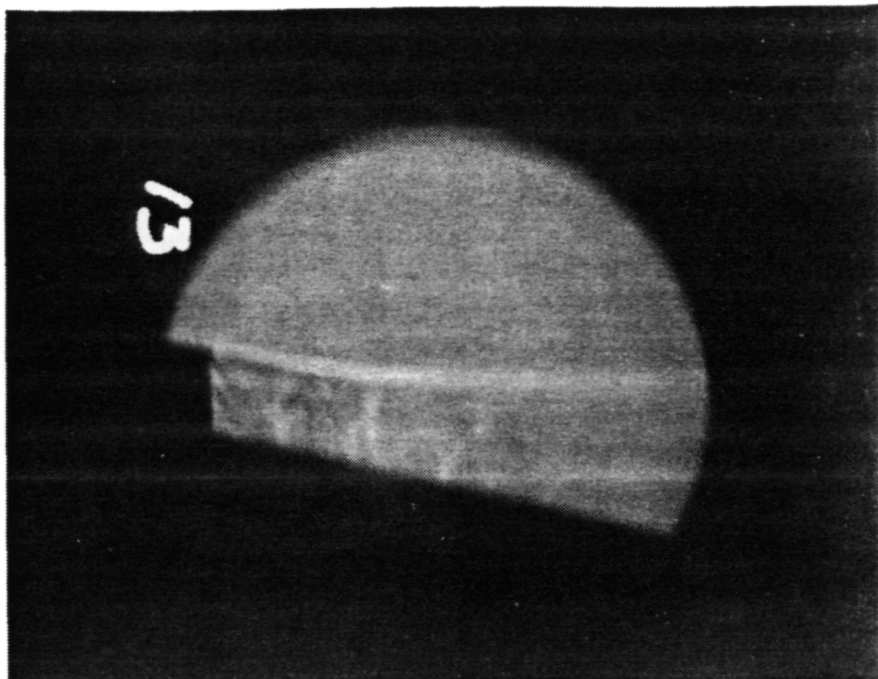
Configuration	<u>6</u>
Test Point	<u>4612</u>
Shadowgraph No.	<u>12</u>



1453

ORIGINAL PAGE IS
OF POOR QUALITY.

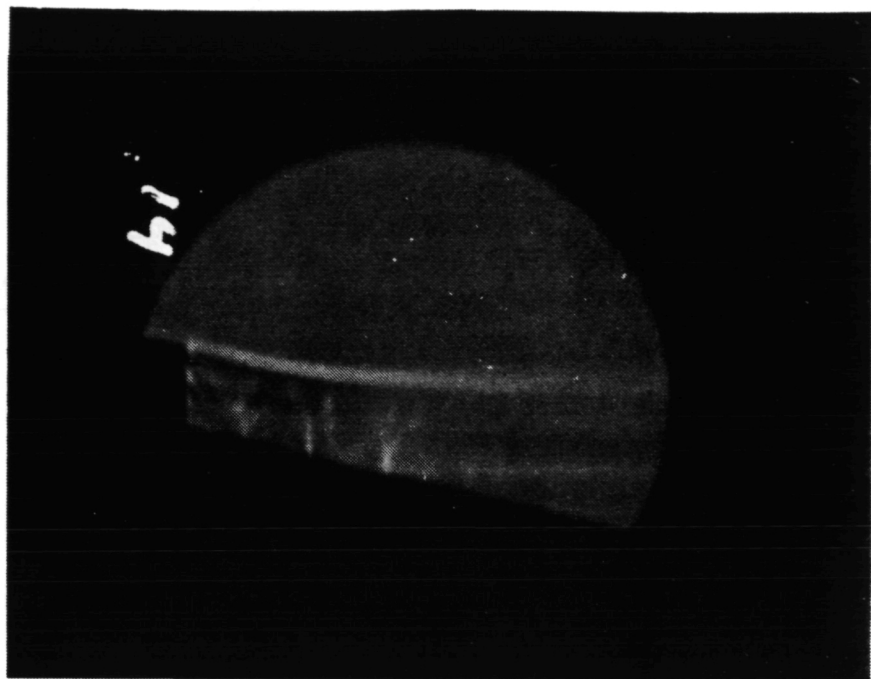
Configuration	<u>6</u>
Test Point	<u>4610</u>
Shadowgraph No.	<u>13</u>



1480

ORIGINAL PAGE IS
OF POOR QUALITY

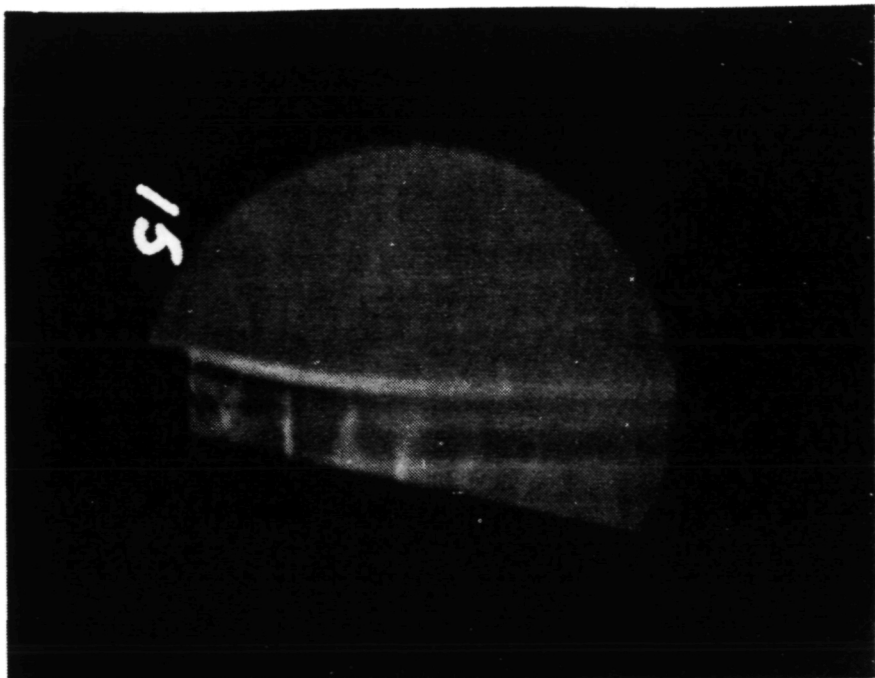
Configuration	<u>6</u>
Test Point	<u>4606</u>
Shadowgraph No.	<u>14</u>



1461

ORIGINAL PAGE IS
OF POOR QUALITY

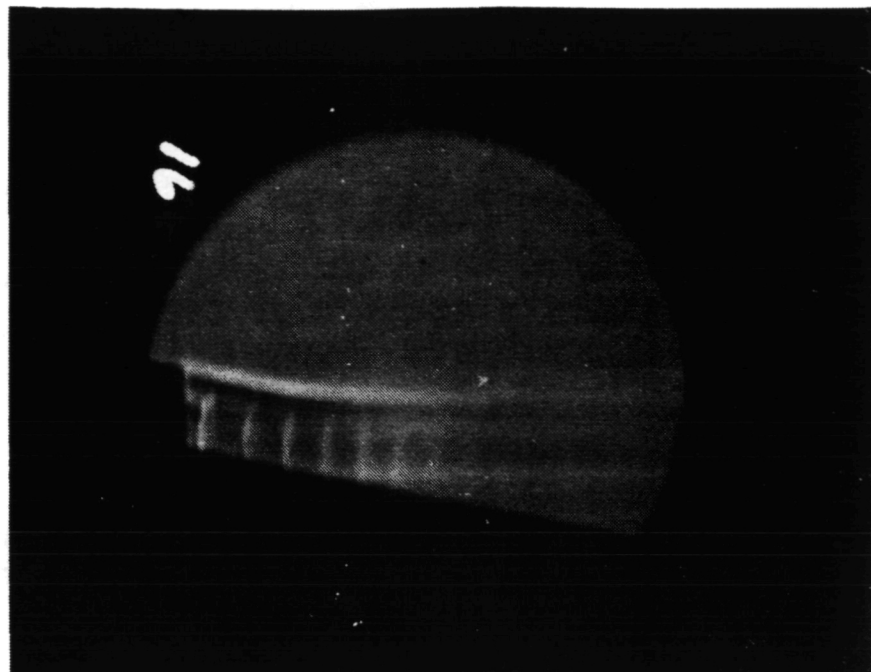
Configuration	<u>6</u>
Test Point	<u>4604</u>
Shadowgraph No.	<u>15</u>



1462

ORIGINAL PAGE IS
OF POOR QUALITY

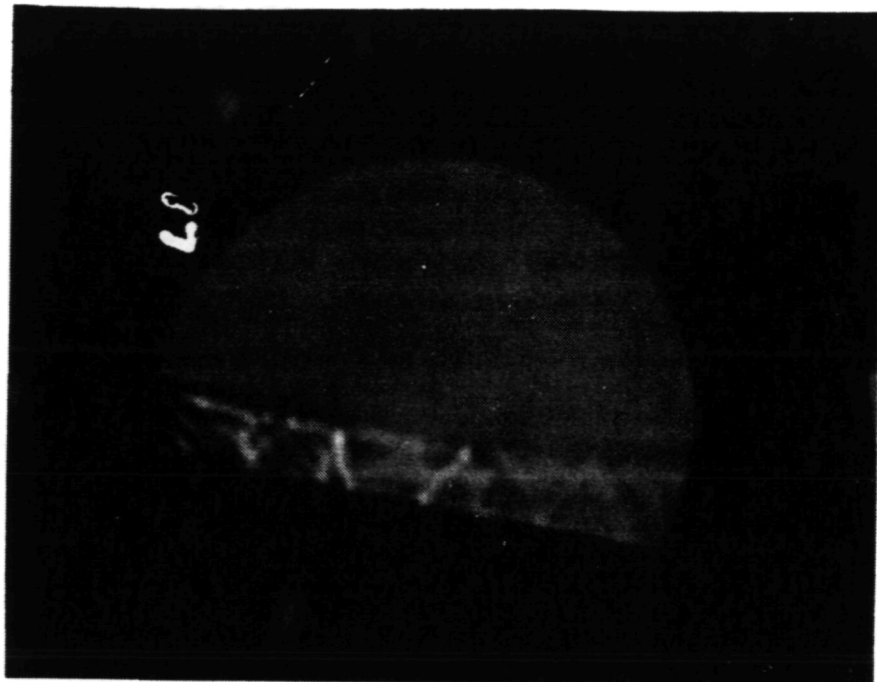
Configuration	6
Test Point	4602
Shadowgraph No.	16



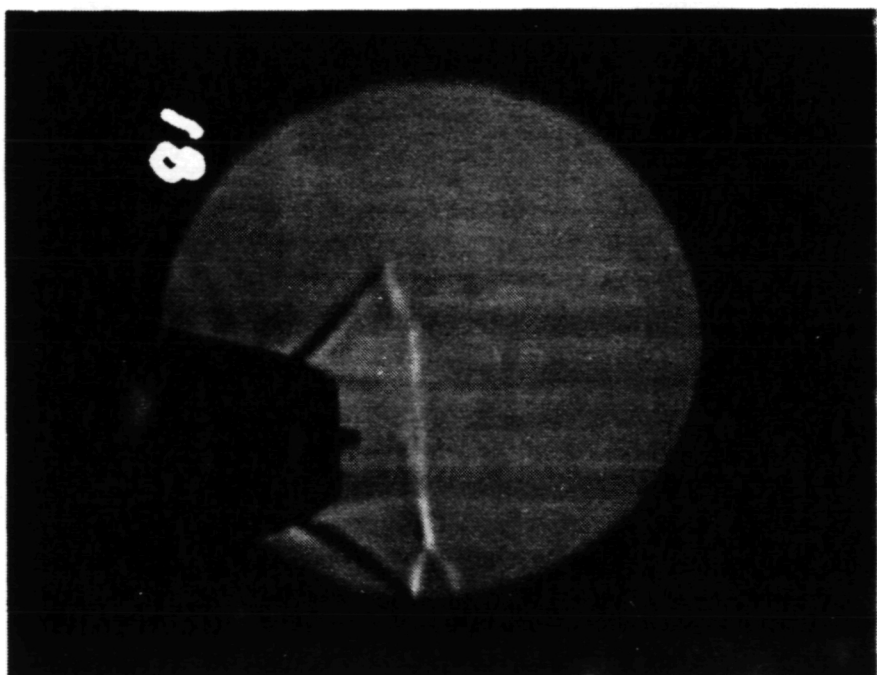
1463

ORIGINAL PAGE IS
OF POOR QUALITY

Configuration	6
Test Point	7614
Shadowgraph No.	17

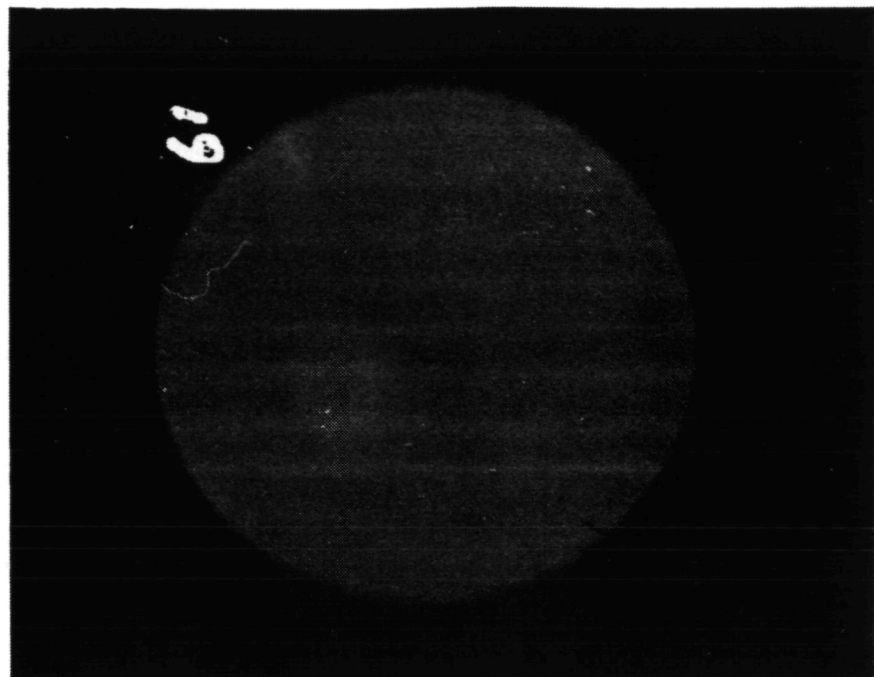


Configuration	6
Test Point	7614
Shadowgraph No.	18

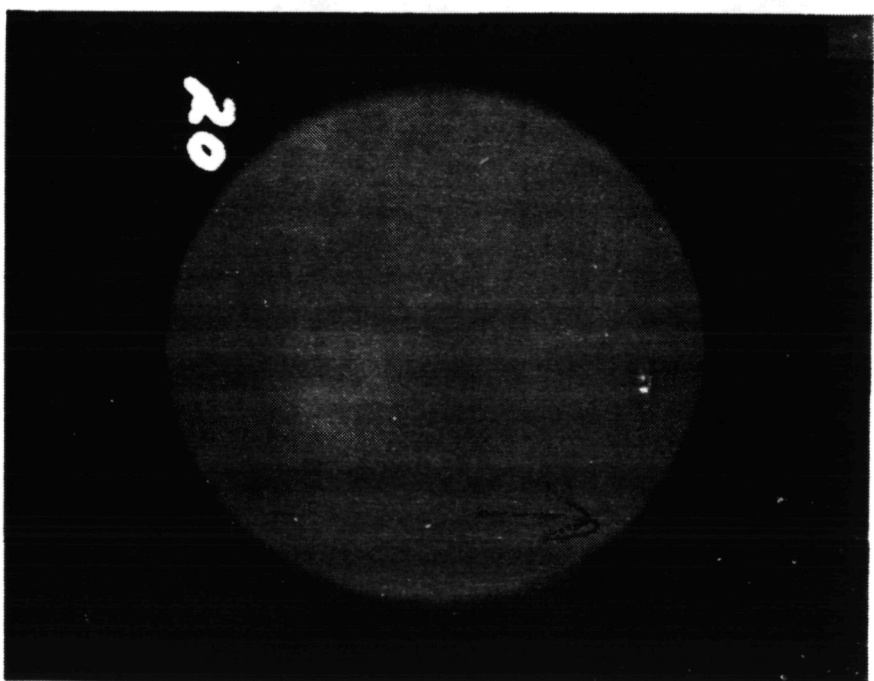


ORIGINAL PAGE IS
OF POOR QUALITY.

Configuration	<u>6</u>
Test Point	<u>7614</u>
Shadowgraph No.	<u>19</u>

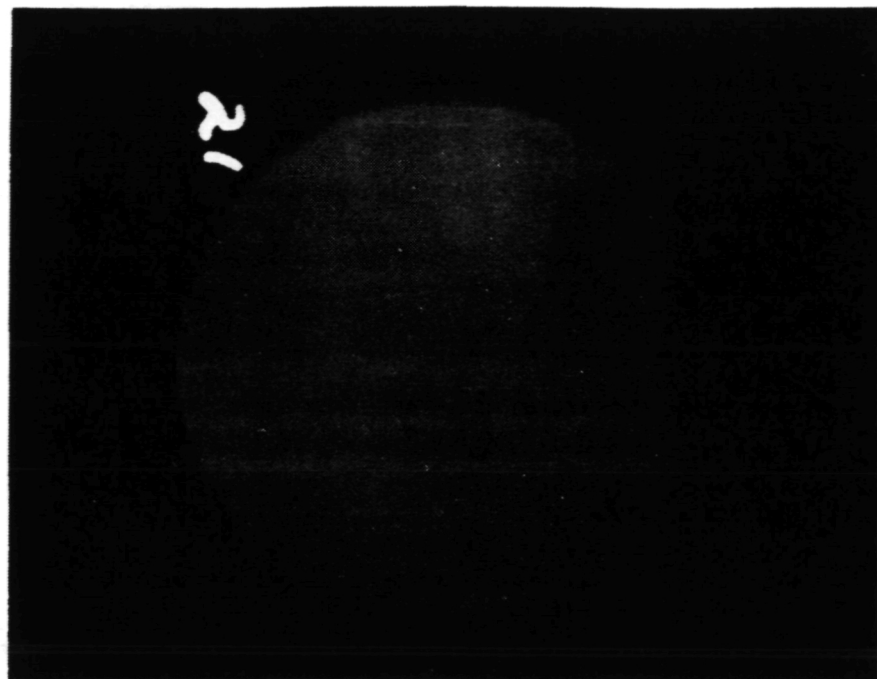


Configuration	<u>6</u>
Test Point	<u>7614</u>
Shadowgraph No.	<u>20</u>



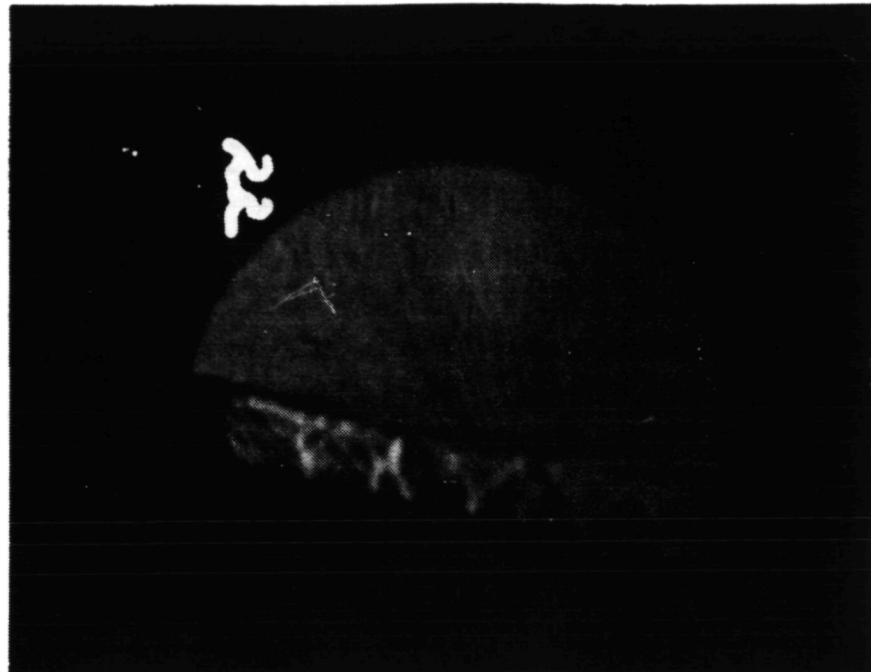
ORIGINAL PAGE IS
OF POOR QUALITY

Configuration	<u>6</u>
Test Point	<u>2614</u>
Shadowgraph No.	<u>21</u>



ORIGINAL PAGE IS
OF POOR QUALITY

Configuration	<u>6</u>
Test Point	<u>7613</u>
Shadowgraph No.	<u>22</u>

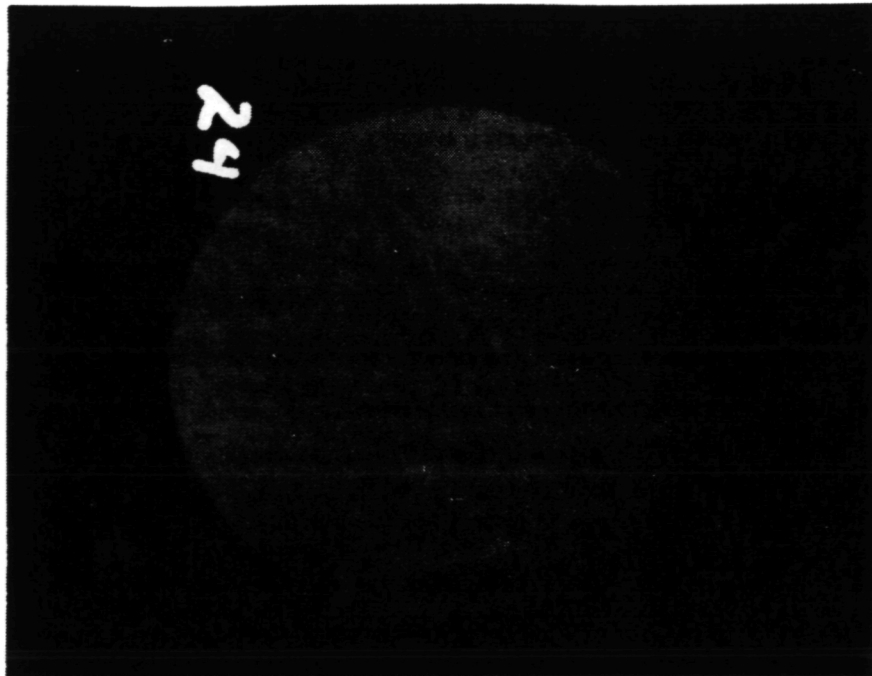


Configuration	<u>6</u>
Test Point	<u>7613</u>
Shadowgraph No.	<u>23</u>

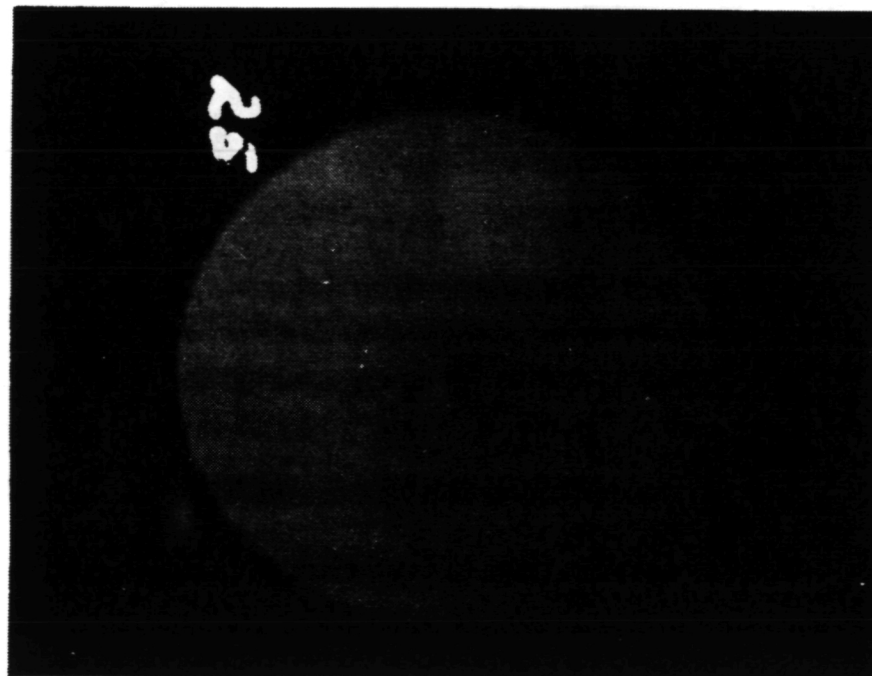


ORIGINAL PAGE IS
OF POOR QUALITY.

Configuration	6
Test Point	7613
Shadowgraph No.	24

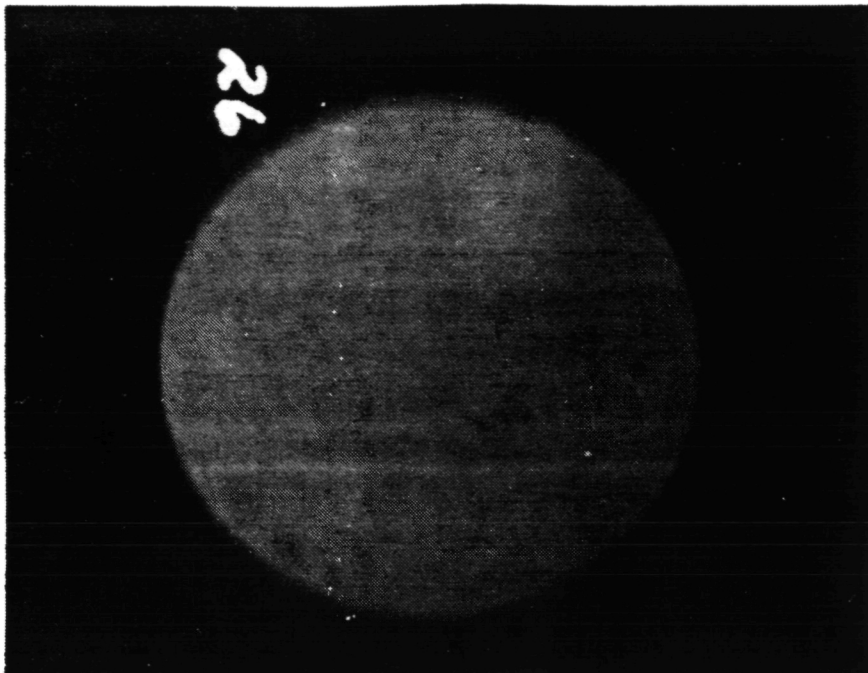


Configuration	6
Test Point	7613
Shadowgraph No.	25



ORIGINAL PAGE IS
OF POOR QUALITY

Configuration 6
Test Point 2613
Shadowgraph No. 26



1462

7.0 STATIC PRESSURE DATA

In order to aid the acoustic and LV results in determining the shock-free operating conditions of the convergent-divergent Models 2,4 and 6, diagnostic static pressure instrumentation has been added on the divergent sections of these model nozzles. In addition, base pressure instrumentation has been applied in the base regions of the chutes of Model 6 in order to obtain an assessment of the base drag and its impact on the nozzle performance. The measured static pressure data are summarized in this section.

7.1 DIAGNOSTIC STATIC PRESSURE DATA

Instrumentation details with Models 2, 4 and 6 are provided in Section 2.0. The locations and identifications of the P_s taps are summarized in this section in Figures 7.1 through 7.3 as follows:

- o 15 P_s taps along the flow passage of convergent-divergent circular nozzle (Figure 7.1)
- o 13 P_s taps on the plug surface and 7 P_s taps on the inner surface of the outer flowpath of the annular convergent-divergent nozzle (Figure 7.2)
- o 24 P_s taps within the convergent-divergent flow passage of the suppressor configuration (Figure 7.3)

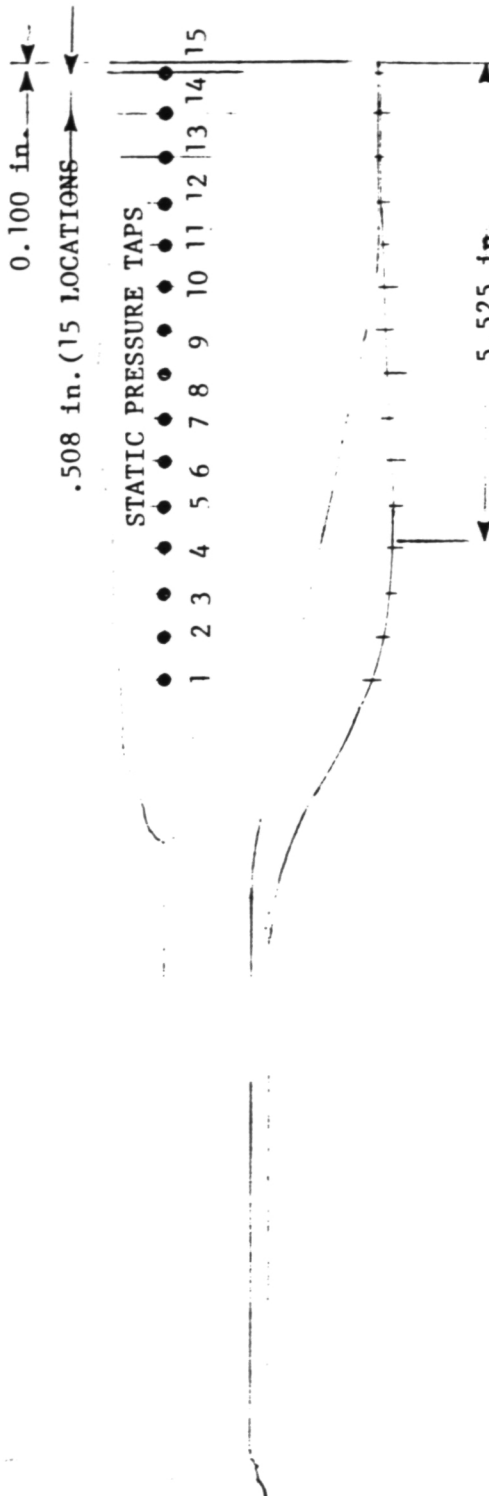
The test data were obtained simultaneously with the acoustic test results. Hence, the aerodynamic flow conditions summarized in Section 3.0 of Volume I for Configurations 2, 4 and 6, respectively, represent also the test points during which the P_s data were obtained.

Tables 7.1 through 7.3 summarize the measured diagnostic static pressure data with Models 2, 4 and 6, respectively.

PRECEDING PAGE BLANK NOT FILMED

SHOCK CELL MODEL 2 (CIRCULAR C-D)

ORIGINAL PAGE IS
OF POOR QUALITY



TYPICAL INSTALLATION
SENSING PORT PERPENDICULAR
TO FLOW SURFACE



1472

Figure 7.1 Application of P_s Instrumentation to Circular Convergent-Divergent Nozzle (Model 2)

ORIGINAL PAGE IS
OF POOR QUALITY

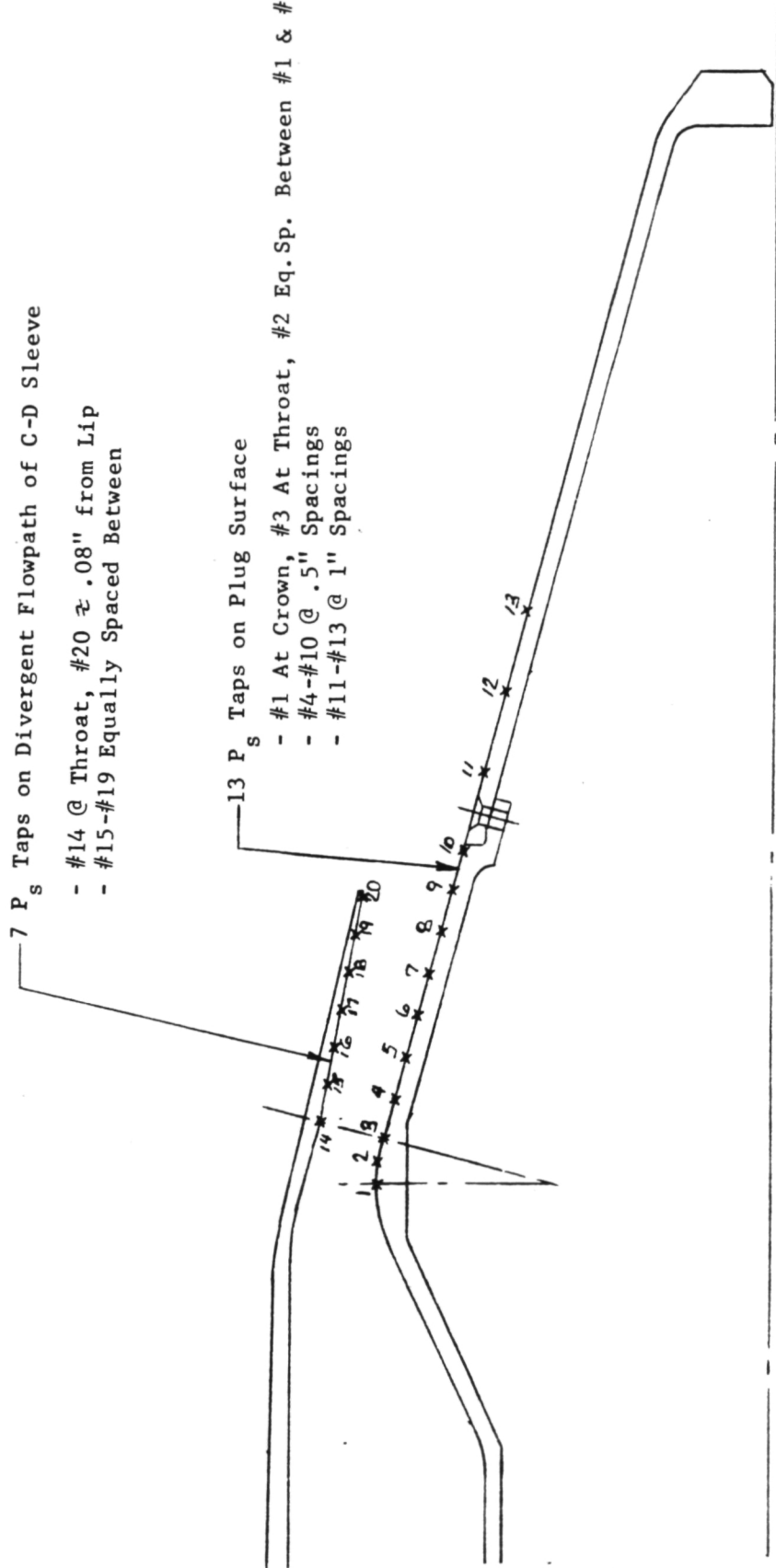


Figure 7.2. Application of P_s Instrumentation to Annular Convergent-Divergent Nozzle (Model 4)

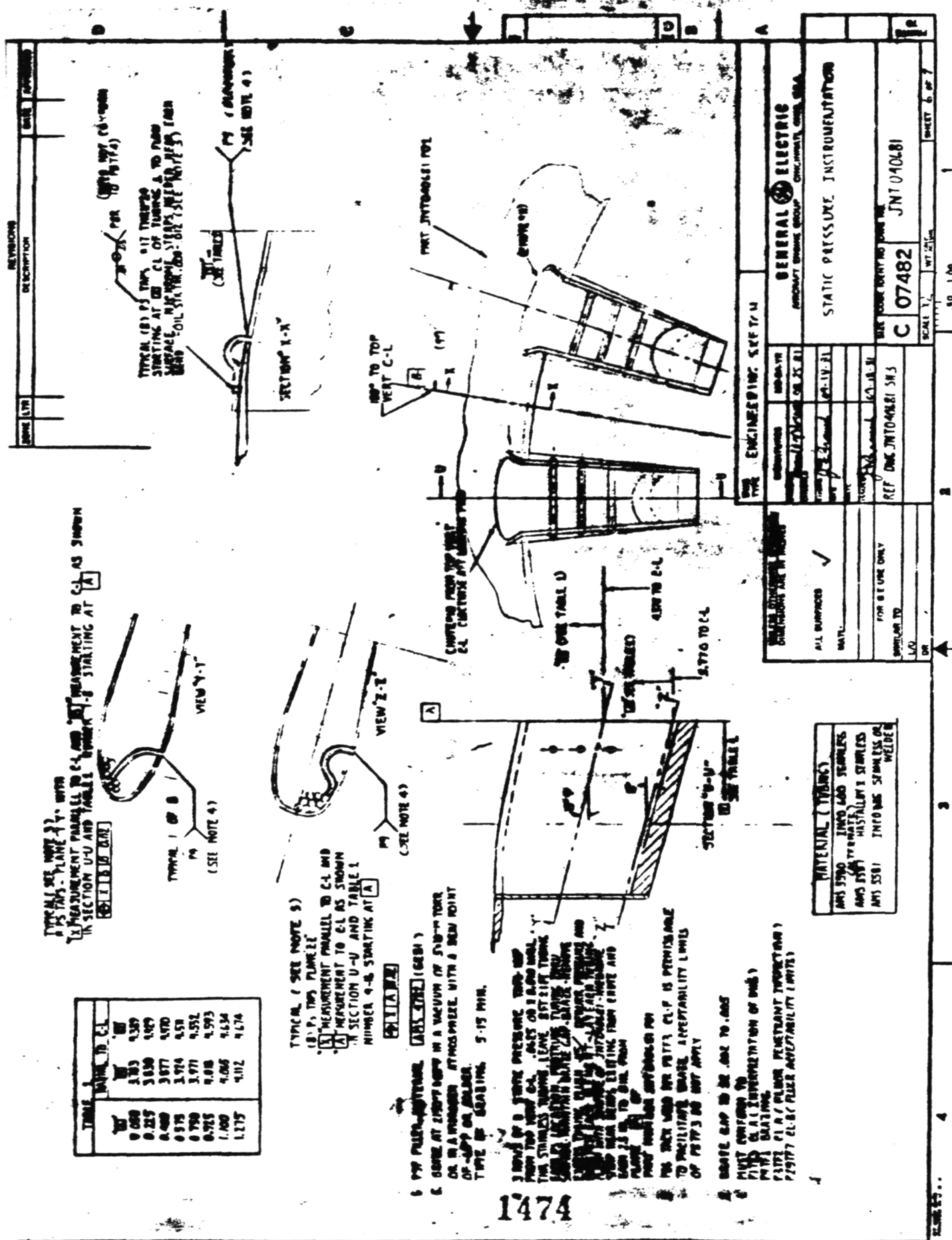


Figure 7.3 Application of P₁ Instrumentation to C-D Flow Passage of 20-Shallow Chute Suppressor Nozzle (Model 6).

Table 7.1. Diagnostic Static Pressure Data of Circular Convergent-Divergent Nozzle (Model 2)

Acous. Test Point	P _a nsia	Tap Number (See Figure 6.1 for Location Details)							
		1	2	3	4	5	6	7	8
201	14.44977	32.701	29.283	25.174	19.476	16.814	16.601	15.962	14.961
202	14.2968	32.182	29.112	25.063	19.365	16.235	16.605	16.835	14.793
203	14.4212	34.449	30.869	26.536	20.466	17.722	17.717	16.546	15.662
204	14.2944	34.424	30.768	26.592	20.535	17.750	17.729	16.798	15.632
205	14.429	35.498	31.792	27.354	21.129	18.282	18.262	17.356	16.157
206	14.2960	35.385	31.725	27.321	21.090	18.220	18.191	17.252	16.036
207	14.4321	36.303	32.515	27.971	21.624	18.692	18.668	17.750	16.579
208	14.2944	36.215	32.479	27.975	21.601	18.676	18.629	17.669	16.937
211	14.4277	36.839	33.063	28.428	21.586	19.019	19.010	18.067	16.812
212	14.2988	36.699	32.900	28.349	21.861	18.936	18.882	17.906	16.656
213	14.4257	37.521	33.605	28.922	22.355	19.330	19.318	18.354	17.081
214	14.2973	37.311	33.436	28.821	22.267	19.241	19.189	19.201	16.941
215	14.4272	38.266	34.279	29.489	22.788	19.699	19.684	19.694	17.395
216	14.3003	38.016	34.080	29.811	22.679	18.610	19.556	18.562	17.269
219	14.4292	38.713	34.694	29.859	23.070	19.952	19.939	18.942	17.631
220	14.2973	38.535	34.541	29.767	23.005	19.995	19.828	18.807	17.500
221	14.4253	39.611	35.674	30.692	23.734	20.526	20.575	19.679	18.128
222	14.2988	39.672	35.561	30.638	23.664	20.499	20.391	19.349	18.000
223	14.4296	42.156	37.783	32.527	25.150	21.755	21.726	20.618	19.152
224	14.2915	41.902	37.633	32.422	25.060	21.607	21.578	20.470	19.038
226	14.2993	31.185	27.959	28.071	18.582	16.069	16.026	15.221	14.159
253	14.4248	46.448	41.707	35.893	27.763	24.017	23.568	22.701	21.155
1205	14.2959	36.400	32.584	27.931	21.374	18.448	18.426	17.530	16.323
1206	14.2998	36.471	32.621	27.971	21.462	16.472	16.430	17.509	16.306
1207	14.2949	37.049	33.182	28.410	21.736	18.776	18.739	17.830	16.588
1208	14.3096	37.133	33.189	28.473	21.765	18.780	18.746	17.817	16.578
1211	14.2929	37.645	33.678	28.874	22.088	19.013	19.057	18.181	16.853
1213	14.2983	37.725	33.740	28.939	22.137	19.105	19.063	18.131	16.953
1214	14.3022	38.262	34.238	29.347	22.456	19.394	19.354	18.414	17.131
1215	14.2939	38.854	34.732	29.814	22.816	19.699	19.664	18.711	17.395
1216	14.3007	38.914	34.818	29.856	22.838	19.704	19.659	18.676	17.369
1217	14.2968	39.441	35.285	30.252	23.136	19.973	19.939	18.963	17.638
1220	14.2927	39.5214	35.322	30.274	23.145	19.963	19.928	18.938	17.601
1221	14.3007	40.047	35.805	30.712	23.486	20.276	20.253	19.258	17.904
1222	14.2951	40.916	35.797	30.617	23.479	20.232	20.204	19.209	17.848

* See Section 3.0 of Vol. I
for Aerodynamic Flow
Conditions

ORIGINAL PAGE IS
OF POOR QUALITY

Table 7.1. (Concluded)

ORIGINAL PAGE IS
OF POOR QUALITY

Accu. Test Point	P _s	Measured Static Pressure, psia (See Figure 6.1 For Location Details)						
		9	10	11	12	13	14	15
201	14.206	14.019	13.742	13.339	12.939	13.157	13.296	
202	14.572	13.953	13.692	13.214	12.824	12.857	13.125	
203	15.570	14.783	14.491	14.047	13.634	13.882	13.85	
204	15.479	14.793	14.998	14.050	13.602	13.745	13.848	
205	15.974	15.229	14.905	14.471	14.047	14.34	14.25	
206	15.900	15.197	14.889	14.48	13.959	14.083	14.086	
207	16.326	15.563	15.267	14.911	14.385	14.660	14.556	
208	16.272	15.551	15.243	14.758	14.290	14.427	14.509	
211	16.609	15.637	15.507	15.045	14.625	14.913	14.777	
212	16.492	15.761	15.475	14.953	14.468	14.641	14.695	
213	16.873	16.098	15.766	15.303	14.868	15.167	15.055	
214	16.769	16.029	15.816	15.202	14.713	14.854	14.924	
215	17.185	16.309	16.077	15.599	15.152	15.456	15.275	
216	17.098	16.373	15.994	15.490	14.986	15.139	15.204	
219	17.125	16.620	16.289	15.801	15.352	15.664	15.472	
220	17.317	16.564	16.196	15.682	15.187	15.327	15.412	
221	17.920	17.081	16.743	16.217	15.784	16.124	15.905	
222	17.625	17.025	16.472	16.140	15.616	15.785	15.847	
223	16.956	16.094	17.717	17.211	16.792	17.049	16.803	
224	16.852	16.010	17.630	17.071	16.574	16.642	16.753	
226	14.019	13.465	13.126	12.714	12.313	12.438	12.207	
253	20.910	19.940	19.545	18.865	18.102	18.261	18.545	
1205	16.093	15.349	15.031	14.594	14.102	13.996	14.355	
1206	16.113	15.218	15.046	14.598	14.060	13.983	14.355	
1207	16.385	15.617	15.208	14.954	14.353	14.270	14.594	
1208	16.394	15.615	15.302	14.860	14.346	14.217	14.605	
1211	16.132	15.862	15.570	15.078	14.576	14.458	14.829	
1211	16.653	15.878	15.548	15.094	14.582	14.450	14.890	
1213	16.916	16.133	15.791	15.256	14.925	14.713	15.063	
1214	16.896	16.106	15.759	15.329	14.775	14.635	15.059	
1215	17.178	16.375	16.020	15.590	15.057	14.937	15.297	
1216	17.173	16.378	16.032	15.574	15.044	14.894	15.310	
1217	17.425	16.416	16.261	15.817	15.263	15.148	15.578	
1220	17.409	16.590	16.272	15.786	15.237	15.094	15.501	
1221	17.698	16.863	16.596	16.049	15.494	15.367	15.756	
1227	17.644	16.824	16.473	15.957	15.460	15.284	15.720	

Table 7.2. Diagnostic Static Pressure Data for Annular Convergent-Divergent Nozzle Model 4.

ORIGINAL PAGE IS
OF POOR QUALITY

Acous. Test Point*	P _a psia	Measured Static Pressure, psia (See Figure 6.2 for Location Details)									
		P _s 1	P _s 2	P _s 3	P _s 4	P _s 5	P _s 6	P _s 7	P _s 8	P _s 9	P _s 10
401	14.4580	26.789	22.215	19.829	17.543	15.625	14.634	13.282	13.395	12.683	13.795
402	14.4472	26.982	22.324	19.870	17.388	15.783	14.471	13.582	13.146	12.697	14.020
403	14.4595	22.997	23.215	20.846	18.366	16.669	15.309	14.427	14.001	13.285	14.162
404	14.4497	28.467	23.501	20.835	18.348	16.600	15.273	14.335	13.699	13.185	13.572
405	14.4560	27.279	24.291	21.615	19.224	17.940	15.995	15.080	14.659	13.820	14.763
406	14.4487	29.143	24.336	21.712	18.999	17.211	15.913	14.892	14.426	13.672	14.444
407	14.4506	29.752	24.681	22.148	19.522	17.660	16.229	15.323	14.994	14.000	15.819
408	14.4541	30.079	24.870	22.186	19.425	17.585	16.196	15.223	14.766	13.997	14.265
411	14.4472	30.224	25.065	22.579	19.843	17.976	16.998	15.573	15.152	14.318	15.266
412	14.4394	30.525	25.235	22.531	19.730	17.879	16.957	15.479	15.003	14.214	14.694
413	14.4550	30.717	25.155	22.995	20.160	18.242	16.767	15.843	15.408	14.546	15.526
414	14.4526	31.061	25.682	22.922	20.003	16.181	16.760	15.792	15.285	14.438	15.243
415	14.4506	31.170	25.822	23.219	20.458	18.573	17.010	16.068	15.635	14.752	15.740
416	14.4506	31.454	25.996	23.234	20.385	18.960	16.998	15.980	15.509	14.664	15.474
419	14.4511	31.764	26.321	23.668	20.654	18.684	17.349	16.402	15.972	15.063	16.074
420	14.4467	31.571	26.473	23.609	20.684	18.748	17.306	16.271	15.830	14.932	15.734
471	14.4531	32.805	27.179	24.465	21.598	19.568	17.947	16.972	16.530	15.576	16.612
472	14.4336	33.984	27.261	24.372	21.375	19.396	17.899	16.853	16.408	15.539	16.277
473	14.4497	34.6203	28.939	25.960	22.906	20.720	17.109	16.070	17.644	16.591	17.690
474	14.4350	34.953	28.968	25.939	22.681	20.629	19.057	17.943	17.490	16.915	17.266
449	14.4443	23.160	19.207	17.213	15.177	13.807	12.703	11.980	11.606	11.600	17.231
451	14.4624	23.752	19.705	17.669	15.603	14.228	13.117	12.337	11.938	11.876	17.202
452	14.4453	23.962	19.852	17.636	15.460	14.021	12.854	12.069	11.648	11.726	17.252
453	14.4511	38.609	31.931	28.794	25.467	23.107	21.393	20.154	19.747	18.511	19.698
454	14.4360	35.652	31.995	28.617	25.188	22.919	21.211	19.957	19.520	18.215	19.169
465	14.4457	30.377	24.820	22.400	20.001	17.881	16.964	15.615	15.196	14.030	15.5107
466	14.4401	30.255	24.739	22.303	19.865	17.815	16.406	15.580	15.130	13.997	15.037
471	14.4420	31.432	25.700	23.197	20.692	18.521	17.050	16.180	15.732	14.535	15.653
472	14.4400	31.609	25.834	23.309	20.771	18.615	17.140	16.234	15.82	14.601	15.708
473	14.4404	31.969	26.195	23.611	21.053	18.649	17.362	16.453	15.901	14.778	15.973
474	14.4080	32.123	26.270	23.697	21.113	18.905	17.415	16.95	16.063	14.849	15.796
475	14.4853	32.355	26.463	23.900	21.302	19.062	17.552	16.645	16.186	14.961	16.111
476	14.4868	34.408	26.522	23.926	21.405	19.073	17.597	16.667	16.232	14.997	16.104

* See Section 3.0 of
Vol. I for Aerodynamic
Flow Conditions

Table 7.2 (Continued)

Measured Static Pressure, psia (See Figure 6.2 for Location Details)												
Acous. Test Point	P _s	Tap Number	11	12	13	14	15	16	17	18	19	20
401	16.925	14.511	14.249	19.545	17.787	16.057	14.535	14.985	13.943	13.136		
402	17.164	14.130	14.835	20.099	17.852	16.073	14.809	14.337	13.733	12.894		
403	16.202	15.213	13.259	20.913	16.628	16.845	15.676	15.208	14.617	13.710		
404	16.635	15.121	13.883	21.158	16.139	16.579	15.628	15.148	14.555	13.575		
405	15.275	15.145	14.497	21.468	16.470	17.623	16.960	15.999	15.288	14.318		
406	15.816	15.920	14.138	21.926	19.543	17.657	16.219	15.730	15.071	14.080		
407	14.946	14.290	14.892	21.109	19.765	17.928	16.667	16.155	15.535	14.545		
408	15.381	15.385	14.530	22.399	19.994	18.047	16.539	16.089	15.465	14.480		
409	14.609	14.017	15.240	22.216	20.04	16.228	16.966	16.423	15.788	14.795		
410	15.035	14.361	15.072	22.879	20.407	18.403	16.882	16.496	15.935	14.587		
411	14.452	14.177	15.535	22.556	20.416	16.528	17.231	16.676	16.053	15.021		
412	14.901	14.210	15.784	23.179	20.867	18.669	17.077	16.584	15.873	14.803		
413	14.278	14.424	15.757	22.901	20.713	18.613	17.482	16.923	16.278	15.238		
414	14.512	15.643	23.049	20.991	19.952	17.354	16.157	16.103	15.433	15.056		
415	14.015	14.666	16.018	23.354	21.142	15.208	17.080	17.283	16.631	15.548		
416	14.545	14.290	15.940	23.819	21.965	19.292	17.660	17.157	16.444	15.320		
417	13.520	14.396	16.269	24.138	21.834	19.192	18.185	17.844	17.197	16.077		
418	13.889	14.250	16.367	24.170	22.273	19.963	18.250	17.744	17.023	15.149		
419	12.402	13.536	16.462	25.576	23.259	21.236	19.619	19.006	16.329	17.101		
420	12.925	13.710	17.400	26.123	23.610	21.183	19.362	18.946	18.067	16.804		
421	14.608	15.281	14.497	17.129	15.370	13.871	12.947	12.579	12.079	11.862		
422	14.249	15.363	14.754	17.623	15.857	14.314	13.316	12.891	12.468	12.235		
423	15.673	15.396	14.746	17.896	15.853	14.227	13.127	12.724	12.180	11.622		
424	10.747	12.001	11.221	28.345	24.001	23.687	21.849	21.186	20.490	19.052		
425	11.156	12.547	11.584	28.857	26.161	23.469	21.478	20.916	20.101	18.649		
426	19.993	14.895	14.887	22.192	20.110	18.294	16.717	16.286	15.642	14.690		
427	15.387	14.932	14.634	22.104	20.022	18.222	16.651	16.229	15.550	14.574		
428	14.631	14.650	13.520	22.982	20.835	18.970	17.311	16.878	16.212	15.780		
429	14.614	14.844	15.758	23.164	20.833	19.050	17.468	16.933	16.232	15.193		
430	14.457	15.000	15.763	23.390	21.201	19.283	17.598	17.156	16.506	15.429		
431	14.693	14.985	15.792	23.524	21.249	19.362	17.693	17.215	16.495	15.998		
432	14.409	15.152	15.916	23.690	21.459	19.519	17.848	17.376	16.686	15.621		
433	14.577	15.123	15.920	23.705	21.431	19.528	17.942	17.371	16.626	15.573		

ORIGINAL PAGE IS
OF POOR QUALITY

Table 7.2 (Continued).

Acous. Test Pt	P _{mh} psia	Measured Static Pressure, psia									
		P _s	Tap Number (See Figure 6.2 for Location Details)	1	2	3	4	5	6	7	8
1419	14.9129	22.783	26.898	24.349	21.659	19.382	17.846	16.915	16.936	16.209	16.370
1420	14.4961	33.008	27.021	24.374	21.749	19.951	17.935	16.999	16.539	15.261	16.405
1421	14.4707	33.424	27.337	24.714	22.048	19.697	18.149	17.215	16.945	15.481	16.635
1422	14.4907	33.376	27.403	24.713	22.071	19.758	18.231	17.262	16.915	16.570	16.614
1426	14.4916	29.14	24.496	21.993	19.502	17.656	16.289	15.426	15.017	13.991	16.899
1448	14.4633	29.787	24.524	21.985	19.429	17.640	16.264	15.386	15.026	13.917	14.133
1470	14.4370	26.799	24.531	21.924	19.263	17.571	16.169	15.261	14.996	13.919	14.795
1499	14.5034	14.852	12.432	11.035	9.815	*	9.701	12.216	14.061	14.492	14.771
9405	14.4980	29.752	24.620	22.118	19.639	17.809	16.483	15.593	15.250	14.225	15.203
9406	14.4938	36.003	24.798	22.183	19.505	17.765	16.400	15.498	15.105	14.019	14.949
9411	14.4912	30.743	25.526	22.959	20.469	18.520	17.170	16.184	15.932	14.767	15.772
9412	14.5073	31.027	25.459	22.968	20.360	18.499	17.160	16.190	15.703	14.539	15.580
9413	14.4902	31.163	25.783	23.179	20.626	18.720	17.356	16.352	16.003	14.916	15.519
9414	14.5004	31.067	25.670	22.984	20.325	18.475	17.041	16.088	15.724	14.594	15.572
9415	14.4999	32.203	26.642	23.961	21.312	19.384	17.925	16.95	16.514	15.406	16.924
9416	14.4985	32.359	26.741	23.944	21.225	19.296	17.809	16.801	16.460	15.221	16.209
9421	14.4893	33.154	27.392	24.655	21.944	19.971	18.435	17.411	17.021	15.882	16.934
9422	14.4848	33.090	27.369	24.499	21.725	19.732	18.229	17.178	16.996	15.562	16.574

Table 7.2 (Concluded).

ORIGINAL PAGE IS
OF POOR QUALITY

Acous. Test Pt	Ps	Measured Static Pressure, psia									
		Tap Number (See Figure 6.2 for Location Details)	11	12	13	14	15	16	17	18	19
1419	14.140	15.046	16.399	24.092	21.808	19.836	19.889	17.635	16.935	15.962	
1420	14.400	15.203	16.375	24.294	21.871	19.905	16.177	17.694	16.957	15.874	
1421	13.798	14.701	16.894	24.953	22.147	20.158	18.585	17.930	17.222	16.095	
1422	14.040	14.913	16.871	24.581	22.164	20.222	18.491	17.983	17.229	16.128	
1461	15.730	15.428	14.532	21.920	19.896	18.084	16.520	16.076	15.464	14.428	
1468	15.377	15.756	14.617	21.946	19.912	17.925	16.466	16.199	15.422	14.324	
1470	15.359	15.635	14.963	22.108	19.996	17.977	16.486	16.020	15.370	14.326	
7401	14.625	14.201	14.621	11.245	10.001	* * *	* * *	11.676	13.755	14.313	
9405	15.030	14.270	14.959	22.787	20.144	15.294	16.892	16.324	15.238	14.642	
9406	16.209	15.792	15.487	23.496	20.397	16.534	17.168	16.906	16.284	15.295	
9411	14.684	14.378	11.001	23.019	20.983	19.065	17.530	17.229	16.265	15.643	
9412	14.695	14.103	15.524	23.299	20.875	18.261	17.276	16.901	16.720	15.032	
9413	14.261	14.406	15.848	23.274	21.030	19.103	17.452	17.081	16.571	15.333	
9414	16.162	14.101	15.571	23.347	20.914	18.866	17.293	16.832	16.135	15.063	
9415	13.841	14.732	16.397	24.017	21.753	19.777	18.022	17.651	17.036	15.844	
9416	14.190	14.894	16.128	24.280	21.750	19.668	18.001	17.525	16.843	15.669	
9421	13.376	14.266	17.153	24.746	22.406	20.289	18.578	18.190	17.563	16.321	
9422	13.826	14.735	16.552	24.716	22.209	20.051	16.372	17.872	17.151	15.961	

Table 7.3. Diagnostic Static Pressure Data of Convergent-Divergent 20-Shallow-Chute Suppressor Nozzle (Model 6)

Acous. Test Point*	P _a psia	Measured Static Pressure, psia										
		P _s	Tap Number	(See Figure 6.3 for Location Details)								
		1	2	3	4	5	6	7	8	9	10	11
601	14.4951	25.349	25.904	19.953	12.307	12.944	12.692	12.751	14.638	30.526	29.276	26.813
602	14.4516	24.607	24.929	18.695	13.199	13.602	11.895	11.718	13.798	30.217	29.053	26.069
603	14.4934	26.905	27.519	21.189	17.918	13.668	13.380	13.277	14.835	32.322	30.986	27.819
604	14.4626	25.997	26.322	19.744	13.924	14.398	12.539	12.154	14.026	31.997	30.465	27.505
605	14.4672	27.615	28.269	21.729	13.324	14.052	13.722	13.559	14.973	33.227	31.842	28.577
606	14.4516	26.719	27.048	20.321	14.265	14.823	12.859	12.406	14.196	32.902	31.538	28.282
607	14.4755	28.787	29.909	22.131	13.863	14.436	14.026	13.806	15.804	34.027	32.611	29.282
608	14.5492	27.423	27.768	20.829	14.626	15.202	13.199	12.654	14.389	33.719	32.307	28.981
611	14.4520	28.789	29.460	22.604	13.974	14.652	14.276	14.013	15.861	34.528	33.141	28.783
612	14.4306	27.750	28.130	21.093	14.764	15.328	13.288	12.725	14.398	34.160	32.682	29.378
613	14.4589	29.736	29.736	22.970	14.729	14.903	14.504	14.212	15.329	35.139	33.686	30.276
614	14.3872	28.209	28.632	21.452	14.974	15.613	13.500	12.928	14.535	34.732	33.279	29.861
615	14.4526	29.655	30.379	23.279	14.571	15.138	14.684	14.397	15.588	35.691	34.213	30.733
616	14.3769	28.625	29.066	21.777	15.193	15.236	14.694	13.699	14.659	35.258	33.789	30.527
619	14.4511	30.127	30.952	23.625	14.763	15.780	14.910	14.606	15.504	36.256	34.756	31.213
621	14.4831	30.697	31.787	24.373	15.088	15.839	15.372	15.037	16.141	37.328	35.777	32.125
622	14.3996	29.614	30.316	22.712	15.102	16.483	14.209	13.526	15.020	36.764	35.725	31.696
623	14.4458	32.773	33.629	25.757	15.992	16.753	16.222	15.917	16.944	37.404	37.773	33.911
624	14.3862	31.701	32.277	24.260	16.624	17.536	15.164	14.729	15.915	37.072	37.467	33.576
626	14.4735	29.059	29.508	22.104	15.430	16.105	13.899	13.282	14.806	35.988	34.336	30.766
605	14.4873	29.786	30.100	22.365	13.306	14.692	14.390	13.248	15.855	34.252	33.064	29.667
607	14.4378	30.415	30.643	23.729	13.585	14.735	14.640	13.447	15.976	35.375	33.637	30.204
611	14.4970	30.833	31.092	23.059	13.742	14.924	14.846	13.620	16.128	35.826	34.113	30.595
613	14.4858	31.305	31.538	23.382	13.906	15.146	15.062	13.804	16.276	36.363	34.615	31.076
615	14.4677	32.046	31.858	23.649	14.368	15.438	15.277	14.398	16.485	36.987	35.217	31.539
619	14.4687	32.770	32.496	24.110	14.641	15.706	15.528	14.576	16.209	37.742	35.947	32.158
621	14.4809	33.127	32.993	24.946	14.727	15.879	15.767	14.760	16.182	38.104	36.324	32.580

* See Section 3.0 of Vol. I for Aero-dynamic Flow Conditions

Table 7.3 (Concluded).

ORIGINAL PAGE IS
OF POOR QUALITY

Measured Static Pressure, psia (See Figure 6.3 for Location Details)															
Acous. Test Pt	P _s	Tap Number	12	13	14,	15	16	17	18	19	20	21	22	23	24
601	23.624	19.962	17.926	17.019	16.742	26.687	27.013	21.521	14.766	15.334	15.986	15.746	12.372		
602	23.310	18.978	17.962	16.600	16.292	26.363	26.740	21.242	14.283	15.437	15.371	13.399	11.840		
603	25.013	20.580	18.966	17.961	17.675	28.728	28.565	22.784	15.600	15.335	16.167	14.615	12.929		
604	24.588	20.029	19.438	17.482	17.120	27.801	28.194	22.410	15.087	15.442	16.209	14.139	12.289		
605	25.680	21.164	19.996	18.418	18.158	28.990	29.358	23.369	15.999	15.334	16.867	15.037	13.174		
606	25.332	20.586	19.009	17.934	17.603	28.609	28.994	23.056	15.498	15.637	16.457	14.560	12.589		
607	26.319	21.701	19.994	18.900	18.611	28.726	30.091	23.974	16.415	15.320	17.237	15.354	13.404		
608	25.936	21.115	19.463	18.379	18.041	29.311	29.726	23.429	15.977	15.432	17.076	14.415	12.821		
611	26.761	22.084	19.204	18.903	18.603	30.218	30.594	24.345	16.697	15.307	17.519	15.570	13.600		
612	26.323	21.924	19.784	18.630	18.300	29.726	30.142	23.963	16.085	15.438	17.312	15.115	12.980		
613	27.205	22.377	20.689	19.522	19.216	30.724	31.002	24.766	16.984	15.313	17.033	15.892	13.794		
614	26.713	21.745	20.013	19.193	19.579	30.126	30.616	24.316	16.378	15.368	17.519	14.398	13.157		
615	27.613	22.726	20.990	19.789	19.509	31.199	31.527	25.101	17.246	15.308	18.085	16.130	13.993		
616	27.136	22.064	20.782	19.177	18.847	30.682	31.009	24.722	16.597	15.369	17.837	15.322			
619	28.036	23.111	21.326	20.108	19.819	31.687	32.078	25.578	17.491	15.309	18.554	16.387	14.194		
621	28.828	23.795	21.974	20.707	20.404	32.629	33.016	26.295	18.017	15.308	18.896	16.903	14.596		
622	28.336	23.071	21.318	20.029	19.691	32.070	32.494	25.817	17.305	15.366	18.526	16.293	13.889		
623	30.468	25.155	23.242	21.874	21.556	34.986	34.568	27.749	19.022	15.330	*	17.696	15.397		
624	29.977	24.944	22.607	21.171	20.978	33.994	34.092	27.357	18.363	15.372	*	17.257	14.690		
626	27.535	22.467	20.699	19.454	19.119	31.159	31.551	25.094	16.825	15.370	18.098	14.398	12.503		
627	26.578	21.873	20.343	19.195	18.953	30.169	31.380	24.224	16.398	15.335	17.827	15.983	13.422		
628	27.009	22.265	20.791	19.525	19.262	30.683	30.923	24.669	16.490	15.338	18.112	16.264	13.628		
629	27.342	22.527	20.958	19.734	19.486	31.099	31.246	24.952	16.879	15.339	18.564	16.514	13.935		
630	27.828	22.902	21.318	20.065	19.837	31.574	31.832	25.367	17.173	15.335	18.607	16.758	14.580		
631	28.174	23.253	21.628	20.337	20.087	32.080	32.307	25.734	17.372	15.337	18.893	16.989	14.505		
632	28.797	23.712	22.039	20.730	20.468	32.717	33.000	26.242	17.700	15.337	19.241	17.335	14.966		
633	29.180	24.070	21.027	20.600	19.148	33.168	33.400	26.575	17.983	15.336	19.499	17.499	14.502		

7.2 SUPPRESSOR BASE PRESSURE DATA

Base pressure instrumentation applied to the convergent-divergent suppressor configuration (Model 6) are described in Section 2.0. The locations and identifications of the 15 P_s taps in the base regions of the chutes are provided in Figure 7.4.

Base pressure measurements were obtained over a range of cycle conditions that are typical of AST/VCE cycle including the shock-free design condition of the suppressor flow elements. The data were recorded with free-jet velocities of 0, 200 and 400 fps. The aerodynamic test conditions of the base pressure test points are summarized in Table 7.4.

Table 7.5 summarized the measured base pressure data corresponding to the aerodynamic flow conditions of Table 7.4.

ORIGINAL PAGE IS
OF PQOR QUALITY

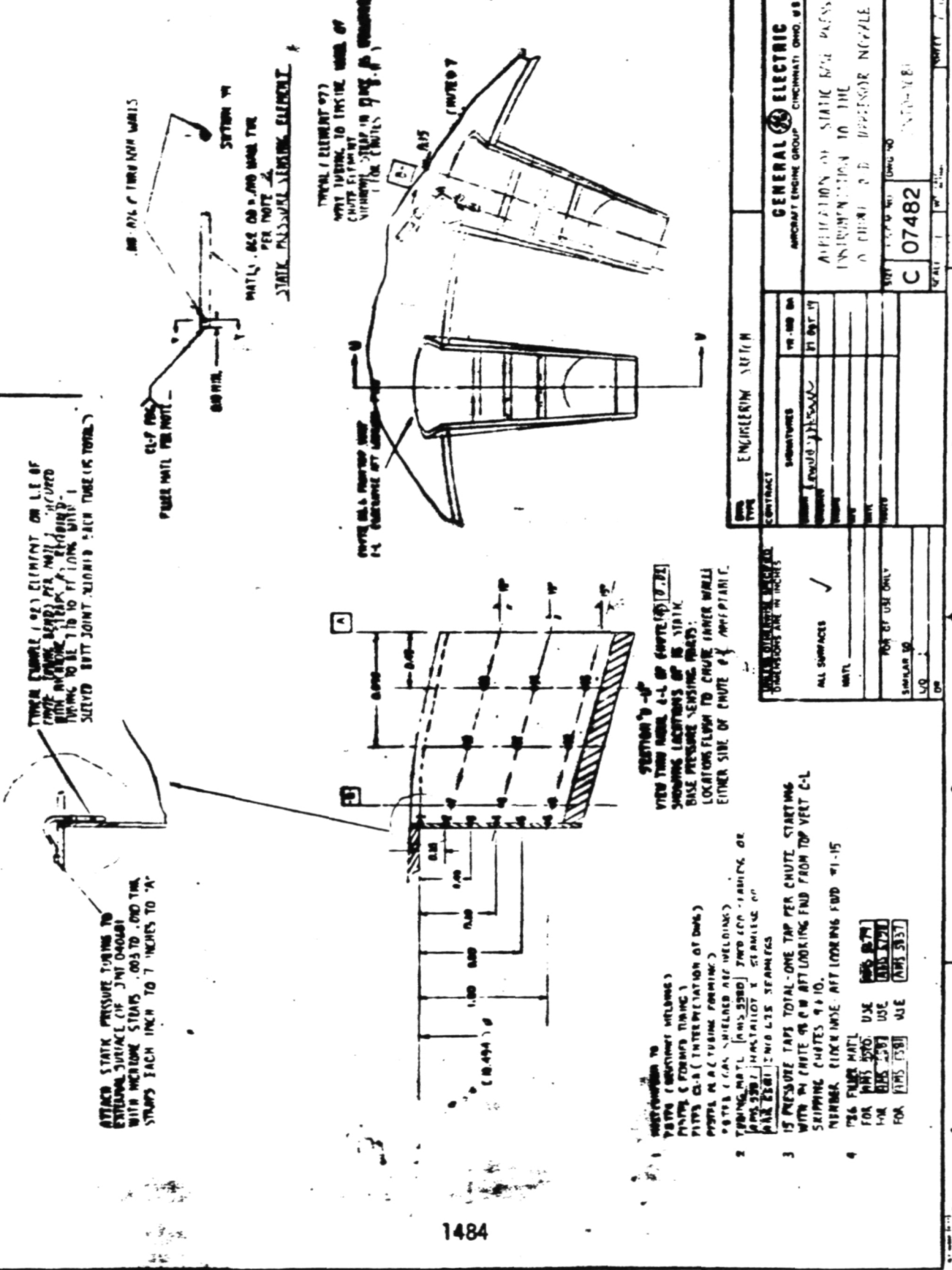


Figure 7.4. Application of Base Pressure Instrumentation to 20-Shallow-Chute Suppressor Nozzles (Model 6).

Table 7.4. Summary of Aerodynamic Flow Conditions of Base Pressure Tests with Model 6.

Base Pressure Test Point	P _r	T _T , °R	V _j , Ft/Sec	V _{a/c} , Ft/Sec
613	3.13	1715	2411	0
614	3.13	1711	2410	400
1613	3.34	852	1727	0
1614	3.34	856	1732	400
1621	3.37	853	1734	0
1622	3.36	854	1734	400
2613	3.13	1718	2412	0
3613	3.24	1716	2442	0
4601	2.38	1578	2051	0
4602	2.37	1591	2055	400
4603	2.73	1739	2300	0
4604	2.72	1732	2290	400
4605	3.02	1727	2388	0
4606	3.02	1733	2390	400
4610	3.21	1740	2451	400
4612	3.42	1730	2499	400
4613	3.35	1712	2468	0
4614	3.72	1725	2566	400
7613	3.26	560	1389	0
7614	3.26	609	1448	400
8602	2.38	1585	2056	200
8604	2.70	1746	2293	200
8608	3.13	1729	2420	200
8612	3.40	1728	2493	200
8614	3.69	1580	2445	200

Table 7.5. Summary of Measured Base Pressure Data for Model 6.

Base * Test Pt.	P _{amb} Press. psia	Measured Base Pressure Data, psia							
		Base Pressure Tap Number (See Fig. 6.4 for Loc. Details)							
		1	2	3	4	5	6	7	8
613	14.3842	14.313	14.308	14.295	14.292	14.325	14.316	14.308	14.270
614	14.3950	13.973	13.726	13.666	13.714	13.708	13.750	13.609	13.664
615	14.4682	14.361	14.378	14.372	14.343	14.372	14.373	14.360	14.319
616	14.4709	13.796	13.737	13.670	13.697	13.794	13.813	13.650	13.506
621	14.4770	14.369	14.365	14.376	14.365	14.363	14.376	14.363	14.316
622	14.4892	13.794	13.722	13.689	13.744	13.751	13.798	13.664	13.694
2613	14.4912	14.390	14.401	14.396	14.396	14.399	14.421	14.396	14.363
3613	14.4934	14.393	14.388	14.393	14.394	14.410	14.398	14.396	14.354
4601	14.4316	14.344	14.353	14.349	14.354	14.364	14.371	14.351	14.344
4602	14.3037	13.820	13.760	13.676	13.719	13.782	13.805	13.684	13.624
4603	14.4336	14.342	14.354	14.344	14.346	14.353	14.369	14.339	14.329
4604	14.3862	13.820	13.738	13.663	13.711	13.756	13.792	13.654	13.539
4605	14.4287	14.346	14.382	14.332	14.331	14.353	14.362	14.329	14.309
4606	14.3862	13.826	13.728	13.666	13.709	13.723	13.780	13.654	13.523
4610	14.3906	13.815	13.703	13.636	13.693	13.726	13.761	13.627	13.499
4612	14.3937	13.777	13.693	13.632	13.674	13.725	13.763	13.601	13.454
4613	14.4955	14.380	14.381	14.376	14.373	14.387	14.401	14.391	14.347
4614	14.3813	13.750	13.679	13.610	13.667	13.699	13.723	13.607	13.495
7613	14.3813	14.288	14.280	14.286	14.278	14.286	14.288	14.276	14.246
7614	14.3896	13.761	13.689	13.605	13.676	13.711	13.779	13.650	13.517
8602	14.4121	14.123	14.109	14.083	14.087	14.124	14.118	14.074	14.022
8604	14.4253	14.141	14.134	14.081	14.114	14.112	14.131	14.084	14.010
8608	14.4350	14.145	14.119	14.093	14.101	14.111	14.129	14.087	13.983
8612	14.4306	14.143	14.112	14.093	14.096	14.112	14.131	14.098	13.970
8614	14.4174	14.119	14.101	14.084	14.087	14.094	14.107	14.082	13.986

ORIGINAL PAGE IS
OF POOR QUALITY

* See Table 7.4 for Aerodynamic Flow Conditions

Table 7.5 (Concluded).

**ORIGINAL PAGE IS
OF POOR QUALITY**

Measured Base Pressure Data, psia								
Base press. pt	Base Test	Press.	Tap No.	(See Fig. 6.4 for Loc. Details)	15	14	13	12
9	10	11	11	14.285	14.261	14.27	14.261	14.287
613	14.296	14.310	14.326	14.319	14.285	14.261	14.27	14.287
614	13.641	13.656	13.685	13.823	13.869	13.929	13.845	13.855
1613	14.372	14.366	14.397	14.390	14.377	14.309	14.359	14.359
1614	13.712	13.625	13.720	13.811	13.866	13.946	13.852	13.852
1621	14.380	14.383	14.405	14.392	14.387	14.334	14.366	14.366
1622	13.730	13.625	13.716	13.835	13.872	13.933	13.822	13.822
2613	14.401	14.395	14.420	14.410	14.374	14.383	14.383	14.392
3613	14.393	14.391	14.399	14.413	14.362	14.328	14.366	14.366
4601	14.346	14.357	14.373	14.369	14.337	14.302	14.340	14.340
4602	13.719	13.594	13.698	13.853	13.830	13.955	13.859	13.859
4603	14.347	14.344	14.372	14.361	14.331	14.285	14.340	14.340
4604	13.676	13.582	13.672	13.832	13.843	13.927	13.833	13.833
4605	14.334	14.341	14.368	14.354	14.316	14.291	14.331	14.331
4606	13.663	13.621	13.620	13.628	13.633	13.919	13.841	13.841
4610	13.637	13.612	13.652	13.718	13.858	13.917	13.830	13.830
4612	13.634	13.624	13.639	13.796	13.853	13.900	13.830	13.830
4613	14.376	14.385	14.403	14.420	14.372	14.342	14.378	14.378
4614	13.644	13.596	13.673	13.784	13.843	13.902	13.815	13.815
7613	14.285	14.261	14.294	14.306	14.276	14.231	14.265	14.265
7614	13.699	13.580	13.700	13.739	13.833	13.878	13.795	13.795
8602	14.091	14.084	14.101	14.155	14.132	14.173	14.173	14.173
8604	14.076	14.084	14.121	14.140	14.151	14.162	14.179	14.179
8608	14.076	14.074	14.114	14.116	14.153	14.168	14.169	14.169
8612	14.084	14.071	14.118	14.157	14.153	14.168	14.173	14.173
8614	14.056	14.049	14.103	14.120	14.134	14.146	14.153	14.153

8.0 NOMENCLATURE

a	Radius of free-jet
c	Speed of sound
C-D	Convergent-divergent
CDR	Comprehensive data report
Corr _T	Turbulence absorption correction
D	Diameter
F	Ideal thrust
f	Frequency
FTFSDR	Flight-transformed full-scale data reduction computer program
F _o , F _x , F _y , F _z	Mutually uncorrelated set of singularities
h	Annular height dimension
ℓ	Path length
k _o	Wave number
k _i	Sample number
LBM	Defined as $10 \log M_j^2 - 1$
LVM	Defined as $10 \log (V_j/a_{amb})$
M	Mach number
N	Number of samples
NF	Normalization factor, defined as $-10 \log (F/F_{ref})(\rho/\rho_{amb})^{\omega-1}$
OAPWL	Overall sound power level
OASPL	Overall sound pressure level
PWL	1/3-octave-band sound power level
P	Pressure
P'	Acoustic pressure
P _s	Static pressure
P _r	Pressure ratio, defined as ratio of inner to outer radius
PNL	Perceived noise level
PNLN	Normalized perceived noise level
PNLT	Tone corrected perceived noise level
R	Gas constant
r	Radial coordinate

PRECEDING PAGE BLANK NOT FILMED

RH	Relative humidity
R_r	Stream radius ratio, defined as ratio of inner to outer radius of a stream
SPL	Sound pressure level
t	Time
T_T	Total temperature
T_s	Static temperature
V	Ideally expanded velocity
VCE	Variable cycle engine
\dot{W}	Weight flow rate
x,y,z	Directional coordinates
θ_i	Microphone angle measured relative to inlet
θ_j	Microphone angle measured relative to exit
μ	Viscosity
ρ	Static density
ω	Density exponent
γ	Ratio of specific heats
α_T	Turbulence absorption coefficient

Subscripts

a/c	Free-jet conditions
amb or o	Ambient conditions
eq	Equivalent
hyd	Hydraulic
i	Individual increment
j	Based on ideal jet conditions
ref	Reference
r	Ratio

Superscripts

mix	Fully mixed conditions
'	Turbulent quantity or coordinates for slant traverses
—	Mean value (overbar)

9.0 REFERENCES

- 2-1 Clapper, W.S., Stringas, E.J., "Investigation of In-flight Aero-Acoustic Effects on Suppressed Exhausts," FAA-RD-76-79,V, G.E. Co., January 1979.
- 2-2 Knott, P.R., Janardan, B.A., et. al., "Free-jet Acoustic Investigation of High-Radius-Ratio Coannular Plug Nozzles," G.E. Co., Final Report Draft, May 1981.
- 2-3 Janardan, B.A., Brausch, J.F., et. al., "Free-jet Investigation of Mechanically Suppressed, High-Radius-Ratio Coannular Plug Model Nozzles," R81AEG484, Comprehensive Data Report Volumes I & II, May 1981.
- 2-4 Bediako, E.D., Yamamoto, K. "Aerodynamic Design and Analysis for Shock Cell Noise Reduction System," R81AEG543, General Electric Company, September 1981.
- 2-5 Brausch, J.F., Majjigi, R.K. & Bediako, E.D., "Model Hardware Design Report for a Thermal Acoustic Shield Concept for AST/VCE Application - Single Stream Nozzle Designs," R81AEG575, General Electric Company, July 1981.
- 2-6 Kozlowski, H. & Packman, A.B., "Flight Effects on the Aero/Acoustic Characteristics of Inverted Profile Coannular Nozzles," United Technologies Corp., NASA Contractor Report 3018, August 1978.
- 3-1 Shields, F.D. and Bass, H.E., "Atmospheric Absorption of High Frequency Noise and Application to Fractional-Octave Bands," University of Mississippi, NASA CR-2760, June 1977.
- IV-1 Knott, P.R., "Supersonic Jet Exhaust Noise Investigation," Vol. I, Summary Report, AFAPL-TR-76-68, July 1976.

APPENDICES

PRECEDING PAGE BLANK NOT FILMED

APPENDIX I
ACOUSTIC TEST FACILITY

All of the acoustic, LV and diagnostic shadowgraph photo tests of this program were conducted in General Electric's Anechoic Free-Jet Facility located in Evendale, Ohio. The facility, schematically shown in Figure I-1, is a cylindrical chamber having a diameter of 13.1 meters and a height of 21.95 meters. The inner surfaces of the chamber are lined with anechoic wedges made of fiber-glass wool to yield a low frequency cutoff below 220 Hz and an absorption coefficient of 0.99 above 220 Hz. Descriptions and results of the tests conducted in order to determine the acoustic characteristics of the anechoic chamber (e.g., inverse square law tests) and the mean velocity and turbulence intensity distributions in the free jet are presented in Reference ~~2-62-1~~.

The facility can accommodate model configurations up to a size of 17.3 cm (6.8 in.) in diameter. The required streams of heated air for a dual flow arrangement, produced by two separate burners, flow through silencers and plenum chambers before entering the test nozzle. The operating domain of the facility in terms of total temperature, pressure ratio, and jet velocity is indicated in Figure I-2 for single and dual flow operation.

The tertiary air system consists of a 250,000-scfm (50 inches water column static pressure) fan and a 3500-hp electric motor. Air supply to the fan is pulled through the existing buildup area inlet silencer. The transition duct-work and silencer route the air from the fan discharge to the tertiary silencer plenum chamber. The silencer reduces the noise level by 30-50 dB. The air is then discharged through the 1.2-m free-jet exhaust. Tertiary flow at its maximum permits simulation up to a Mach number of 0.41. Mach number variation is obtained by varying the tertiary airflow rate which is achieved by an adjustment in the fan inlet vanes. The combined airflow is exhausted finally through a "T" stack directly over the nozzles in the ceiling of the chamber.

A schematic of the anechoic chamber, along with microphone locations, is presented in Figure I-3. An overhead view of the tertiary exhaust surrounding a conical test nozzle is shown in Figure I-4.

The effect of tertiary flow on the background noise level at 50°, 90°, and 150° microphone locations is shown respectively in Figures I-5 through I-7. In each of these figures, background noise spectra with tertiary flow velocities equivalent to $M_{\infty} = 0$, 0.2, and 0.3 are compared with one another and with a static spectra of a typical coannular nozzle operating with a mixed velocity of $V_{mix}^{ac} = 325$ mps (1066 fps). An examination of these figures indicates the level of jet noise to be considerably higher compared to background noise with tertiary flow only. Therefore, the tertiary flow is not expected to appreciably influence the levels of jet noise at the jet velocities of interest in this program.

ORIGINAL PAGE IS
OF POOR QUALITY

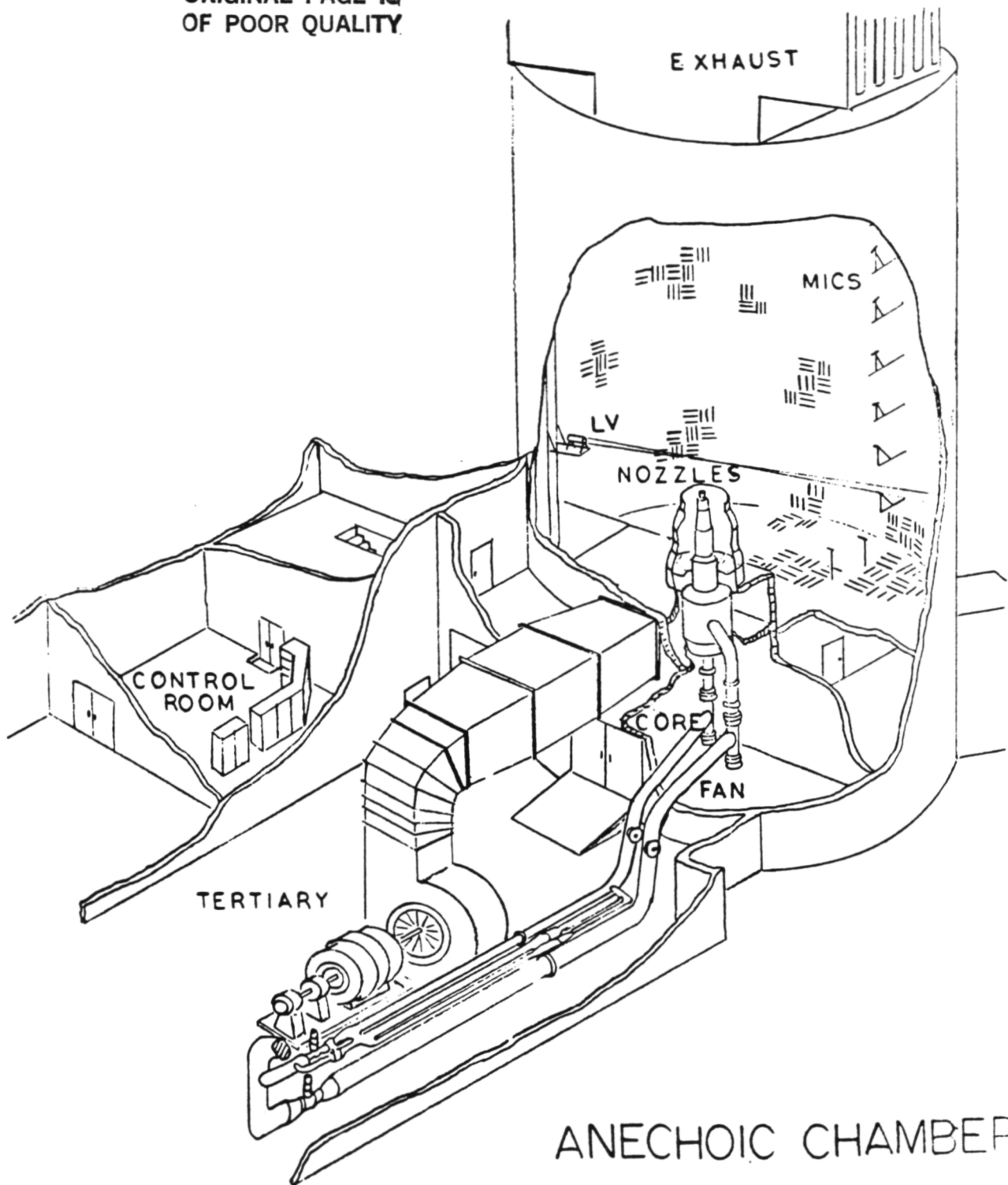


Figure I-1. Schematic of the General Electric Anechoic Free-Jet Acoustic Facility.

ORIGINAL PAGE IS
OF POOR QUALITY

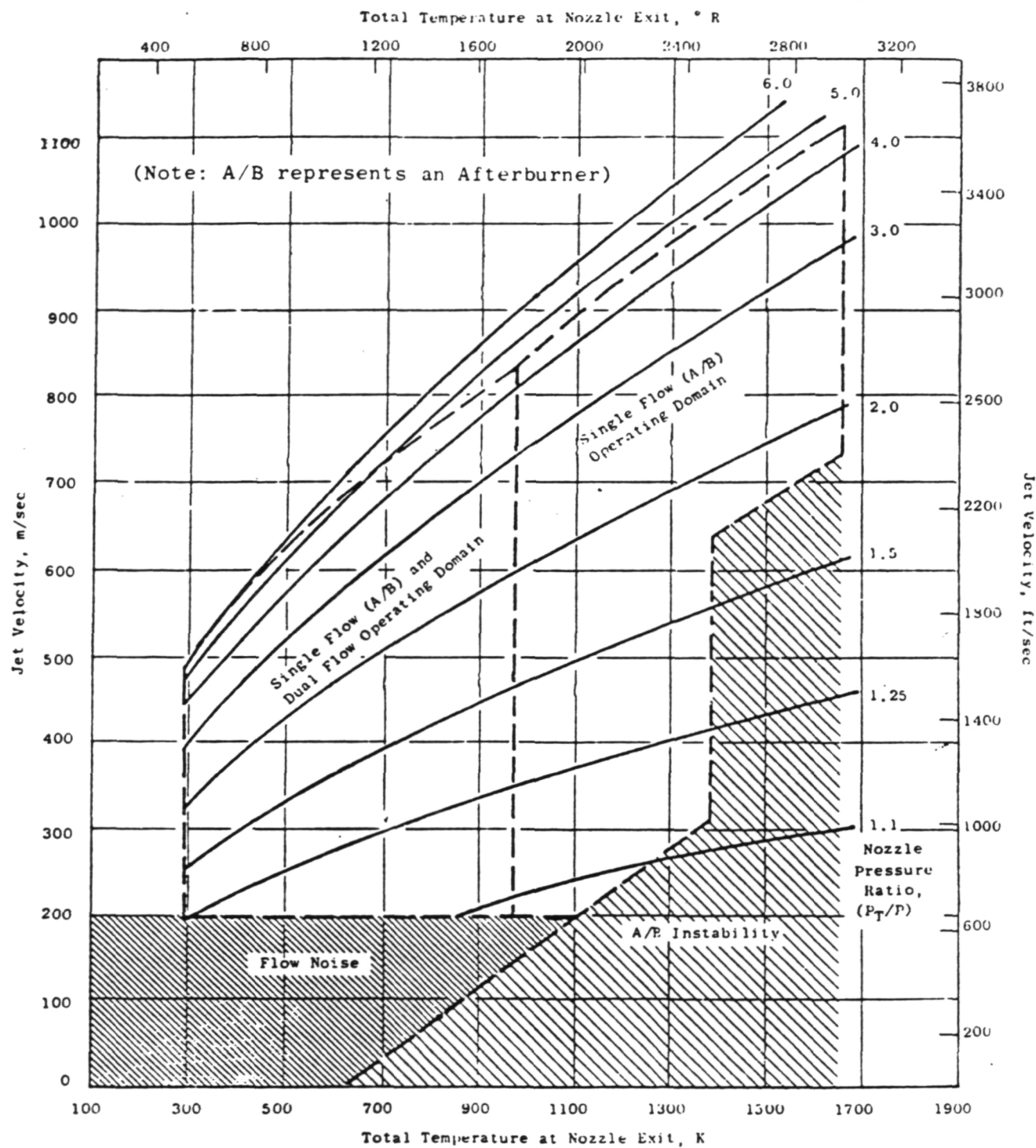


Figure I-2. Operating Domain of General Electric's Anechoic Chamber.

ORIGINAL PAGE IS
OF POOR QUALITY

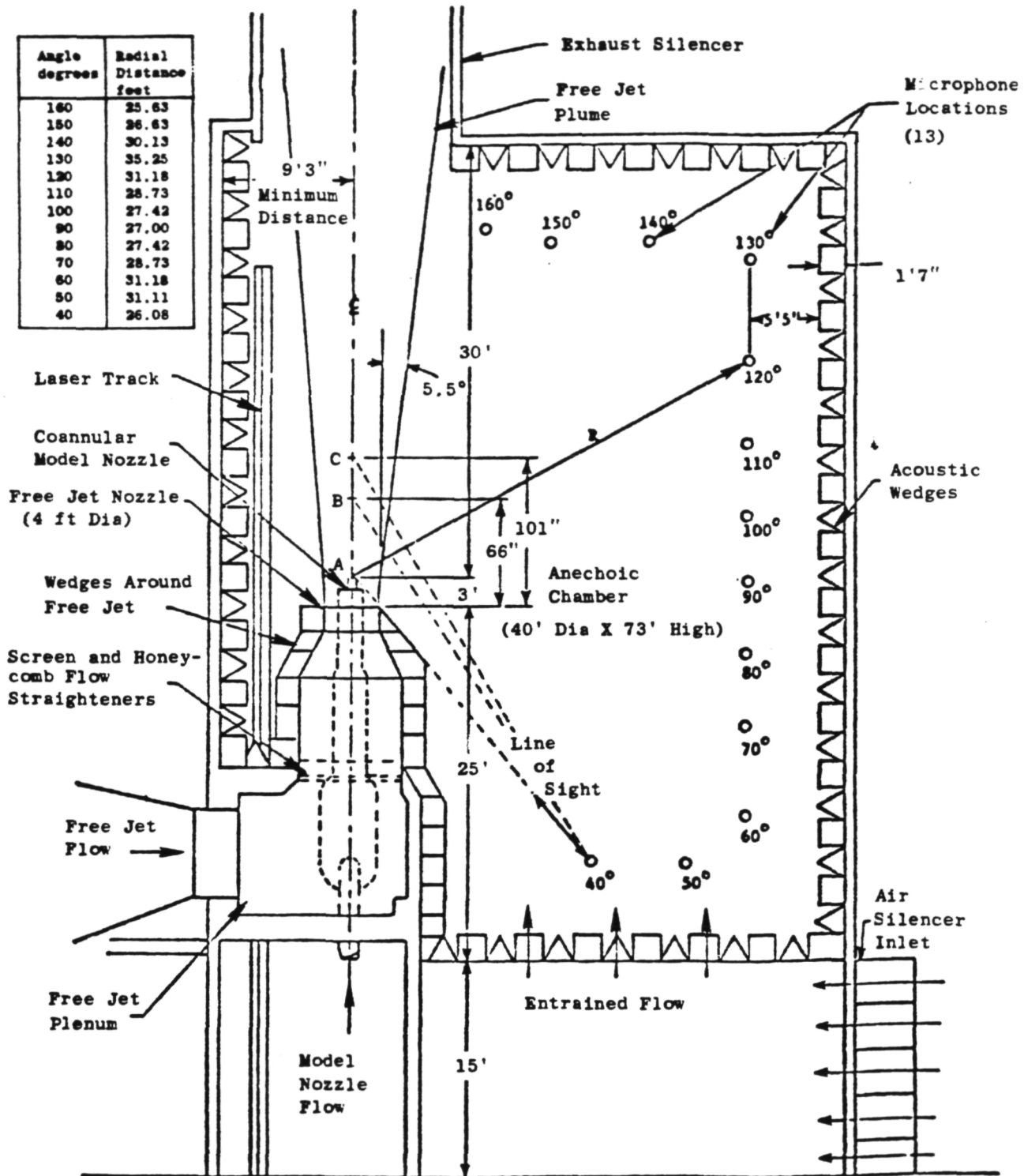


Figure I-3. Free-Jet Arrangement in Anechoic Facility (Cell 41).

ORIGINAL PAGE IS
OF POOR QUALITY

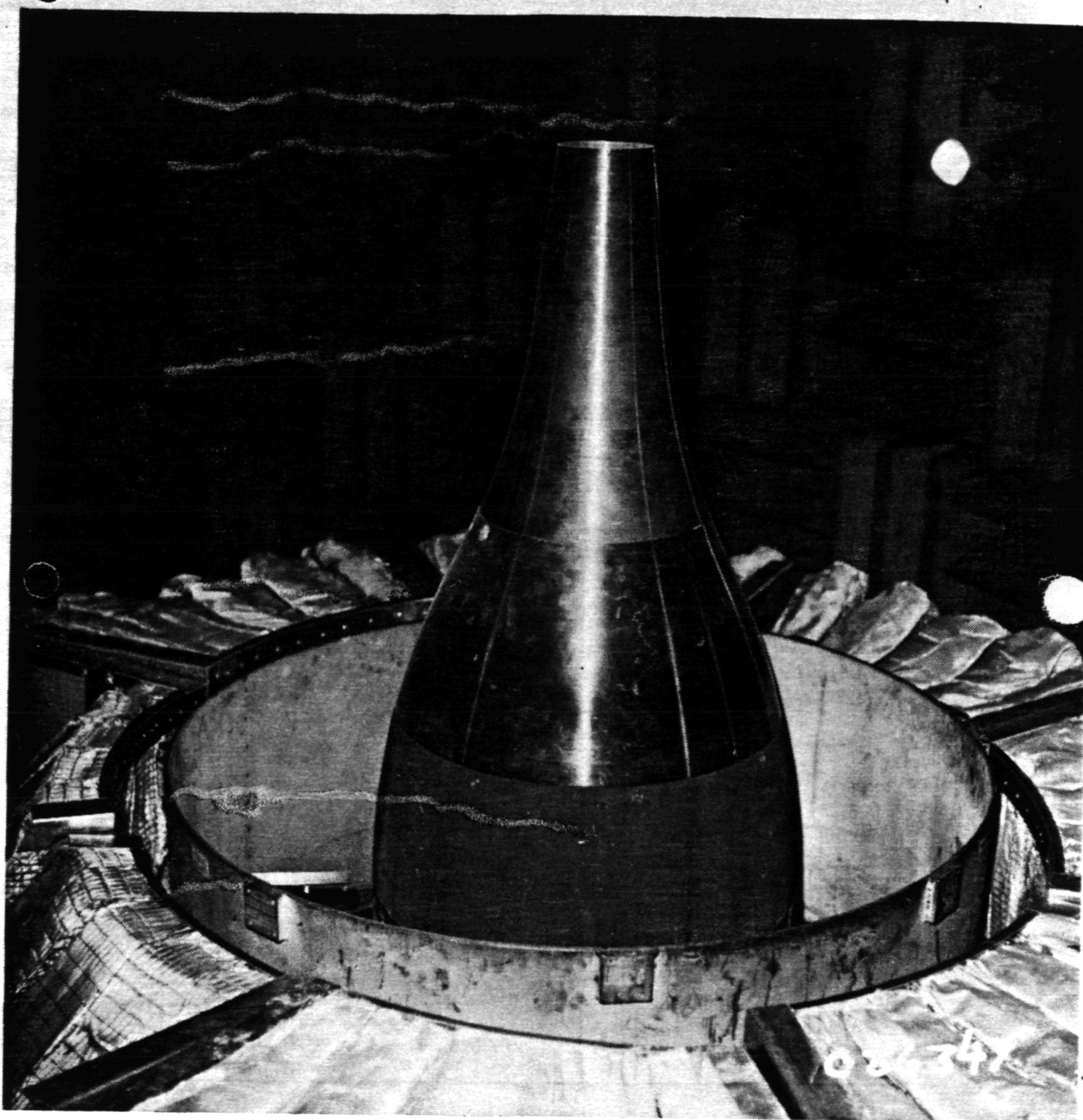


Figure I-4. Overhead view of the Tertiary Exhaust Surrounding a Circular Convergent (conical) Nozzle.

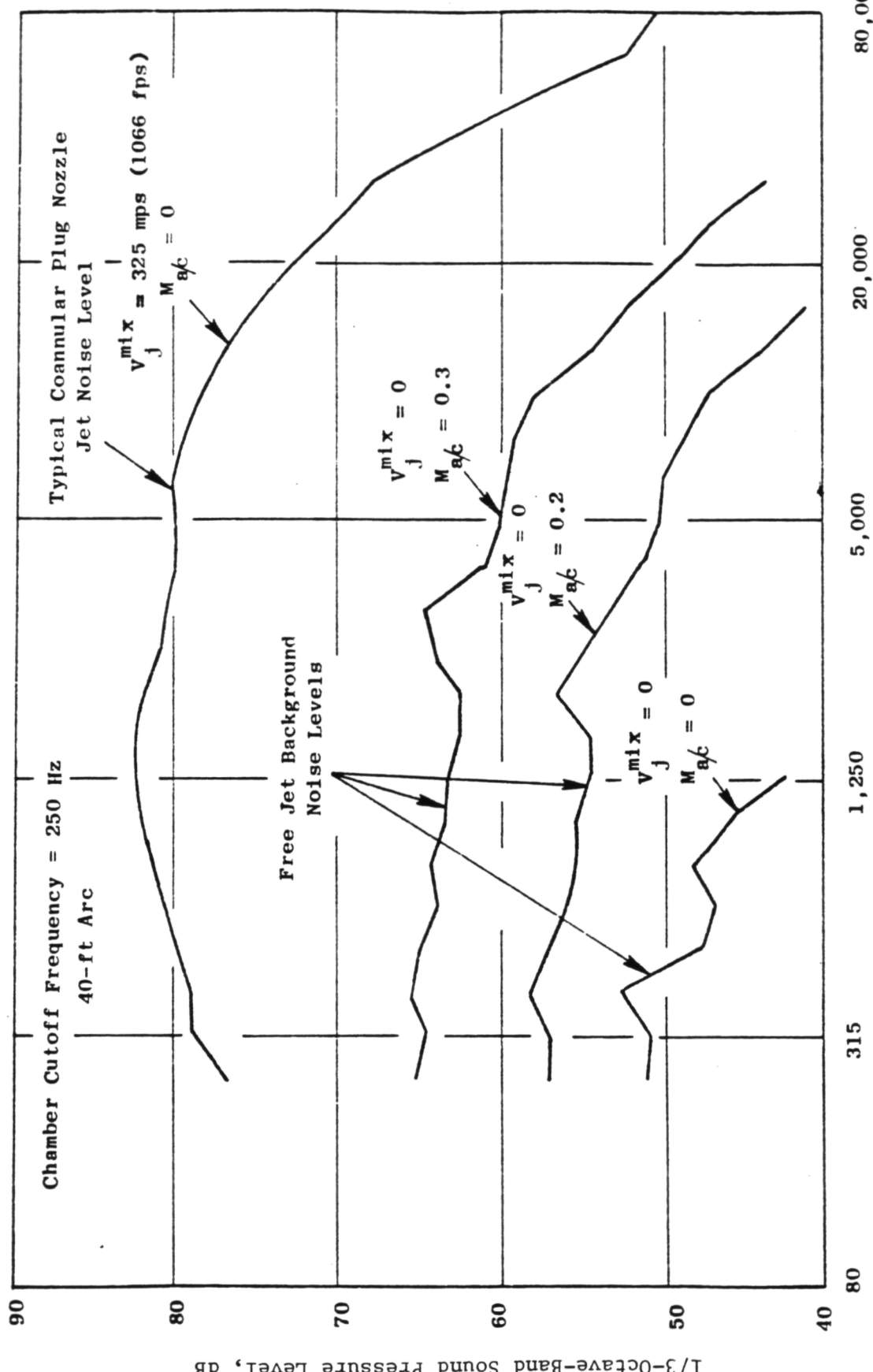


Figure I-5. Comparison of Coannular Jet Noise Spectra with Tertiary (Background) Noise Spectra at $\theta_i = 50^\circ$.

ORIGINAL PAGE IS
OF POOR QUALITY

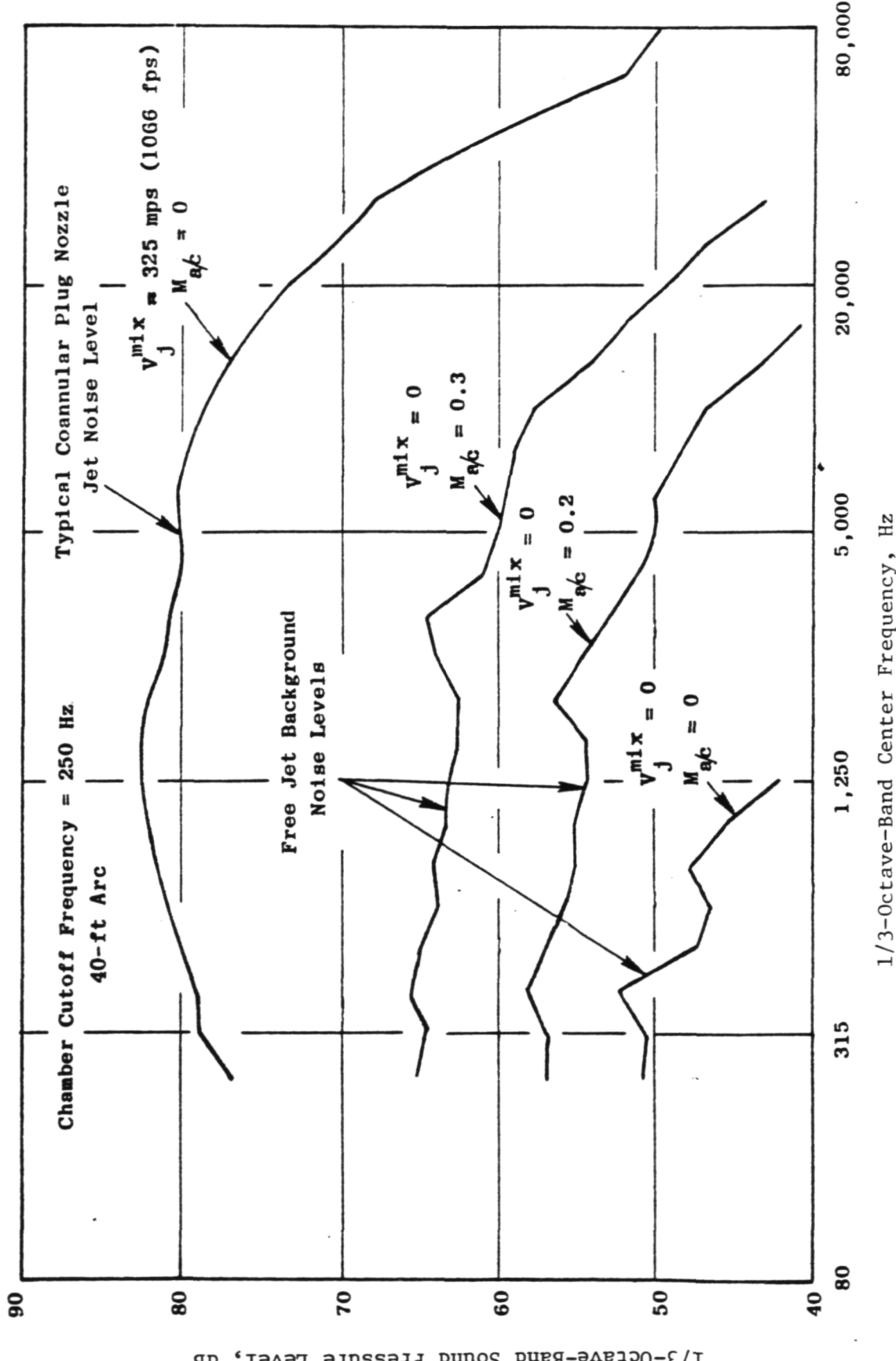


Figure I-6. Comparison of Coannular Jet Noise Spectra with Tertiary (Background) Noise Spectra at $\theta_i = 90^\circ$.

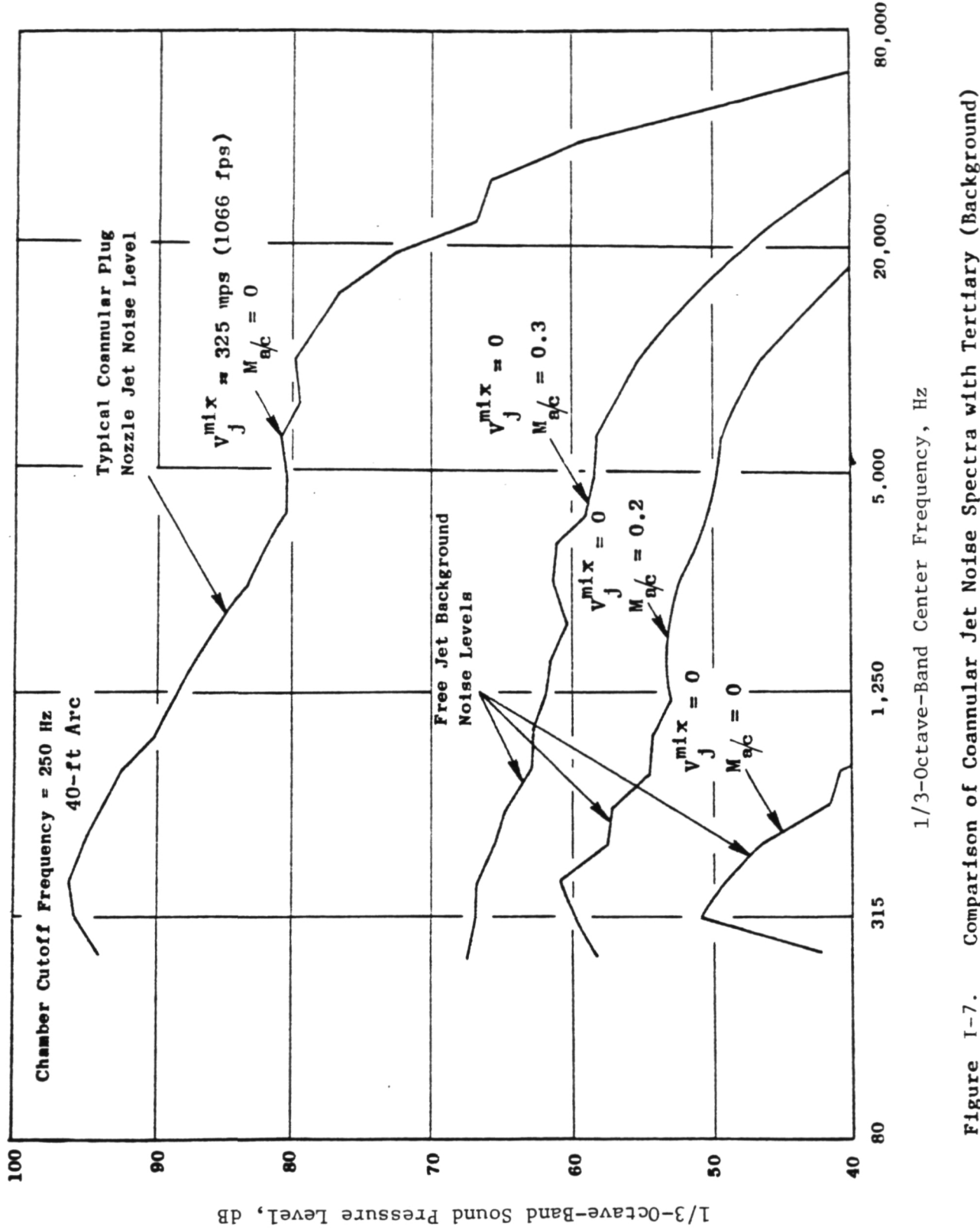


Figure I-7. Comparison of Coannular Jet Noise Spectra with Tertiary (Background) Noise Spectra at $\theta_i = 150^\circ$.

APPENDIX II

ACOUSTIC DATA ACQUISITION AND REDUCTION PROCEDURES

1.0 ACOUSTIC DATA ACQUISITION AND REDUCTION PROCEDURES

A flow chart of the acoustic data acquisition and reduction system is shown in Figure II-1. This system is optimized for obtaining the acoustic data up to the 80 kHz 1/3-octave-band center frequency. The microphones used to obtain 80 kHz data are the B&K 4135, 0.64 cm, condenser microphones with the microphone grid caps removed to obtain the best frequency response. The cathode followers used in the chamber are transistorized B&K 2801 power supply operated in the direct mode.

The output of the power supply is connected to a line driver adding 10 dB of amplification to the signal as well as adding "preemphasis" to the high frequency portion of the spectrum. The net effect of this amplifier is a 10-dB gain at all frequencies, plus an additional 3 dB at 40 kHz and 6 dB at 80 kHz due to preemphasis, thus increasing the ability to measure low amplitude, high frequency data. In order to remove low frequency noise, high pass filters with attenuations of approximately 26 dB at 12.5 Hz decreasing to 0 dB at 200 Hz are installed in the system.

The tape recorder amplifiers have a variable gain from -10 dB to +60 dB in 10-dB steps and a gain trim capability for normalizing incoming signals. High pass filters are incorporated in the acoustic data acquisition systems to enhance high frequency data previously lost in the tape recorder electronic noise floor for microphones from 110° to 160°. The microphone signal below the 20 kHz 1/3-octave band is filtered out, and the gain is increased to boost the "signal-to-noise" ratio of the remaining high frequency signal. For microphones from 110° to 160°, both the filtered and unfiltered signals are recorded on tape. The sound pressure levels for frequencies below 20 kHz are calculated using the filtered signal. The jet noise spectra at a given angle are obtained finally by computationally merging these two spectra.

The prime system used for recording acoustic data is a Sangamo/Sabre IV, 28-track FM recorder. The system is set up for wideband Group I (intermediate band double extended) at 120-ips tape speed. Operating at 120-ips tape speed provides the improved dynamic range necessary for obtaining the high frequency/low amplitude portion of the acoustic signal. The tape recorder is set up for ±40% carrier deviation with a recording level of 8 volts peak-to-peak. During recording, the signal gain is adjusted to maximum without exceeding the 8 volt peak-to-peak level.

Individual monitor scopes are used for observing signal characteristics during operation. On-line data monitoring was available for this program via a Rockland narrow-band analyzer or a General Radio 1921 1/3-octave analyzer with their outputs on display scopes or hard copy via Tektronic plotter.

ORIGINAL PAGE IS
OF POOR QUALITY

Standard data reduction is conducted in the General Electric AFG Instrumentation and Data Room (IDR). The data tapes are played back on a CDC3700D tape deck with electronics capable of reproducing signal characteristics within the specifications indicated for wideband Groups I and II. An automatic shuttling control is incorporated in the system. In normal operation, a tone is inserted on the recorder in the time slot designed for data analysis. Tape control automatically shuttles the tape, initiating an integration start signal to the analyzer at the tone as the tape moves in its forward motion. This motion continues until an "integration complete" is received from the analyzer at which time the tape direction is reversed and the tape restarts at the tone in the forward direction advancing to the next channel to be analyzed until all the channels have been processed. A time code generator is also utilized to signal the tape position of the readings as directed by the computer program control. After each total reading is completed, the number of tape channels at each point is advanced to the next reading.

All 1/3-octave analyses are performed on a General Radio 1921 1/3-octave analyzer. Normal integration time is set for 32 seconds to ensure good interaction for the low frequency content. The analyzer has 1/3-octave filter sets from 12.5 Hz to 100 kHz and has a rated accuracy of $\pm 1/4$ dB in each band. Each data channel is passed through an interface to the GEPAC 30 computer. Here the data are corrected for the frequency response of the microphones. Also the data are corrected to standard day (59° F, 70% RH) atmospheric attenuation conditions using the Shields and Bass model (Reference 3-1) and then processed to calculate the perceived noise level and OASPL from the spectra. For calculation of the acoustic power, or scaling to other nozzle sizes, or extrapolation to different far-field distances, the data are sent to the Honeywell 6000 computer for data processing. This step is accomplished by transmitting the SPL's via a direct time-share link to the 6000 computer through a 1200 Band Modem. In the 6000 computer, the data are processed through the Flight-Transformed Full-Scale Data Reduction (FTFSDR) program where the appropriate calculations are performed. The data printout is accomplished on a high-speed "remote" terminal.

The detailed FTFSDR program flow chart is shown in Figure II-2. The as-measured data are first extrapolated from the measured distance to a common 40-ft arc. This is accomplished by subtracting both the distance correction [i.e., $20 \log (40\text{-ft distance}/\text{measured distance})$] and the atmospheric attenuation correction over the Δ distance (i.e., where Δ distance = 40-ft measured distance). The Shields and Bass Pure Tone Method (Reference 3-1) is used for all atmospheric attenuation corrections. The data are then converted to standard day at the 40-ft arc location by adding in the standard day correction (i.e., $\Delta \text{dB} = a_{\text{amb}} - a_{\text{std day}}$). The data are printed in tabulated form for SPL, OASPL, and PWL (for full sphere and based on the lossless data). For this program, model scale data below the chamber cutoff frequency of 250 Hz should be ignored.

The model scale data are corrected next for background noise using the background noise spectra obtained with the tertiary jet at the required simulating flight velocity. The corrected model scale data are processed next through a flight transformation procedure, described in the next subsection,

ORIGINAL PAGE IS
OF POOR QUALITY

to obtain data that are representative of the noise produced in actual flight. In addition, the FTFSDR program writes a magnetic tape for CALCOMP plotting of the data used in the course of data analyses of the test results.

2.0 THE FLIGHT TRANSFORMATION TECHNIQUE

The objective of the General Electric free-jet transformation process is to employ far-field SPL spectra at various angles to the inlet axis (typically $40^\circ \leq \theta_i \leq 160^\circ$ in increments of 10°) obtained in a free-jet experiment and transform it to yield SPL spectra as would be measured in a true moving frame experiment.

The concept employed is as follows: proper aerodynamic simulation of the effects of forward flight is achieved in a free-jet experiment; but, acoustic simulation of the effects of uniform flow over the primary jet plume noise sources is achieved to a limited extent only. In other words, the free jet achieves the effect of a right source mix radiating into an environment that nearly approaches a static environment rather than an environment of sources shrouded by either a finite or infinite extent of uniform nonturbulent flow. (The basis of several previous investigations has been to assume that a well-defined region is taken as a doubly infinite cylinder of a constant circular section equal to the cross section of the free-jet exhaust plane.). The acoustic sources in a free jet, of course, do not radiate into a completely static environment; hence, some propagation effects of the free-jet flow have to be taken into consideration.

Based on the above picture, the broad outline of the procedure adopted is as follows. Defining the "static" directivity as the directivity pattern (in various frequency bands) that the sources (of the primary jet exhaust plume altered by the effects of relative velocity due to imposition of the free-jet) may be expected to produce if they radiated into a quiescent environment, the "static" directivity is deduced first from the measured free-jet experimental data by correcting the latter for propagation effects of the free jet. Since the free-jet flow field includes intensely turbulent shear layers through which the sound field of the sources must pass before reaching the far-field microphones (located in the quiescent ambient), some degree of empiricism (especially for the high frequency sound) is involved in attempting to account for these propagation effects. These are described in detail later in this Section.

Once such a static directivity is extracted, it still remains to deduce what the noise signature of the source distribution would be if the source distribution was not stationary relative to the ambient, but moving relative to the ambient at the flight velocity. A multiple decomposition procedure suitable for the broadband jet noise problem, which attempts to synthesize the static directivity by ascribing it to a mix of uncorrelated singularities, was developed in order to predict the flight noise. Once such a decomposition is completed, the dynamic exponent applicable to each singularity can be applied to derive the flight noise signature.

In summary, the method starts with narrow-band directivities from the free-jet experiment in various 1/3-octave bands, corrects these directivities for free-jet propagation effects in a frequency-dependent manner to retrieve the "static" directivity, synthesizes the "static" directivity by a suitable mix of uncorrelated singularities, and finally applies the dynamic effect appropriate to each singularity to predict the flight noise. It is an inherent feature of the method that it works separately with each 1/3-octave-band directivity pattern. The final flight predictions can then be summed to yield either OASPL or PNL directivities or flight SPL spectra at various angles to the jet axis (Doppler shift effects on the frequency are fully accounted for during the analyses.)

A detailed algorithm description is given in Figure II-3.

The two phenomena involved in the change in the directivity of the noise radiated by the sources associated with the jet plume, when the jet is exhausting into a free-jet environment as opposed to a static environment, are

1. Refractive Effects of the Free-Jet Flows

To deduct the refractive effects of the free-jet flow, the following procedure is adopted:

- a. At low frequencies ($k_0 a < 3$), the plug flow model solution for a point pressure source is used.

$$p' = (1 - M_{at} \cos \theta_i)^{-2}$$

- b. At high frequencies ($k_0 a > 3$), the asymptotic high-frequency solution for a pressure source is used

$$p' \approx (1 - M_{at} \cos \theta_i)^{-1}$$

At these values of the frequency parameter ($k_0 a < 3$) the exhaust arc was used to deduce the refractive effect following the method due to Schubert*. In this method,

- First the refractive dip in dB along the jet exhaust axis is determined as being proportional to the product of the jet Mach number and the frequency parameter.

$$R\theta_j \quad \propto M_{at} k_0 a \quad \text{where } \theta_j = 180 - \theta_i$$

- Then a shape factor that is essentially Mach number and frequency independent is used to determine the refractive

*Schubert, "Numerical Study of Sound Refraction by a Jet Flow; Wave Acoustics," J. of Acoustical Society of America, September 1971.

dip at other angles. For the range $3 < k_o a < 6$, Ribner's results were used with a linear extrapolation in the range $6 > k_o a > 1.25$.

- Based on experimental data, the refractive dip in the exhaust arc for $k_o a > 6$ was considered independent of $k_o a$, but still linearly proportional to $M_{a/c}$.

2. Absorptive Effects of the Fine Grain Turbulence in the Shear Layer of the Free Jet

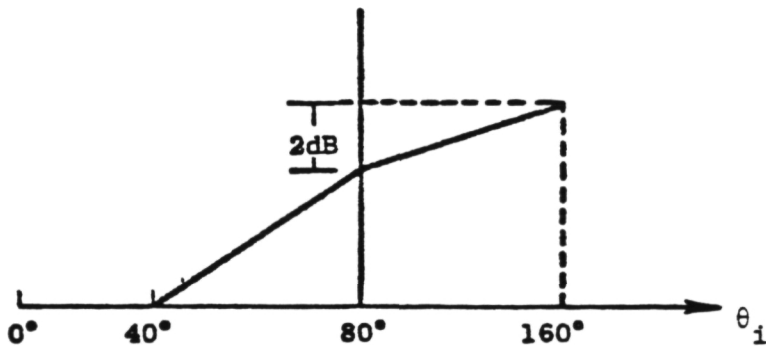
This relates to the fact that fine-grained turbulence in the shear layer of the free jet can absorb sound, especially at high frequencies. This correction is based on Crow's* theory which states that the effective absorption coefficient is proportional to the frequency, the distance the sound traveled in the shear layer, and the square of the Mach number, i.e.,

$$\alpha_T = f M_{a/c}^2 \frac{l}{a} \ell$$

where $M_{a/c}$ = free-jet Mach number

ℓ = path length

Based on the path length that the sound has to traverse, the absorption coefficient is assumed to vary with θ_i as shown in the figure below



*Crow, S.C., "Viscoelastic Character of Fine-Grained Isotropic Turbulence," Physics of Fluids, Volume 10, July 1967.

ORIGINAL PAGE IS
OF POOR QUALITY

The absorption was calculated assuming an eddy viscosity of 70μ for $M_{at} = 0.25$ and $f = 50$ KHz. This yields corrections for $k_0 a > 30$. The actual expressions used were

$$\text{Corr}_T \left|_{\theta_i = 90^\circ} \right. = \begin{cases} 2 \left(\frac{M_{at}}{1/4} \right)^2 \times \frac{k_0 a}{38.4} & \text{for } ka \geq 30 \\ 0 & \text{otherwise} \end{cases}$$

$$\text{Corr}_T \left|_{\theta_i > 90^\circ} \right. = \text{Corr}_T \left|_{\theta_i = 90^\circ} \right. + 2 \left(1.5 - \frac{180 - \theta_i}{60} \right)$$

The above correction modification term for aft angles is limited to 3 dB.

$$\text{Corr}_T \left|_{\theta_i < 90^\circ} \right. = \text{Corr}_T \left|_{\theta_i = 90^\circ} \right. \times \left(2.8 - \frac{180 - \theta_i}{50} \right)$$

From the measured free-jet data, the refraction and turbulence absorption corrections are added to obtain the "basic" directivity of the sources.

The basic directivity obtained above is assumed to be generated by a set of singularities, F_0 , F_x , F_y , etc., such that the sound field is a solution to

$$\frac{\nabla^2}{p} + k_0^2 p = F_0 \delta(x) \delta(y) \delta(z) + F_x' (x) \delta(y) \delta(z) + F_y (x) \delta(y) \delta(z)$$

where F_0 , F_x , F_y are mutually uncorrelated, so that they contribute to the far field only additively. As the mean square pressure of any singularity is symmetric about both $\theta_i = 0^\circ$ and $\theta_i = 90^\circ$, the inlet and exhaust arc are synthesized separately.

The procedure adopted to determine the dynamic effect is as follows:

1. From the "basic" directivity pattern, obtain the normalized SPL's based on the least SPL in both the forward and aft quadrants.
2. Determine the linearized levels using the question

$$\overline{p'^2} = 10 \frac{\text{SPL}-\text{SPL}_{\min.}}{10}$$

3. Decide on a level of fitting by using the criterion that the data ought to be reconstructed to within an average error of 2 dB. Assuming that the data ought to be reconstructed with the least singular distribution of uncorrelated sources possible, the problem

ORIGINAL PAGE IS
OF POOR QUALITY

simplifies to one of solving a least squares problem of the type find \underline{x} to minimize $|\underline{r}| = (\underline{A}\underline{x} - \underline{b})$ subject to nonnegative constraining $\underline{x} \geq 0$. This is done by using an algorithm based on the Kuhn-Tucker theorem of optimization theory.

4. The singularities obtained by using the Kuhn-Tucker theorem are combined to obtain the least singular decomposition of the sources.
5. The appropriate dynamic effect is applied to each singularity type to determine the correction that is applied to the measured free-jet data corrected for refraction and turbulence absorption. If the mean square of the sound pressure is obtained by adding the singularities as

$$P_0'^2 = F_0 C^6 + F_x C^4 S^2 + F_y C^2 S^4 + F_z S^4$$

where $C = \cos \theta_i$

$S = \sin \theta_i$

the dynamic effect is calculated using the relation

$$\text{Dynamic effect} = 10 \log_{10} \frac{P_F'^2}{P_S'^2} = 10 \log_{10} \frac{\frac{F_0 C^6}{K^8} + \frac{F_x C^4 S^2}{K^8} + \frac{F_y C^2 S^4}{K^8} + \frac{F_z S^4}{K^6}}{P_S'^{12}}$$

where $K = (1 + M_{ac} \cos \theta_i)$

6. The levels are then corrected to

$$\text{SPL}_{\text{flight at free-jet frequency}} = \text{SPL}_{\text{basic}} + \text{dynamic effect}$$

7. Doppler frequency shift results in a flight frequency given by

$$f_{\text{flight}} = \frac{f_{\text{free jet}}}{(1 + M_{ac} \cos \theta_i)}$$

8. Then, $\text{SPL}_{\text{flight}} (\text{at } f_{\text{flight}}) = \text{SPL}_i (\text{at } f_{\text{free jet}})$.

Thus by using the above transformation, the free-jet data are transformed into flight data. Further discussion of this procedure is found in Ref. 2-1.

ORIGINAL PAGE IS
OF POOR QUALITY

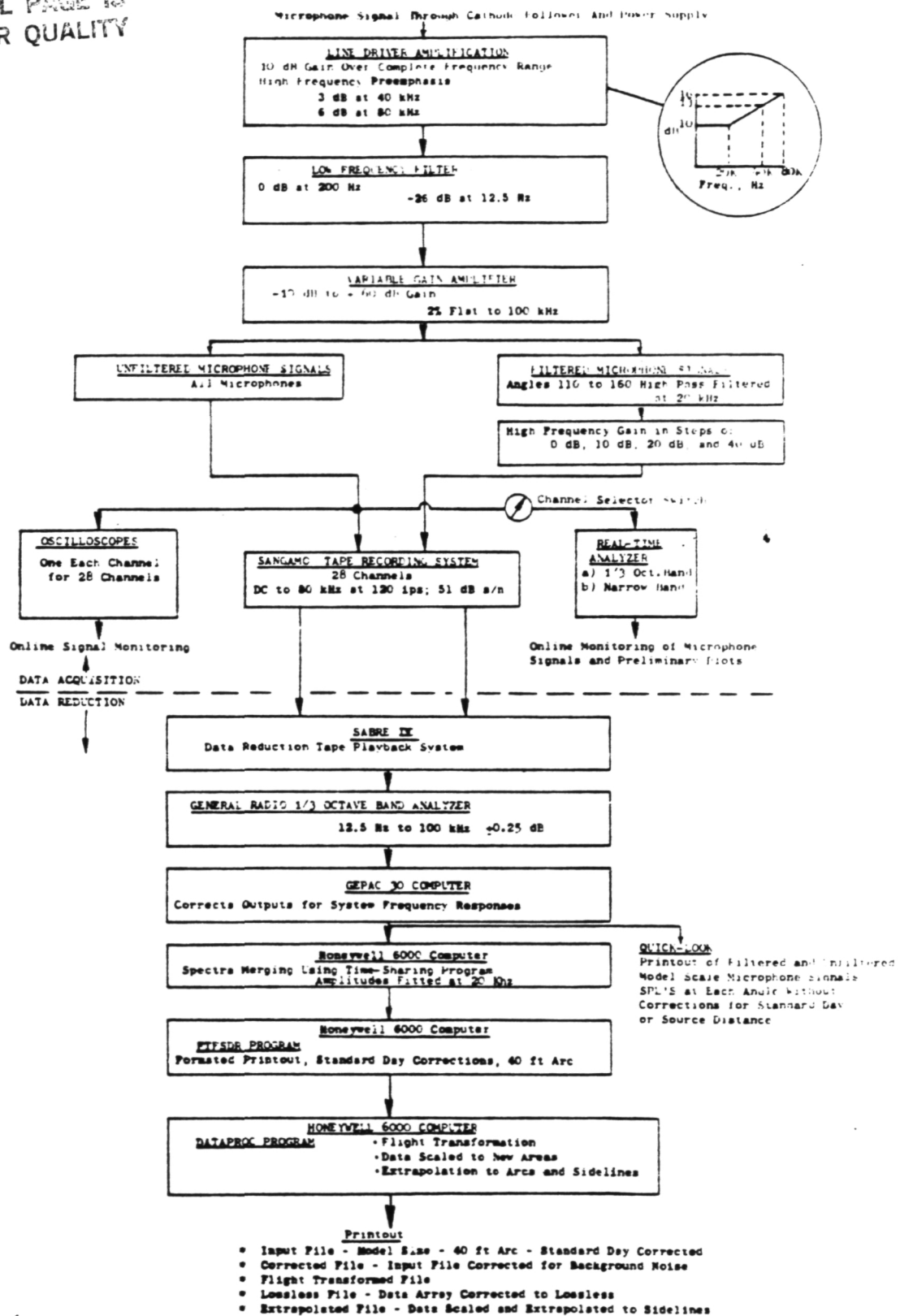


Figure II-1. Acoustic Data Acquisition and Reduction System.

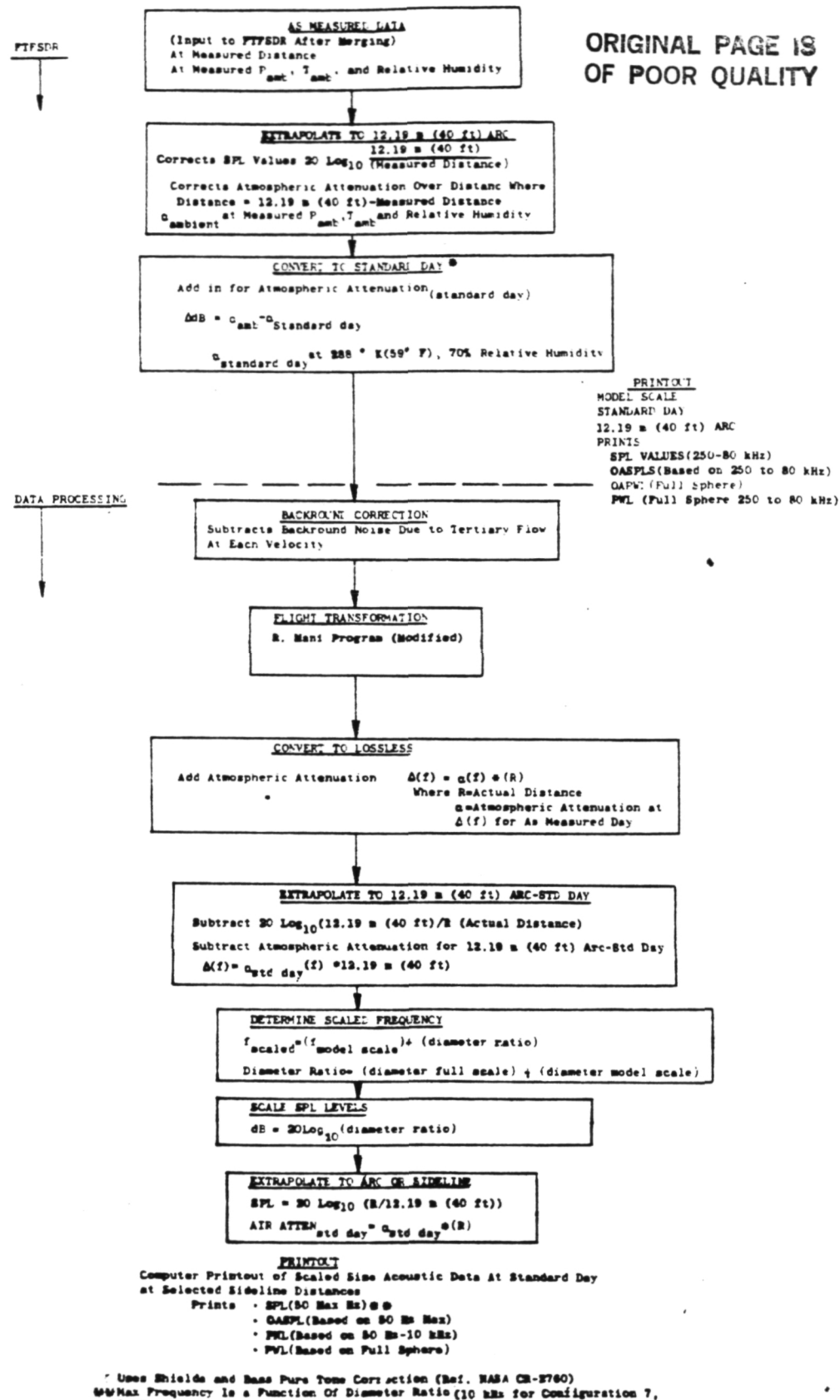


Figure II-2. Acoustic Data Processing Flow Chart.

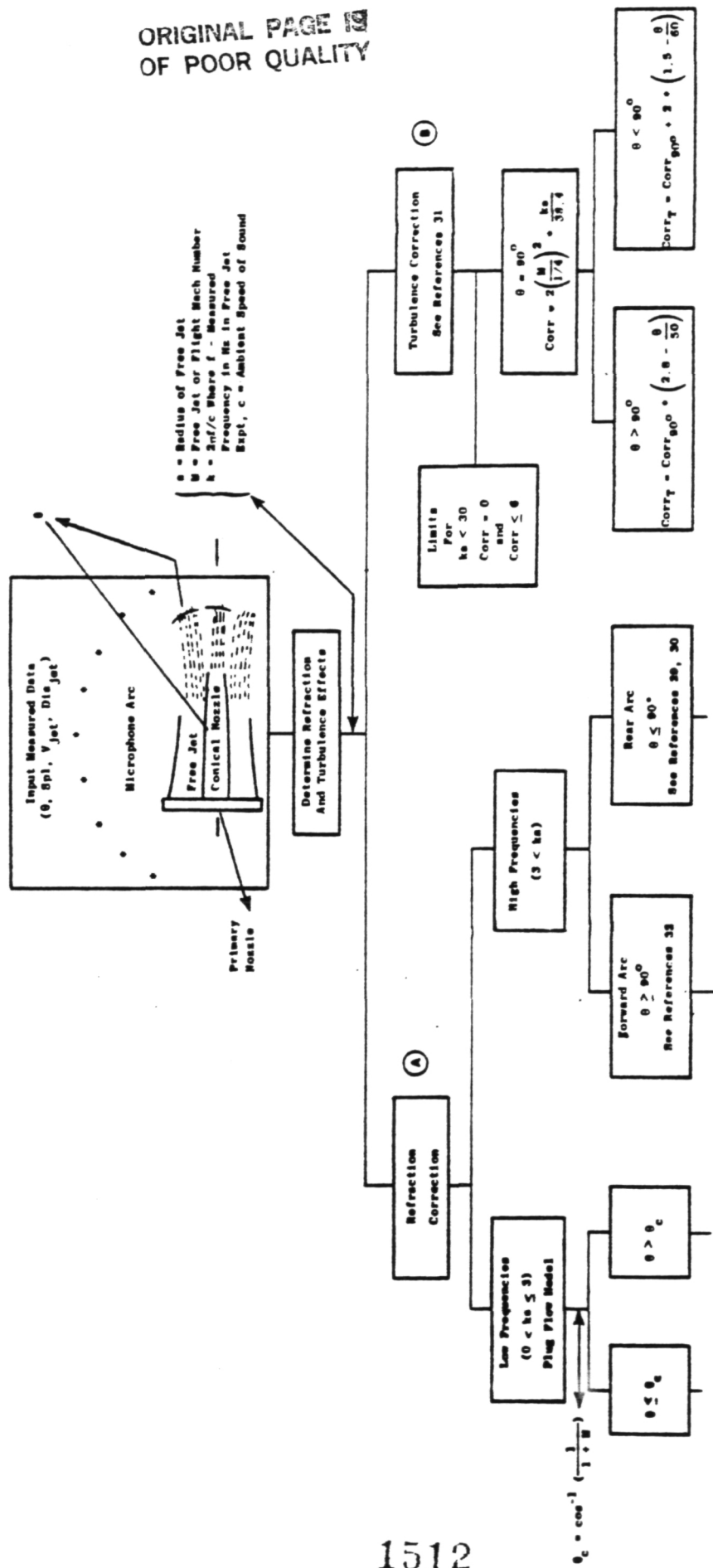


Figure II-3. Algorithm Description.

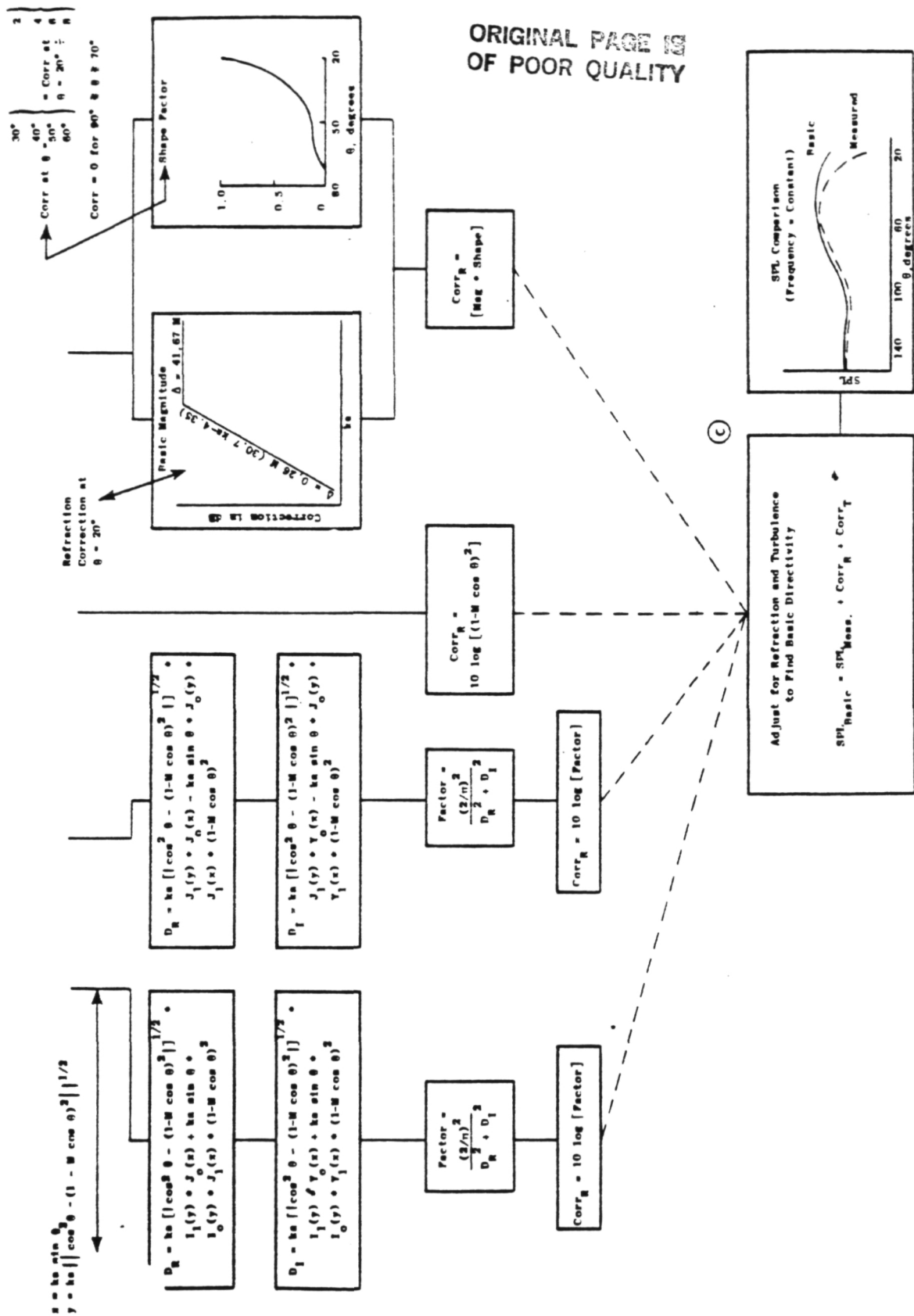


Figure 11-3. Algorithm Description (Continued).

ORIGINAL PAGE IS
OF POOR QUALITY

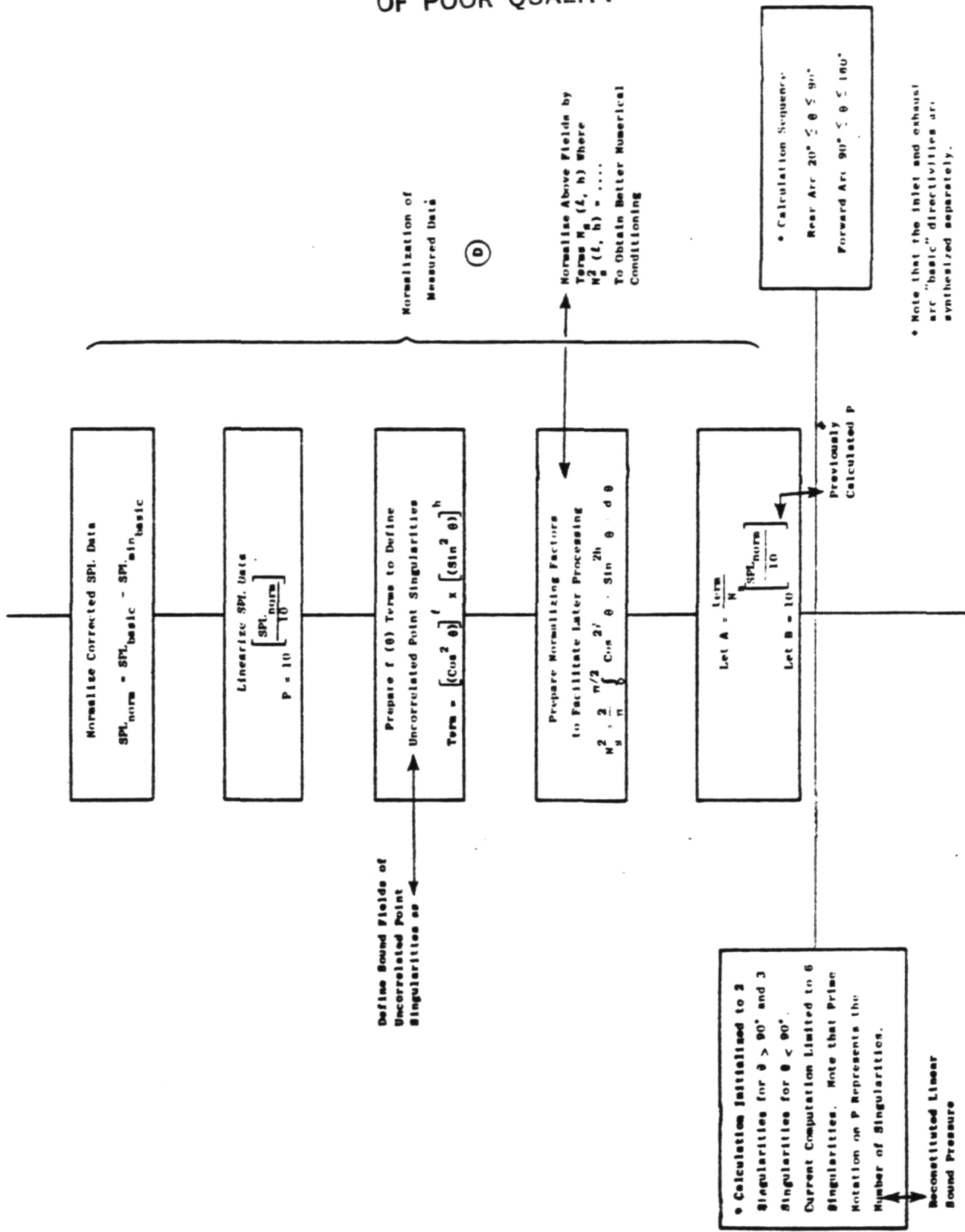


Figure II-3. Algorithm Description (Continued).

ORIGINAL PAGE IS
OF POOR QUALITY

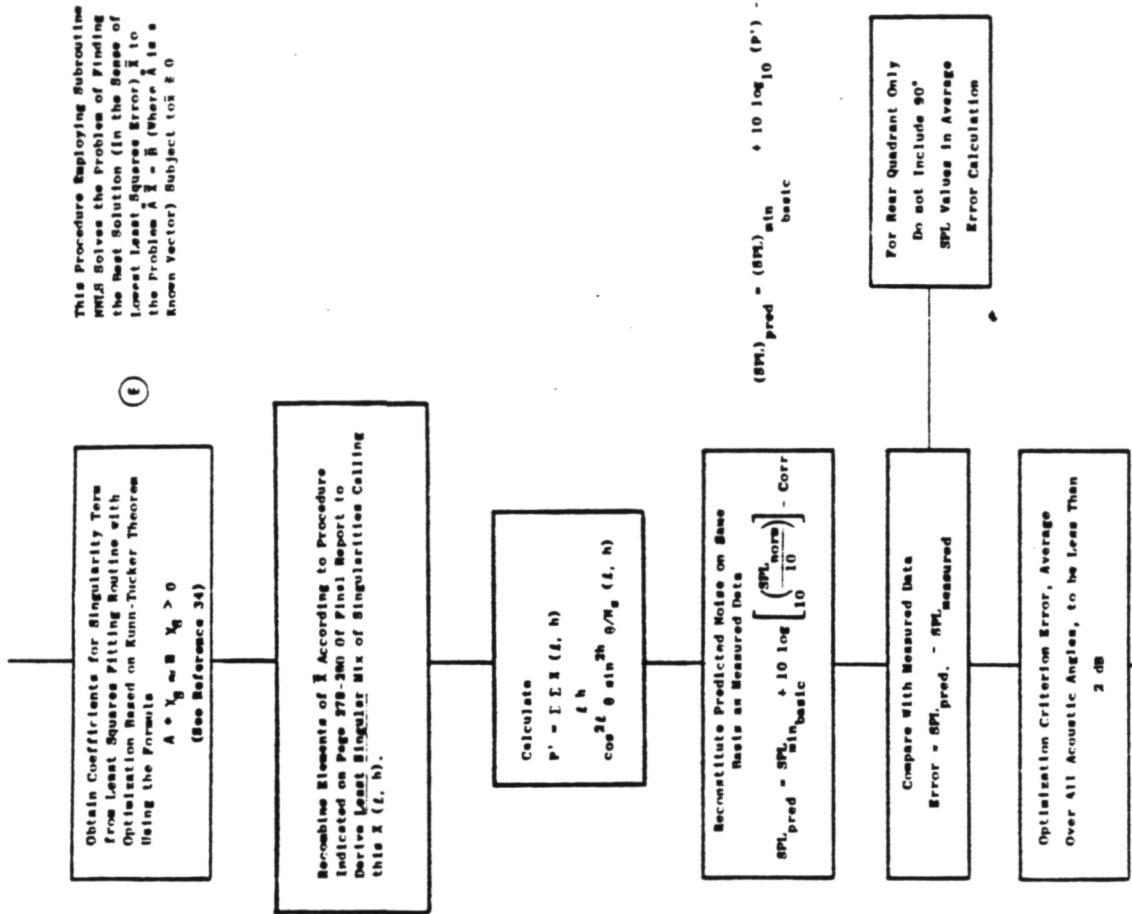
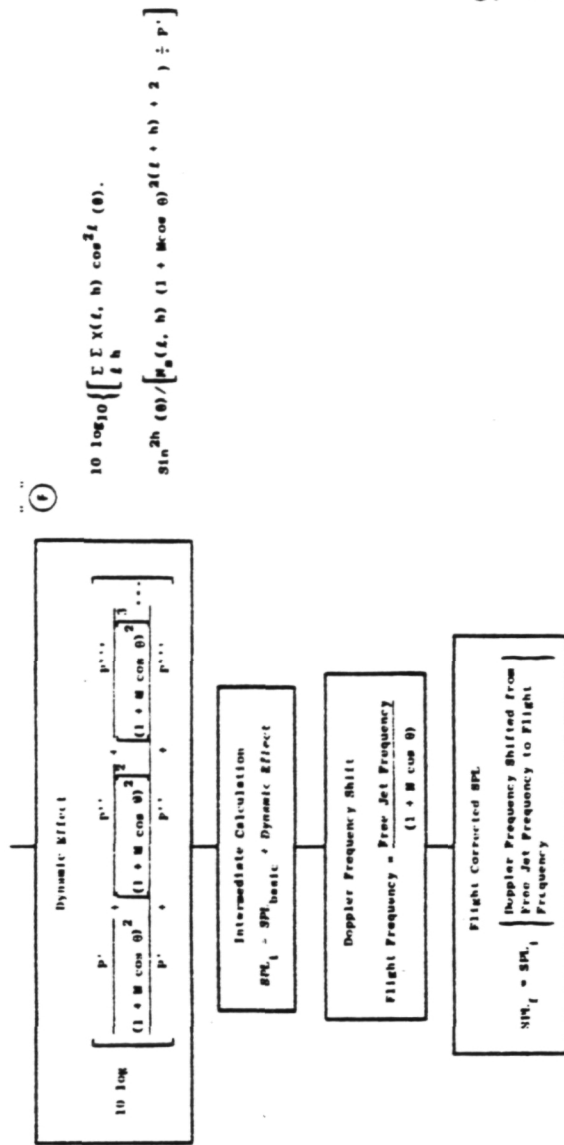


Figure 11-3. Algorithm Description (Continued).



List of Symbols

A	An Input Matrix to the Least Squares Fitting Procedure	I	Numerical Value Varies with Level of Singularity Considered
M	An Input Vector to the Least Squares Fitting Procedure	M	Mach Number = (Free Jet Velocity) / (Ambient Speed of Sound)
$n(t, h)$	An Array used to Identify the Refraction and/or Turbulence Correction	S	Normalizing Factor, Function of Singularity
P		p_{ref}	Linear Bound Pressure
P _{ref}		R	0.0003 Microbars
		Subscript for Refraction Correction	
		S	Singularity Subscript
		T	Sound Pressure Level = $10 \log (p^2/p_{ref}^2)$
		X	Subscript for Turbulence Correction
		x	Basel Function Argument, $x = k \sin \theta$
		y	A Vector Derived from Least Squares Fitting, Function of Singularity
D_n	Real Root of Denominator Term in Solution of the Sound Pressure for the Free Flow Model	y	Bessel Function Argument, $y = k \sin^2 \theta - (1 - M \cos \theta)^2$
n_i	Imaginary Root of Denominator Term in Solution of the Sound Pressure for the Free Flow Model	$y_n(x)$	Bessel Function of the Second Kind of Order n, Argument x
r	Subscript for Flight Corrected SPL	θ	Angle from the Jet Axis Referred to the Emissive Critical Angle that Defines the Jet Zone of Silence = $\cos^{-1}(1/M)$
s	Numerical Value Varies with Level of Singularity Considered	T	
t	Subscript on SPN to Identify an Intermediate Calculation	x	
i		y_n	
$I_n(x)$	Multivalued Bessel Function of the First Kind of Order n, Argument in $is\ x$	y	
$I_n(r)$	Multivalued Bessel Function of the First Kind of Order n, Argument in $is\ y$	$y_n(x)$	
$J_n(x)$	Bessel Function of the First Kind of Order n, Argument in $is\ x$	θ	
$J_n(y)$	Bessel Function of the First Kind of Order n, Argument in $is\ y$	θ_c	
k	Frequency Parameter = (Free Jet Frequency Band of Interest in Hertz per Second) = (Free Jet Radius in feet) : (Ambient Speed of Sound in feet)		

Figure II-3. Algorithm Description (Concluded).

APPENDIX III
AERODYNAMIC DATA ACQUISITION AND REDUCTION PROCEDURES

The facility operating parameters are monitored during testing at the control console to (1) ensure that prescribed facility limits are not exceeded and (2) set the test point conditions.

The core and fan discharge pressures are measured from a single element on their respective rakes and are used for setting the desired nozzle pressure ratios. These parameters also are routed through the Dymec scanning system and recorded along with nozzle performance data by the aerodynamic data handling (ADH) system.

Facility temperatures are monitored at the control console using a Doric multichannel temperature indicator. The unit has a 24-channel capability and is designed for use with Type K thermocouples (chromel-alumel). It is used for safety monitoring and setting test point temperatures for the dual flow system. A system schematic is shown on Figure III-1.

1.0 NOZZLE PRESSURE AND TEMPERATURE MEASUREMENTS

A critical parameter used in evaluating acoustic test results is nozzle exhaust velocity. Determination of this velocity depends on an accurate determination of the exhaust temperature and pressure, which in turn depend on adequate sampling across the stream to account for profile effects. Special multielement rakes have been designed for use on the single and dual flow systems.

The system uses two rakes, each having three pressure and three temperature elements with spacing of the elements corresponding to centers of six equal area annular segments of the flow stream. These rakes use shielded Type K thermocouples (chromel-alumel) which have a recovery factor very close to unity.

Pressure measurement accuracy is controlled by the accuracy of the transducer used for the measurement. The scanivalve transducers that are used are rated at 0.1% of full-scale range.

2.0 PERFORMANCE DATA PROCESSING

Aerodynamic parameters are calculated based on the acquired temperature and pressure information. The input information for nozzle performance consists of ambient pressure (P_{amb}), nozzle discharge total temperature (T_T), and nozzle total pressure (P_T).

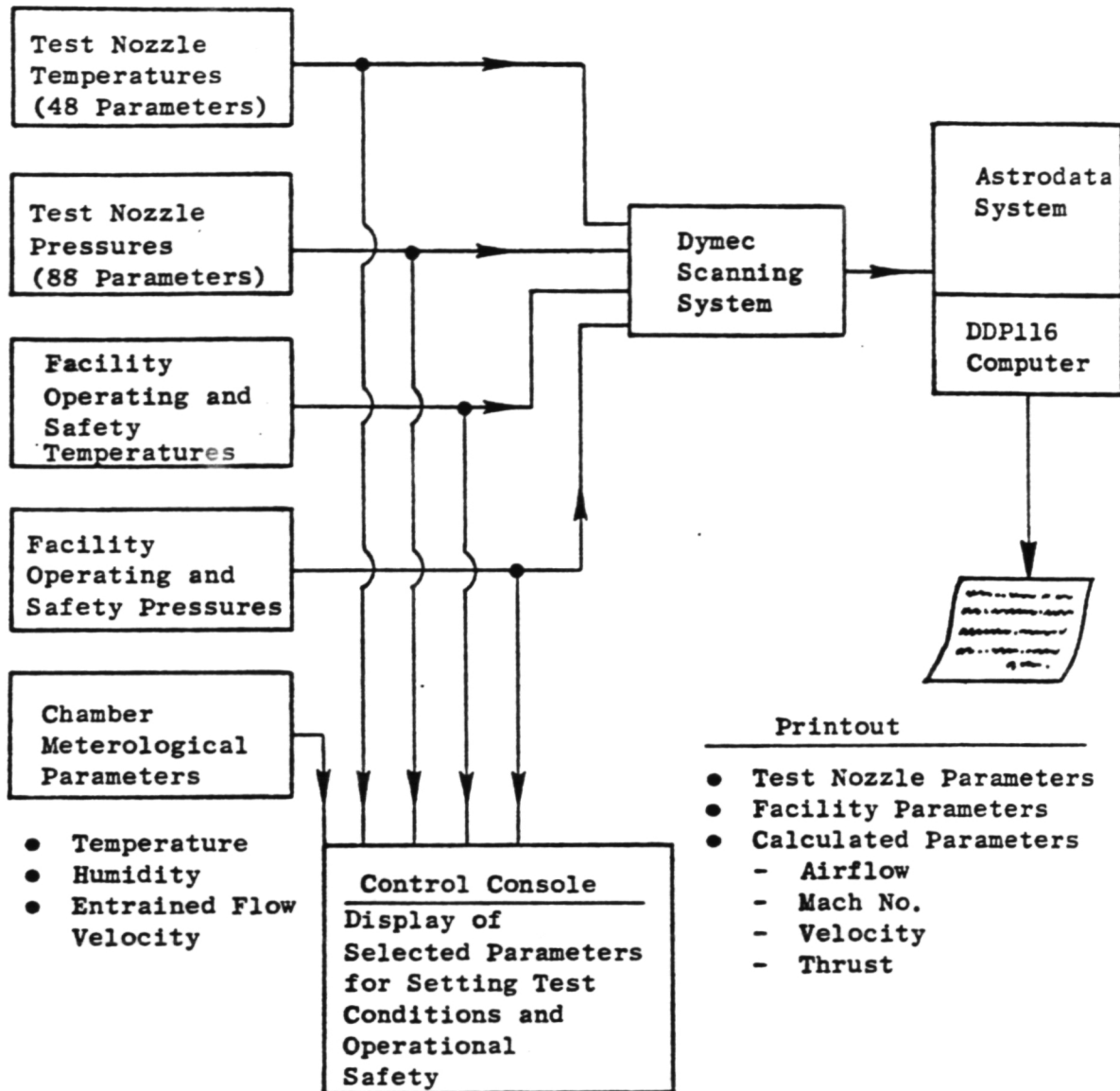


Figure III-1. General Electric Anechoic Chamber Aerodynamic Data Processing System.

Output of the processing program consists of tabulations of the individual input parameters with their identification, averages of similar parameters (i.e., P_T rake average), and calculated parameters as indicated in the following paragraphs:

1. Gamma

For $T_S \leq 440^\circ K$ ($788.3^\circ R$); $\gamma = 1.4$

For $T_S > 440^\circ K$ ($788.3^\circ R$); $\gamma = \frac{2.23708}{(T_S)^{0.070271}}$
with T_S in $^\circ R$

2. Isentropic or Ideal Mach number

$$M_j = \left(\frac{2}{\gamma-1} \right)^{1/2} \left(\left(\frac{P_T}{P_{amb}} \right)^{\frac{\gamma-1}{\gamma}} - 1 \right)^{1/2}$$

$$\frac{T_T}{T_S} = 1 + \left(\frac{\gamma-1}{2} \right) M_j^2$$

$$T_S = T_T / \left(\frac{T_T}{T_S} \right)$$

T_S is initially assumed to be equal to T_T . Starting with the gamma calculation, the above steps are repeated by an iteration procedure until the difference in T_S between iterations is <1.0.

3. Local Sonic Velocity

$$c = \sqrt{\gamma R T_S}$$

4. Ideal Velocity (fully expanded)

$$V_j = M_j c$$

5. Calculated Ideal Thrust

$$F = V_j \dot{W}$$

3.0 HUMIDITY AND TEMPERATURE MEASUREMENT

One of the parameters necessary for correcting acoustic data for atmospheric absorption is the humidity content of the air through which the signal is propagating. Since varying nozzle operating conditions may cause changes in the chamber environment during the course of testing, a means of remote humidity readout is required. This is accomplished through the Hygrometrix Model 8501 Relative Humidity System. This system utilizes a Xeritron sensor that is an assembly of hygromechanical crystallite structures and pieoresistive silicon strain gages on a common substrate. The sensing element responds to changes in relative humidity by a dimensional change reflected in the strain gage resistance with its resistance being proportional to the relative humidity.

Temperature at the humidity sensor location is measured using a Type K thermocouple. Readout of both temperature and relative humidity is provided at the cell control panel and is logged for each test point. Provision exists for humidity readout from any of the microphone positions; however, the sensor is mounted at the 40° microphone position, since this location represented a good approximation of mean chamber conditions as determined from the environmental survey. The manufacturer's stated accuracy for this system is ±2% over the range of -40° C to +1250° C.

APPENDIX IV
LASER VELOCIMETER SYSTEM

1.0 GENERAL ARRANGEMENT

The laser velocimeter (LV) arrangement used during this program is a system developed under a USAF/DOT-sponsored program and reported in detail in Ref. IV-1. The basic optics system is a differential Doppler, backscatter, single-package arrangement that has the proven feature of ruggedness for the severe environments encountered in high velocity, high temperature jets. Fig. IV-1 shows a photograph of the LV system in the General Electric Anechoic Test Facility. Fig. IV-2 is a schematic arrangement of the laser package. The laser beams are projected from below the lens, forming an angle , that keeps the major axis of the control volume ellipsoid to a minimum. The dimensions of the control volume are 0.635 cm (0.25 inch) for the major axis and 0.518 cm (0.020 inch) for the minor axis. The range of the LV control volume from the laser hardware is 2.16 m (85.0 inch). The three steering mirrors and the beam splitter are mounted on adjustable supports, all of the same aluminum alloy, which eliminates temperature-alignment problems.

2.0 LV ACTUATOR AND SEEDING

Two remotely actuated platforms are available, i.e., normal traverse platform and slant traverse platform. The normal traverse platform has three axes: vertical, horizontal, and axial. Travel capabilities are 0.813 m (32 in.), 0.813 m (32 in.), and 5.79 m (228 in.), respectively. Resolution is 0.1588 cm ($\pm 1/16$ in.) for each axis except for the last 5.28 m (208 in.) of axial travel, which has a resolution of 0.3175 cm ($\pm 1/8$ in.).

The slant traverse platform enables LV traverse to be made along the axis that is parallel to the plug surface. Travel capability is 0.508 m (20 in.) in the axial direction parallel to the plug surface (which makes an angle of 15° to the nozzle axis). Resolution is 0.1588 cm ($\pm 1/16$ in.).

Seeding is by injection of aluminum oxide (Al_2O_3) powder, nominal 1-micron diameter, into the supply air to the burner and into the region of the nozzle so as to seed the entrained air. The powder-feeder equipment used is described in Ref. IV-1 except that the fluidized bed column supply air is currently heated to about 394.1 K (250° F) to prevent powder aggregation by moisture absorption.

3.0 SIGNAL PROCESSING AND RECORDING

The LV signal processor used is a direct-counter (time-domain) type similar to that reported in Ref. IV-1 but with improvements. These improvements result in a lowered rate of false validations and improved linearity and resolution. Turbulent velocity probability distributions (histograms) are recorded by an NS633 pulse-height, 256-channel analyzer. All the data acquired from the laser unit is transmitted to a microcomputer system which stores the data on floppy disk and performs all the necessary data reduction functions.

The processing capabilities of the General Electric LV system are as follows:

- Velocity range - 35 to 5000 fps
- Random error for single particle accuracy (error associated with system inaccuracies such as fringe spacing, linearity, stability, burst noise) - 0.75%
- Bias error for mean velocity - 0.5%
- False data rejection capability (possibility of accepting bad data) - <0.0002%.

The GE System uses a 16-fringe control volume where all of the 8 center fringes are used in the data acceptance/rejection testing.

4.0 LV DATA REDUCTION

The concept of using LV measurements for obtaining the mean and turbulent velocity profiles may be described as follows: two beams of monochromatic light intersect at a point in space and set up a fringe pattern of known spacing (see Figure IV-3). The flow is seeded with small particles which pass through the measuring volume. The light scattered from the particles is collected, and the laser signal processor measures the time it takes for the particles to pass through each fringe. Knowing the distance and time for each validated particle enables the construction of the usual histogram (see insert on Figure IV-3). Then by statistical techniques, the mean value (which corresponds to the mean velocity) and the standard deviation (which corresponds to the turbulent velocity) are constructed. Although the principle of measurement is easy, the practical aspects associated with the design of an electronic processing unit to monitor the valid particles are quite challenging. Investigators have had great difficulty performing measurements even in low velocity jets, and the extension to heated supersonic jet measurements represents a major achievement. The method of calculation used to obtain the mean and turbulent velocities from LV measurements is described below.

1. Histogram

A histogram is an estimate of the first-order probability density of the amplitude of a given sample. To obtain a velocity histogram, the time-dependent LV velocity, $V(t)$, is accumulated and divided into classes bounded by values of velocity increments V_i . For each independent sample of velocity, a class interval is formed such that $V_{i-} < V(t) < V_{i+}$. During a measurement period, k_i number of velocity samples are accumulated in each sample class V_i . From the total sample of measured velocity points, the histogram is constructed as shown in Figure IV-3. The mean velocity and turbulent velocity derived from the histogram are obtained as described below.

2. Mean Velocity

The mean velocity of the jet, \bar{V}_j , obtained from the discrete velocity sample is calculated by:

$$\bar{V}_j = \sum \left(\frac{V_{i+1} + V_i}{2} \right) \frac{k_i}{N}$$

All Class
Intervals

where

$\frac{V_{i+1} + V_i}{2}$ is the value of the sampled axial velocity component at the center of the class interval

k_i is the number of velocity samples in the class interval

N is the total number of velocity samples ($= \sum k_i$) in the histogram

3. Turbulent Velocity

To obtain the turbulent velocity, V' , from the sampled data contained in the histogram, the standard square root of the statistical variance is performed. This calculation is performed using the following equation:

$$V' = \left[\sum_{\text{All Class Intervals}} \left(\frac{\frac{V_{i+1} + V_i}{2} - \bar{V}_j}{\frac{N}{k_i}} \right)^2 \right]^{1/2}$$

4. Statistical Errors for LV Mean and Turbulent Velocity Measurements

With any large data sample, as obtained through the collection of velocity samples in an LV histogram, guidelines for estimating the accuracy of each measurement are required. Tables IV-I and IV-II provide estimates of the percent error obtained for a mean velocity or turbulent velocity LV measurement.

Table IV-I lists the percent error for a 95% confidence statement of mean velocity measurement as a function of the total number, N , of velocity samples contained in the histogram and the turbulence level, V'/\bar{V}_j . Table IV-II gives the percent error for a 95% confidence statement of the turbulent velocity estimate as a function of N , the total velocity sample. As can be seen from Table IV-I, a fairly small sample of velocity measurements is required to obtain a good estimate of the mean velocity. For the turbulent velocity, the number of data samples required for a good estimate increases substantially. The usual number of samples obtained with the General Electric LV during a

routine data-taking measurement performed during this program is approximately 1000 samples. For simple and quick diagnostic-type information, this amount of samples is sufficient. For more advanced measurements, such as turbulence spectra or two-point cross correlations, many more data samples are required than are obtained currently on a routine basis.

5.0 LV TRAVERSES FOR MEAN VELOCITY PROFILES

In addition to the above described stationary mode of OV operation for the determination of mean and turbulent velocities at discrete points, the LV is operated also in a traversing mode to obtain continuous profiles of mean velocities. These traverses are possible along any of the three axes with the normal traverse platform and along the slant axis parallel to the plug surface with the slant traverse platform. During these traverses, the data describing the velocity levels and the location of the measurement volume are recorded continuously on an X-Y plotter. The traversing speeds are adjusted as well as traverses repeated for obtaining well-defined mean velocity profiles.

As one of the new features incorporated in the present LV test efforts, a new micro-computer software has been developed that enables mean velocity data to be obtained during any traverse mode (i.e., axial or radial, chordwise and slant axial) from mini-histograms in the form of plots of mean velocity versus traverse distance. During the present tests, the mean velocity data measured with the mini-histograms were acquired from the acceptable data samples set to 20. This number of samples yields an estimated 5% error in the LV mean velocity measurements with a statistical 95% confidence level for a given turbulence intensity of 10%.

ORIGINAL PAGE IS
OF POOR QUALITY

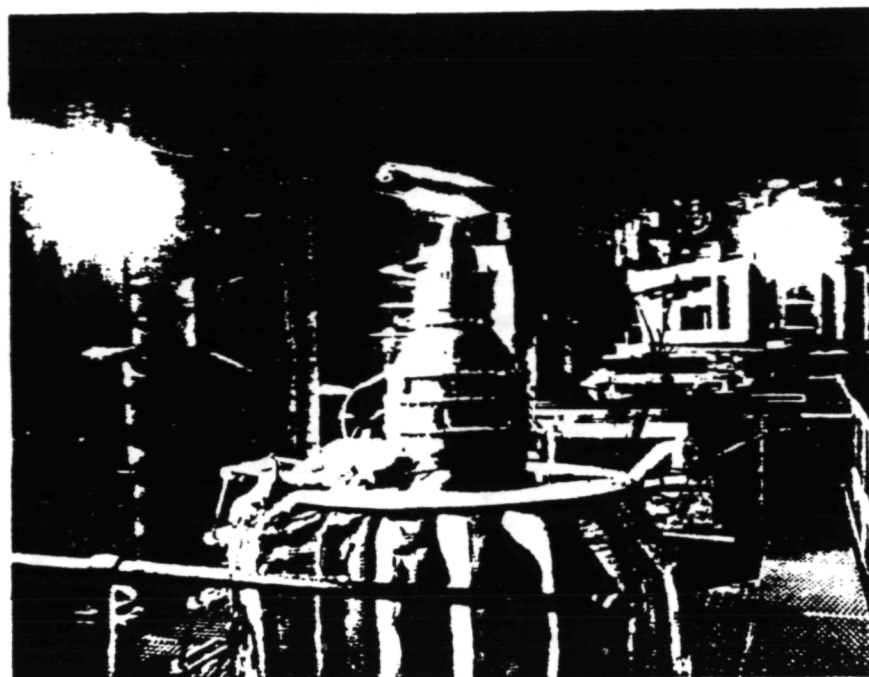


Figure IV-1. Laser System in the GE Anechoic Jet Noise Test Facility.

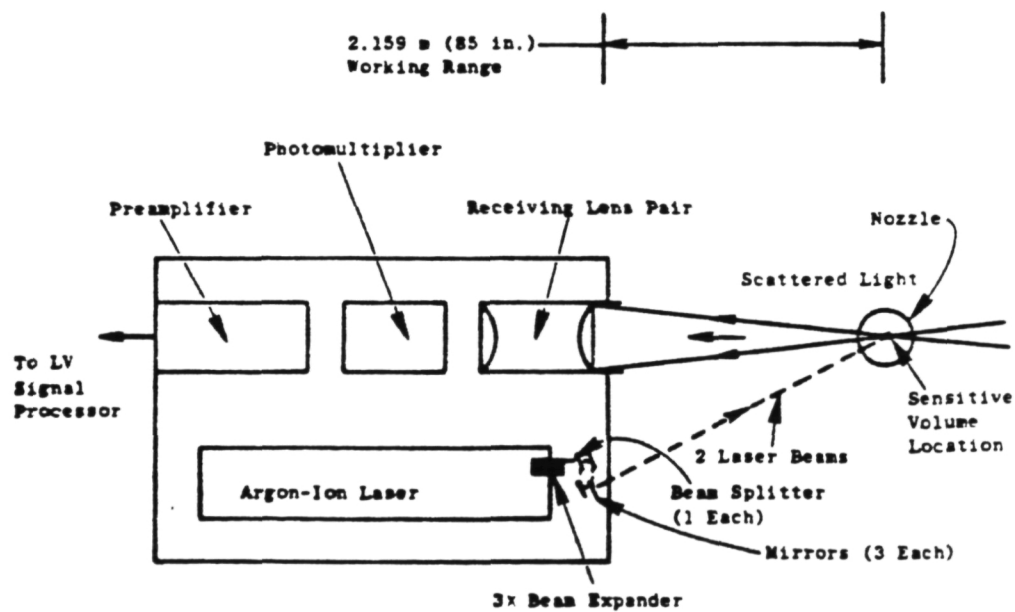


Figure IV-2. Laser Velocimeter Optics Package.

ORIGINAL PAGE IS
OF POOR QUALITY

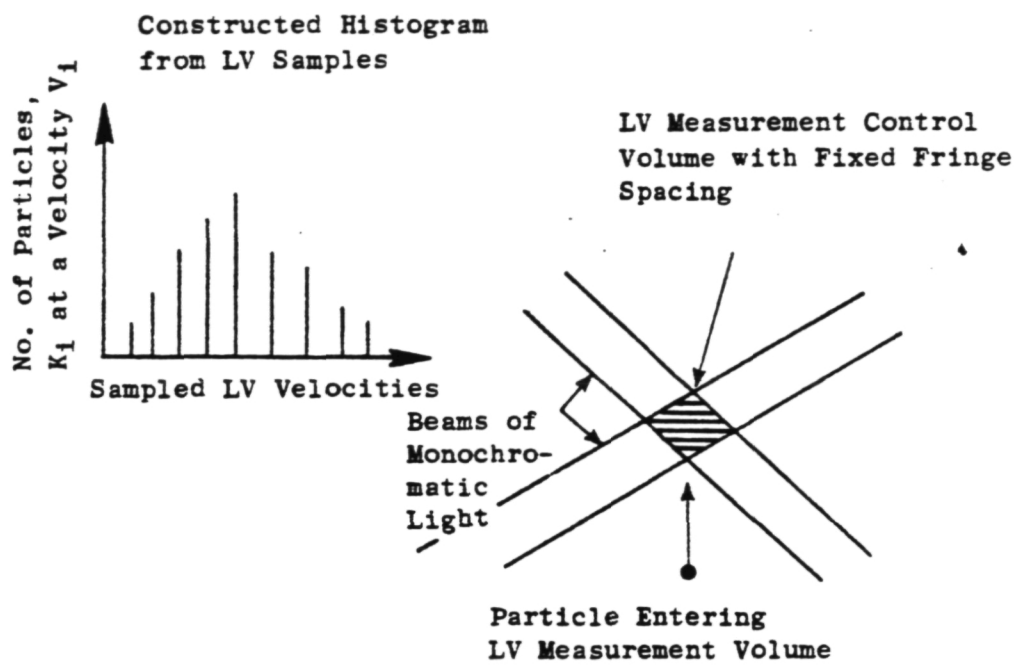


Figure IV-3. Schematic of Laser Velocity Measurements.

Table IV-I. Estimated Percent Error in the LV Measurement
of Mean Velocity with 95% Confidence.

N	u'/\bar{v}_j			
	0.2	0.1	0.05	0.025
10	14.1	7.0	3.5	1.76
20	9.3	4.7	2.3	1.20
30	7.4	3.7	1.9	0.93
40	6.3	3.2	1.6	0.80
60	5.0	2.6	1.3	0.65
120	3.6	1.8	0.9	0.45

Table IV-II. Estimated Percent Error for LV Turbulent
Velocity Measurements with 95% Confidence.

N	Percent Error
20	31.50
40	21.80
60	17.80
120	12.60
240	9.12
480	6.45
960	4.56
5,000	2.00
25,000	0.89

APPENDIX V

SHADOWGRAPH SYSTEM

A shadowgraph system was installed in GE's anechoic free-jet facility to perform diagnostic flow visualization tests. To obtain the shadowgraph photos of good resolution, the system was mounted in near proximity of the jet nozzle. The light source mounted on the optical bench was of steady-state type. Collimation of the light through the test volume was achieved by means of a reflective mirror system of 10-inch diameter. Shadowgraph images were backdropped on a screen which has a sufficient size to encompass the total test section of the given flow and is located at 12 feet 2 inches from the jet nozzle. A mounting platform for the steady-state light source, reflective mirror and camera system is remotely controlled to position the shadowgraph system for an approximately three (3) foot vertical flow field study. The schematic arrangement of the shadowgraph setup in GE's anechoic free-jet facility is shown in Figure V-1.

PRECEDING PAGE BLANK NOT FILMED

ORIGINAL PAGE IS
OF POOR QUALITY.

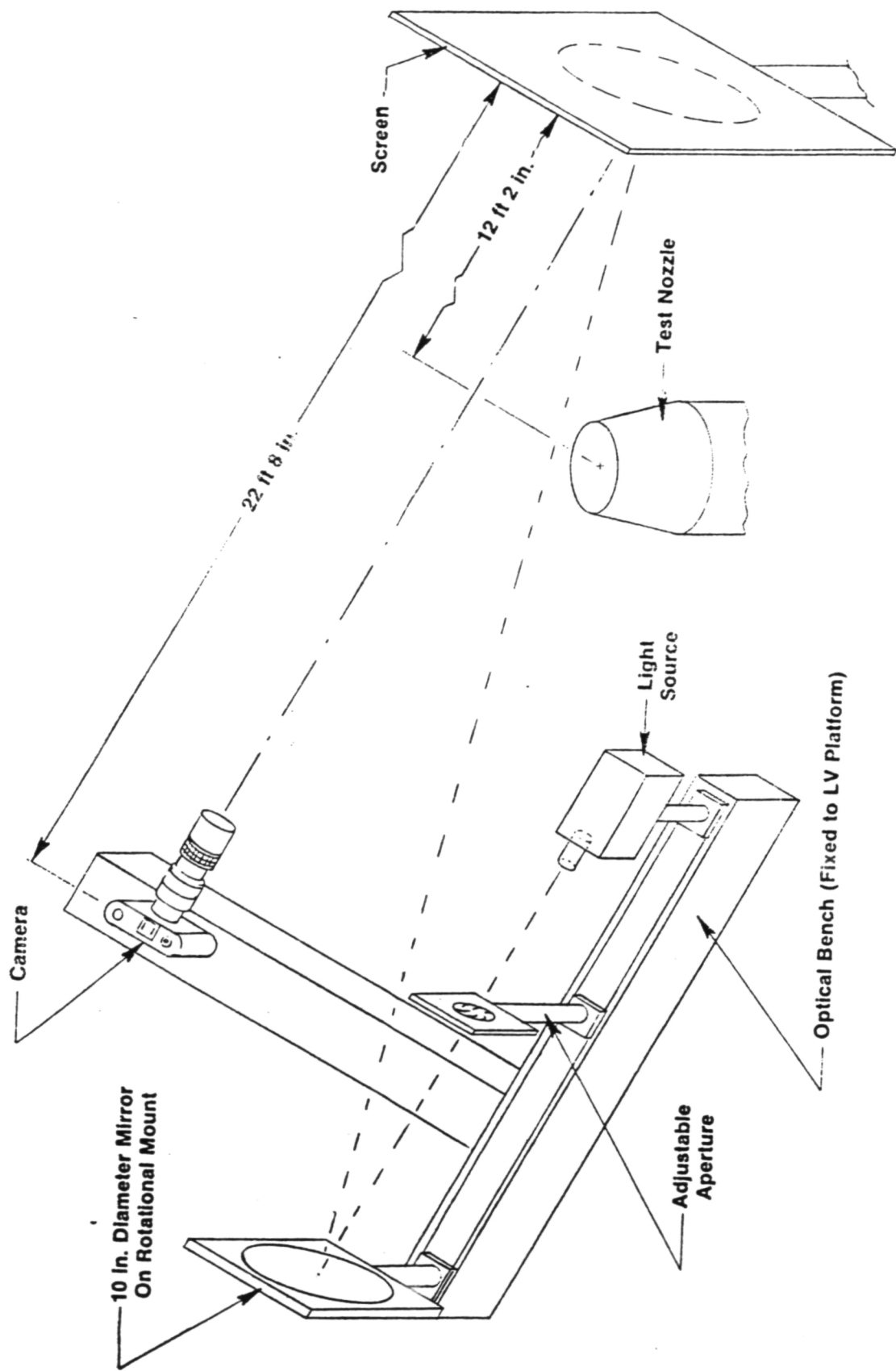


Figure V-1. Schematic Arrangement of the Shadowgraph Setup in the Anechoic Jet Facility.

APPENDIX VI

DESIGN DRAWINGS OF SCALE MODEL NOZZLES

Detailed design information relative to the seven test configurations delineated in Section 2.0 is included within this Appendix. Note: For ease of reference, Table 2-1 of Section 2.0 is repeated as Table VI-1. It summarizes the test configurations and all applicable schematics, drawings and photos.

**ORIGINAL PAGE IS
OF POOR QUALITY**

Table VI-1. Summarization Scale Model Nozzles with Applicable Text and Appendix Figures.

Configuration No.	Description	Figure Numbers Within Text				Figure Numbers Within Appendix VI			
		Geom. Schem.	Photos	Instr. Schem.	Instr. Photos	Geometric Details	Photos	Instr. Details	Instr. Photos
1	Baseline Conical-Convergent Nozzle	2-1	2-2	N/A	N/A	VI-1	-	N/A	N/A
2	Circular Convergent-Divergent Nozzle	2-3	2-4	2-5	2-6	VI-2 & -3	VI-4 and -5	VI-3	VI-5
3	Baseline Contoured-Convergent Annular Plug Nozzle	2-7	2-8	N/A	N/A	VI-6,-8,-10,-12, -14,-17,-19, & -21	VI-7,-9,-11,-13, -15,-16,-18, & -20	N/A	N/A
3 With Tabs	Baseline Contoured-Convergent Annular Plug Nozzle with Shock Screech Tabs	2-9	2-10 & 2-11	N/A	N/A	Same as 3 & Ref. Fig. 2-9	Same as 3 & Ref. Fig. 2-10 & 2-11	N/A	N/A
4	Convergent-Divergent Annular Plug Nozzle	2-12	2-13	2-14	2-15	VI-6,-8,-10,-12, -14,-17,-19, & -22	VI-7,-9,-11,-13, -15,-16,-18, -20, & -23	VI-24,-25, & -26	VI-9,-11, & -23
5	20-Chute Annular Plug Suppressor; Convergent Flow Element Termination	2-16	2-17	N/A	N/A	VI-28,-30, &-31	VI-32	N/A	N/A
6	20-Chute Annular Plug Suppressor; Convergent-Divergent Flow Element Termination	2-18	2-19 & 2-20	-	2-21 & 2-23	VI-27,-29,-30, & -31	VI-33	VI-34 & VI-35	Ref. Fig. 2-21 & 2-23

ORIGINAL PAGE IS
OF POOR QUALITY

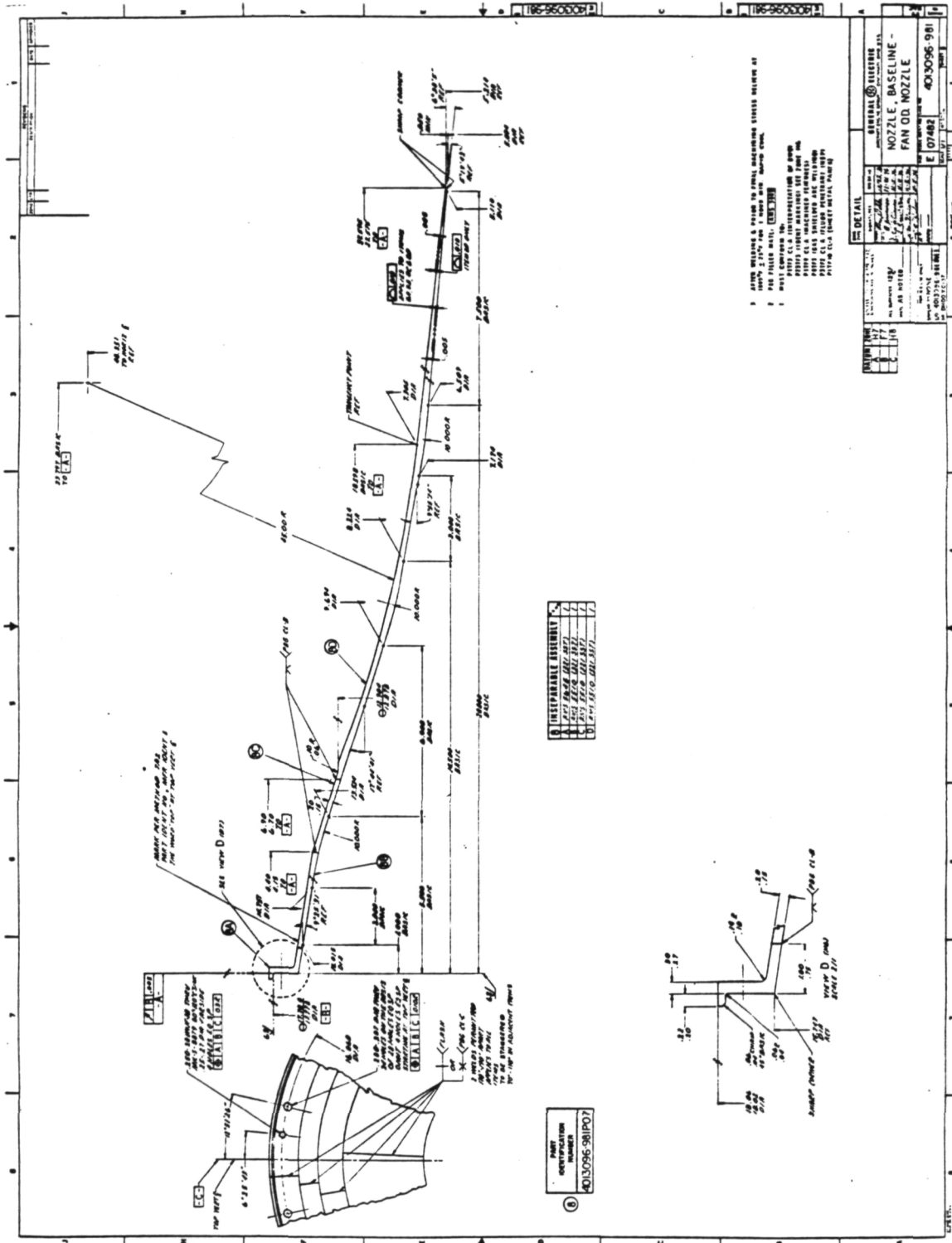


Figure VI-1. Drawing of Model 1; Baseline Conical-Convergent Nozzle, 4013096-981, Item 8, P07.

ORIGINAL PAGE IS
OF POOR QUALITY

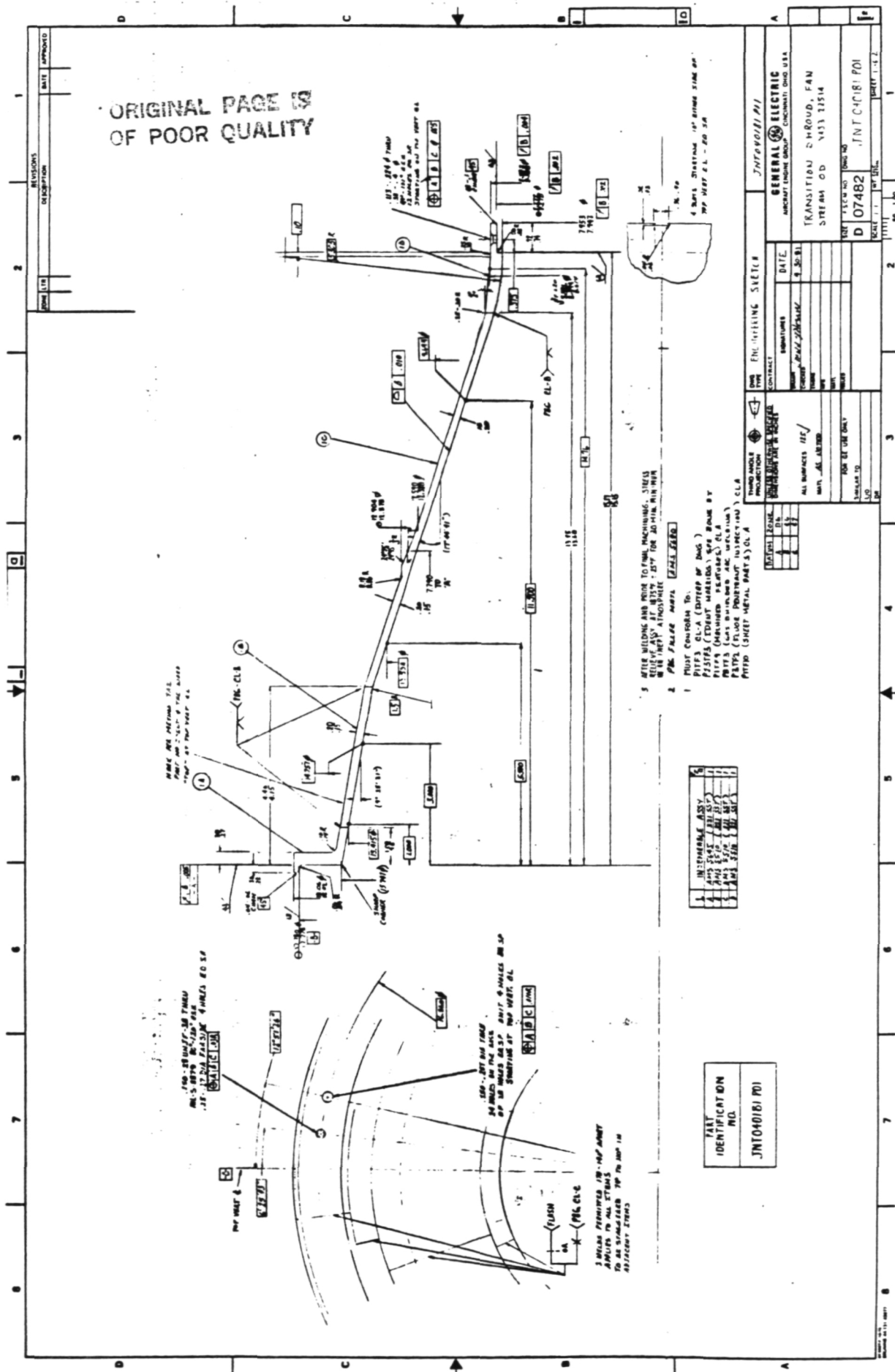


Figure VI-2. Drawing of Model 2's Transition Shroud, JNT040181P01.

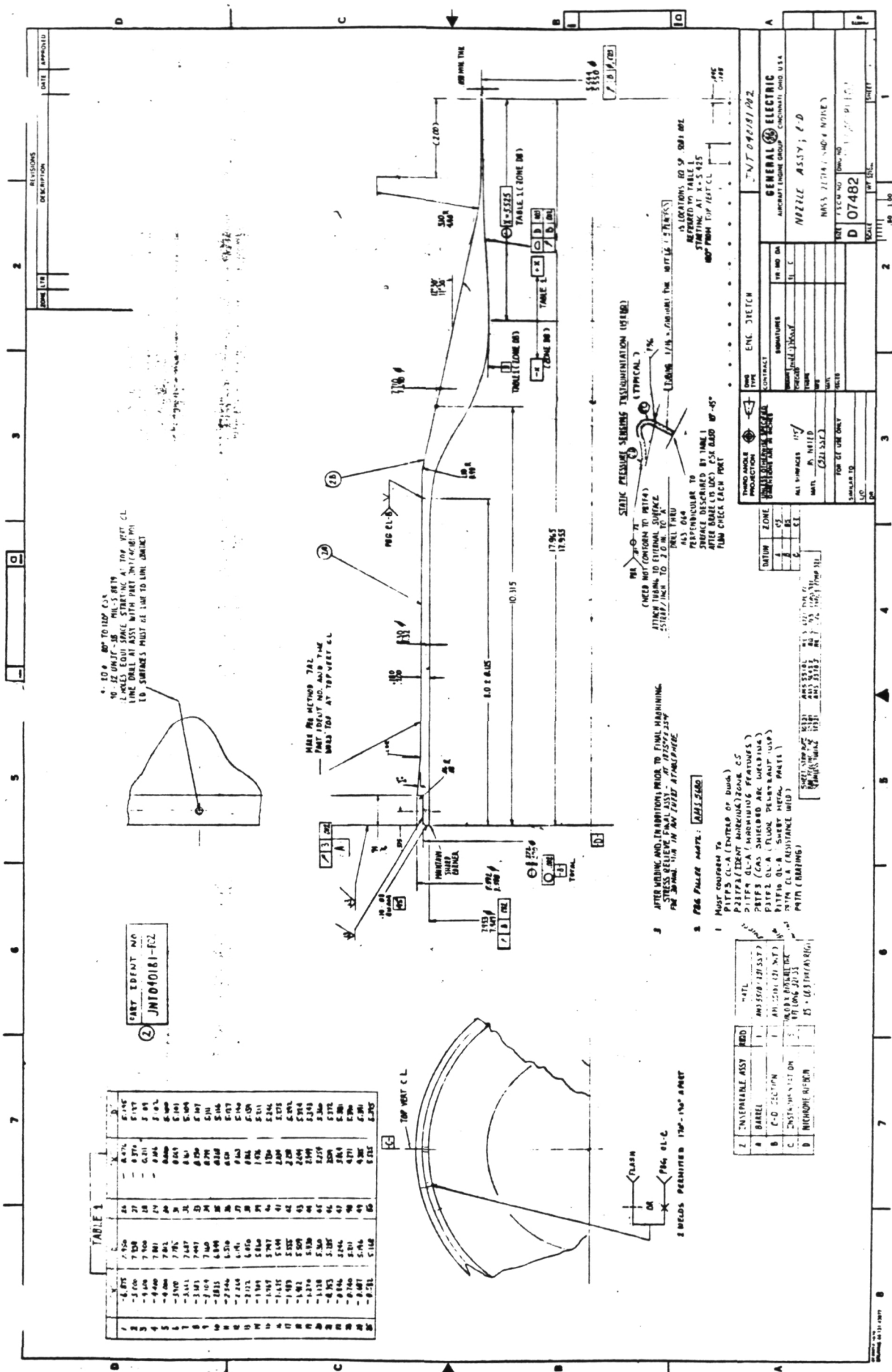


Figure VI-3. Drawing of Model 2's C-D Nozzle. JNT040181P02.

ORIGINAL PAGE IS
OF POOR QUALITY

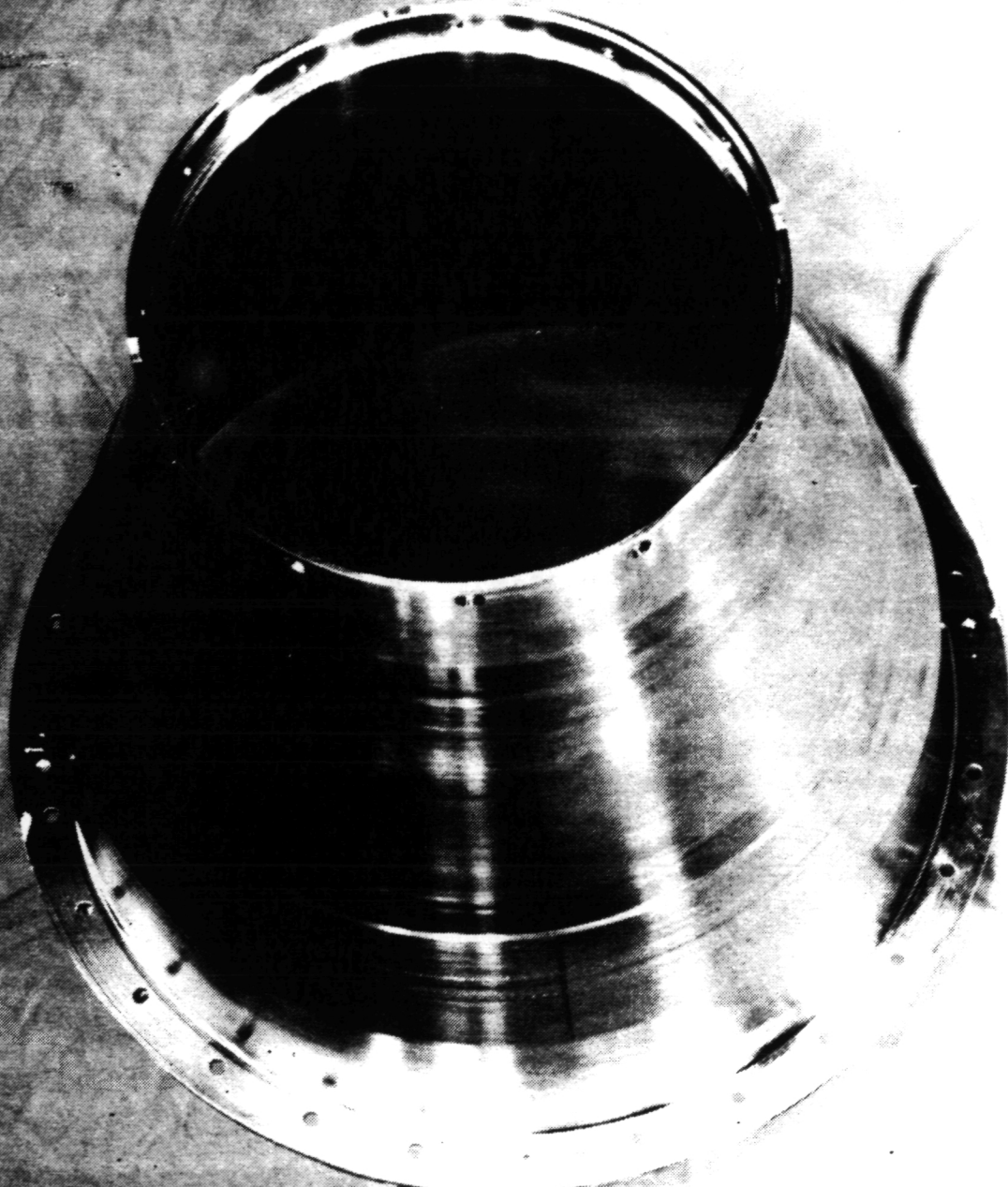
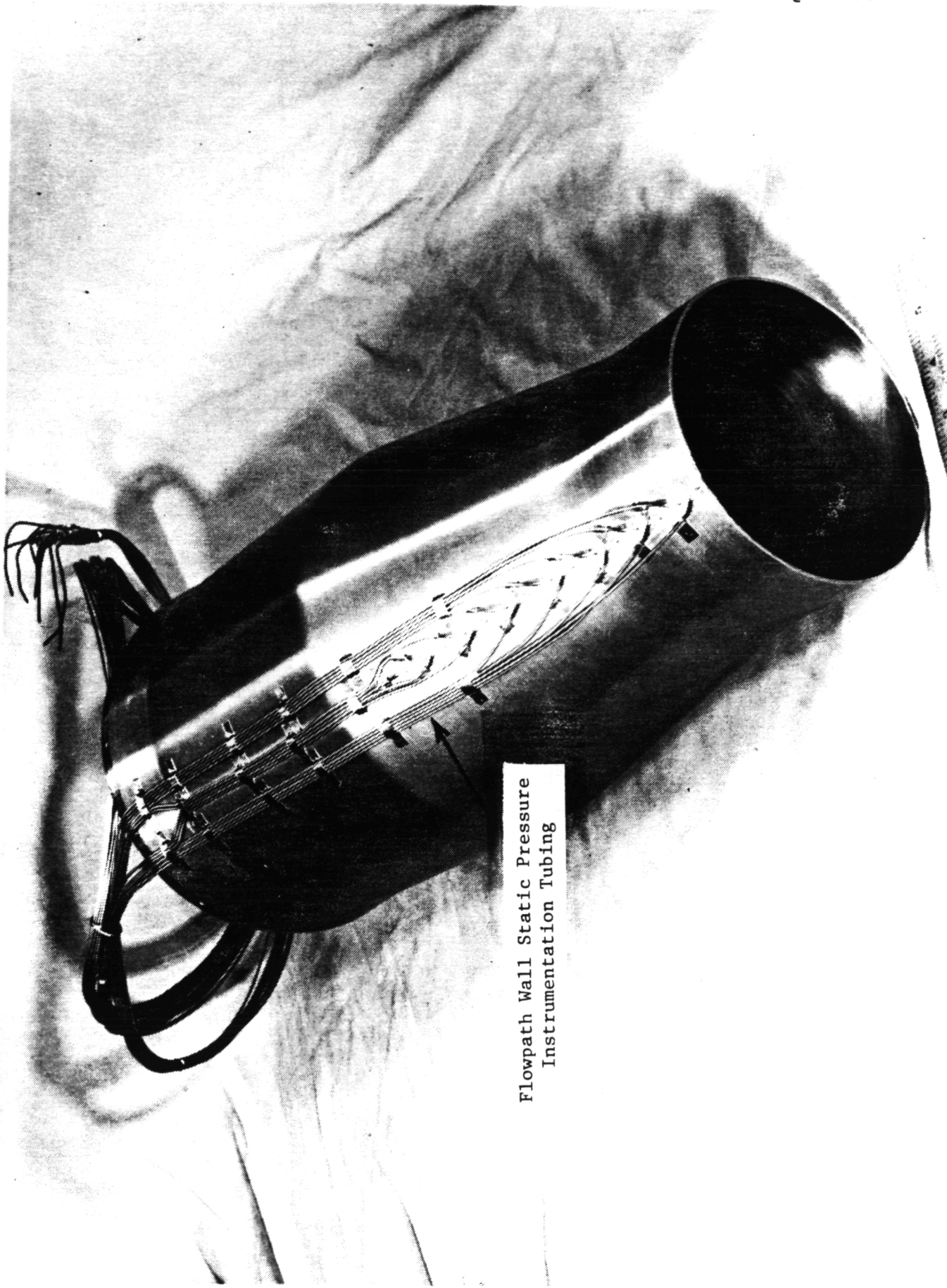


Figure VI-4. Photo of Model 2's Transition Shroud, JNT040181P01.

ORIGINAL PAGE IS
OF POOR QUALITY



Flowpath Wall Static Pressure
Instrumentation Tubing

1537

Figure VI-5. Photo of Model 2's C-D Nozzle, JNT040181P02.

ORIGINAL PAGE IS
OF POOR QUALITY

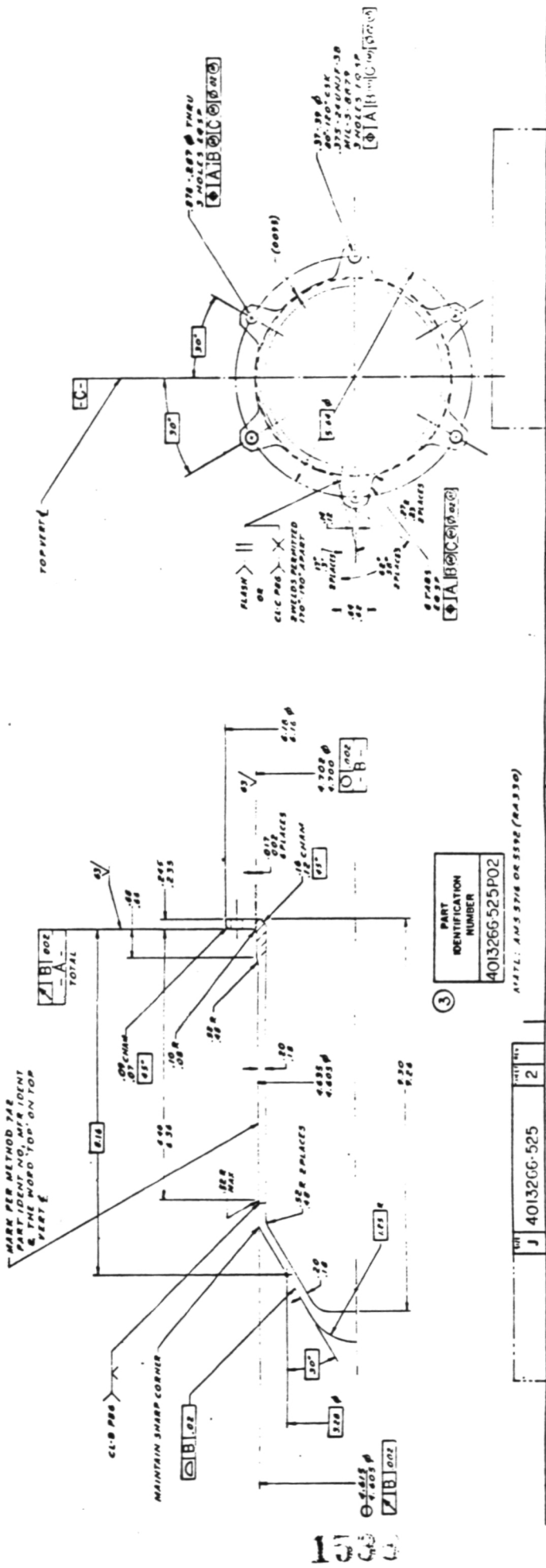


Figure VI-6. Drawing of Models 3 and 4 Plug Forebody, 4013266-525 Item 3, P02.

ORIGINAL PAGE IS
OF POOR QUALITY

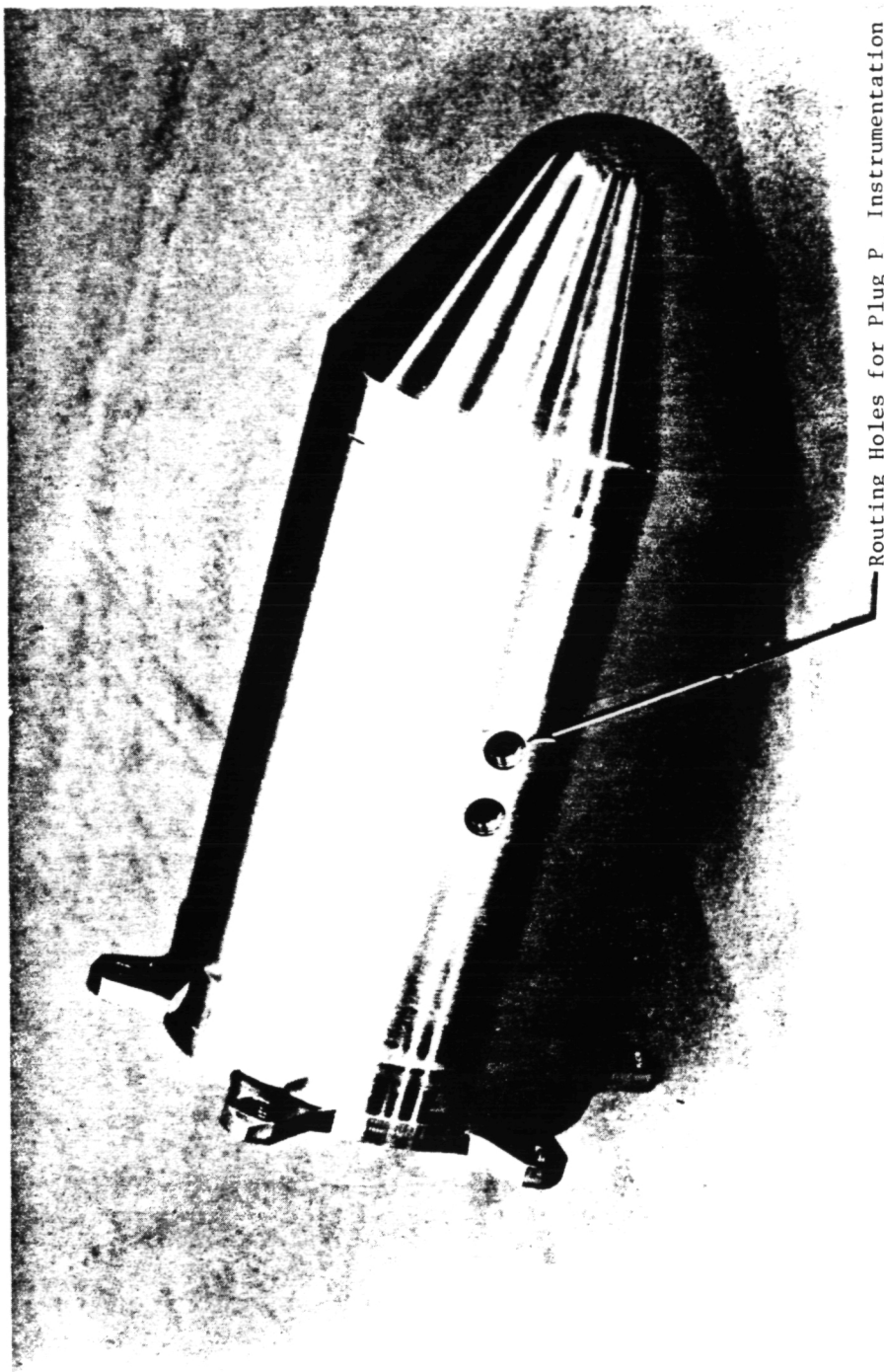
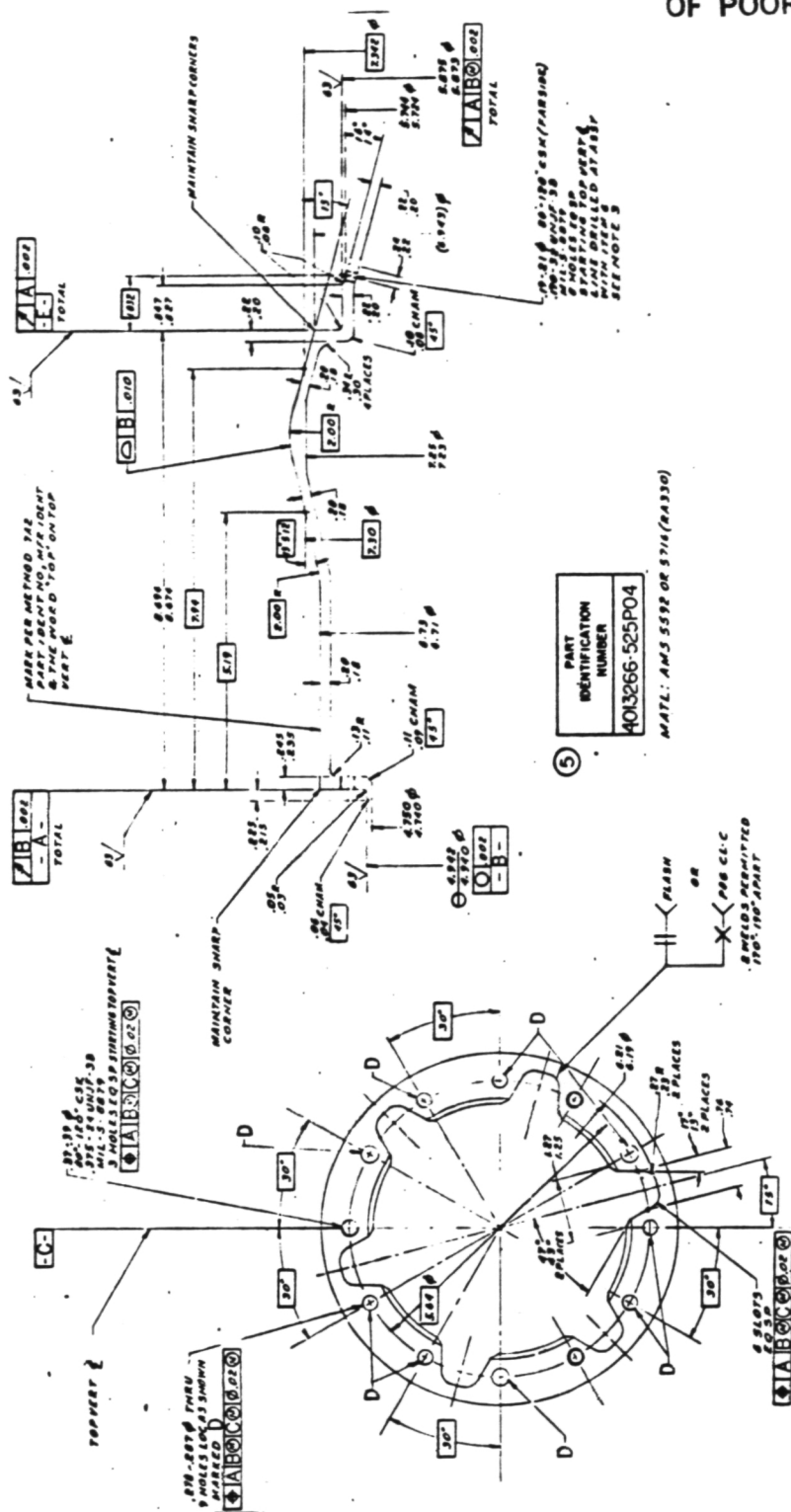
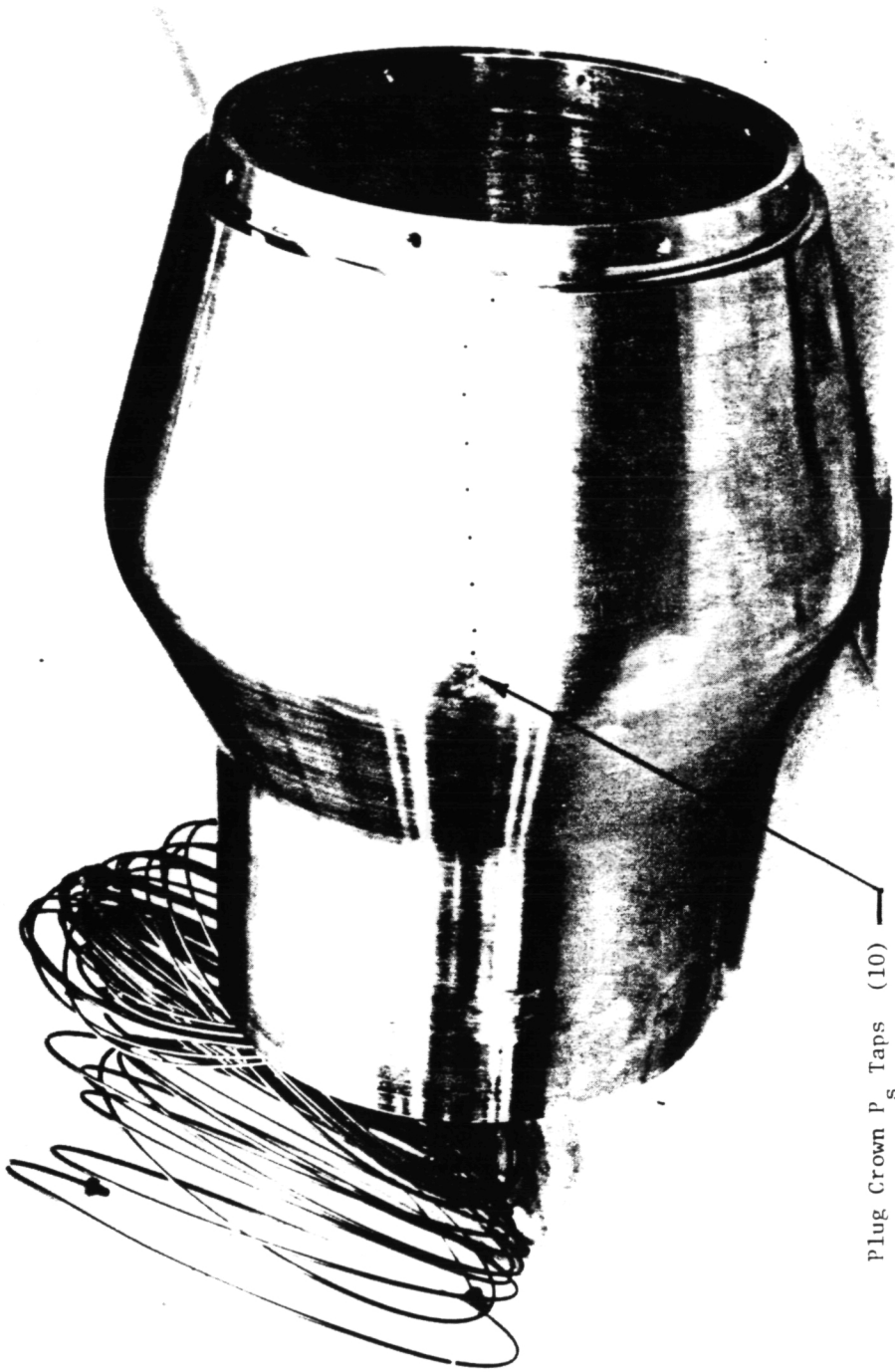


Figure VI-7. Photo of Models 3 and 4 Plug Forebody, 4013266-525 Item 3, P02

ORIGINAL PAGE IS
OF POOR QUALITY



ORIGINAL PAGE IS
OF POOR QUALITY



Plug Crown P_s Taps (10)

Figure VI-9. Photo of Models 3 and 4 Plug Crown, 4013266-525, Item 4, P03

ORIGINAL PAGE IS
OF POOR QUALITY

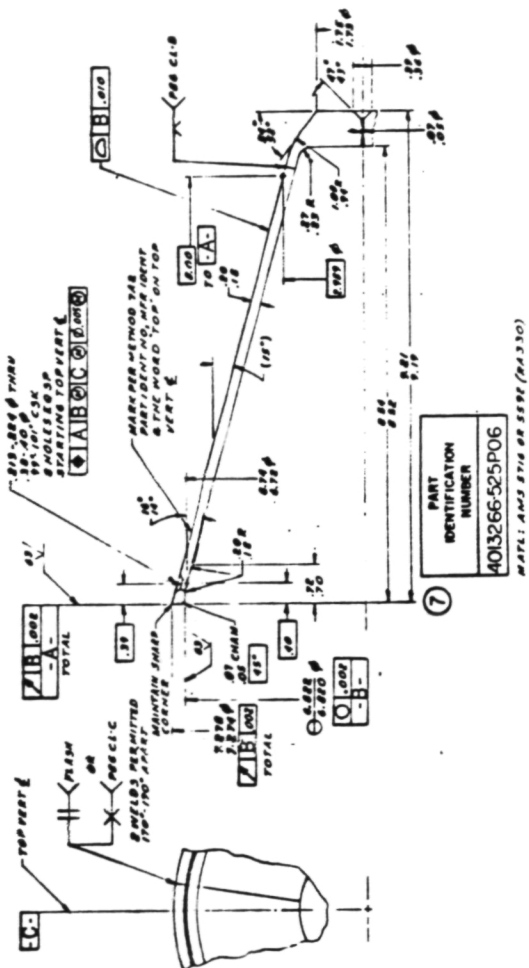


Figure VI-10. Drawing of Models 3 and 4 Plug Closure, 4013266-525 Item 7, P06.

ORIGINAL PAGE IS
OF POOR QUALITY

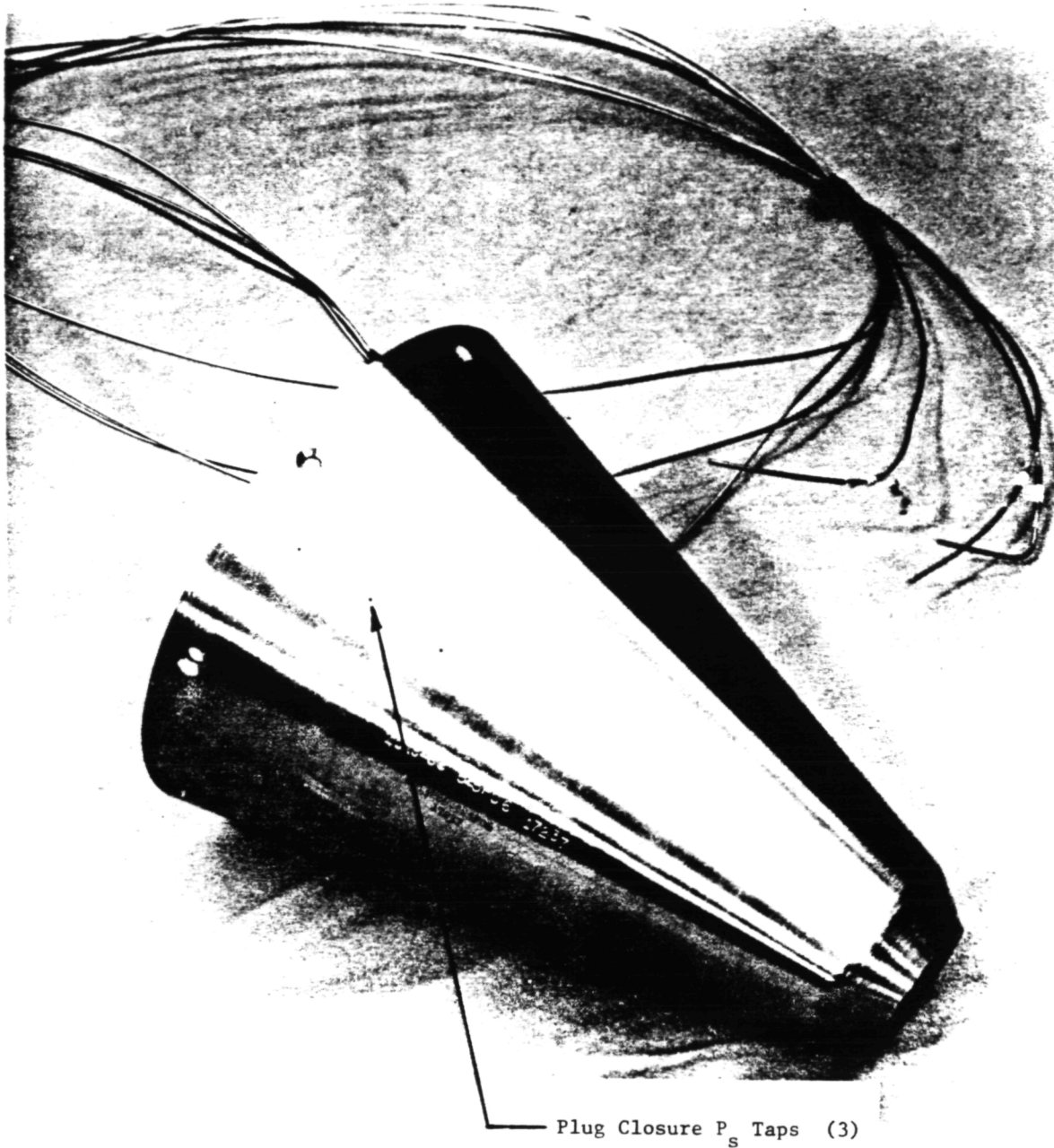


Figure VI-11. Photo of Models 3 and 4 Plug Closure, 4013266-525, Item 7, P06

ORIGINAL PAGE IS
OF POOR QUALITY

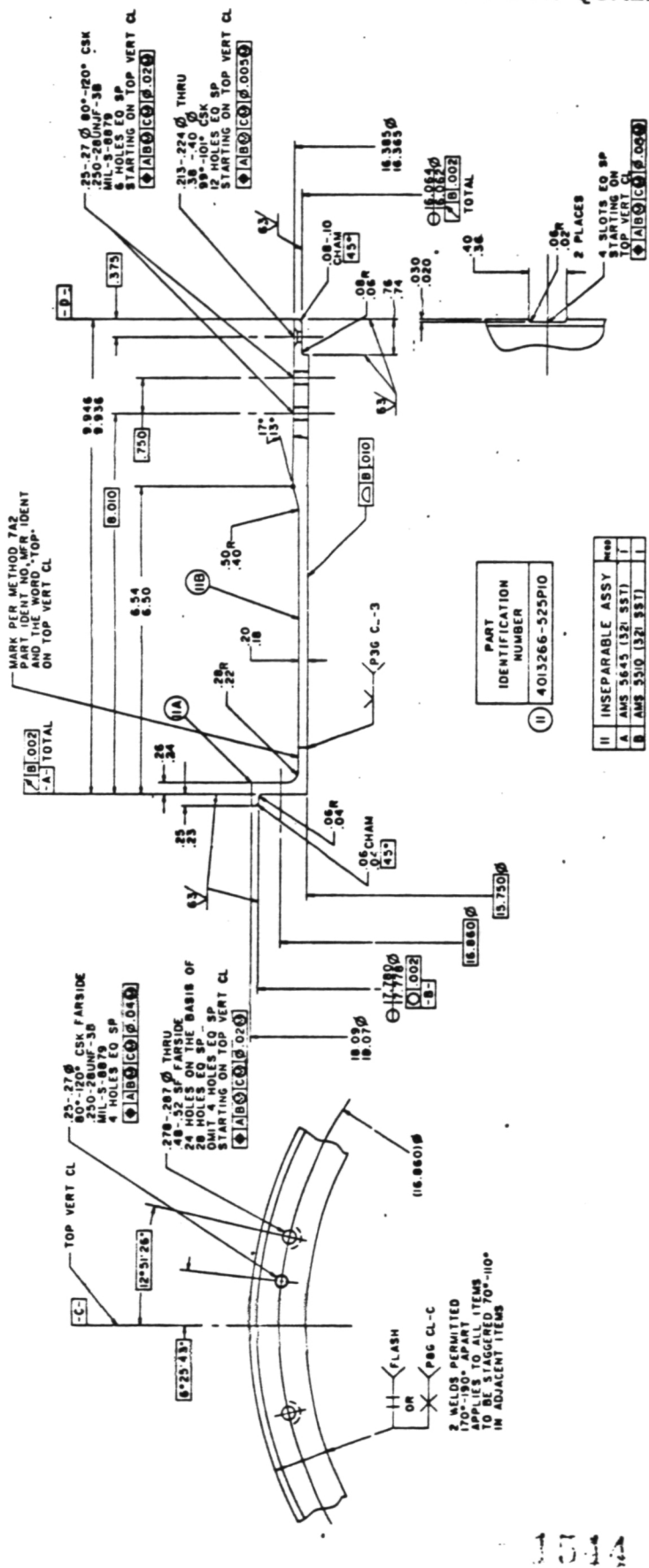


Figure VI-12. Drawing of Models 3 and 4 Transition and Centering Sleeve, 4013266-525 Item 11, p10.

ORIGINAL PAGE IS
OF POOR QUALITY

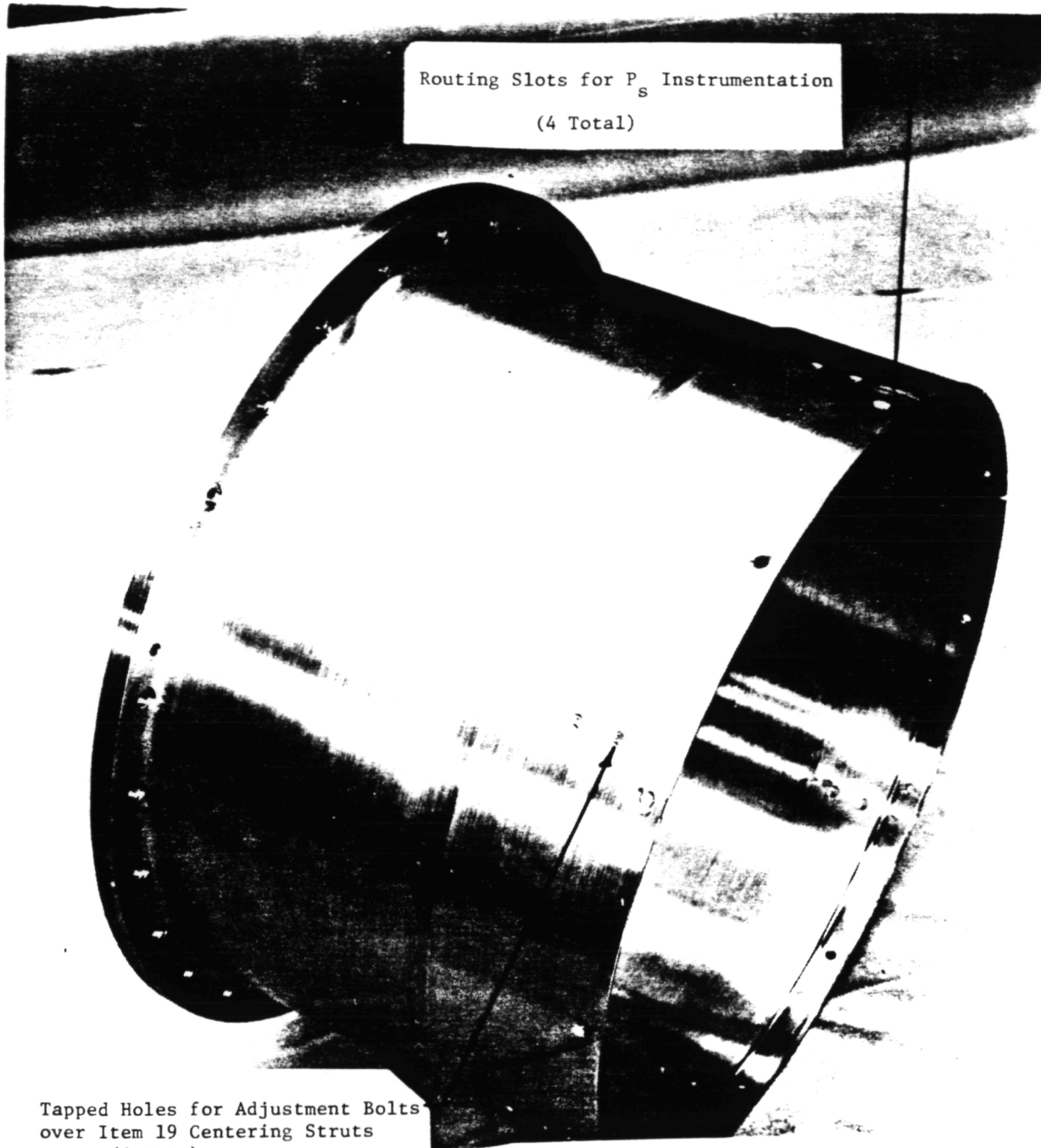


Figure VI-13. Photo of Models 3 and 4 Transition and Centering Sleeve, 4013266-525, Item 11, P10

ORIGINAL PAGE IS
OF POOR QUALITY

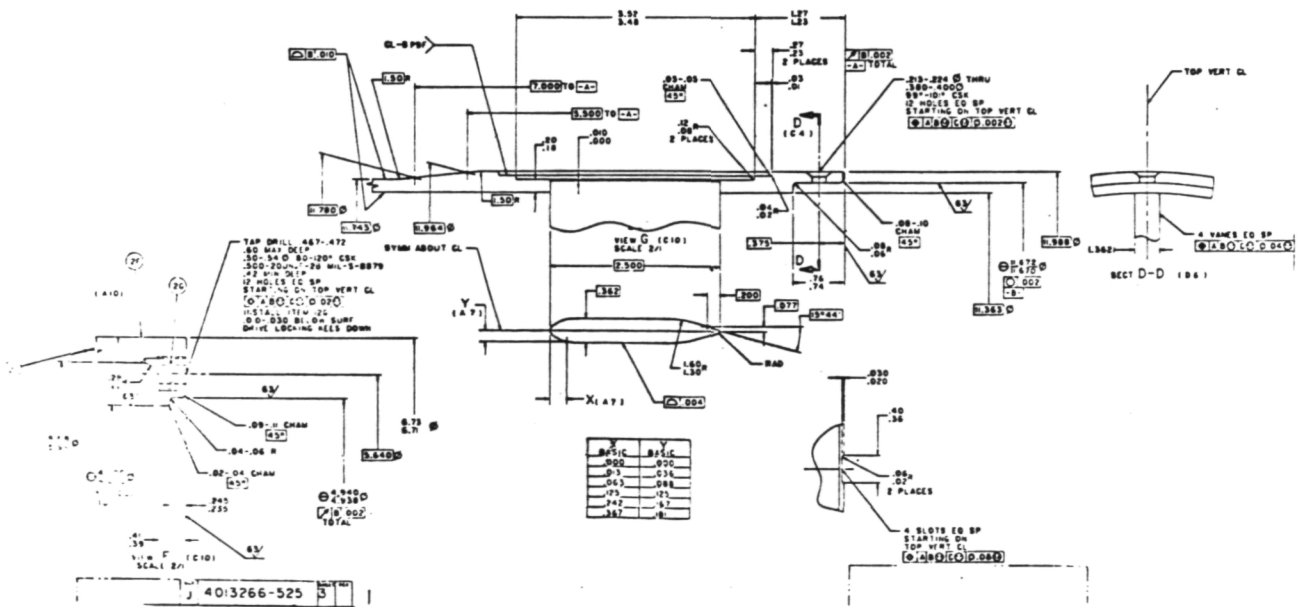
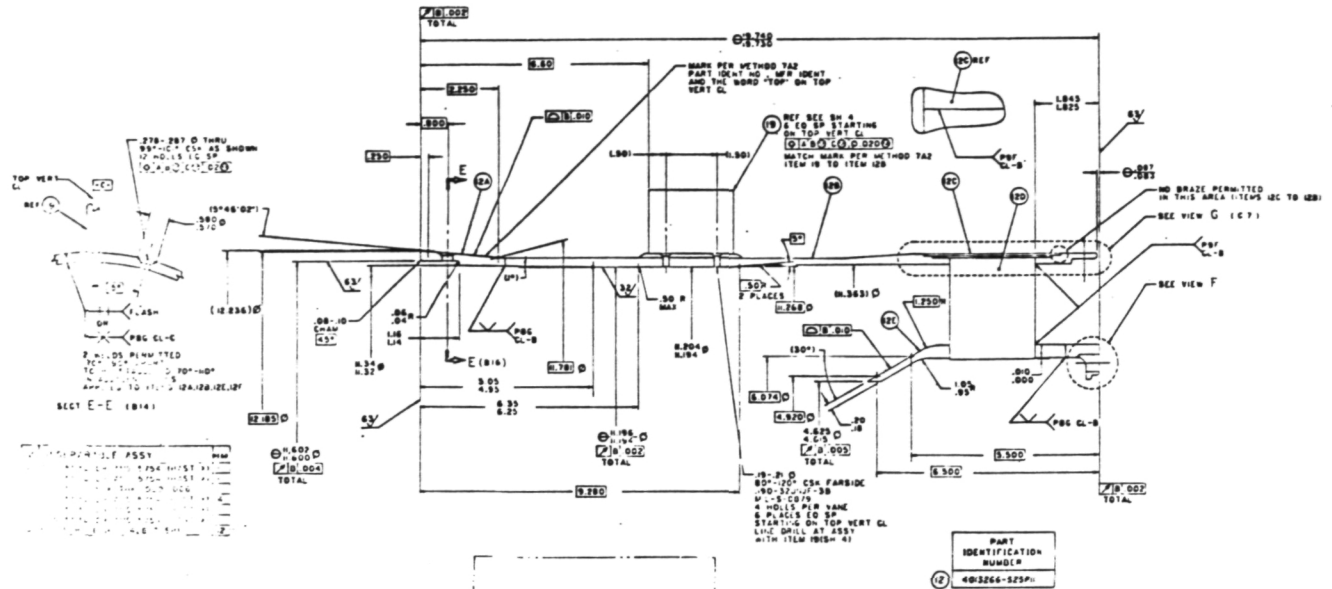


Figure VI-14. Drawing of Models 3 and 4 Core Nozzle Support Structure, 4013266-525 Item 12, Pl1.

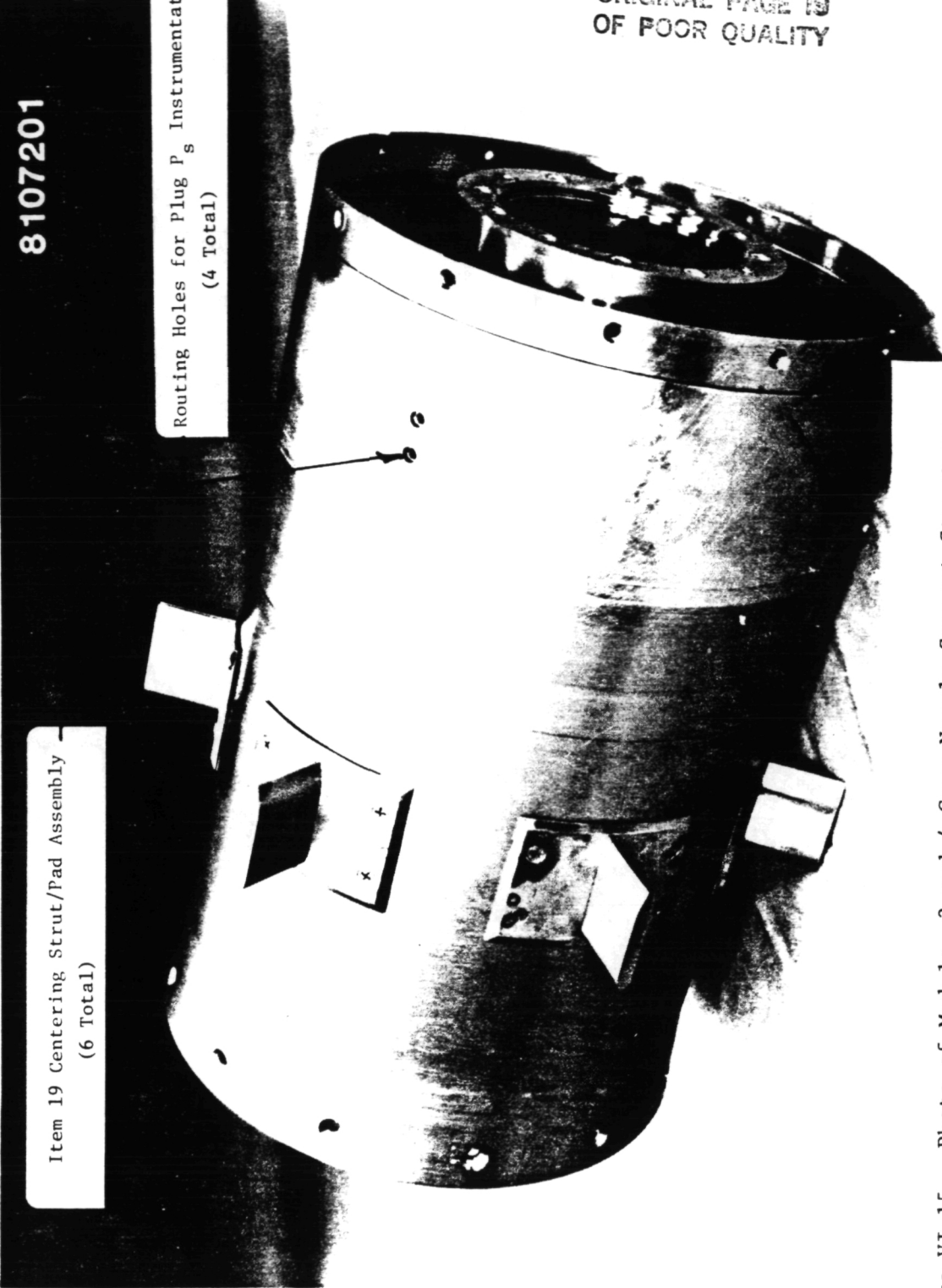


Figure VI-15. Photo of Models 3 and 4 Core Nozzle Support Structure, 4013266-525, Item 12, P11; Side View.

8107199

Holes through Struts for Routing
Plug P_s Instrumentation (4 Total)

- Internal Support Strut (4 Total)

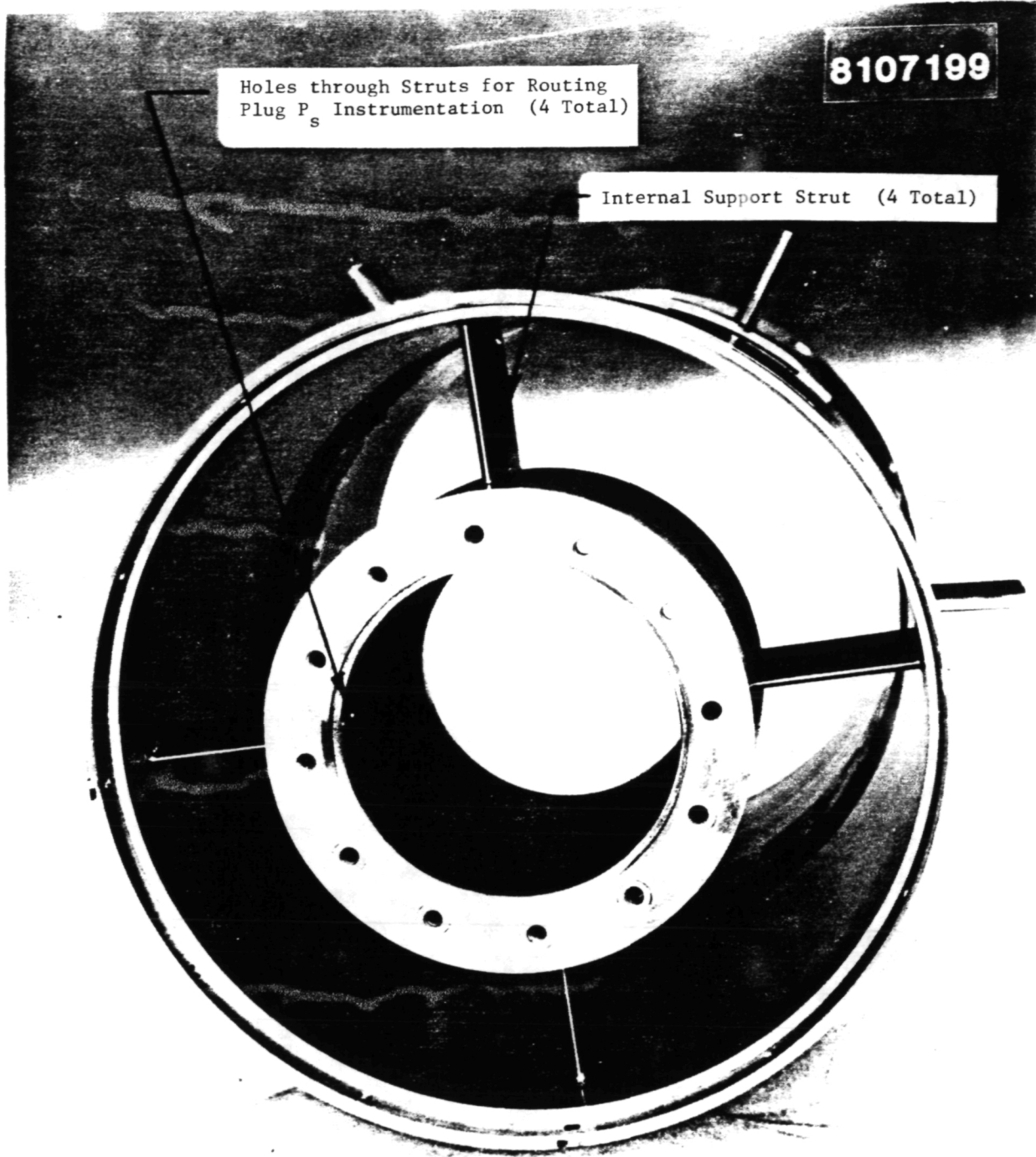


Figure VI-16. Photo of Models 3 and 4 Core Nozzle Support Structure,
4013266-525 Item 12, Pl1; End View.

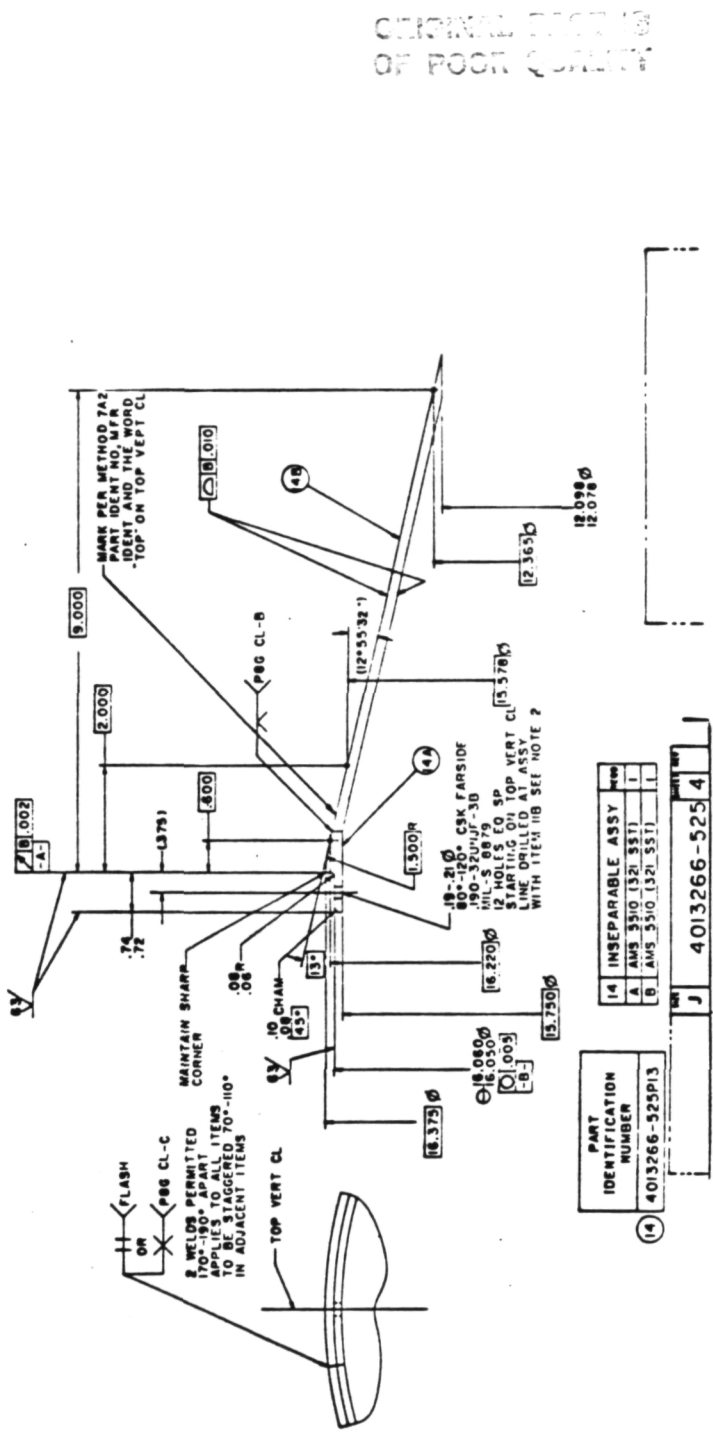
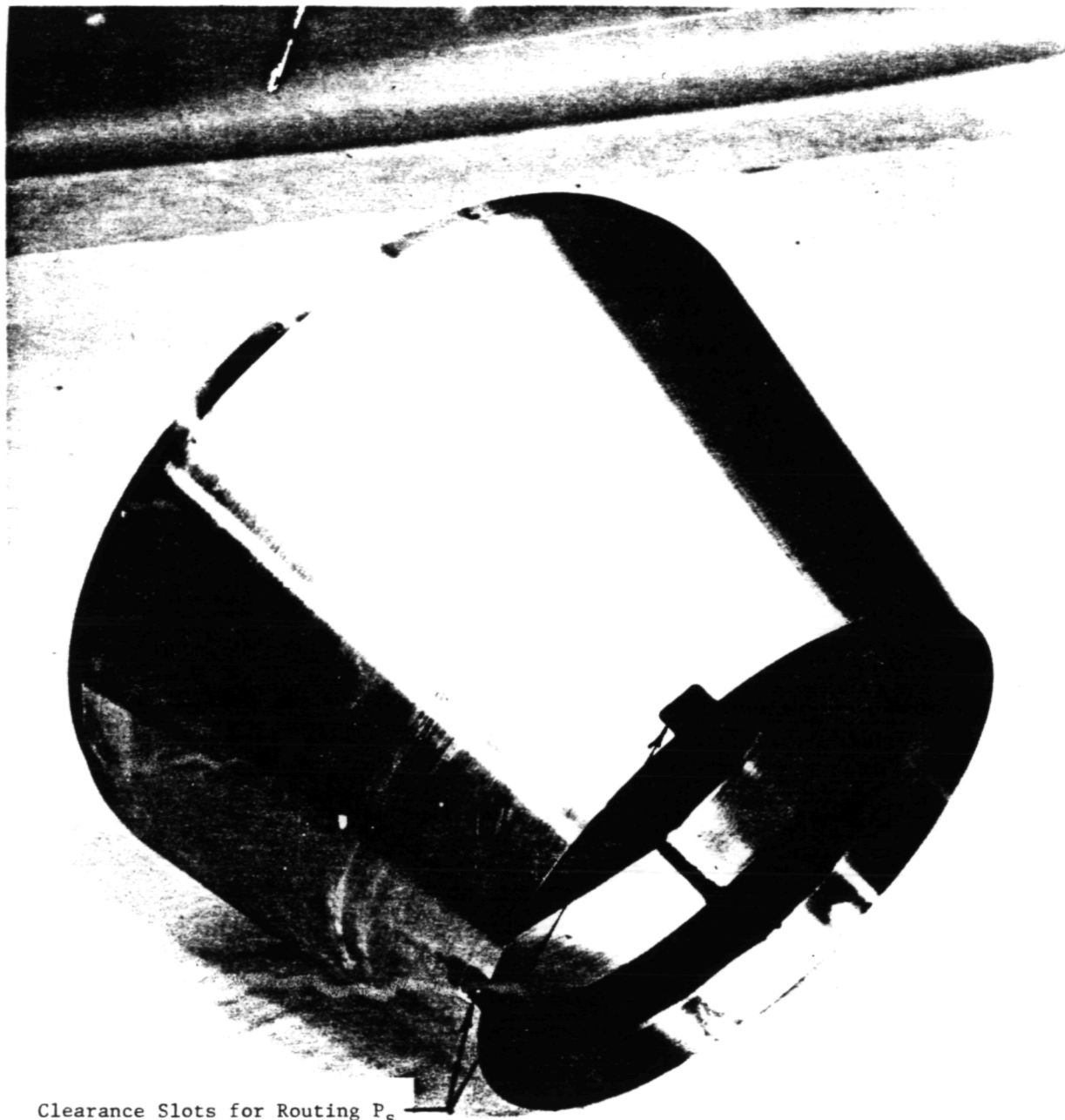


Figure VI-17. Drawing of Models 3 and 4 Aft Free Stream Closure, 4013266-525 Item 14, p13.

ORIGINAL PAGE IS
OF POOR QUALITY



Clearance Slots for Routing P_s
Instrumentation on Baseline
Cylindrical, C-D & 32-Chute
Nozzles

Figure VI-18. Photo of Models 3 and 4 Aft Free-Stream Closure,
4013266-525 Item 14, P13.

ORIGINAL DRAWING
OF POOR QUALITY

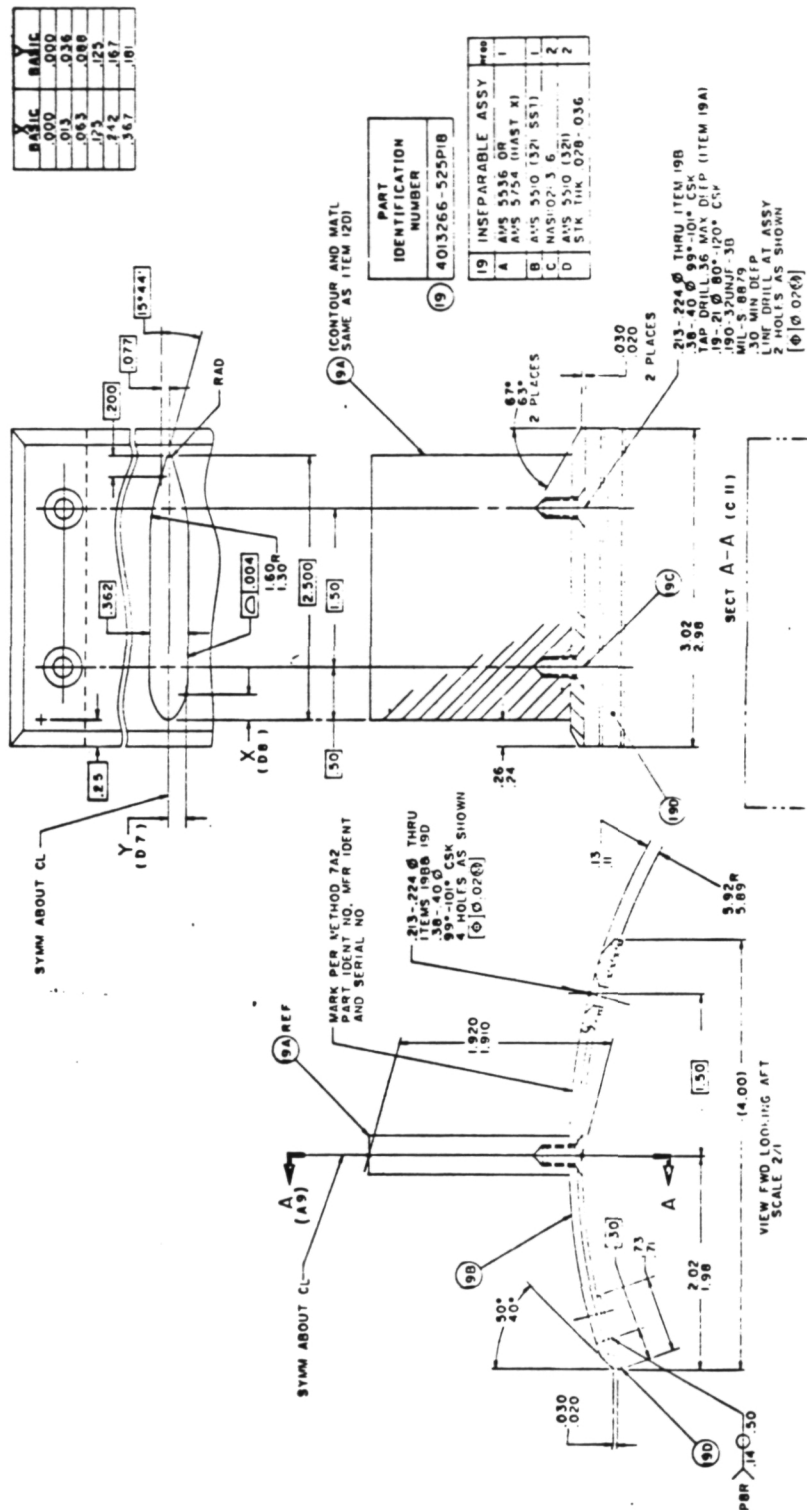


Figure VI-19. Drawing of Models 3 and 4 Centering Strut/Pad Assembly, 4013266-525 Item 19, P17.

ORIGINAL PAGE IS
OF POOR QUALITY

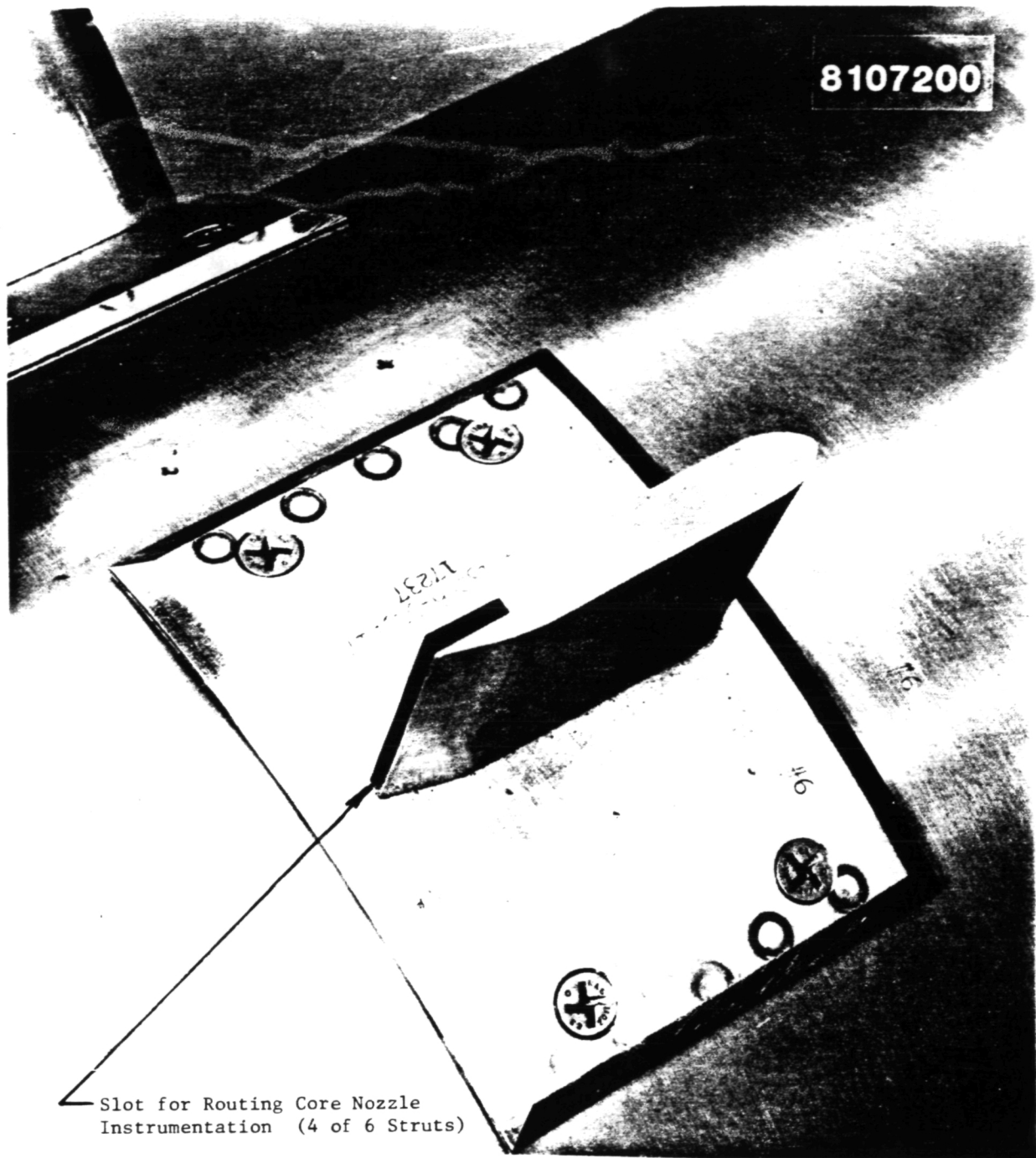


Figure VI-20. Photo of Models 3 and 4 Centering Strut/Pad Assembly,
4013266-525 Item 19, P17.

ORIGINAL PAGE IS
OF POOR QUALITY

This technical drawing illustrates a mechanical assembly, likely a bearing housing or similar component. The drawing includes several views and detailed dimensions:

- Dimensions:**
 - Vertical height: 7.7045
 - Bottom width: 7.7135
 - Top width: 7.7145
 - Left side width: 7.7135
 - Bottom thickness: 1.50
 - Top thickness: 1.50
 - Bottom shoulder width: 1.50
 - Top shoulder width: 1.50
 - Bottom shoulder height: 1.50
 - Top shoulder height: 1.50
 - Bottom shoulder depth: 1.50
 - Top shoulder depth: 1.50
 - Bottom shoulder angle: 45°
 - Top shoulder angle: 45°
 - Bottom shoulder radius: 0.50
 - Top shoulder radius: 0.50
 - Bottom shoulder height: 1.50
 - Top shoulder height: 1.50
 - Bottom shoulder depth: 1.50
 - Top shoulder depth: 1.50
- Part Numbers:**
 - 1A: Located at the top center.
 - 1B: Located at the top right.
 - 1C: Located at the bottom center.
 - 1D: Located at the bottom right.
 - 1E: Located at the bottom left.
 - 1F: Located at the top left.
 - 1G: Located at the top center.
 - 1H: Located at the top right.
 - 1I: Located at the bottom center.
 - 1J: Located at the bottom right.
 - 1K: Located at the bottom left.
 - 1L: Located at the top center.
 - 1M: Located at the top right.
 - 1N: Located at the bottom center.
 - 1O: Located at the bottom right.
 - 1P: Located at the bottom left.
 - 1Q: Located at the top center.
 - 1R: Located at the top right.
 - 1S: Located at the bottom center.
 - 1T: Located at the bottom right.
 - 1U: Located at the bottom left.
 - 1V: Located at the top center.
 - 1W: Located at the top right.
 - 1X: Located at the bottom center.
 - 1Y: Located at the bottom right.
 - 1Z: Located at the bottom left.
- Manufacturing Instructions:**
 - FLASH ON TOP MACHINING CL-C
 - FLASH ON TOP MACHINING CL-B
 - FLASH ON TOP MACHINING CL-A
 - FLASH ON TOP MACHINING CL-D
 - FLASH ON TOP MACHINING CL-E
 - FLASH ON TOP MACHINING CL-F
 - FLASH ON TOP MACHINING CL-G
 - FLASH ON TOP MACHINING CL-H
 - FLASH ON TOP MACHINING CL-I
 - FLASH ON TOP MACHINING CL-J
 - FLASH ON TOP MACHINING CL-K
 - FLASH ON TOP MACHINING CL-L
 - FLASH ON TOP MACHINING CL-M
 - FLASH ON TOP MACHINING CL-N
 - FLASH ON TOP MACHINING CL-O
 - FLASH ON TOP MACHINING CL-P
 - FLASH ON TOP MACHINING CL-Q
 - FLASH ON TOP MACHINING CL-R
 - FLASH ON TOP MACHINING CL-S
 - FLASH ON TOP MACHINING CL-T
 - FLASH ON TOP MACHINING CL-U
 - FLASH ON TOP MACHINING CL-V
 - FLASH ON TOP MACHINING CL-W
 - FLASH ON TOP MACHINING CL-X
 - FLASH ON TOP MACHINING CL-Y
 - FLASH ON TOP MACHINING CL-Z
- Marking Method:**

MARK PER METHOD 1A
PART IDENT NO.
MPC IDENT NO.
TOP ON TOP MACH
TOP ON TOP MACH C.L.
- Identification Number:**

JNT0404-1 PC1
- Welds:**

WELDS PERMITTED
TIG-OR-GAS
APPLIES TO ALL ITEM'S
TO BE STAG-ERIC TD - HD
IN ASSEMBLY STAGE

1553

Figure VI-21 Drawing of Model 31-a Convergent Annular Sleeve. INT030981-1P01

**S AFTER WELDING UP TO 10 STRESSES BELIEVE WELDED ASSEMBLIES AT
NINETY PER CENT FOR 30 MINUTES WHEN IN AN INERT ATMOSPHERE.**

Z PFG FILLER MATEL AAMS STRG (HAST W)

- 1 MUST CONFIRM TO:
- PATS CLA (INTERFACIAL TENSION OF DME)
- PATS CLA (PENETRATION FEATURES)
- PATS CLA (SHEARING AND WELDING)
- PATS CLA (IDENT PENETRANT TEST)

MUST COMPORT TO:

- PATF1 CLA (INTERPENETRATION OF DNG)
- PATF2 CLA (MINIMISE FEATURES)
- PATF3 KAS SIGHTED AND MELTING
- PATF4 IDENT MARKING
- PATF5 CLA (FLUORINE PENETRANT INSP)

**ORIGINAL PAGE IS
OF POOR QUALITY**

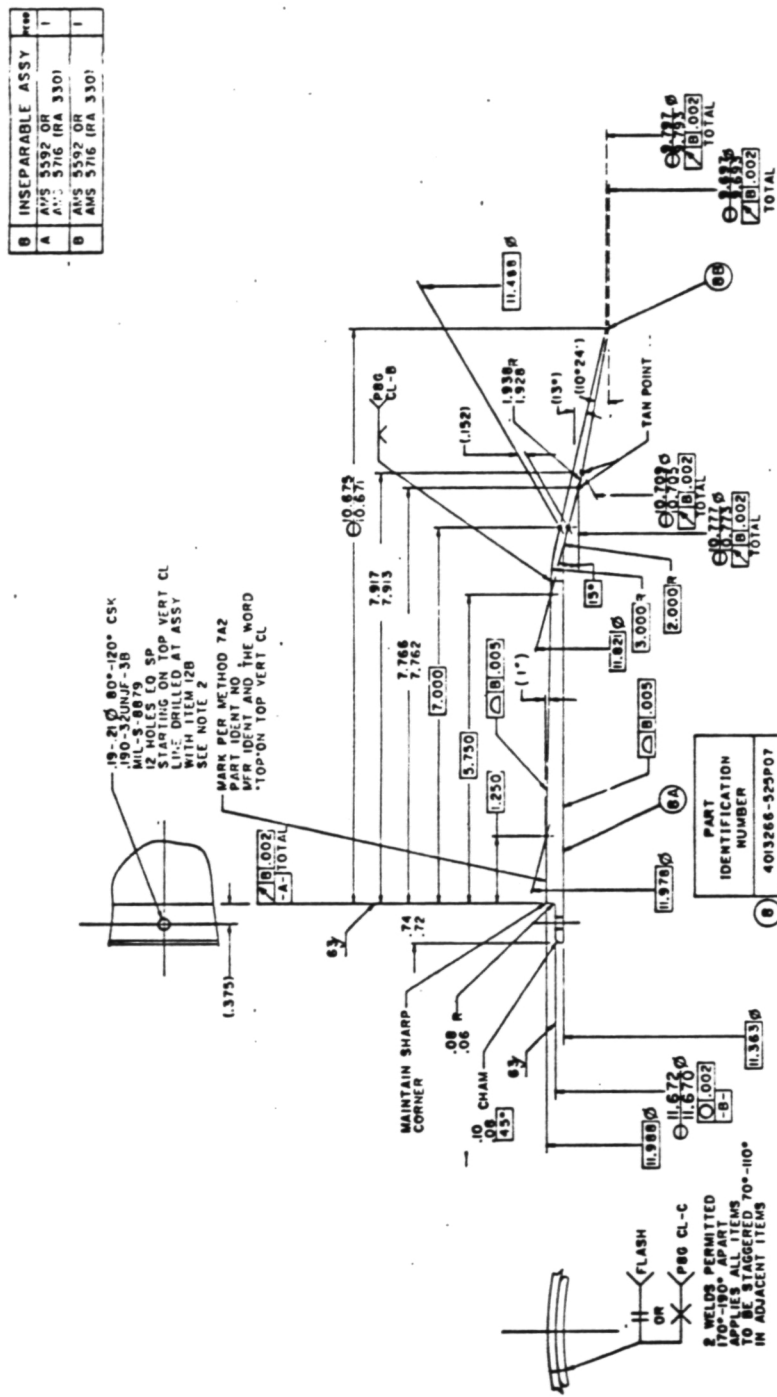


Figure VI-22. Drawing of Model 4's Convergent-Divergent Annular Sleeve, 4013266-525 Item 8, P07.

ORIGINAL PAGE IS
OF POOR QUALITY



4013266-52G-P07

C - 3

1555

Figure VI-23. Photo of Model 4's Convergent-Divergent Annular Sleeve, 4013266-525 Item 8, P07.

TABLE 1		
INSTRUMENTATION	X	O
ITEM NO.		
1	7.1L	120°
2	7.37	120°
3	7.62	120°
4	8.102	120°30'
5	8.586	120°18'
6	9.069	120°57'
7	9.552	120°36'
8	10.035	123°15'
9	10.516	123°54'
10	11.001	120°
	Φ A C Ø .02	

ORIGINAL PAGE IS
OF POOR QUALITY

INSTRUMENTATION APPLICATION TO ITEM ④ 4013266-525 P03 PLUG CROWN FOR BASELINE CYLINDRICAL C-D NOZZLES	TNT 050181	SHT 10512	BRN 1/61
--	------------	-----------	----------

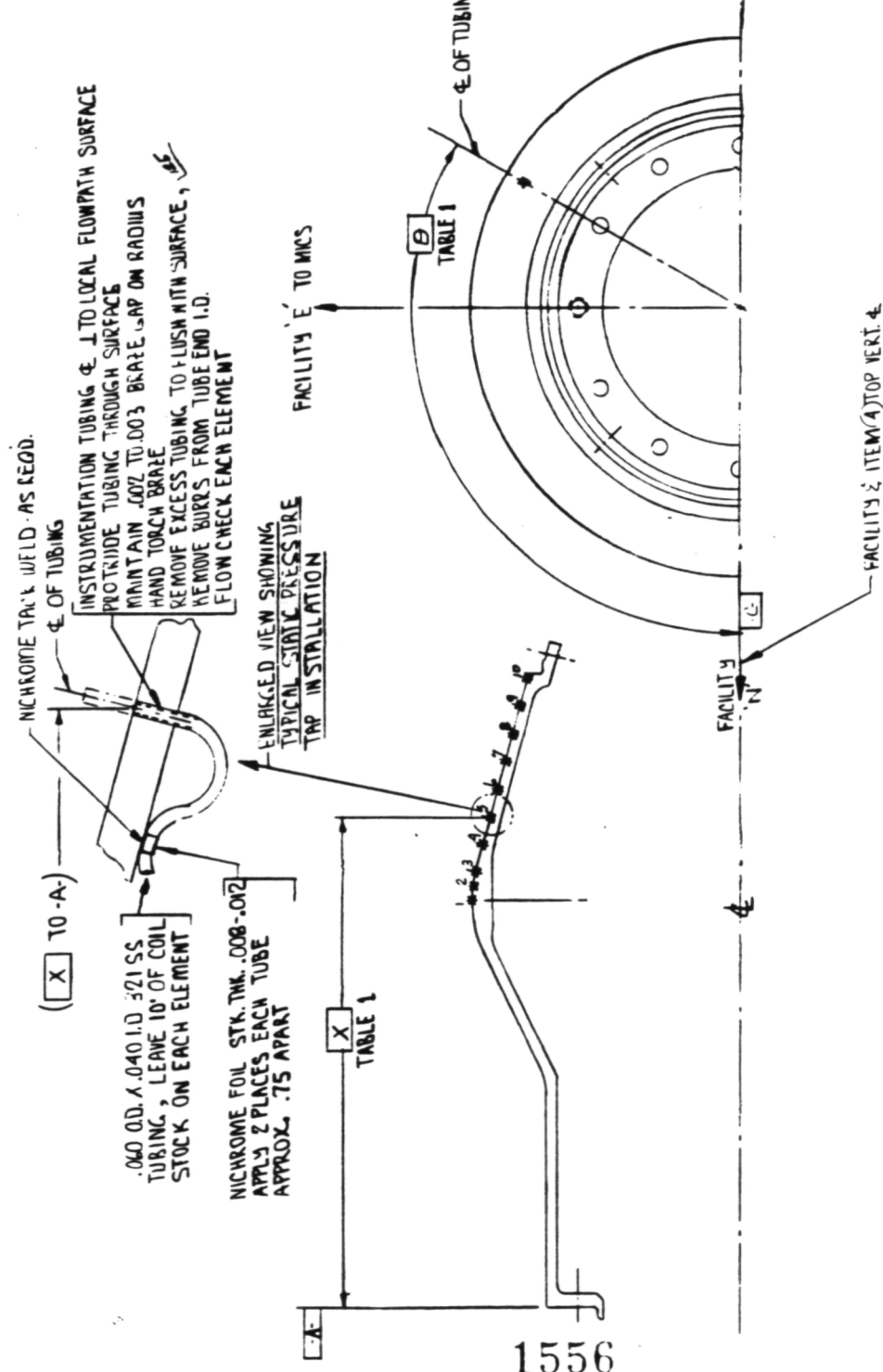


Figure VI-24. Drawing of Static Pressure Instrumentation Application to Model 4's Plug Crown, 4013266-525, Item 4, P03.

TABLE 1		X	Θ
INSTRUMENTATION ITEM NO.		.867	W ⁰
11		1.832	W ⁰
12		2.778	V ⁰
13			V ⁰
		Φ	A C D .02

ORIGINAL PAGE IS
OF POOR QUALITY

INSTRUMENTATION APPLICATION TO	
ITEM (7) 4013266-525 POC	
PLUG CLOSURE FOR BASELINE CYLINDRICAL	
C-D NOZZLES	

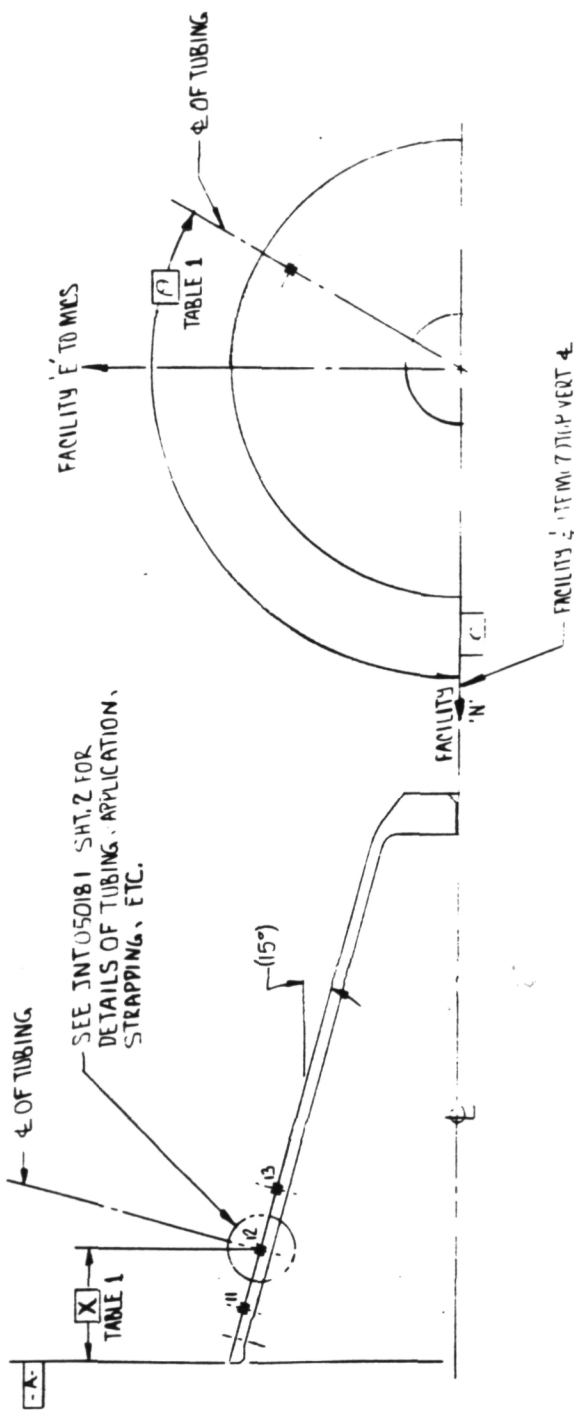


Figure VI-25. Drawing of Static Pressure Instrumentation Application to Model 4's Plug Closure, 4013266-525, Item 7, P06.

ORIGINAL PAGE IS
OF POOR QUALITY

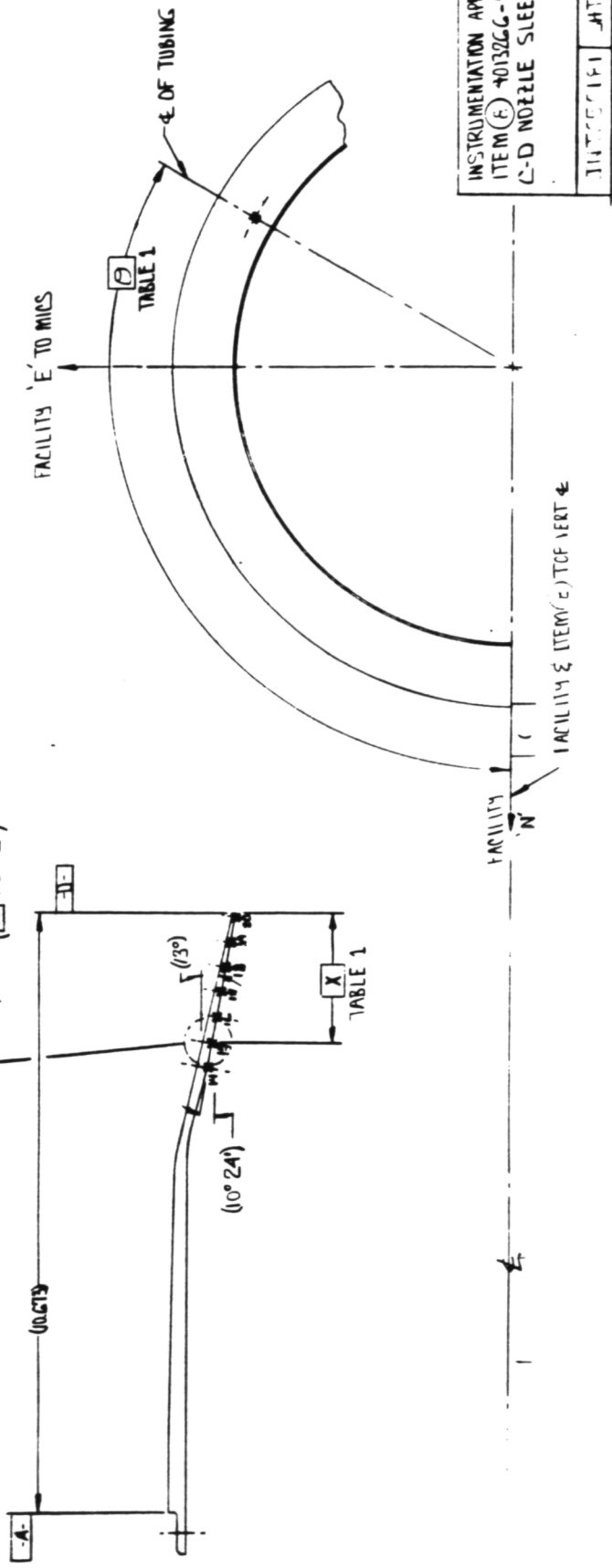
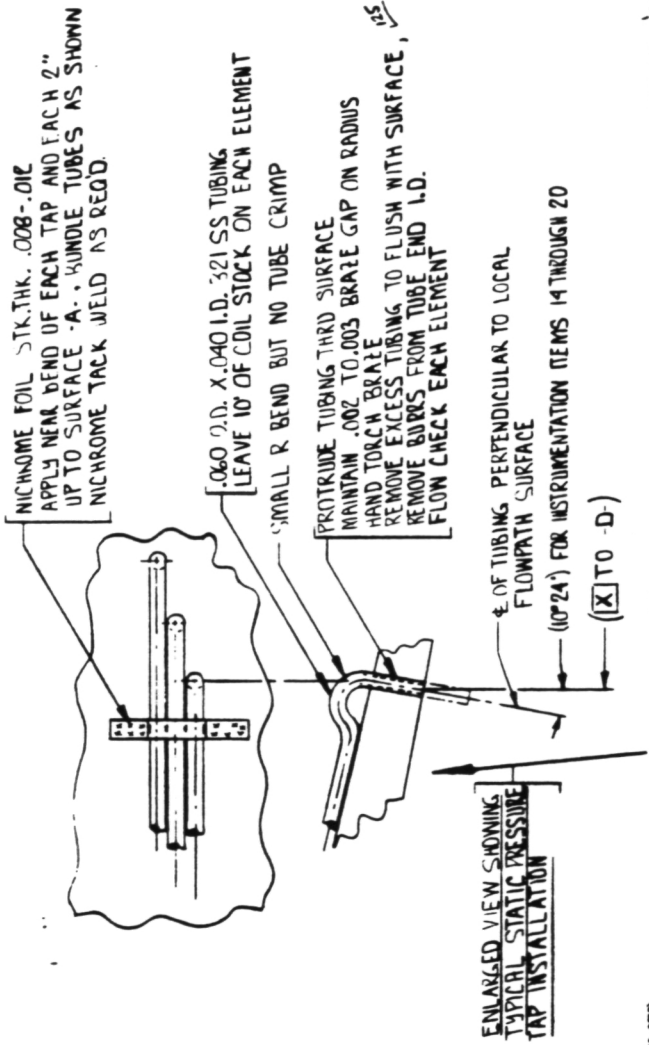
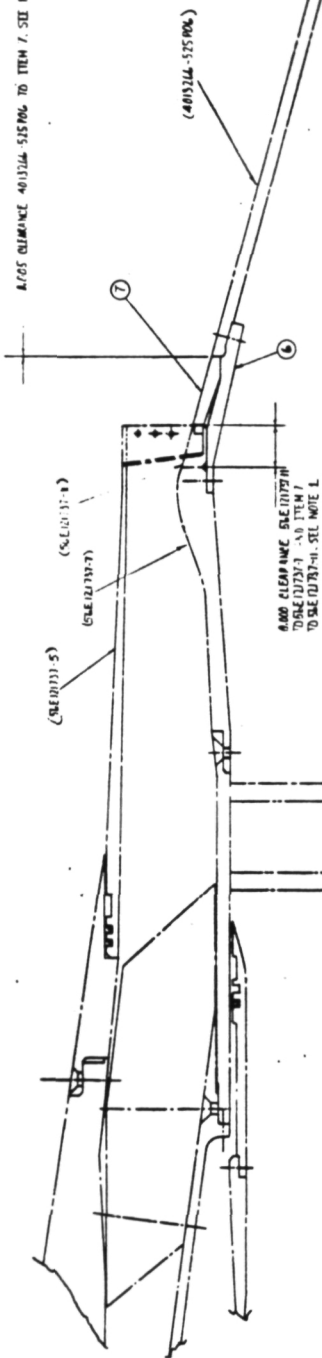


Figure VI-26. Drawing of Static Pressure Instrumentation Application to Model 4's C-D Annular Sleeve, 4013266-525 Item 8, p07.

ORIGINAL PAGE IS
OF POOR QUALITY

1 DECEMBER 1995 GALLAGHER ET AL.



NOTE 1. TRANSFER (8) EIGHT HOLE LOCATIONS FROM ITEM 40157N SYSTEM TO ITEM 40157N SYSTEM.
2. INC. CLEARANCES SHOWN ARE THE ITEMS 6-7 SEC 11111-7 SEC 11111-7
AND PART 40157N SYSTEM. EIGHT HOLE STABILIZER AT TOP OF TIP WHT. CL.
CL. 11111-7, ATT. LOCATING END TIP MARE ITEM 40157N SYSTEM.

ASSY IDENT No. INT-418162
INTERVIEW NAME A. FLEMING

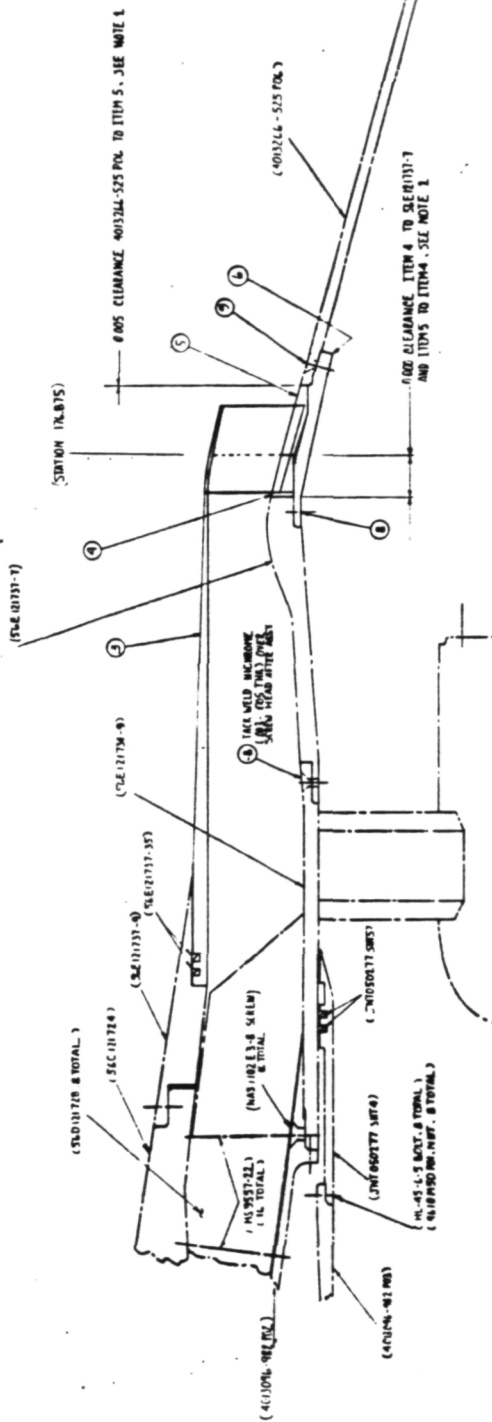
17-07-81 09HRS
MAS-22514
EQUILIBRIUM STATES

卷之三

Figure VI-27. Assembly Drawing, Model 5.

ORIGINAL PAGE IS
OF POOR QUALITY

ITEM NO.	INFORMATION OR NAME	SPECS		MANUFACTURER		DATE APPROVED
		STOCK NO.	QTY	STOCK NO.	QTY	
1	P-10001, II CHUTE C.D. KIT, IN CHUTE CONVENT	1	1	4 AND 5H14 5 AND SH17		1/18 1/18
2	101, CHUTE SHROUD ASSY	1	1			
3	102, FUEL FILLER RING, C.D.	1	1			
4	103, TAIL END, E.D.	1	1			
5	104, TRANSITION RING	1	1			
6	105, ATT. FILLER RING, CONVENT	1	1			
7	106, OIL FILTER	1	1			
8	107, OIL FILTER SCREEN	1	1			



WELL 1. TUNNELS, LOCATED IN THE LOCATIONS FROM ELEM 401524-401526 TO ELEMENT 401528-401529.
SECOND MING LAYER AT 45'-0" DEPTH AND 401524-401525.
FIRST MING LAYER AT 50'-0" DEPTH AND 401526-401527.

卷之三

ASSEMBLY NUMBER
18444

Figure VI-28, Assembly Drawing, Model 6.

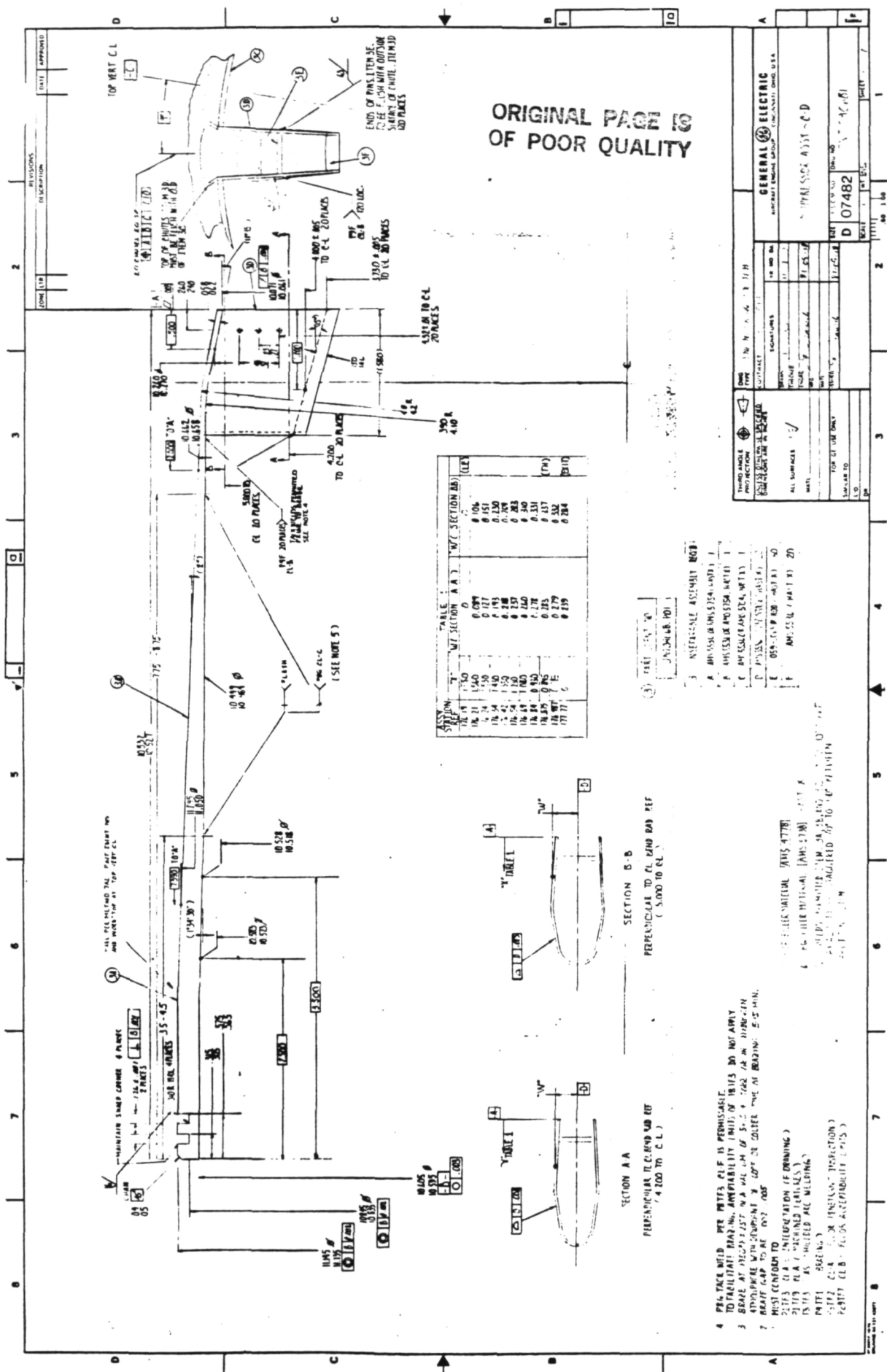


Figure VI-29. Detailed Drawing, Model 6.

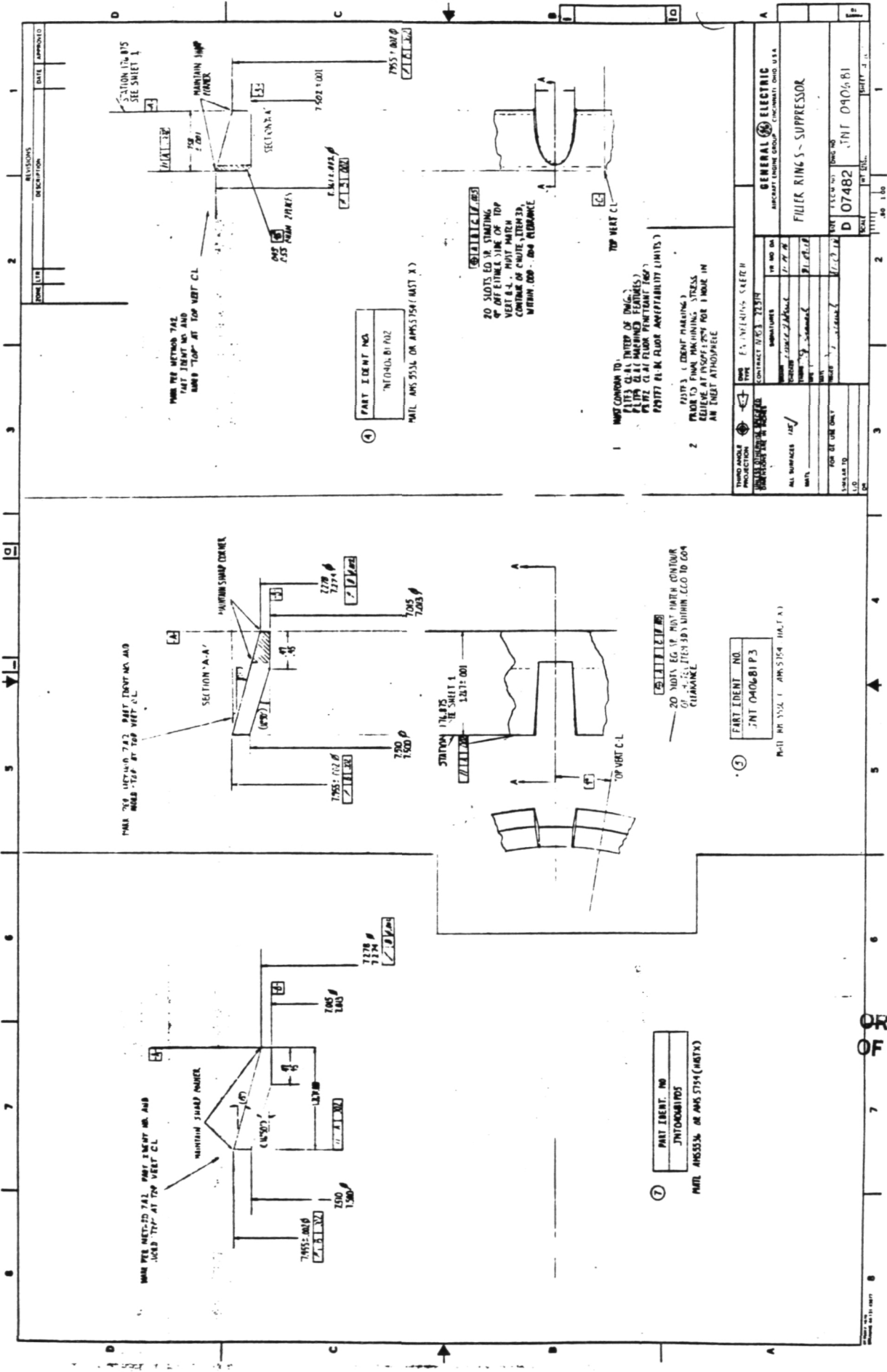
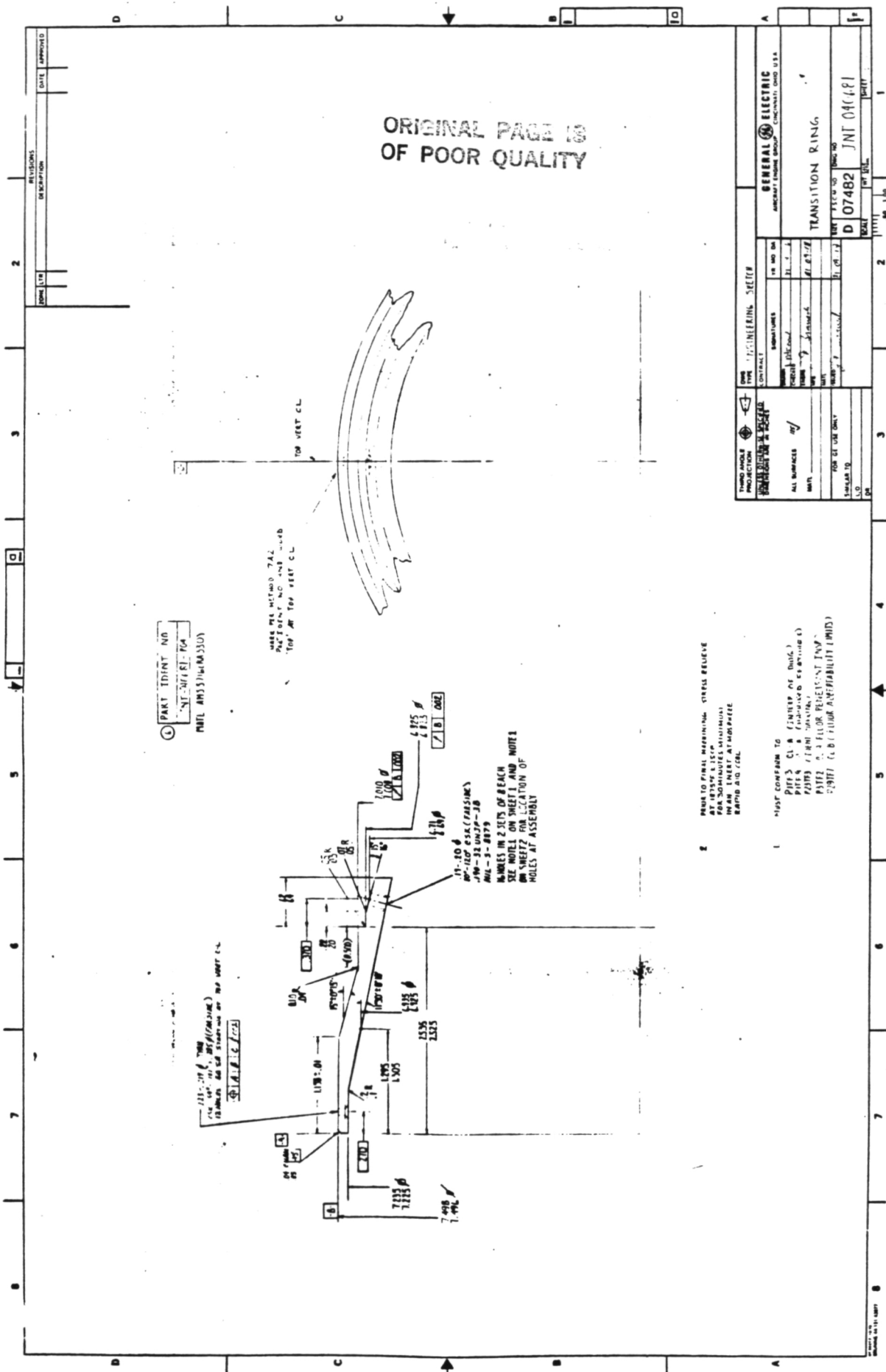


Figure VI-30. Detailed Drawing, Models 5 and 6.

ORIGINAL PAGE IS
OF POOR QUALITY



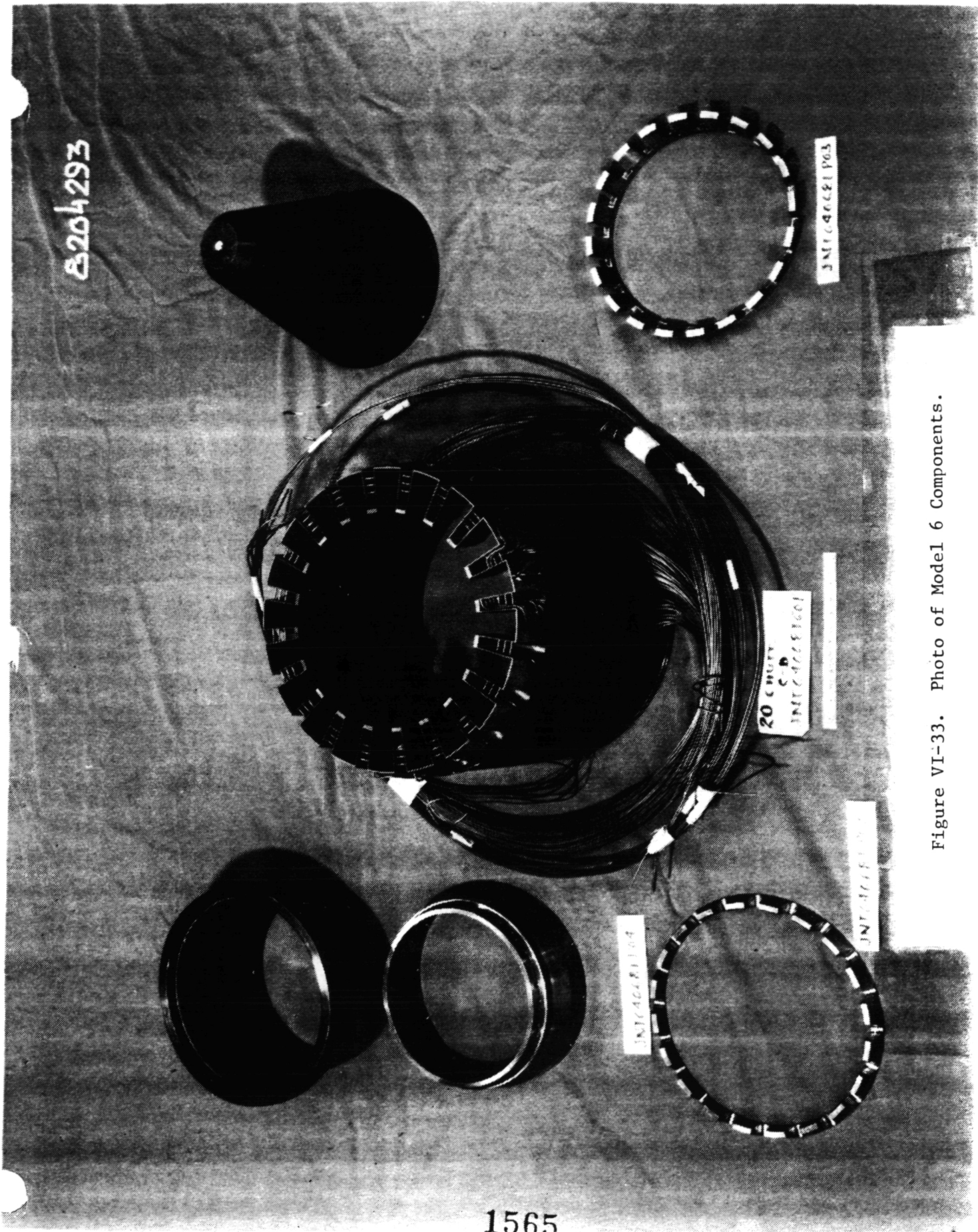
ORIGINAL PAGE IS
OF POOR QUALITY

C71097

1564

Figure VI-32. Photo of Model 5 Components.

8204293



1565

ORIGINAL PAGE IS
OF POOR QUALITY

ORIGINAL PAGE IS
OF POOR QUALITY

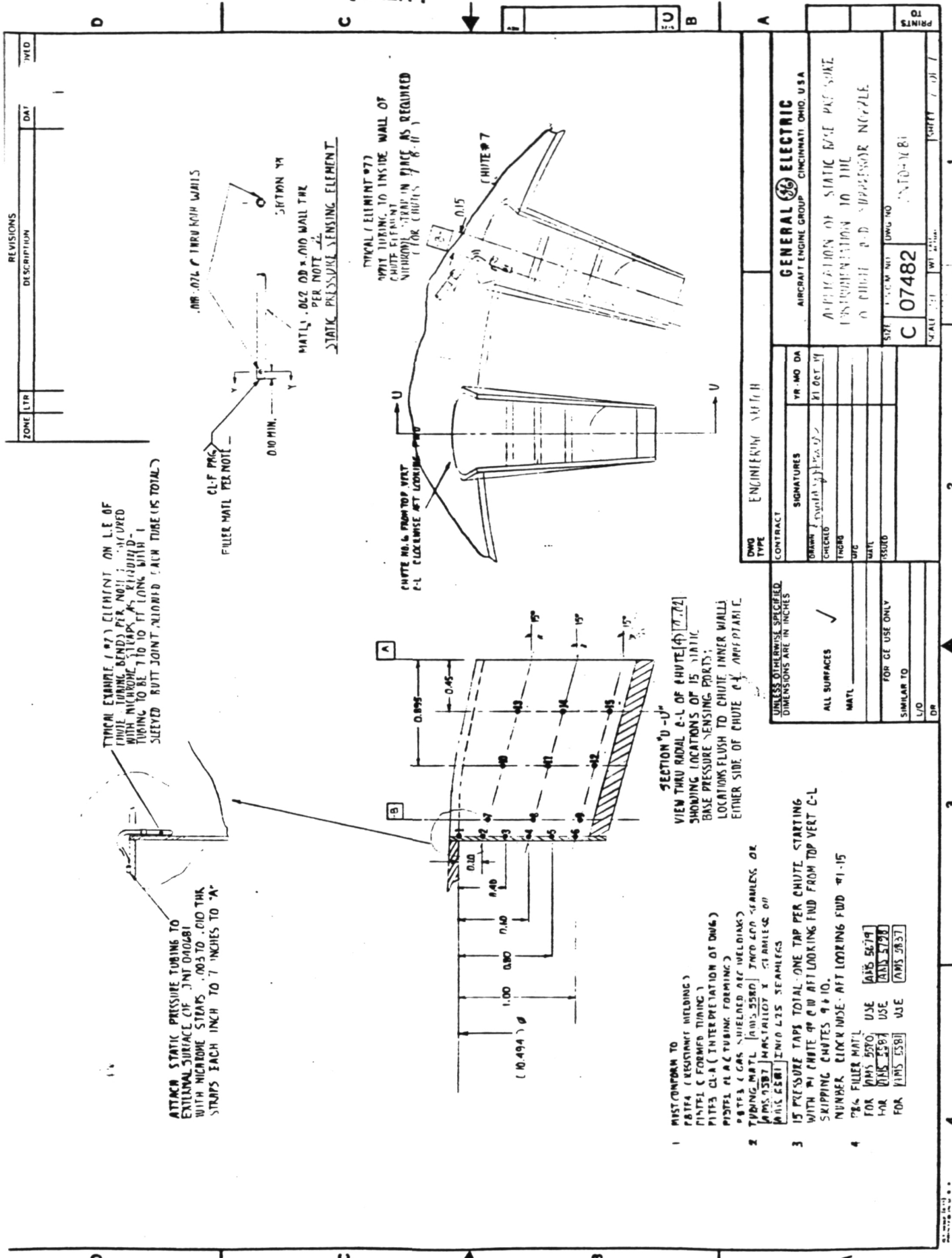


Figure VI-35. Application of P_s Instrumentation to Base Area of Model 6 20 C-D Chute Suppressor.